Spring 1-1-2017

A Thermo-Poromechanics Finite Element Model for Predicting Arterial Tissue Fusion

Douglas P. Fankell
University of Colorado at Boulder, fankell@colorado.edu

A Thermo-Poromechanics Finite Element Model for Predicting Arterial Tissue Fusion

By

Douglas P. Fankell

B.S., University of Wyoming, 2011
M.S. University of California Berkeley, 2012
M.S. University of Colorado Boulder, 2015

A thesis submitted to the
faculty of the Graduate School of the
University of Colorado in partial fulfillment
of the requirements of the degree of
Doctor of Philosophy
Department of Mechanical Engineering
2017

This thesis entitled:

A Thermo-Poromechanics Finite Element Model for Predicting Arterial Tissue Fusion

written by Douglas P. Fankell

has been approved by the Department of Mechanical Engineering

_____

Mark E. Rentschler

_____

Virginia L. Ferguson

Date: _____

The final copy of this thesis has been examined by the signatories and we find that both the content and the form meet acceptable presentation standards of scholarly work in the above mentioned discipline.

Fankell, Douglas P. (Ph.D., Mechanical Engineering)

A Thermo-Poromechanics Finite Element Model for Predicting Arterial Tissue Fusion

Thesis directed by Associate Professor Mark E. Rentschler

This work provides modeling efforts and supplemental experimental work performed towards the ultimate goal of modeling heat transfer, mass transfer, and deformation occurring in biological tissue, in particular during arterial fusion and cutting. Developing accurate models of these processes accomplishes two goals. First, accurate models would enable engineers to design devices to be safer and less expensive. Second, the mechanisms behind tissue fusion and cutting are widely unknown; models with the ability to accurately predict physical phenomena occurring in the tissue will allow for insight into the underlying mechanisms of the processes. This work presents three aims and the efforts in achieving them, leading to an accurate model of tissue fusion and more broadly the thermo-poromechanics (TPM) occurring within biological tissue. Chapters 1 and 2 provide the motivation for developing accurate TPM models of biological tissue and an overview of previous modeling efforts. In Chapter 3, a coupled thermo-structural finite element (FE) model with the ability to predict arterial cutting is offered. From the work presented in Chapter 3, it became obvious a more detailed model was needed. Chapter 4 meets this need by presenting small strain TPM theory and its implementation in an FE code. The model is then used to simulate thermal tissue fusion. These simulations show the model's promise in predicting the water content and temperature of arterial wall tissue during the fusion process, but it is limited by its small deformation assumptions. Chapters 5-7 attempt to address this limitation by developing and implementing a large deformation TPM FE model. Chapters 5, 6, and 7 present a thermodynamically consistent, large deformation TPM FE model and its ability to simulate tissue fusion. Ultimately, this work provides several methods of simulating arterial tissue fusion and the thermo-poromechanics of biological tissue. It is the first work, to the author's knowledge, to simulate the fully coupled TPM of biological tissue and the first to present a fully coupled large deformation TPM FE model. In doing so, a stepping stone for more

advanced modeling of biological tissue has been laid.

Dedication

To my parents, Don and Tricia, as well as my siblings Jacquie, Mandi, Joel, Brenna, and Vicki, who have provided an unimaginable amount of support, joy and love throughout my life.

Acknowledgments

I would like to express my extreme gratification to those who have provided support throughout the course of my doctoral studies. First, thank you to all of my colleagues in the AMTL for your countless discussions and ideas, in particular, Dr. Eric Kramer for his great experimental aid, Micah Prendergast for his ability to seemingly always catch the bugs in my code and to provide a relaxed lab atmosphere, Dr. Madie Kern for her calm intelligence and Carlye Lauff for her enthusiastic support. Additionally, I would like to thank my labmates and colleagues, Joan Ortega, Alex O'brien, Greg Formosa, Chelsea Heveran, Levi Pearson, Dr. Levin Sliker, Nick Anderson, Kristin Calahan, and Karl Johannes.

I am forever indebted to my advisors and mentors. Thank you Dr. Mark Rentschler for providing an incredible lab culture and the all-encompassing guidance to help me grow into the researcher, scientist and academic I am today. Thank you Dr. Rich Regueiro for your calm guidance through the challenges of implementing FEA code. And thank you Dr. Virginia Ferguson for you aid in my experiments and writing.

Portions of this work were funded by Conmed Electrosurgery, and I would especially like to thank, Ken Taylor, Renee Merchel and Kelli Barnes for their help.

Lastly, I would like to express my appreciation to all of the family and friends who put up with my incessant ramblings about science, school and research and helped me understand the bigger picture of life. I would not be where I am without your love and support.

Contents

List of Tables

List of Figures

Chapter 1: Introduction

This work focuses on the development of a finite element (FE) model used to simulate the heating and deformation of biological tissue, in particular the processes of cutting and fusing arteries with laparoscopic surgical devices. Several finite models from initial theory through final development are presented. The first, put forth in Chapter 3, is a thermo-mechanical model implemented in commercial FE software to simulate the cutting of an artery. From this work, the need for more detailed modeling of the physics occurring during the tissue fusion process arose and thus the full thermo-poromechanics finite element models are presented in Chapters 4 through 7. The work consists of four main parts. The first comprises of Chapters 1 and 2 and introduces the tissue fusion process, past attempts at modeling the TPM of biological tissue, and the ever increasing need for more advanced models. The second section of this dissertation comprises of Chapter 3 which introduces the experimental development of a novel damage parameter and its implementation in the commercial finite element program Abaqus. Chapter 4 presents the theory and implementation via custom written code of a small deformation finite element model. From this model, the need for a large deformation FE model was obvious, and chapters 5, 6, and 7 show the development, detailed linearization, and implementation of large deformation TPM into a custom written Galerkin FE code. Lastly, chapter 8 presents an overall summary of the work and the potential for the expansion of these modeling efforts.

1.1   Background of Energy Treatment of Tissue

Treating biological tissue with energy to either cauterize or ablate - to remove or destroy the function of - it can be traced back as far as the year 1500 B.C. in ancient Egypt [1]. The

ancient Roman doctor Claudius Galenus was the first to propose and conduct experiments to ligate or close off blood vessels and nerves with heat (200 A.D.)[1] though the practice did not become applied in medicine until the middle ages by Ambrose Pare [2]. The process has since been continuously refined and surgeons now treat tissue with energy via lasers, direct heat, or electrical current in numerous applications such as Lasik surgery [3], [4], electrocautery [5], [6], ablation of tumors [7], and fusion of bowel [8], skin [9], and arterial tissue [10], [11]. This dissertation will primarily focus on the cutting and fusing of arterial tissue.

Currently surgeons employ electrosurgical devices to fuse and cut arteries during laparoscopic surgery. Doing so provides several advantages over traditional mechanical methods that use scalpels, clips and sutures. These advantages include the elimination of long term foreign bodies, reduced infection rates, reduced scarring, and faster surgeries [11]–[13].

1.2 Current Surgical Techniques and the Need for an Accurate Model

In order to cut or fuse tissue a device must apply pressure and heat to cause changes in the tissue properties. While pressure must be applied mechanically, several different mechanisms can be used to heat arteries including lasers [14], ultrasonic vibration [13], bi-polar current [11], [13] and direct heat [15]. Several devices are available commercially and a good deal of research has been conducted on tissue fusion, yet, the mechanisms behind these tissue devices remains widely unknown [16]–[18]. Therefore, development of an accurate model is necessary for two primary reasons. First, a predictive model would allow for numerous design iterations to be created and evaluated computationally, allowing for more refined designs, and consequently, less expensive, more effective, and safer devices than those created using the current, costly, time intensive empirical studies. The second reason to develop a physically accurate model of tissue fusion is that such a model would shed valuable insight into the

unknown mechanisms behind tissue fusion. Developing a truly accurate model, supplemented by experimental data, would provide essential insights into the physical phenomena occurring during the fusion process.
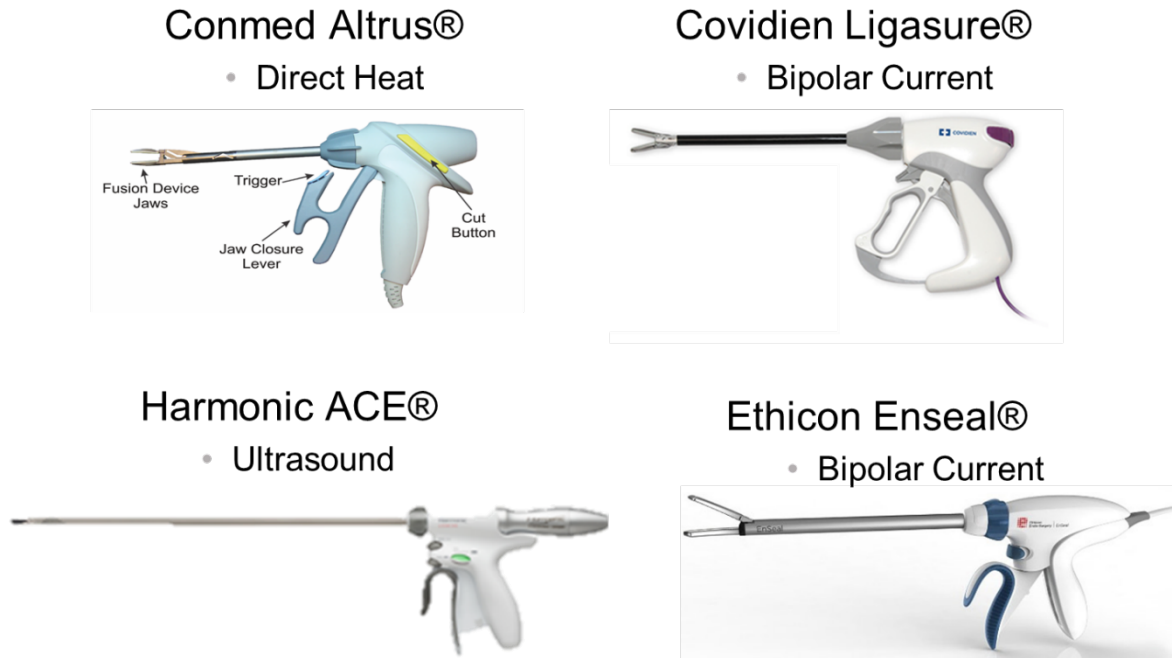
Figure 1.1: Images of current tissue fusion devices. The Conmed Altrus applies direct heat, the Covidien Ligasure and Ethicon Enseal bipolar current and the Harmonic ACE ultrasound to heat biological tissue.

1.3 Research Aims

Due to the benefits that would be provided by a comprehensive model of tissue fusion the following research aims were developed. They are as follows:

Research Aim 1: Develop a thermo-mechanical finite element model of exact geometry of an artery that solves for the stress and temperature in the tissue during the fusion process. Then use this model to predict arterial cutting.

Research Aim 2: Develop a two dimensional unsaturated thermo-poromechanics (TPM) small deformation model that represents the heat transfer, mass transfer
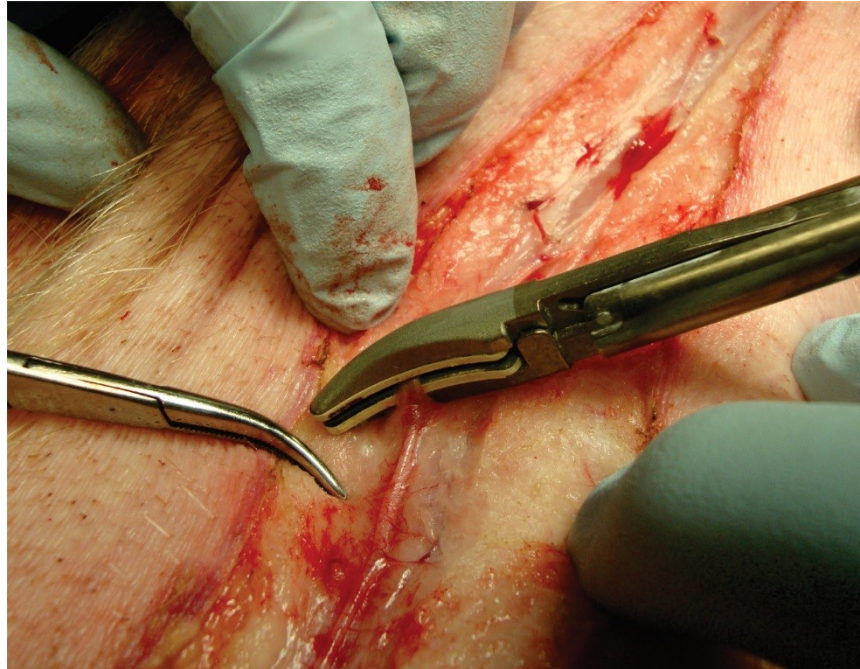
Figure 1.2: Image of a tissue fusion device sealing a gastric vein.

and deformation of a porous medium and use this model to simulate the tissue fusion process.

Research Aim 3: Extend the small strain TPM theory developed in Aim 2 to include large deformation theory and implement this theory in two dimensional FE code.

As no models currently exist with the ability to combine heat transfer and the structural mechanics of thermal tissue fusion, the purpose of Aim 1 is to address this need. Additionally, as current devices only successfully cut arteries on 90% of attempts during surgery, the ability to model the capability of certain devices to cut arteries became the final aim of the combined thermo-mechanical model. Initially, modeling arterial fusion with this same thermo-mechanical model was the obvious next step. However, as more research was conducted towards this goal it became apparent using the empirically based model developed in Aim 1 would not suffice; thus Research Aim 2 was born. Water in an artery has been shown to have a significant impact on the ability of tissue to be fused [19]. The model developed in Aim 2 not only models the structural deformation and the and heat transfer of the tissue, but

also includes the transport and phase change of the water. By doing this, a more physically intuitive model, based in the physics of mechanically and thermally loading tissue is created. Lastly, arterial tissue typically undergoes large deformations [20]. This is especially true when clamped on by fusion devices; therefore, while the model developed in Aim 2 is able to match experimental measurements of temperature, water content, and tissue deformation reasonably well, it is significantly limited by its assumptions of small deformations ($< 10\%$ strain). Aim 3 expands unsaturated TPM theory to include large deformations, something unseen in literature of any field, providing a novel and robust model with the ability to model biological tissue under a very wide range of conditions.

1.4 Motivation for a Large Deformation TPM Model beyond Arterial Fusion

Although this thesis is primarily focused on modeling arterial cutting and fusion, the author would like to draw the reader to the novelty of a fully coupled large deformation TPM finite element model. Tissue with properties similar to that of porous media exists commonly in the human body. This includes cartilage [21], vertebral discs [22], skin [23], ligaments[24], and numerous other tissues. Interactions between thermal sources and syncs, (in the form of surgical devices, wearable electronics, implanted electronics, etc,) are becoming evermore prevalent [25]–[27]. As these interactions increase, the need for the ability to accurately model the physics occuring within the biological tissue increases as well. Additionally, to the author's knowledge no such model exists in literature, and such a model would provide a valuable advancement to fields as wide ranging as geomechanics [28], food processing [29], and biomechanics as a whole. Therefore, the models currently being developed in Aims 2 and 3 will not only be applicable to thermal tissue fusion, but they will also provide a framework from which many studies can be conducted.

Chapter 2: Background

Numerous efforts have been made to model the structural mechanics of arteries and of human body tissue. Additionally, several efforts have been made to model the transport processes of water, chemicals, and heat through biological tissue. This section will first provide a brief introduction to the anatomy and physiology of an artery. It will then discuss the potential mechanisms behind thermal tissue fusion and, lastly, introduce the reader to these past approaches of modeling the physics of biological tissue. The goal of Chapter 2 is to provide the reader with a brief understanding of what has been done and the current needs in this field of biomechanical modeling.

2.1   Anatomy of an Artery

Arteries consist of three primary layers, the adventitia, the media, and the intima. The innermost layer, the intima, comprises of a single muscular layer of endothelial cells. The media is the middle layer and consists of mostly muscular cells interwoven with a three dimensional mesh of collagen and elastic fibers. Layers of collagen and elastin fibers form the adventitia, the outermost layer of the artery. The layers of crosslinked elastin and collagen in the media and adventitia constitute most of the extracellular matrix (ECM) and provide the structural strength of the artery. Typically, the collagen and elastin fibers exhibit a form of orientation causing the artery to behave in an anisotropic manner when loaded. The last component of the ECM is water, which can move freely through the ECM or be bound to proteins. When the ECM is heated, as in fusion processes, the collagen is denatured and much of this water vaporizes and is driven out of the artery.
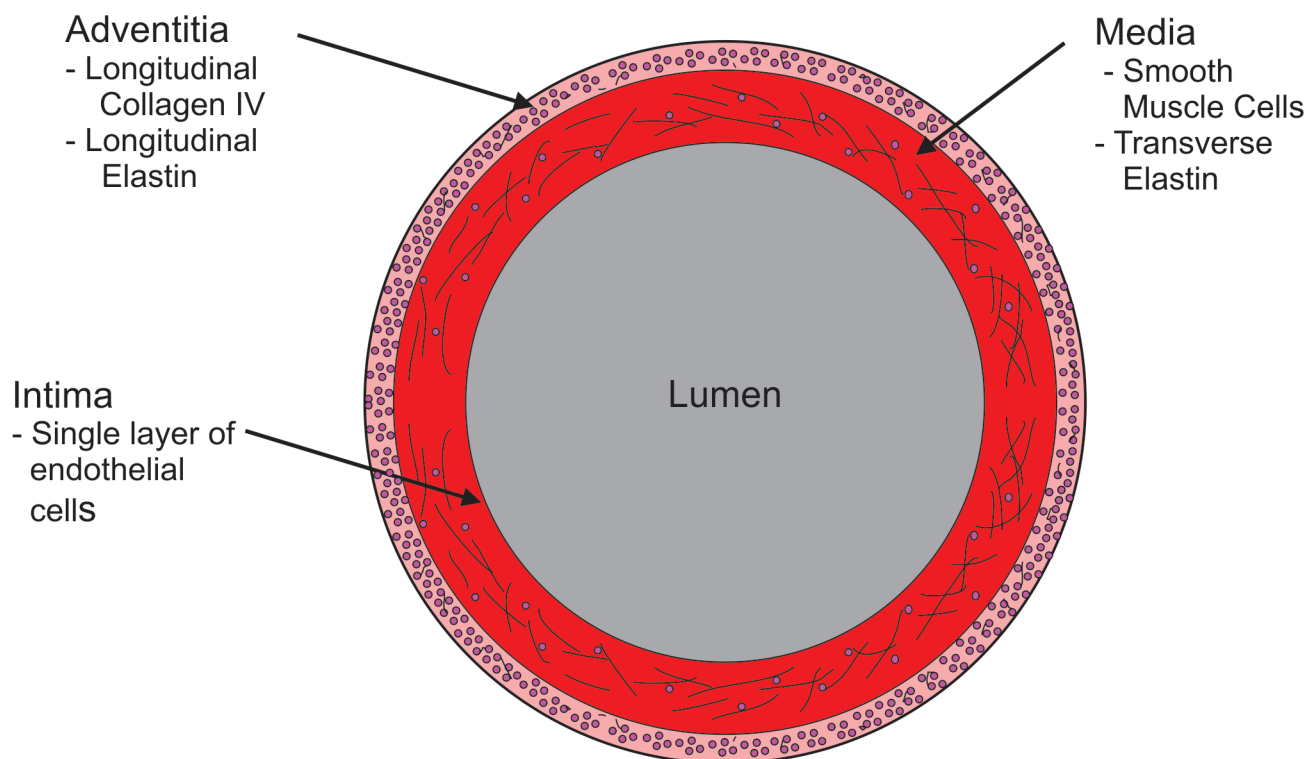
Figure 2.1: A depiction of the artery. Three layers, the intima, the media, and the adventitia make up the artery wall.

2.2 Mechanisms of Tissue Fusion and Cutting

Although several theories exist on the binding mechanics of thermal tissue fusion and the process of thermal cutting, the fundamental mechanisms behind each process remain elusive [14], [30]. Collagen denatures when heated above 60 °C [30]. Thus, traditional theories propose that tissue is bonded together through the destruction (during heating) of crosslinks and the reformation of new crosslinks as the tissue cools [31], [32]. Recent studies have been conducted challenging the validity of this theory. Combining evidence that water content of the tissue impacts fusion bond strength [33] and recent work done by Kramer et. al. on the role of the hydrophilic Glycosaminoglycans (GAGs), a new theory has been developed which implies that the bonding mechanisms of fusion are the result, not of reforming crosslinks, but of hydrogen bonds forming when water is driven out of the tissue [18]. Experimental studies are being conducted to validate or disprove these theories, but currently they only remain

theories. Thus, a model with the ability to evaluate the energy and water transport in the tissue would be an immense aid in validating these theories and designing experiments to further explore the bonding mechanisms. Attemts to elucidate the fundamental mechanisms of cutting arteries using heat are much more limited. The prevailing theory stems from a theory of tissue ablation. The theory proposes that microexplosions caused by the rapid heating and expansion of water vapor create pressures that damage arterial tissue [34], [35]. This theory is supported by the observation that it is difficult to cut dry tissue, even when heated to 270 °C. Once again, due to limited knowledge of the structural damage caused in arteries by electrosurgical devices the work presented here explores development of a damage parameter and its implementations within an FE model to provide insight into the fundamental mechanisms of arterial cutting.

2.3   Modeling

Countless efforts have been made by scientists to represent physical processes and their impact on biological tissue. As with most science, these efforts initially came in the form of several forms of physics (*e.g.* heat transfer, solid mechanics, fluid mechanics) and even separate fields. With the highly coupled nature of biological tissue and the advent of ever more powerful computers, models combining several forms of physics have become increasingly important, and efforts to create them are occurring frequently. In this section, the author attempts to provide the reader with a thorough background in the history of modeling heat transfer, mass transfer, and deformation of biological tissue, in particular arterial tissue. Initially each of these phenomena is introduced separately and their development followed into the highly coupled theories of current modeling efforts.

2.3.1 Solid Mechanics of an Artery

Modern biomechanics is considered to start with Y.C. Fung although the field can be traced back to Galileo Galilei and further. In his book "Biomechanics" Fung applies traditional continuum mechanics theory, including hyperelasticity and viscoelasticity to various biological tissue and includes a chapter on the artery [36]. As discussed earlier, the artery is an anisotropic material and it can experience large deformations. Therefore, Fung proposed to model the artery with a pseudoelastic stress-strain relationship represented by an exponential strain energy function [37],

$$W = \frac{C}{2}exp(a_1E_{\theta\theta}^2 + a_2E_{zz}^2 + 2a_4E_{\theta\theta}^2E_{zz}^2) \tag{2.1}$$

where C, a_1, a_2, and a_4 are constants found by fitting the equation to experimental data and $E_{\theta\theta}$ and E_{zz} are the strains corresponding to arbitrary stresses in the same directions. This approach has been widely used on a vast range of cardiovascular tissue of cardiovascular tissue [20], [38]. The current gold standard of modeling the solid mechanics of arteries was developed by Holzapfel, Gasser and Ogden [39]. In the Holzapfel-Gasser-Ogden theory the artery is treated as an incompressible hyperelastic composite tube with two fiber directions represented by the strain energy function,

$$\psi I_1, I_4, I_6 = \frac{c}{2}(I_1 - 3) + \frac{k_1}{k_2} \sum_{i=4,6} exp(k_2(I_i^* - 1)^2 - 1) \tag{2.2}$$

where c is the shear modulus of the tissue, k_1 and k_2 are material constants and I_i is the psuedo-invariant of the stretch in the ith direction. With this function a physically meaningful constitutive model was born with the first, neo-hookean term, representing the cellular material of the artery and the second term representing the mechanics of the fibrous ECM. This equation has been the basis for numerous studies employing FE modeling of arteries [40]–[44]. The most interesting FE modeling with regards to tissue fusion simulate

the interaction of surgical clamps occluding arteries performed by Famaey [41], [45], Gasser [9], Yang [46], and Farkoush[47]. These clamping models provide the basis for the clamping portion of the thermal tissue fusion process simulated in Aim 1.

As constitutive behavior of arteries is now well understood, attempts have been made to expand this to represent the damage of arterial tissue. These include structural mechanical modeling of the damage caused by balloon angioplasty, stent implantation and hypertension [48]–[52]. It should be noted that all of the current structural damage modeling efforts are limited to purely mechanical or poromechanical mechanisms. None of the current models combine arterial structural mechanics with heat transfer nor take into account the structural effects of thermal damage. As discussed earlier, this provides the basis for Aim 1.

2.3.2   Heat Transfer

Considerable effort around the world has been put forth to model heat transport in biological tissue as models provide insight into the effects of processes ranging from surgical treatment (e.g. cryotherapy, thermal ablation, laser treatment, etc) to hyperthermia [29]. As such a wide range of applications exist, this section will focus primarily on the origins of bioheat transfer and then on the develepment of the heat transfer in porous media. The first effort to model the heat transfer in biologcial tissue can be traced back to Pennes' effort to model the heat transport in the human forearm through modification of the conductive heat transfer equation[53],

$$\rho c_p \frac{\partial T}{\partial t} = \nabla \cdot (k \nabla T) + q_g, \tag{2.3}$$

where ρ, c, and k are the density, specific heat and thermal conductivity of the tissue, q_g, is the source term and T is the temperature of the tissue. Though criticized severely at times for being overly simple, this equation has been the basis for countless modeling efforts over the past 70 years[54]. Still widely used, the Pennes equation makes several simplifying

assumptions. First, it treats the tissue as a homogenous material, which as discussed earlier is rarely the case in biological media. Also, it assumes a non-directional, all-encompassing heat source, neglecting the directional effects of fluid (usually blood) leaving the tissue. To address these issues several modifications were suggested by Weinbaum and Jiji [55] and Wissler [56] by modifying the heat source term (q_g), but they still do not account for the heterogenous nature of biological tissue. Thus, for more accurate models representing the true nateure of biological tissue, a theory of porous media had to be used [57]. The first to use this theory in the context of bioengineering were Xuan and Roetzel [58] where they solve the combined energy equations of the blood and solid phases. Finally, Nakayama and Kuwahara present a "general bioheat transfer model based on the theory of porous media" [59] that again extends the equation from a two phase model to a three phase model, which can be summarized as:

$$\rho_\alpha\big(\frac{\partial T}{\partial t} + \boldsymbol{u}_\alpha \bigtriangledown T\big) = \bigtriangledown \cdot (k_\alpha \bigtriangledown T) + q_\alpha, \tag{2.4}$$

with $\boldsymbol{u}_\alpha$ as the velocity vector of the α phase. Applications of this equation and its modified forms through finite element modeling of biological tissue are very widespread. Those relevant to thermal treatment of tissue are: burn injury [60], tissue ablation [61], [62], laser treatments [63] and tissue fusion [64]–[67] .

2.3.3   Mass Transport - Flow through Porous Media

Modeling mass transport through biological tissue has traditionally been done in two ways, the first method is to use the diffusion equation. The second method is to use as variant of the Navier-Stokes equations, typically in the form of Darcy's law. Using the diffusion equation can be valuable when concentration of mass in a certain location is desired, such as when modeling drug treatment [68] or mass transport in the brain [69]. However, typically modelers consider tissue as a porous media. In fact, as seen in equation 2.4 the velocity of

each phase ($\boldsymbol{u}_\alpha$) is needed as an input to the heat equation. Modified versions of the Navier-Stokes equations address this need. Darcy developed the first and most widely used theory of fluid flow through porous media [70]. The equation provides a linear relationship between the pore pressure and fluid velocity by neglecting both fluid inertial effects and boundary effects. Darcy's law is shown as,

$$\boldsymbol{u} = -\frac{\boldsymbol{K}}{\mu}\frac{\partial P}{\partial \boldsymbol{x}} \tag{2.5}$$

where $\boldsymbol{u}$ is the fluid velocity, $\boldsymbol{K}$ is the permeability, P is the pressure and μ is the fluid viscosity. Darcy's theory has been used in many biomedical applications such as ligaments and tendons [24], [71], vetebral discs [72] and the arterial wall [73]. If the assumptions put forth by Darcy are not valid then additional terms must be added to the equation. The most common of examples including additional terms are the Brinkman equation [74] which provides an additional term to account for the effect of fluid boundaries and the Brinkman-Foreheimer-Darcy [57] equation which includes the inertial effects of the fluid as well. In this work, only Darcy's law will be used in the poromechanical and thermo-poromechanical models discussed later.

2.3.4 Poromechanics and Thermo-poromechanics - Historical Development

The primary theory and modeling efforts of poromechanics originated in the field of soil mechanics. Terzaghi and Fullinger provided the start to the field with their studies on the mechanics of liquid-filled rigid porous solids [75]. Maurice Biot continued their work and is generally credited with establishing poromechanics as field through his development of a theory of elasticity and consolidation of a fluid saturated porous media [75]–[77]. In 1972, Biot expanded his theory to include finite deformations [78]. Numerous researchers have since expanded upon Biot's theories and it is outside of the scope of this work to describe in detail each contribution. Thus, the author will only highlight major developments that

lead to the theories of thermo-poromechanics presented in this thesis. The reader is invited to visit detailed reviews by de Boer [75], [79], [80] for more in depth historical review. Highlights in the development of poromechanics include Nunziato, Passman and Walsh's efforts to develop the concept of using volume fractions as a constraint [81]–[83] and Bowen's efforts to use this idea to represent incompressible and compressible porous media [75], [79]. Coussy published on the thermo-mechanics of saturated porous media in the finite strain regime in 1989[84] and, in 1992, Li and Li presented theory on the thermo-poromechanics of fluid saturated media. Li and Li's theory was expanded and firmly established by de Boer and Kowalski in 1995 [85]. Modeling the phase transition between materials in porous media is necessary when looking at the heating and cooling of biological material. First efforts to do this involved trying to model the freeze-thaw-evaporation cycle in soils. According to de Boer, the first attempts to discuss these effects in partially saturated media were conducted by Kowalski [86]. Several efforts have since been put forth in adding freezing and drying phase transitions to porous media theory [79], [87], [88]. With this theory established, the obvious next step was to employ it with numerical simulations.

2.3.5 Application of Thermo-poromechanics to Biological Tissue and Finite Element Modeling

Many researchers have implemented poromechanics theories in finite element models; this work includes only those modeling efforts that have had significant impacts in the field of biomechanics. The first attempt to use poromechanics theory to model biological tissue was conducted by Van Mow in 1980, where he developed a binary mixture model to represent articular cartilage [89]. Continuing Mow's work, Lai developed a "Triphasic theory for the swelling and deformation of articular cartilage to represent the coupling of chemistry with biphasic poromechanics. Electric current and potential are then added to the theory by Huyghe and Janssen [90]. Additionally, Snijders, Simon, Van Campen, Oomenns and Jayaraman have applied mechanics of porous media theories to soft biological tissues including:

skin, cartilage, vertebral discs and the artery wall [23], [73], [91]–[93] . Ehlers et. al. [94] provides an overview of these theories and gives a general theory for modeling saturated biological tissue. It should be noted, while these theories are thermodynamically consistent, none of them include heat transfer through the tissue nor mass phase change of the fluid. As scientists applied poromechanics theory to more and more biological tissues in the 1980's and 1990s computer scientists continued to exponentially increase computing power. Consequently, solving the coupled partial differential equations present in poromechanical theories through numerical methods became increasingly popular. Researchers utilized finite element (FE) analysis to primarily model the poromechanics in two biological tissues initially, vertebral discs and articular cartilage. Initial efforts were conducted by Simon and Snijders [92], [93], [95] (vertebral discs) and Spilker and Suh[96] (articular cartilage). These efforts have spurred numerous FE modeling attempts which can be found summarized in review papers on FE modeling of the vertebral discs [22]and articular cartilage [97]. Efforts to employ poromechanical FE modeling on other biological tissues are limited in scope but have been conducted on cardiac tissue [98] and lung tissue [99]. All poromechanics FE models mentioned in this section examine only a fully saturated biphasic (solid and liquid) or a triphasic (solid, fluid and chemical potential) biological tissue.

To the author's knowledge no FE models exist that couple triphasic (partially saturated) poromechanics and heat transfer through biological tissue. To find computational modeling efforts employing such a theory the fields of geomechanics and food processing must be examined. Theories of partially saturated thermo-poromechanics consider a solid skeleton with its voids filled with more than one fluid *e.g.* water and air, or water and oil. The first implementation of such a model, which allowed for water and air flow, including phase transition, using finite elements was done by Li, Zienkiewicz and Xie [50], [100]. This was extended to include heat transfer by Schrefler and Xiaoyong [101], [102] and fully explored in the second edition of Lewis and Schrefler's book "The Finite Element Method in the Static and Dynamic Deformation and Consolidation of Porous Media" [103]. Wang et. al. also presented a fully coupled TPM FE model to simulate the effects of heated foundation [104],

[105]. The coupled TPM FE models of Lewis, Schrefler and Wang provide the basis for the finite element model presented in Chapter 4.

Perhaps the finite element model simulating physics most similar to those seen in arterial tissue fusion is the TPM model developed by Dhall and Datta [106] which simulates the cooking of hamburger patty and a potato slab. However, this model typically neglects deformation of the tissue or considers the effects of changing geometry as minor. As the conditions presented in the this model are close to those seen during tissue fusion, Dhall and Datta's works are heavily relied on for mechanical properties.

All of the TPM models mentioned thus far in this paper do not consider finite strain nor large deformations. In fact, a full large deformation triphasic TPM FE model is missing in the literature. Borja, Song, Reguiero, Ebrahimi and Wong have made great inroads in presenting thermodynamically consistent static and dynamic large deformation models of biphasic porous media [99], [107]–[109], but do not incorporate thermal effects. Additionally, strides have been made by Sun to develop a full large deformation TPM FE model of fully saturated biphasic porous media [28], but this theory has yet to be expanded to a triphasic media.

2.3.6   Commentary on Material Properties

A major consideration in the development of increasingly complex finite element models of biological tissue is providing correct material parameters. Experimentally measuring material properties of biological tissue proves difficult on many fronts. First, inherent variability exists throughout all biological tissue. Specimens can vary from individual to individual and even upon location within an individual [20]. Secondly, measureing biological tissue properties can be experimentally difficult. As a living tissue works as part of a larger biological system, it is desirable to measure tissue properties in-vivo. However, this proves to be costly, difficult and often impossible to accomplish without damage to the specimen. Therefore, tissue is typically extracted and tested ex-vivo which can lead to measurement

of unrepresentative material properties [33] unless extreme care is taken to preserve all material conditions. Due to the difficulties discussed here, several gaps in the knowledge base of biological tissue properties exist. For instance, extensive research has been conducted on the structural material properties of arteries [20], [110] and their thermal conductivities [67], [111] yet little data exists on the permeability of the tissue. The modeler must weigh the benefits of a more accurate in-depth theory with numerous material constants potentially not well known with a less accurate model using fewer, but more accurately measured material parameters. Additionally, for models utilizing parameters not directly measured, it is essential for the modeler to calibrate and validate their simulations with experiments. In this work, two methods are employed to address these issues. In Chapter 3 when needed material properties were unknown, experiments were developed and conducted to ascertain these values. In Chapters 4 and 7 literature was scoured for known values of materials similar in composition to that of the artery wall. The results of the simulations were then compared and calibrated to experimental results.

2.4 Summary and Commentary

While countless modeling efforts have been put forth with regards to using the finite element method to model biological tissue as a porous media, several opportunities exist to expand this field both with regards to thermal tissue fusion and, more broadly, in the modeling of soft biological tissue and porous media.

2.4.1 Current State of Modeling Thermal Tissue Fusion

Modeling efforts relating to thermal tissue fusion and the occlusion of arteries are currently implemented in two ways, structural mechanics or heat and mass transport. Structural mechanics models [41], [47] only represent arterial clamping and evaluate damage based solely on stresses in the artery wall. They do not account for heat or mass transfer within the

tissue. On the opposite end of the spectrum, heat and mass transport models [66] of thermal tissue fusion evaluate damage purely based on temperature. To the author's knowledge, no current model exists that combines both heat transfer and structural mechanics into one model. Chapter 3 presents a combined heat transfer and structural mechanics model, including a method of evaluating structural damage as a function of both temperature and pressure (through strain-energy). This model, however, treats tissue as a homogeneous material with temperature dependent thermal properties. Also, the model is limited in the fact that it cannot predict fusion strength as studies have shown such a dependence on water transport [19][18] and pressure [112][113]. Thus, the need for a more advanced model, fully describing the underlying physics of the fusion process is very apparent, and the aims leading to Chapters 3-7 were born.

2.4.2   Current State of Thermo-poromechanical Finite Element Modeling of Biological Tissue

Scientists have put forth numerous FE modeling efforts to represent biological tissue as a porous medium. Currently, these efforts mainly fall into one of two categories. The first category treats the tissue as a saturated porous medium and the models solve for deformation and fluid flow or fluid pressure in the tissue as a saturated porous medium and the models solve for deformation and fluid flow or fluid pressure within the tissue. Models in the first category do not account for heat transfer within the tissue. These models have primarily focused on either vertebral disc or articular cartilage, though lung tissue and myocardial tissue have been examined on a limited basis. The second category of models treat tissue as either biphasic (solid and liquid), triphasic (solid, liquid, and vapor) or 4-phase (solid, liquid, vapor and chemical species) and examine the heat, mass and chemical transport through the tissue, neglecting deformation and its effects. Not yet in literature has a model been presented that uses a fully coupled unsaturated TPM formulation to simulate biological tissue. With increasing device-tissue interaction through surgical devices, wearable

technology and implanted electronics, these models are becoming more necessary to fully understand the impact of foreign bodies and procedures on tissue. A major reason for the lack of TPM modeling of biological media is the, almost universal, large deformations tissue typically undergoes. While unsaturated TPM have been implemented in soil mechanics models [103], [105] and food processing [106] these models are limited to small deformations, limiting their effectiveness to biological tissue. Recently, a TPM FE model presented by Sun includes large deformations, but only for the fully saturated case, neglecting phase change and triphasic materials. Thus, a true triphasic (solid, liquid, gas) TPM FE model remains undeveloped at this time. Chapters 5-7 attempt to fill this void and provide an essential step towards all encompassing multi-phase models. Such models are essential if the goal of patient, specific models of exact surgical procedures, simulations of large deformation thermal geomechanics, or accurate modeling of porous high explosives is desired.

Chapter 3: A novel parameter for predicting arterial cutting in finite element models

3.1 Overview

Current efforts to evaluate the performance of laparoscopic arterial fusion devices are limited to costly, time consuming, empirical studies. Thus, a finite element (FE) model, with the ability to predict device performance would improve device design and reduce development time and costs. This study introduces a model of the heat transfer through an artery during electrosurgical procedures that accounts for changes in thermal material properties due to water loss and temperature. Experiments then were conducted by applying a known heat and pressure to carefully sectioned pieces of porcine splenic arteries and measuring cut completeness. From this data, equations were developed to predict at which temperature and pressure arterial tissue is cut. These results were then incorporated into a fully coupled thermomechanical FE model with the ability to predict whole artery cutting. An additional experiment, performed to examine the accuracy of the model, showed that the model predicted complete artery cut results correctly in 28 of 32 tests. The predictive ability of this FE model opens a gateway to more advanced electrosurgical fusion devices and modeling techniques of electrosurgical procedures by allowing for faster, cheaper and more comprehensive device design. The work in Chapter 3 has undergone successful peer review and has been published in the *Annals of Biomedical Engineering* [16]. It is reproduced here in its entirety.

3.2 Introduction

Currently surgeons employ electrosurgical devices during laparoscopic procedures to join and cut biological tissue. Clinical applications of electrosurgical devices range from ligation [10] and cutting [114] of blood vessels to fusion of colorectal tissue [8]. Devices apply the energy and pressure necessary to fuse and cut tissue through jaws utilizing bipolar current, ultrasonic vibration, or ceramic heaters. Advantages of tissue fusion over current mechanical methods, such as clips and sutures, include the elimination of long-term foreign bodies, reduced infection rates, reduced scarring and faster surgeries [11]–[13]. Therefore, development of ever more precise and effective laparoscopic tissue fusion devices will greatly benefit the surgical community as the technology moves into other application areas. Despite prior research into tissue fusion, the specific mechanisms of the process that bond two apposing tissue layers remain elusive [17]. Thus, researchers and device designers have relied solely on empirical evidence to evaluate the performance of laparoscopic tissue fusion devices. Furthermore, to our knowledge, no comprehensive finite element (FE) models exist with the ability to predict if a device will cut or fuse an artery. Such a model would allow for numerous device design iterations and reduced development time and costs. Current FE modeling efforts concentrate on either the structural mechanics of an artery when occluded [41], [50], [111], [115] or on the heat-transfer through the tissue [64], [66] but an inclusive model containing a coupled thermomechanical analysis has not been developed. While clamping models provide a reasonable representation of the stresses and strains induced in an artery when clamped, these models have yet to take into account changes in material properties due to supraphysiological pressure and temperature. Studies show both applied pressure[112], [116] and tissue temperature [64], [117] affect the cutting and fusing of arteries; therefore, a combined thermomechanical model is necessary to accurately predict arterial cutting. Thus, the objective of the present study was to create a finite element model that combines both the structural mechanics and the heat transfer of arterial fusion and cutting. To accomplish this aim, a heat transfer FE model was developed, verified and expanded to include the structural mechan-

ics of the artery. Next, to determine the conditions at which an artery cuts, experiments were conducted on sectioned rectangular tissue specimen strips and a damage parameter which includes the detrimental effects of temperature and pressure was developed. Finally, this damage parameter was incorporated into the thermostructural FE model providing a method of predicting if a whole artery will cut during the procedure. This developed model has potential to aid in device optimization and provide insight into the important mechanisms underlying thermal vessel sealing and ultimately to provide steps towards improved medical devices, improved surgeries and the potential development of tissue anastomosis.

3.3 Materials and Methods

3.3.1 Heat Transfer Equation Development

Traditionally, the Pennes Bioheat Equation is used to define heat transfer through biological tissue [98]. It accounts for heat sinks and sources, including blood flow and metabolic heat generation. For the case examined herein, both of these phenomena can be neglected as the artery will be clamped preventing blood flow and the metabolic heat generated is orders of magnitude less than the applied heat. Thus, the bioheat equation can be written as,

$$\rho c_{eff} \frac{\partial T}{\partial t} = \triangledown \cdot (k_{eff} \triangledown T) + q_g \tag{3.1}$$

where ρ is the tissue density, c_{eff} is the specific heat, T is the temperature, t is the time, k_{eff} is the effective thermal conductivity and q_g is the generated heat.

Tissue specific heat and thermal conductivity change as water leaves the tissue; thus, the bioheat equation must be modified to accurately represent the heat transfer through the tissue. Building on work by Chen et. al. [64] and Yang et. al. [46] an empirical water loss model was developed by modifying Chen's equation for modeling water content during microwave ablation to enable it to represent water content data collected during direct heat

fusions by Cezo [19], [117]. The resulting material model is

$$WC = \frac{A * WC_{25°C}}{1 + Ce^{Z_o}} + WC_{180°C} \tag{3.2}$$

$$Z_0(T) = B(T - D). \tag{3.3}$$

The water content, WC, is a function of temperature. $WC_{25°C}$ and $WC_{180°C}$ are water contents measured at 25 °C and 180 °C respectively [118] and A,B,C, and D are constants derived using a nonlinear regression (NonLinearModel.fit, Matlab R2012b) to fit equation 3.2 to data collected in previous studies [19], [118].

A water content term is added in the expressions for the effective thermal conductivity, k_{eff}, and effective specific heat, c_{eff}, to incorporate the role water content plays on the material properties. The modification of k_{eff} is

$$k_{eff} = k_f + \left(k_{W25°C} + 0.001575(T - 25°C)\right)WC(T), \tag{3.4}$$

where k_f is the thermal conductivity of dry tissue, $k_{W25°C}$, the thermal conductivity of water at 25°C (0.5653 W/mK)[119], $WC(T)$ the water content defined by equation 3.2, and T the temperature. The specific heat is defined by

$$c_{eff} = c_f + c_w WC(T) + c_\ell \dot{W}C(T), \tag{3.5}$$

where c_f is the specific heat of the dry tissue. The second term multiplies the specific heat of water, c_w (4181.3 J/kgK) [119] by the water content of the tissue, $WC(T)$, effectively representing specific heat of the water bound in the tissue. The final contribution accounts for the latent heat of vaporization of the water in the artery, found by multiplying the latent heat of vaporization of water, c_ℓ, by th rate of water lost in the tissue, $\dot{W}C(T)$. To determine the properties of dry tissue (k_f and c_f), equations 3.5 and 3.4 are set to established values ($k_{eff} = 0.45$ W/mK and $c_{eff} = 3314.2$ J/kgK at 25°C) [120] and k_f and c_f are solved to be

0.009144 w/mK and 145.83J/kgK, respectively.

3.3.2 Heat Transfer Model Validation

Once the Pennes Bioheat Equation was modified, a heat transfer simulation was developed to model the heat transfer through the tissue. The results were then compared to published experimental data to validate the model. The simulations were conducted using COMSOL multi-physics finite element modeling software (COMSOL 4.2a, COMSOL, Inc. Burlington, MA, USA). The 3 mm x 12 mm x 0.4 mm rectangular block of tissue displayed in Figure 3.1 represents that of a flattened artery. The compressed region within the device jaws has a thickness 0.2 mm and a width of 3.5 mm; the jaws are 3.5 mm 9 2 mm with a corner radius of 0.25 mm. COMSOLs standard meshing engine was used to create the mesh of 20-node tetrahedral elements. A mesh dependency study was conducted, and a maximum element size of 0.715 mm with a minimum curvature ratio of 0.40 was determined to provide accurate results at minimal computational cost.
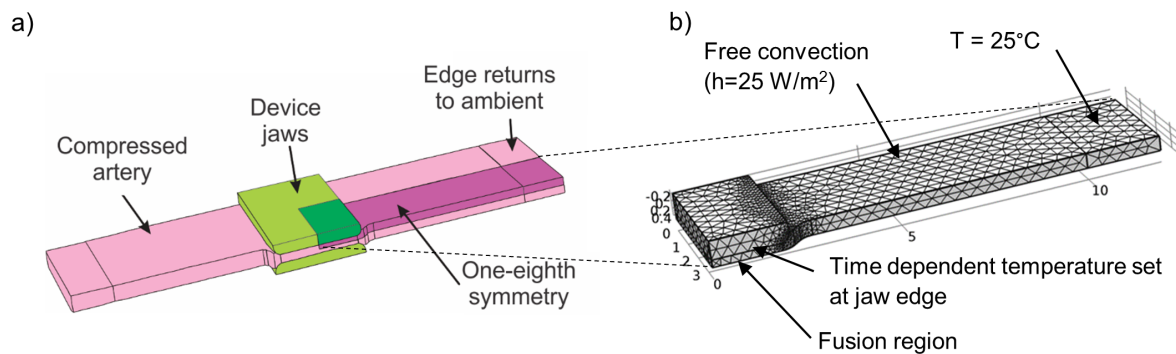
Figure 3.1: a: Depiction of a full flattened artery compressed in the device jaws. b: The mesh of a 1/8th cutout of the artery used in the heat transfer finite element simulation.

To limit computational resources, 1/8th symmetry is used and a symmetric boundary condition implemented on the three planes of symmetry (Fig. 3.1b). The edges at the end of the artery are assumed to remain at ambient temperature and are fixed at a temperature of 25 °C. All other edges not in contact with the jaws are represented by a free convective boundary condition with a heat transfer coefficient, h, set to $25W/m^2$. This represents a mixture of water and air for the ambient surroundings. Energy is added to the tissue through a transient temperature boundary condition on the edges of tissue in contact with the jaws. The temperature of the jaws at each time is interpolated from measured experimental data. A time dependent simulation is run for 3 s with set time steps of 0.25 s. A standard backward Euler method and a Multifrontal Massively Parallel Sparse direct solver (standard settings in COMSOL 4.2a) were used to solve the differential equations for temperature at each node. Once the simulation was complete, the thermal spread through the tissue was compared to results measured by an intra-luminal array (ILA) published by Cezo [15] to validate the material model.

3.3.3 Structural Mechanics Theory

After the material model for the heat transfer was verified, a fully combined thermo-structural model was developed. Conservation of momentum provides the governing equation used to represent the solid mechanics of an artery [121],

$$\rho\boldsymbol{a} + \frac{\partial\boldsymbol{\sigma}}{\partial\boldsymbol{x}} + \rho\boldsymbol{f} = 0 \quad in \quad body \quad \Omega \tag{3.6}$$

$$\boldsymbol{\sigma} \cdot \boldsymbol{n} + \boldsymbol{t} = 0 \quad on \quad boundary \quad \Gamma \tag{3.7}$$

where $\boldsymbol{a}$ is the acceleration, $\boldsymbol{f}$ is the body force, $\boldsymbol{t}$ is the traction vector and $\boldsymbol{\sigma}$ is the stress in the body.

It has been shown that using an incompressible hyperelastic material model with two composite fiber directions can accurately represent the structural properties of an artery. This is achieved using the Holzapfel-Gasser-Ogden (HGO) strain energy density function [122]:

$$\psi_{iso}(I_1, I_4, I_6) = \frac{c}{2}(I_1 - 3) + \frac{k_1}{k_2} \sum_{i=4,6} exp(k_2(I^*_i - 1)^2 - 1), \tag{3.8}$$

$$I_1 = \lambda_r^2 + \lambda_\theta^2 + \lambda_z^2, \tag{3.9}$$

$$I^*_{4,6} = I_1\kappa + (1 - 3\kappa)I_{4,6}, \tag{3.10}$$

$$I_{4,6} = \lambda_\theta^2 cos^2\phi + \lambda_z^2 sin^2\phi, \tag{3.11}$$

$$\boldsymbol{\sigma} = 2J^{-1}\boldsymbol{F}^T \frac{\partial \psi}{\partial \boldsymbol{C}}\boldsymbol{F}. \tag{3.12}$$

The isochoric strain energy density function, ψ_{iso} has a Neo-Hookean term to represent the isotropic, cellular, portion of the artery and two anisotropic terms which represent the energy potential due to stretch in the direction of the ECM fibers. The isotropic term is a function of the first invariant, I_1, which is a sum of the squares of the stretch in the three directions, λ_i, and the shear modulus, c. The anisotropic terms are a function of the psuedo-invariants, $I_{4,6}$, which represent the stretch in the fiber directions (Fig. 3.2) and two material constants, k_1 and k_2. A fiber dispersion factor, κ modifies the psuedo-invariants to account for a normal distribution of the about their primary directions. Seperate material properties were used for the adventitia and media (Table 3.1) and were taken from published studies[110].

Constant	μ (kPa)	k_1 (kPa)	k_2	κ	φ_1 (deg)	φ_2 (deg)
Media	122.3	24.7	16.5	0.16	6.9	173.1
Adventitia	138.2	178.4	48.4	25.9	25.9	154.1

Table 3.1: Material constants used for HGO strain energy density function
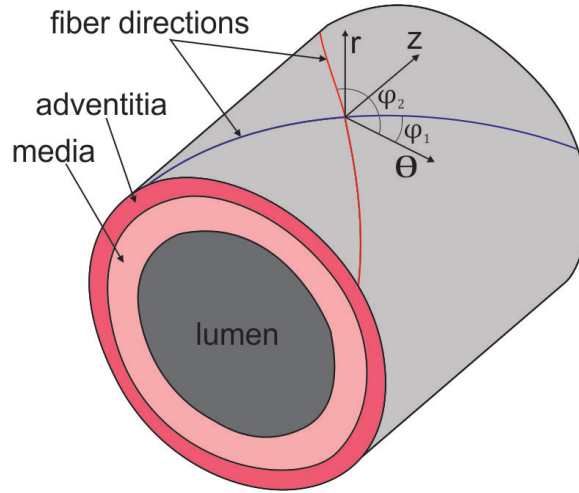
Figure 3.2: Geometric representation of an arterial section. The radial (r), circumferential (θ) and longitudinal(z) directions along with the fiber directions are shown for a point.

3.3.4   Proposed Damage/Cut Parameter

A parameter, $D(\psi_{iso}, T)$, has been proposed that is a function of both the elastic strain energy in the tissue determined by the HGO strain energy density function (Eqn. 2.2) and the temperature of the tissue determined by the solution to the Pennes Bioheat Equation (Eqn. 2.3). This damage parameter, $D(\psi_{iso}, T)$. is used as a measure of the overall energy in the system. The equation is defined such that a damage value of 1 represents the point at which the arterial tissue is significantly degraded by heat and pressure such that it loses all strength. A damage value of 0 means the arterial tissue remains undamaged. Damage values between 0 and 1 represent the corresponding percentage of damage occurring in an element (*e.g. if $D(\psi_{iso}, T) = 0.25$, the element loses 25% of its strength*). During a finite element simulation, the parameter, $D(\psi_{iso}, T)$, will be evaluated at each integration point. If the damage is greater than zero the stiffness of each element is modified as such:

$$c = c_{initial}(1 - D(\psi, T)), \tag{3.13}$$

$$k_1 = k_{1_{initial}}(1 - D(\psi, T)), \tag{3.14}$$

$$k_2 = k_{2_{initial}}(1 - D(\psi, T)). \tag{3.15}$$

It should be noted to ensure stability in the model, the value of the shear modulus, c, was limited to a minimum of 10% of its original value. The effect on thermal conductivity due to damage to the ECM was neglected as free water and vapor still exist within the damaged tissue. The heat transport and conductivity of water and vapor are on an order of magnitude greater than the conductivity of the ECM.

3.3.5 Damage Parameter Characterization

To develop both the equation for the damage parameter and the damage thresholds an experiment was designed and conducted. Several porcine spleens were obtained from an abattoir (Innovative Foods LLC, Evans, CO) and kept on ice for less than five hours before harvesting the main splenic artery. The arteries were cut into sections (15 mm long) and then flash frozen by placing each on a a cork backing and coating each artery in the tissue embedding medium Tissue Tek OCT. The backing and arteries were immersed in chilled (160 °C) isopentane and stored at -80°C until needed. On the day of testing each artery was thawed (37 °C, 0.9% phosphate buffered saline (PBS);15-60 minutes). All arteries were frozen and thawed using methods shown to retain mechanical properties consistent with those of fress tissues [123]. Once thawed the arteries were cut into 2.5 mm wide rectangular strips with longitudinal lengths ranging from 15 to 25 mm.

To determine the cutting temperature and strain energy, a custom environmental chamber with Conmed Altrus jaws was built (Fig. 3.3) and affixed to a uniaxial material testing system (MTS; MTS Insight 2 Electromechanical Testing System, MTS System Corporation,
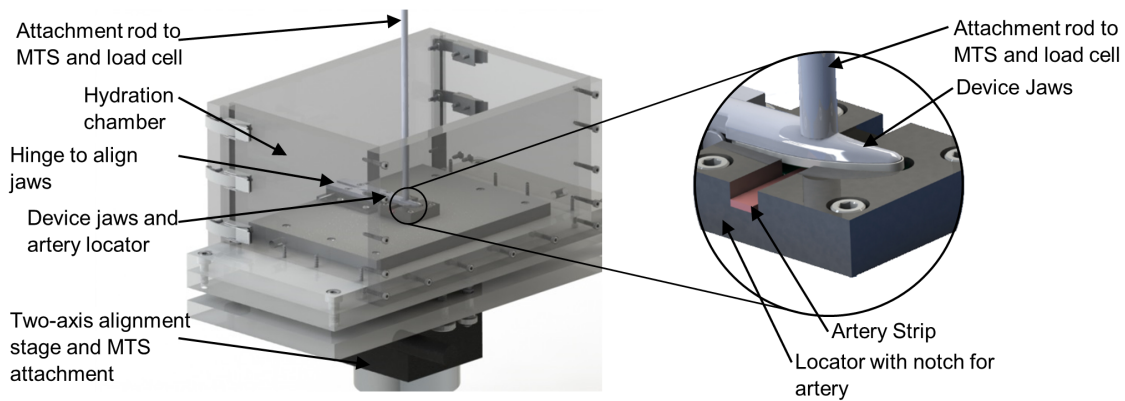
Figure 3.3: Left, a full view of the experimental setup. During the experiments the environmental chamber was filled with 0.9% PBS, an artery placed in the device jaws and a vertical load applied by the MTS through the vertical rod. Right, inset shows a magnified view of the device jaws with an artery strip lying within a positioning channel.

USA). In the custom chamber a locating feature was 3-D printed (Makerbot Replicator 2, Makerbot Industries, LLC) and placed around the lower jaws. A depression in the locating feature ensures each arterial section contacts the jaws in the same location, minimizing error caused by a temperature gradient along the length of the jaws. The jaws were connected and aligned using a hinge attached to the lower plate ensuring consistent parallel contact between the jaws. The chamber was filled with 0.9% PBS to completely submerge the arterial strip during testing allowing for a constant water content among strips to be maintained. For each test, an arterial strip was placed, adventitia side up, in the jaws. Using the MTS, load was applied to the jaws using a 10 mm diameter attachment rod. The applied force was measured with a 2.0 kN load cell and a proportional-integral-derivative (PID) controller controlled the applied force through a feedback loop. Once the desired force was reached, after approximately 4 s, the heaters were activated and the applied temperature held for 2 s. At the completion of each test, a partial, full, or no cut result was recorded based

upon visual and manual inspection of the tissue. Tests were conducted for 99 different, randomized, temperature-force combinations with applied force varying from 15 to 115 N and applied temperature ranging from 140 to 225 C.
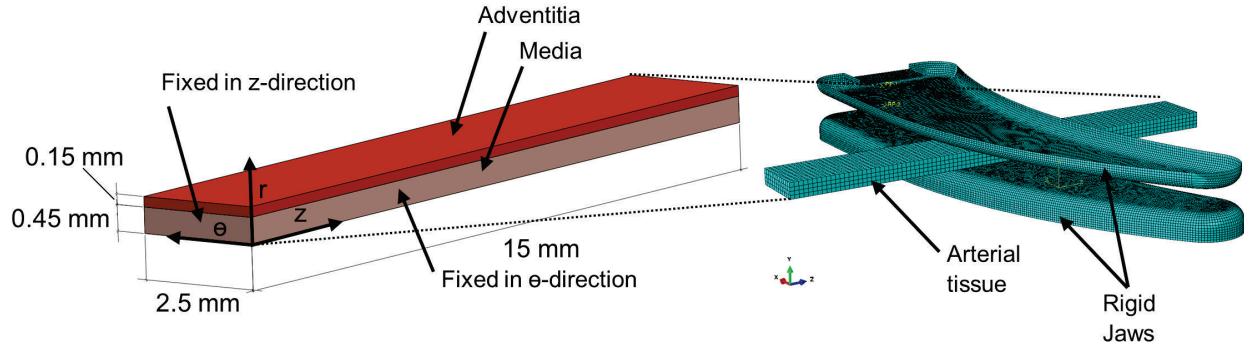
Figure 3.4: Left, a depiction of the arterial strip used in the finite element simulations. Right, a depiction of the mesh used for both the jaws and tissue. Frictionless contact is used to represent the interaction of the jaws and tissue. The jaw is displaced until the desired reaction force is reached, then the strain energy in the tissue is recorded

To determine the stain-energy induced in each tissue by the applied load, an inverse FE method was used. An FE model of the jaws and strip was constructed in Abaqus\Explicit v6.13 (Dassalt Systems Inc., Lafayette, CO). The geometry consists of a 1.5 mm x 15 mm x 0.6 mm strip located at the center of the jaws. The strip is segmented into a 0.15 mm thick adventitia layer and a 0.45 mm thick media layer (Fig. 3.4). A material constitutive model was coded using the VUANISOHYPER subroutine function to accurately represent the theory presented previously and rigorously validated through comparison with Abaqus' built-in HGO anisotropic material model. Material parameters for each layer were found in the literature [110]. To aid in convergence of the FE model an additional volumetric term was added to the strain energy function implemented in the subroutine. This was

$$\psi_{vol} = \frac{1}{D}\Big[\frac{J^2 - 1}{2} - ln(J)\Big] \tag{3.16}$$

where D, a measure of compressibility, is a constant set to 0.001 to ensure a nearly incompressible material and J is the Jacobian of the deformation gradient. In the FE model, all boundaries of the artery are left unconstrained except one longitudinal edge of the center of the artery which is constrained in the transverse direction and one end of the artery which is fixed in the longitudinal direction, to represent the constraints placed on the artery by the experimental locating feature. The jaws are considered rigid as they are several orders of magnitude stiffer than arterial tissue. Each jaw is constrained through rigid body motion. To simulate the applied pressure, the bottom jaw is spatially fixed while the top jaw's displacement is prescribed, representing the experiments conducted. The jaw is displaced until the desired reaction force is reached. The artery mesh uses 8 node, linear, hexahedral elements (C3D8) sized to be 0.2 mm x 0.2 mm x 0.2 mm and was generated by Abaqus' automatic meshing software. The jaws were meshed using rigid tetrahedral elements sized to have edge lengths on the same order of magnitude as the arterial elements to limit contact complications. Frictionless, "hard" contact is assumed between the jaws and arterial tissue and implemented through Abaqus' built-in algorithm. All simulations conducted were quasi-static, meaning time steps were sufficiently long enough to neglect dynamic effects ($1x10^6$). To ensure the analysis remained in a quasi-static state the kinetic energy was compared to the total energy in the tissue and found to be several orders of magnitude less.

One simulation was run for each applied load on the tissue and the average isochoric strain energy along the centerline (cutting line) of the jaws in the adventitial and medial layers of tissue was recorded. These results were then combined with the temperature reached in the arterial strip. The damage function was fit to the data using a non-linear regression analysis (Minitab 16, Minitab, Inc., State College, PA, USA) with the response variable being 1 if the artery was cut and 0 it the artery remained uncut. The independent variables were the temperature and strain energy occurring in the arterial strip. An analysis was conducted

and equation developed for both the adventitia and media.

3.3.6   Thermo-Structural Model

Once the cutting model was developed using sectioned tissue, a full thermo-structural FE model was developed in Abaqus\Explicit v6.13 to be used in the prediction of whole artery cutting and fusing. The model is similar to that of the sectioned strips and consists of a full artery in between two Conmed Altrus jaws (Fig. 3.5). One end of the artery is fixed in the longitudinal direction and each end is set to the ambient temperature. For each simulation, the radius and thickness of the artery were set to the desired size while the length was left at a consistent 15 mm. The artery mesh was generated using Abaqus automatic meshing capabilities and consists of 8 node, hexahedral, thermomechanical elements (C3D8RT). Each node of the element has 4 degrees of freedom, 1 for temperature and 3 for displacement. A mesh dependency study was conducted and the mesh was refined until the strain energy within the tissue varied less than 1% and the cut area less than 5% when the mesh density was increased by 25% at this point the finer mesh was chosen. The maximum mesh size for each artery ranged between 0.1 and 0.2 mm with a maximum deviation factor of 0.1. As a monotonic damage parameter was used, regularization methods were considered, but deemed unnecessary for the current geometries as the experimental results were consistently similar to the simulation results. The HGO constitutive model is used to represent the structural mechanics of the artery with properties found in the literature [110]. The heat transfer theory presented earlier is implemented through the tabular temperature dependent capabilities provided in the Abaqus material property interface. Thermal energy is imparted on the artery through a time-dependent temperature boundary condition on the jaw surface. The thermal conductivity of the jaw tissue contact condition was set to be several orders of magnitude higher than the tissue conductivity in order for the temperature on the tissue to match the jaw temperature. To represent the cutting process, a two part simulation is needed. First, the jaws are displaced until the desired reaction force is reached. Once the

applied force is reached a specified temperature boundary condition is applied and held for 2 s to match the heating profile of the experiments. During each time increment the user subroutine calculates and registers the damage parameter (D) value for each element using the calculated strain energy and temperature. This value is then used to modify the strength of each element accordingly.
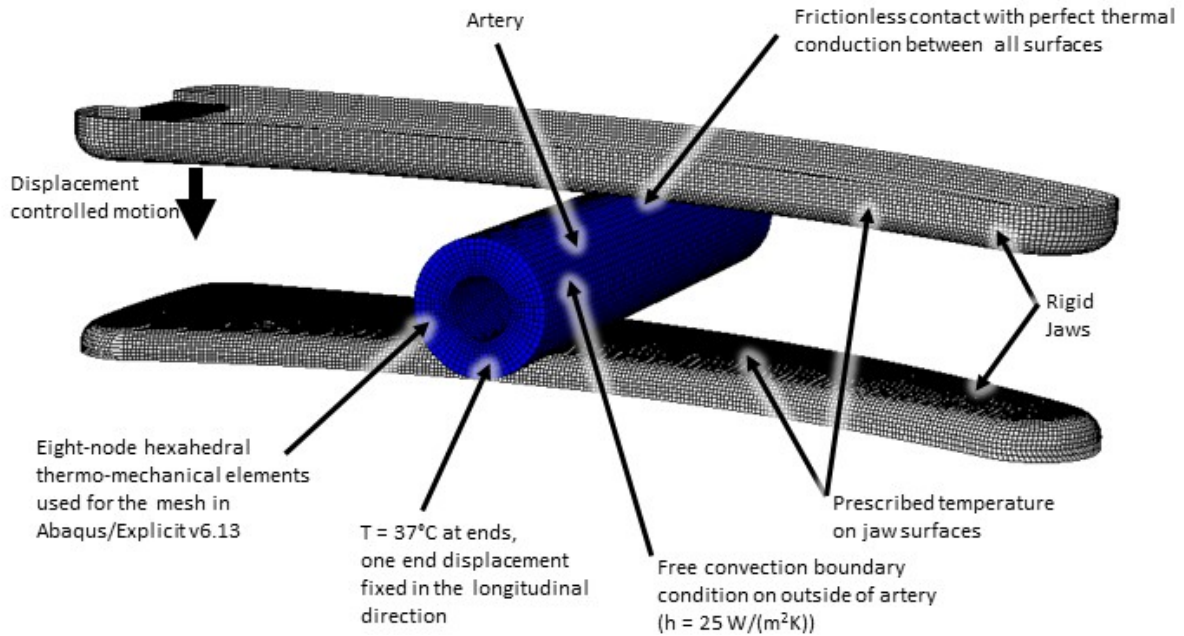
Figure 3.5: Image showing the full FE geometry, mesh, and boundary conditions. The artery mesh contains 8-node thermo-mechanical elements and is sized so that bending effects are negligible. The ends are fixed in temperature. All exterior edges have a free convection boundary condition representing the 0.9% PBS solution. The jaws are treated rigid. All contact is frictionless and allows for perfect heat transfer. The upper jaw is displaced until the reaction force reaches the desired limit. Then a temperature boundary condition is applied to the jaw surfaces to simulate heating.

In order to validate the model's predictive capabilities, 32 tests were conducted on full arteries using the environmental chamber setup described earlier. Before each test the thickness (0.69 ± 0.10 mm) of the arterial wall and the circumference (6.92 ± 0.80) of the artery was measured. For each test, a desired applied force (20 to 70 N) and temperature (170 to 225 °C) was set, the settings of the test run and the percentage of the artery cut was recorded. Cuts were recorded to the nearest 10 percent through the visual measurement along the centerline of the jaws. A cut was considered "full" if the artery was split into completely

separated sections. A "no cut" was recorded if there was no visual separation of the artery. Each of the 32 tests were then simulated using the FE model and simulation results were compared to the experimental results.

3.4   Results

3.4.1   Heat Transfer Finite Element Model
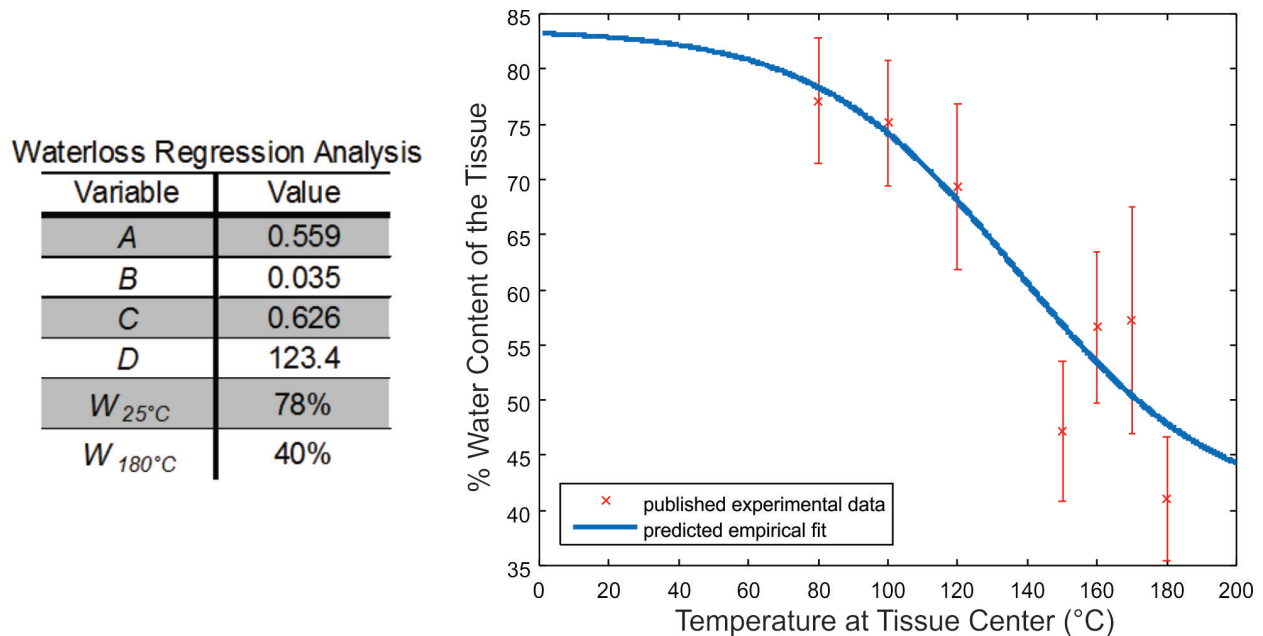
Figure 3.6: Left, results of the regression analysis the water content equation (Eqns. 3.2-3.3) are compared to the reproduced published water loss data [117] shown in the plot on the right. The parameters shown result in an average NRMSE value of 0.323. The water loss data has a very high variation.

Water loss predictions (*i.e.* Eqns. 3.2-3.3) forecasted water content in the tissue to decrease as a function of temperature. Comparison of theoretical results to published experimental data yields an average normalized root mean square error (NRMSE) of 0.32 (Fig. 3.6). This data was then used for the heat trasfer portion of the finite element simulations. The temperature in the tissue at the end of a three second 163 °C heating cycle reaches a maximum of 162.6°C in the center of the tissue, tissue temperature remains constant in the tissue

between the jaws, but decreases as a function of distance from the jaws (Fig. 3.7a). Both the simulation accounting for water loss and the one neglecting water loss predict tissue temperatures that fall within error bars of previously published experimental data from our lab using the Altrus [117] (Fig. 3.7b). The model including water loss effects predicts temperatures closer to the mean of the measured experimental temperatures than the model assuming a constant water content.
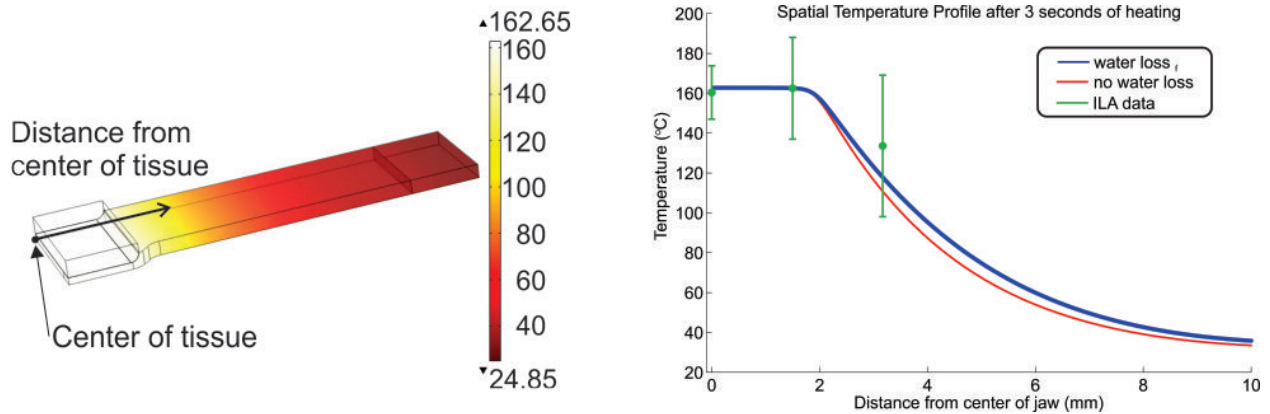
Figure 3.7: Left, temperature of the tissue during a fusion heating cycle. Right, the spatial temperature profile from the center of the jaw at the end of the fusion heating cycle (t=3 s). The model accurately predicts the temperature in the jaws and is slightly below the measured average temperature as the distance from the center of the jaw increases.

3.4.2 Damage Parameter Development

The experimental cutting results for tissue strips demonstrate a quadratic relationship between isochoric strain energy and temperature (Fig. 3.8). As the strain energy increases, the necessary cut temperature drops as a function of temperature squared. From this data, equations representing the damage function of strain energy and temperature were developed using non-linear regression for each arterial layer as follows:

$$D_{adv}(\psi_{iso}, T) = 0.00724\psi_{iso} + 0.00210T^2 - 0.0472T, \tag{3.17}$$

$$D_{med}(\psi_{iso}, T) = 0.00835\psi_{iso} + 0.00213T^2 - 0.0484T, \tag{3.18}$$

for the adventitia and media, respectively. ψ_{iso} is the isochoric strain energy density in KJ/m^3 and T, the temperature in °C. The upper curve (red in Fig. 3.8) represents the conditions at which full cutting of the material occurs and corresponds to a D value of 1, the lower (blue) curve represents the conditions at which the material begins to cut and corresponds to a D value of 0. The standard error of fit was 0.24 for the media and 0.25 for the adventitia.
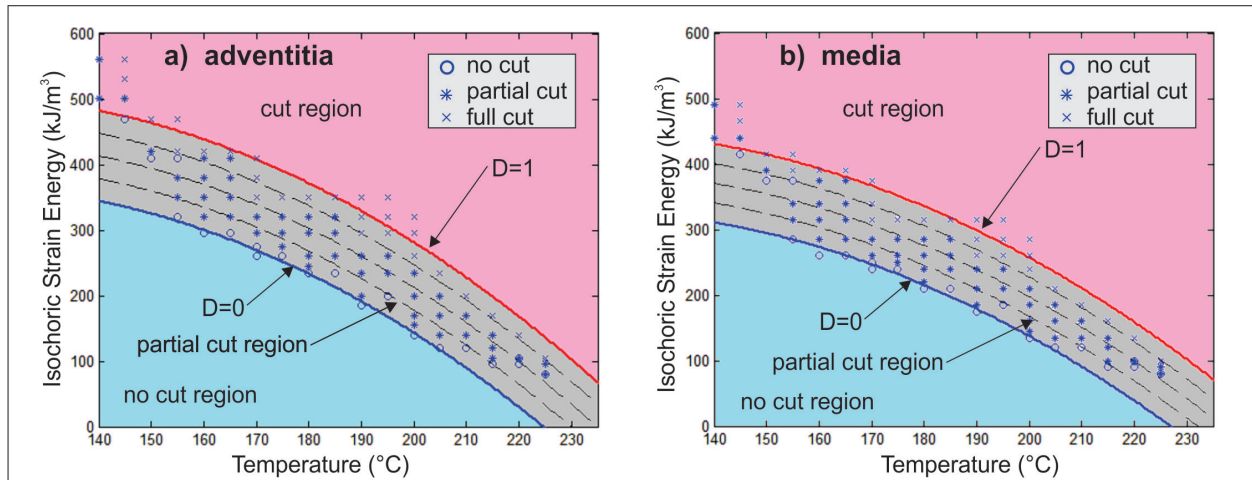
Figure 3.8: Isochoric stain energy per unit volume and temperature for the adventitia (left) and media (right) are plotted for each experimental strip test. An x represents a test with a fill cut, and o no cut and a * a partial cut. A non-linear regression was used to find and equation for the damage parameter of each layer. The blue curve represents the equation when $D = 0$, where area below the line represents an undamaged artery. The red curve represents a $D = 1$, where area above this line represents cutting conditions. The gray region represents a partially damaged artery, each dashed line corresponds to a 25% increment of damage.

3.4.3   Validation

Comparison of experimental images to simulation results for a full cut, partial cut and no cut scenario for full arteries display the simulations ability to predict the cutting result for each of three scenarios (Fig. 3.9). The simulation accurately predicts full cuts 95% of the

time and no cuts 83% of the time. Partial cuts are predicted to within 20% of the artery cut 83% of the time. Each simulation that predicts a cut result with error greater than 20% of the experimental result occurs at a load of 40 N or less.

3.5   Discussion

This study provides a method for using FE modeling to simulate the heat transfer through arterial tissue during direct heat tissue fusion and cutting by accounting for water loss through the modification of thermal tissue properties. Utilizing this method, a fully coupled thermostructural predictive FE model that predicts the cutting of an artery with laparoscopic fusion devices was developed. The model incorporates a novel parameter which was proposed and developed through experiments in order to accurately predict the strain energy and temperature at which arterial tissue is completely cut. Once developed, the predictive capabilities of the model were tested through comparison with experimental tests. The simulations accurately predicted the cutting result for 28 of 32 (88%) experimental tests.

3.5.1   Heat Transfer Water Loss Model

The results of the water loss regression analysis do not represent an exact fit (NRMSE = 0.323) to the published water loss data. This is primarily due to the wide experimental variations in water content. The resulting error due to these variations is most likely the cause of the slightly lower predicted temperatures. Both the material model accounting for water loss and a material model neglecting water loss effects can accurately predict the tissue temperature in the clamped region (2 mm from the center of the tissue). At 3 mm from the center of the tissue both models predict temperatures within the error range of the experimental results, but the model neglecting water loss shows a lower temperature than the model including water loss. This discrepancy is due to the change in thermal conductivity and specific heat caused by the decrease in water content. One limitation of this approach

is the effect of water loss is only accounted for through the modification of the material parameters. The energy lost with the water leaving the tissue is not taken into account. Even with this omission the presented material model accurately predicts the temperatures in the clamped tissue region and still predicts the temperature within the error range of measured experiments outside of the tissue fusion region.

3.5.2   Damage Parameter Development and Validation

As with any biological tissue a wide range of tissue composition likely exists in the porcine artery, and can be the cause of substantial variation in experimental results. The contributions to experimental measurement uncertainty were minimized by cutting all arterial strips into sections 2.5 mm wide, placing them in the same spot on the jaws and controlling their water content. While splitting the artery into the media and adventitia more accurately represent the artery in the model, the exact compositions of the artery, such as amount of collagen, elastin and cellular material are not considered in the model; thus, variation in the results of thermally cutting strips still exists. For the three representative experiments and their corresponding simulations (Fig. 3.9) each simulation predicts whether the artery is cut or not as well as the shape of the cut. However, over the 32 validation tests conducted some differences between simulations and experiments exist due to simplifying assumptions. Currently, the simulation assumes a perfectly conductive contact situation, meaning the edge of the tissue matches the exact temperature of the jaws. This may not be an accurate assumption for loads 40 N (approximately 750 kPa) and below[112]. As noted earlier, other variance may be induced by the differing composition of each artery. Again, geometric variance is taken into account, but differences in the collagen, elastin and cellular content are not. Expanding, while porcine splenic arteries have been shown to be a good representation of human arteries,[117] it may be beneficial to observe the effects on arteries with different compositions such as the aortic or carotid arteries. Moreover, both thickness and diameter appear to play a role in the cutting of an artery to some extent, but the metric

of volume per length of tissue may not be an accurate indicator of the potential for cutting success. The heat transfer through the cutting region is primarily dependent on the thickness of the artery, but the strain energy of the tissue is dependent on both the thickness and the diameter as changes in either can impact how the artery deforms. Thus, knowledge of both the thickness and diameter of the arterial wall is necessary to predict if an artery will be cut. It was noted earlier that water content plays a significant role in the cutting and fusing of tissue. Currently, this role is only taken into account through the impact of water loss on the thermal conductivity and specific heat of the tissue. During experimentation the tissue was cut while submerged in a 0.9% PBS bath to maintain full hydration and ensure that water content was largely consistent across specimens. However, surrounding conditions and location of a cut during surgery may cause a variation of the water content in an artery. Therefore, it is desirable to expand the damage equation to include a term accounting for the water content in an artery during a procedure. This inclusion would result in expansion of the lines in Fig. 3.8 to surfaces, with axes of temperature, strain energy, and water content. Expanding further, a more accurate representation of the energy in the tissue could be modeled using a poromechanical model. Taking into account tissue permeability and fluidstructure interactions would allow the model to represent the energy being absorbed and removed from the tissue by vaporization of water and provide a more accurate insight into the stresses on the ECM caused by the rapid expansion of water vapor. Currently, the coupled thermomechanical model presented is only able to represent arterial damage caused by devices imparting heat and pressure. Work is currently underway to expand the FE model to incorporate data published on the ideal temperatures and pressures for arterial fusion into a threshold value. When the threshold value is reached then fusion of the arterial walls will be simulated through a contact interaction condition. Applying this threshold value will then allow modeling of both the fusion and cutting applications of current laparoscopic energy devices. In conclusion, two primary steps have been taken towards the development of a thermostructural FE model of the cutting and fusing of an artery. First, a heat transfer model was developed, allowing for the determination of temperature in an artery during fu-

sion or cutting. Second, a novel parameter predicting structural damage to an artery during fusion or cutting was developed. These techniques were then combined into a structural mechanics FE model resulting in the ability to predict arterial damage and cutting with use of a direct heat laparoscopic fusion device. Though this damage model currently only uses temperature and strain energy to model cutting of tissue, it has shown the ability to predict the cutting of arteries. Also, the model could easily be expanded to represent the modeling of tissue fusion as well; thus, providing a gateway into a better understanding of the tissue fusion process and more accurate FE models of arterial fusion with the potential to lead to more advanced, safer, surgeries and surgical devices.

3.6   Acknowledgments
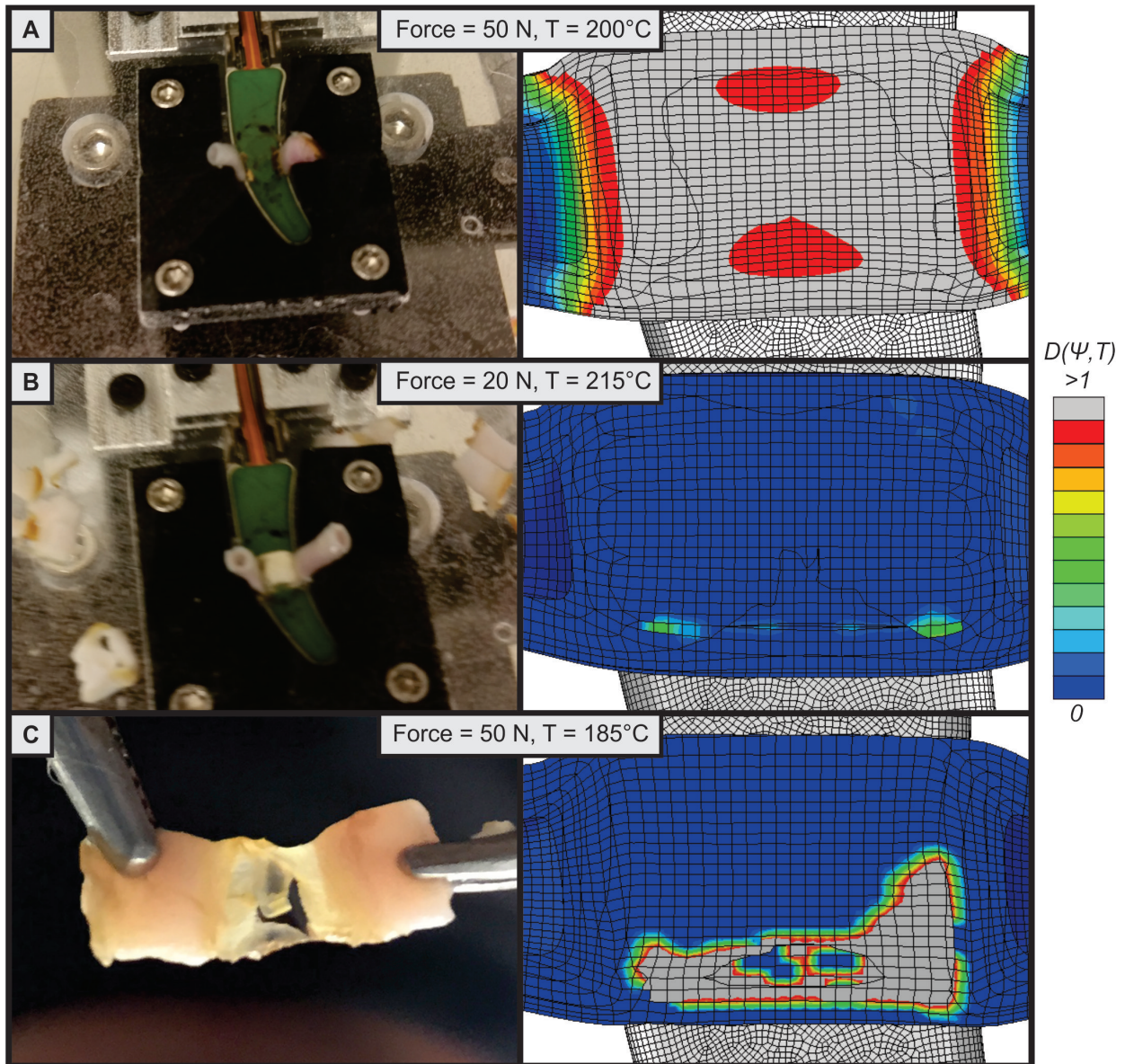
Figure 3.9: The visual experimental results of three different attempts to cut a full artery and their corresponding simulations. Gray elements in the simulations are cut elements. In part A, an artery that was completely cut in both experimental tests and the simulation. Part B shows an uncut artery and the same predicted simulation. Section C shows a 60% cut artery and the simulation prediction that 40% of the artery will be cut.

Chapter 4: A small deformation thermo-poromechanics finite element model and its application to thermal tissue fusion

4.1 Overview

Understanding the impact of thermally and mechanically loading biological tissue to supra-physiological levels is becoming of increasing importance as complex multi-physical tissue-device interactions increase. The ability to conduct accurate, patient specific computer simulations would provide surgeons with valuable insight into the physical processes occurring within the tissue as it is heated or cooled. Several studies have modeled tissue as porous media, yet fully coupled thermo-poromechanics (TPM) models are limited. Therefore, this study introduces a small deformation theory of modeling the TPM occurring within biological tissue. Next, the model is used to simulate the mass, momentum, and energy balance occurring within an artery wall when heated by a tissue fusion device and compared to experimental values. Though limited by its small strain assumption, the model predicted final tissue temperature and water content within one standard deviation of experimental data for seven of seven simulations. Additionally, the model showed the ability to predict the final displacement of the tissue to within 15% of experimental results. These results promote potential design of novel medical devices and more accurate simulations allowing for scientists and surgeons to quickly, yet accurately, assess the effects of surgical procedures as well as provide a first step towards a fully coupled large deformation TPM finite element model.

4.2 Introduction

Biological tissue undergoes loading in several manners ranging from surgical devices that heat or cool biological tissue to cauterize or ablate it [16], [61], [62], [66], to natural causes such as hyperthermia or frostbite [29]. Scientists and physicians seek to understand these processes and their impact on tissue mechanics to create novel, safer, and more effective medical devices and procedures. With tissue device interaction becoming ever more prevalent in the form of more complex medical devices, wearable electronics, and implanted electronics, experimental testing is becoming increasingly expensive in time and resources. Computer simulations of these interactions, when calibrated to experimental data, provide essential insight into the underlying physics occurring in biological tissue when deformed and heated, allowing for streamlined design work and ultimately more effective devices and safer procedures. Additionally, models with the ability to accurately and quickly predict surgical outcomes will help satisfy the growing desire for patient specific, near real time, simulations for surgical procedures [124]. A good deal of biological tissue is non-homogenous and typically contains several materials, often in different phases[29]. For example, the artery wall has an extracellular matrix made up of collagen, elastin, and glycosaminoglycans. While water is attracted to molecules within the tissue through polar interactions, it readily moves through interstitial spaces. Thus, this tissue can be considered a porous medium. Studies attempting to model biological tissue, including vertebral discs[22], articular cartilage[97], lung tissue[99], arterial tissue[73], skin[29], and myocardial tissue[98] as a porous medium exist throughout literature; however, these attempts have failed to completely represent the complex physics occurring within the tissue. Typically, models representing biological tissue as porous media fall into one of two categories. The first neglects deformation and only heat and/or mass transfer is represented[29], [60], [66]. The second category of models uses solid mechanics and mass transport to model tissue deformation and coupled pore fluid flow, but thermal transport is not considered [22], [99], [125]. To the authors knowledge no model exists that demonstrates the coupled solid phase (skeleton) mechanics, mass transfer, and

heat transfer (thermo-poromechanics (TPM)) occurring in biological tissue. In this chapter a small deformation, TPM finite element model with the ability to represent the heating and deformation of biological tissue is presented and its results are validated by comparison to measured experimental results of thermal arterial tissue fusion.

4.3 Theory

4.3.1 Initial Definitions

Throughout this chapter it will be assumed the biological tissue being modeled will be partially saturated triphasic (also called unsaturated) porous media. Meaning the tissue will consist of some solid skeletal matrix and multiple fluid constituents (gas and liquid) occupying the voids between the solid matrix. It will be assumed the voids will be filled with liquid water and gaseous water vapor (Fig. 4.1).
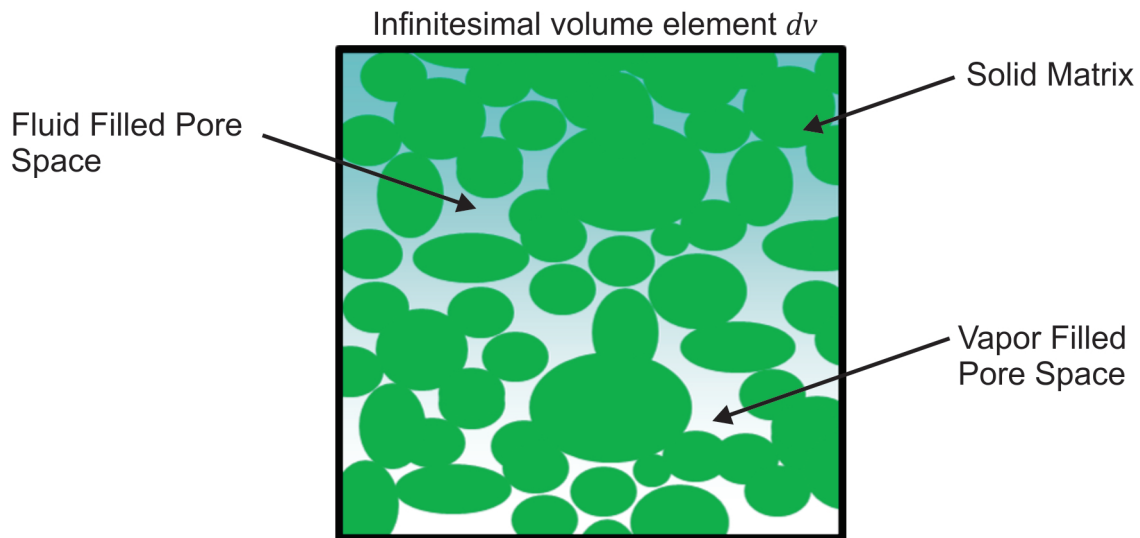
Figure 4.1: A representative infinitesimal volume element of triphasic porous media. It consists of a solid matrix with pores filled with liquid and gas fluids.

To fully describe a partially saturated triphasic porous medium, several definitions must be prescribed and constraints given. Considering a total differential volume, dv, with a total

differential mass, dm, it can be seen that the total differential volume and mass are equal to the sum of the differential volumes and masses of each phase $\alpha(s = solid, \ell = liquid, g = gas)$, at a continuum point.

$$dv = \sum_{\alpha=s,\ell,g} dv_\alpha, \tag{4.1}$$

$$dm = \sum_{\alpha=s,\ell,g} dm_\alpha. \tag{4.2}$$

Thus, we can define the volume fraction of each phase, n^α, as

$$n^\alpha = \frac{dv_\alpha}{dv}. \tag{4.3}$$

With equation 4.3 it can be seen that

$$1 = n^s + n^\ell + n^g = n^s + n \tag{4.4}$$

where n is the volume fraction of the pore space, or porosity. The differential mass of each phase can be written as

$$dm_\alpha = \rho^{\alpha R} dv_\alpha = \rho^{\alpha R} n^\alpha dv \tag{4.5}$$

where $\rho^{\alpha R}$ is the true (real) mass density of the α phase. With equation 4.5 it can be shown that the partial mass density, ρ^α, is

$$\rho^\alpha = \rho^{\alpha R} n^\alpha. \tag{4.6}$$

Lastly, it is beneficial to define the saturation of the liquid and gas phases, S_f, as the volume fraction of the pore space occupied by each fluid phase,

$$S_f = \frac{n^f}{n} \quad f = \ell, g, \tag{4.7}$$

$$1 = S_\ell + S_g. \tag{4.8}$$

4.3.2 Kinematics

To fully understand the physical processes occurring within porous media when loaded, it is necessary to examine the kinematics of a volume element and its constituents. From fundamental continuum mechanics and the theory of porous media [79], [126], it can be said each phase undergoes some motion $\boldsymbol{\chi}_\alpha$ defined as

$$\boldsymbol{x} = \boldsymbol{\chi}_\alpha(\boldsymbol{X}_\alpha, t) \tag{4.9}$$

where $\boldsymbol{x}$ is the current "smeared" position of all phases at time, t, and $\boldsymbol{X}_\alpha$ is the initial location of the α phase as shown in Figure 4.2. Thus, the deformation gradient, $\boldsymbol{F}_\alpha$, for the α phase is

$$\boldsymbol{F}_\alpha = \frac{\partial \boldsymbol{\chi}_\alpha(\boldsymbol{X}_\alpha, t)}{\partial \boldsymbol{X}_\alpha} = \frac{\partial \boldsymbol{x}(\boldsymbol{X}_\alpha, t)}{\partial \boldsymbol{X}_\alpha}. \tag{4.10}$$

Examining the volumetric change of the differential volume element it is seen that

$$dv = J_\alpha dV_\alpha, \tag{4.11}$$

$$dv_\alpha = n^\alpha J_\alpha dV_\alpha, \tag{4.12}$$

where J_α is the determinant of the deformation gradient, $\boldsymbol{F}_\alpha$, and dV_α is the reference differential volume for the α phase. To this point, all variables are still non-linear geometric and valid for large deformations, they will be simplified later to the linear (small deformation) theory.

4.3.3 Governing Equations

Three governing equations will be used in the finite element formulation: balance of mass, balance of linear momentum, and balance of energy for the three phase mixture. While these equations can be arranged to solve for numerous variables, in this chapter the desired field
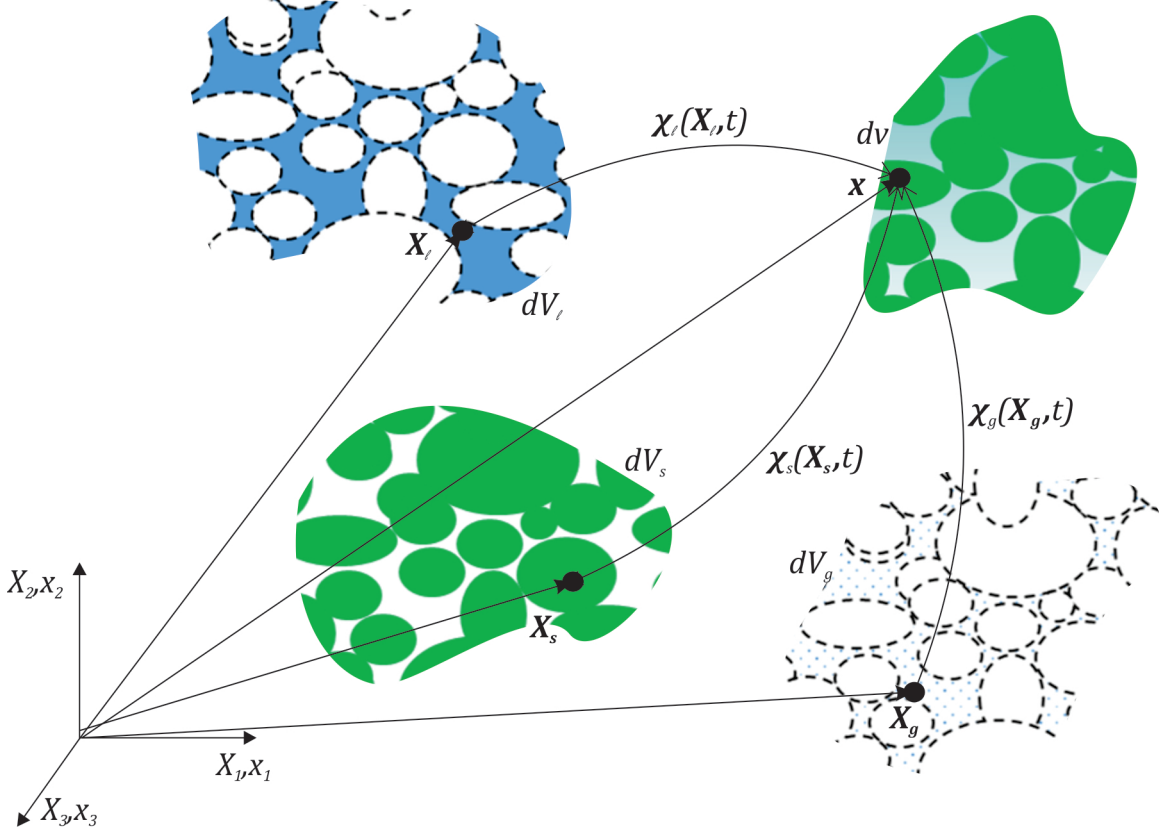
Figure 4.2: A depiction of the deformation of each phase from its initial differential volume, dV_α, in their respective reference configurations to the final "smeared" differential volume, dv, in the final current configuration.

variables are the solid skeleton phase displacement, $\boldsymbol{u}$, the liquid pore pressure, p_ℓ, and the average temperature of the smeared mixture, θ. In geomechanics it is traditional to split the gas mixture into a combination of dry air and water vapor adding another balance of mass equation to solve for gas pressure [105]. However, in this work it is assumed no dry air exists in the biological tissue and all gas is water vapor. Therefore, gas (vapor) pressure can be directly solved for with a constitutive equation such as the Clausius-Clapeyron equation as demonstrated later. Figure 4.3 illustrates the problem set up including generalized boundary conditions, which include: for the solid skeleton - prescribed displacements, $\boldsymbol{u}^{fixed}$, and applied traction, $\boldsymbol{t}$, for the water species - prescribed liquid pore pressure, p_ℓ^{fixed}, and flux, q_ℓ, in the form of vapor or liquid, and for energy - prescribed temperature, θ^{fixed}, and energy flux, q_θ.
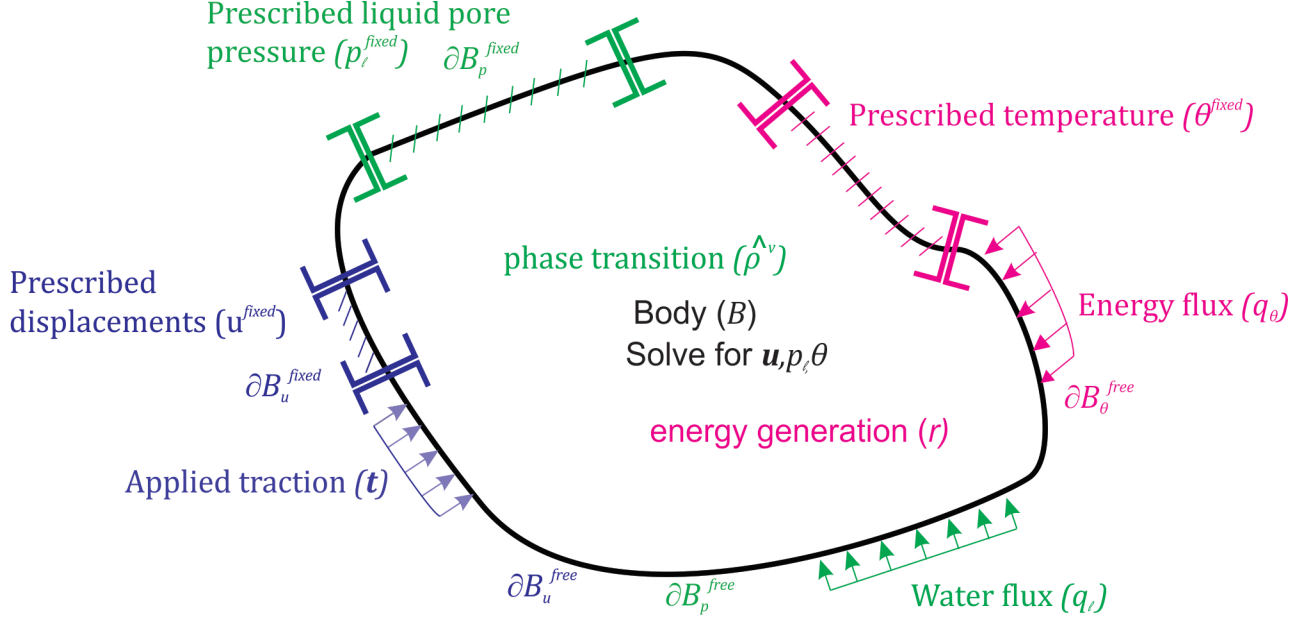
Figure 4.3: Depiction of the problem set up for the balance equations where, $\boldsymbol{u}$, p_ℓ, and θ are the desired field variables. Fluxes and prescribed boundary conditions act on surfaces (∂B) while heat source (r) and phase transition ($\hat{\rho}^v$) act throughout the body (B).

4.3.4 Balance of Mass

The balance of mass of the α phase for a total differential volume element can be written as

$$\frac{D^\alpha m^\alpha}{Dt} = \frac{D^\alpha}{Dt} \int_B \rho^\alpha dv = \int_B \hat{\rho}^\alpha dv \tag{4.13}$$

where $\frac{D^\alpha m^\alpha}{Dt}$ is the material time derivative of mass with respect to the α phase and $\hat{\rho}^\alpha$ is the mass supply term [121]. It is assumed that the solid matrix cannot gain or lose mass ($\hat{\rho}^s = 0$) and that the water can change from liquid to vapor or vice versa, but that no water is added or lost,

$$\hat{\rho}^g = -\hat{\rho}^\ell = \hat{\rho}^v. \tag{4.14}$$

Applying these assumptions, localizing the integral, and applying the definition of partial mass density (Eqn. 4.6) to equation 4.13 gives the balance of mass for each phase as

$$\frac{D^s n^s}{Dt} + n^s div \boldsymbol{v}_s = 0, \tag{4.15}$$

$$\frac{D^\ell n^\ell}{Dt} + n^\ell div \boldsymbol{v}_\ell = -\frac{\hat{\rho}^v}{\rho^{\ell R}}, \tag{4.16}$$

$$\frac{D^g n^g}{Dt} + n^g div \boldsymbol{v}_g = \frac{\hat{\rho}^v}{\rho^{gR}}, \tag{4.17}$$

where $div\boldsymbol{v}_\alpha$ is the divergence of the velocity, $\boldsymbol{v}_\alpha$, of the α phase and $\hat{\rho}^v$ is the change in water mass due to vaporization or condensation. Arguments by Lewis and Schrefler [103] state the material time derivatives, $\frac{D^\alpha p_\alpha}{Dt}$, of the pressure, p_α, of the α phase can be related to the change in its density, $\rho^{\alpha R}$, and temperature, θ^α, through the materials bulk modulus, K_{bulk}^α, and thermal expansion coefficient, β_α^θ, as

$$\frac{D^\alpha p_\alpha}{Dt} = \frac{1}{\rho^{\alpha R}} \left[K_{bulk}^\alpha \frac{D^\alpha \rho^{\alpha R}}{Dt} - \beta_\alpha^\theta \frac{D^\alpha \theta^\alpha}{Dt} \right] \tag{4.18}$$

such that the material time derivative of the mass density, $\frac{D^\alpha \rho^{\alpha R}}{Dt}$, is

$$\frac{D^\alpha \rho^{\alpha R}}{Dt} = \rho^{\alpha R} \left[\frac{1}{K_{bulk}^\alpha} \frac{D^\alpha p_\alpha}{Dt} - \beta_\alpha^\theta \frac{D^\alpha \theta^\alpha}{Dt} \right]. \tag{4.19}$$

Assuming the solid and liquid phases are incompressible, thus,

$$\frac{1}{K_{bulk}^s} \frac{D^s p^s}{Dt} = 0, \tag{4.20}$$

and

$$\frac{1}{K_{bulk}^\ell} \frac{D^\ell p^\ell}{Dt} = 0, \tag{4.21}$$

but allowing for density change due to temperature [103] and treating gas as ideal, the solid and liquid balance of mass equations balance of mass equations become

$$\frac{D^s n^s}{Dt} + n^s div \boldsymbol{v}_s - \beta_s^\theta n^s \frac{D^s \theta}{Dt} = 0 \tag{4.22}$$

and

$$\frac{D^\ell n^\ell}{Dt} + n^\ell div\boldsymbol{v}_\ell - \beta_\ell^\theta n^\ell \frac{D^\ell \theta}{Dt} = -\frac{\hat{\rho}^v}{\rho^{\ell R}}. \tag{4.23}$$

Water vapor is assumed ideal in this work thus,

$$\rho^{gR} = \frac{p_g M_g}{\theta^g R} \tag{4.24}$$

where p_g is the gas pressure, M_g is the molar mass of the gas, θ^g is the gas temperature and, R is the ideal gas constant. This assumptions allows the material time derivative of the real gas density, $\frac{D^g \rho^{gR}}{Dt}$, to be written as

$$\frac{D^g \rho^{gR}}{Dt} = \rho^{gR} \left[\frac{1}{p_g} \frac{D^g p_g}{Dt} - \frac{1}{\theta^g} \frac{D^g \theta^g}{Dt} \right]. \tag{4.25}$$

Applying equation 4.25 to 4.17 gives

$$\frac{D^g n^g}{Dt} + n^g div\boldsymbol{v}_g + n^g \left[\frac{1}{p_g} \frac{D^g p_g}{Dt} - \frac{1}{\theta^g} \frac{D^g \theta^g}{Dt} \right] = \frac{\hat{\rho}^v}{\rho^{gR}}. \tag{4.26}$$

A Lagrangian formulation is used for the finite element (FE) formulation such that all material time derivatives must be put in terms of the solid phase (*i.e.* the mesh will follow the solid skeleton motion). Therefore, it is beneficial to define [121],

$$\frac{D^\alpha(\bullet)}{Dt} = \frac{D^s(\bullet)}{Dt} + grad(\bullet) \cdot \tilde{\boldsymbol{v}}_\alpha \tag{4.27}$$

where $\bullet$ represents any quantity and $\tilde{\boldsymbol{v}}_\alpha$ is the relative velocity of the α phase with respect to the solid phase. Defining the Darcy fluid velocity, $\boldsymbol{v}_f^D$, as

$$\boldsymbol{v}_f^D = n^f(\boldsymbol{v}_f - \boldsymbol{v}_s) \tag{4.28}$$

and applying equation 4.27 and the definition of saturation (Eqn. 4.7) to equations 4.22, 4.23 and 4.26 allows for the total balance of mass of the mixture to be written as

$$
\begin{aligned}
(\rho^{\ell R} S_\ell + \rho^{gR} S_g) div \boldsymbol{v}_s &- \left[(1-n)(\rho^{\ell R} S_\ell + \rho^{gR} S_g)\beta_s^\theta + n\rho^{\ell R}\beta_s^\theta \right] \frac{D^s\theta}{Dt} \\
&+ n(\rho^{\ell R} - \rho^{gR})\frac{D^s S_\ell}{Dt} + nS_g \frac{D^s \rho^{gR}}{Dt} + div(\rho^{gR}\boldsymbol{v}_g^D + \rho^{\ell R}\boldsymbol{v}_\ell^D) = 0.
\end{aligned}
\tag{4.29}
$$

4.3.5 Balance of Linear Momentum

According to de Boer [79], Holzapfel [121], and Coussy [87] the balance of linear momentum for the α phase can be written as

$$
\int_B \left[\boldsymbol{v}_\alpha \frac{D^\alpha \rho^\alpha}{Dt} + \rho^\alpha \boldsymbol{a}_\alpha + \rho^\alpha div\boldsymbol{v}_\alpha \right] dv = \int_B (\rho^\alpha + \boldsymbol{b}^\alpha + \hat{\boldsymbol{h}}^\alpha) dv + \int_{\partial B} \boldsymbol{t}^\alpha da
\tag{4.30}
$$

where $\boldsymbol{t}^\alpha$ is the traction acting on surface, ∂B, $\boldsymbol{a}_\alpha$ is the acceleration, $\boldsymbol{b}^\alpha$ is the body force, and $\hat{\boldsymbol{h}}^\alpha$ is the drag body force of all other phases acting on the α phase such that

$$
\sum_{\alpha=s,\ell,g} \hat{\boldsymbol{h}}^\alpha = \boldsymbol{0}.
\tag{4.31}
$$

Localizing and applying Cauchy's theorem, equation 4.30 can be written as

$$
\boldsymbol{v}_\alpha \frac{D^\alpha \rho^\alpha}{Dt} + \rho^\alpha \boldsymbol{a}_\alpha + \rho^\alpha div\boldsymbol{v}_\alpha = \rho^\alpha \boldsymbol{b}^\alpha + \hat{\boldsymbol{h}}^\alpha + div\boldsymbol{\sigma^\alpha}
\tag{4.32}
$$

where $\boldsymbol{\sigma}^\alpha$ is the partial Cauchy stress of the α phase. Summing over all phases, neglecting inertia terms and applying equation 4.31, the total mixture balance of linear momentum is

$$
\boldsymbol{0} = \rho^{eff}\boldsymbol{b} + div\boldsymbol{\sigma}
\tag{4.33}
$$

where

$$
\rho_{eff} = (1-n)\rho^s + n(S_\ell \rho^{\ell R} + S_g \rho^{gR}),
\tag{4.34}
$$

$$\boldsymbol{b}^\alpha = \boldsymbol{b}, \tag{4.35}$$

and the total Cauchy stress of the mixture, $\boldsymbol{\sigma}$, is defined by the effective stress principle as

$$\boldsymbol{\sigma} = \boldsymbol{\sigma}' - (\chi p_\ell + (1 - \chi)p_g)\mathbf{1}, \tag{4.36}$$

where $\boldsymbol{\sigma}'$ is the effective stress of the solid skeleton, p_ℓ and p_g are the pore pressure of each fluid phase, and χ is the effective stress parameter representing the portion of the stress taken by the liquid and gas phases [103].

4.3.6 Balance of Energy

The first law of thermodynamics provides the balance of energy for the mixture and can be written for the α phase as

$$\dot{E}^\alpha + \dot{K}^\alpha = P^\alpha + \dot{Q}^\alpha + \int_B \hat{e}^\alpha dv \tag{4.37}$$

with

$$\dot{E}^\alpha + \dot{K}^\alpha = \int_B \left[\hat{\rho}^\alpha \left(\frac{\boldsymbol{v}_\alpha \boldsymbol{v}_\alpha}{2} + e^\alpha \right) + \rho^\alpha \frac{D^\alpha e^\alpha}{Dt} \right] dv, \tag{4.38}$$

$$P^\alpha = \int_B \left[\boldsymbol{\sigma}^\alpha : \frac{D^\alpha \boldsymbol{\epsilon}^\alpha}{Dt} - \hat{\boldsymbol{h}}^\alpha \cdot \boldsymbol{v}_\alpha \right] dv, \tag{4.39}$$

$$\dot{Q}^\alpha = \int_B [\rho^\alpha \boldsymbol{r}^\alpha - div \boldsymbol{q}_\theta^\alpha] dv. \tag{4.40}$$

The material time derivatives of the α phase of internal energy, $\dot{E}^\alpha$, and kinetic energy, $\dot{K}^\alpha$, are a function of the partial mass density, ρ^α, the source or sink of mass density, $\hat{\rho}^\alpha$, the velocity, $\boldsymbol{v}_\alpha$, and the per unit mass internal energy e^α of the α phase. The rate of heat transfer to the α constituent, $\dot{Q}^\alpha$, is dependent both on an energy supply source, $\boldsymbol{r}$, and the heat flux, $\boldsymbol{q}_\theta^\alpha$, to each phase. P^α is the power imparted on the α phase (here the assumption of small deformations begins). Lastly, $\hat{e}^\alpha$ is the per unit mass energy supply rate of the α constituent from all other constituents. Localizing and summing over all constituents,

equation 4.37 becomes

$$\sum_{\alpha=s,\ell,g} \boldsymbol{\sigma}^\alpha : \frac{D^\alpha \boldsymbol{\epsilon}^\alpha}{Dt} + \hat{\boldsymbol{h}}^\alpha \cdot \boldsymbol{v}_\alpha - \rho^\alpha \left(\frac{\boldsymbol{v}_\alpha \boldsymbol{v}_\alpha}{2} \right) + \rho^\alpha \frac{D^\alpha e^\alpha}{Dt} - \rho^\alpha r^\alpha + e^\alpha \hat{\rho}^\alpha = 0. \tag{4.41}$$

4.3.7 Closure of Theory

Although the balance equations provide the backbone to TPM, additional equations, often called constitutive equations are needed to reach a closed theory. In this work, several equations will be used to close the theory.

The second law of thermodynamics is used to motivate constitutive forms and can be written in the local form for the α constituent as

$$\hat{\rho}^\alpha \eta^\alpha \theta^\alpha - \rho^\alpha r^\alpha + \rho^\alpha \theta^\alpha \frac{D^\alpha \eta^\alpha}{Dt} + div\boldsymbol{q}_\theta^\alpha - \boldsymbol{q}_\theta^\alpha \cdot \frac{grad\theta^\alpha}{\theta^\alpha}, \tag{4.42}$$

where η^α is the entropy per unit mass of the α phase. The Gibb's free energy per unit mass, g^f, of a fluid $(f = \ell, g)$ phase is defined as

$$g^f = e^f - \frac{p_f}{\rho^{fR} - \theta^f \eta^f}. \tag{4.43}$$

Taking the material time derivative with respect to f of equation 4.43, substituting it into equation 4.42 and combining with balance of mass (Eqn 4.13) and balance of energy (Eqn. 4.41) yields the entropy inequality for the fluid phases as,

$$\sum_{f=\ell,g} \rho^f \frac{\boldsymbol{v}_f \boldsymbol{v}_f}{2} - \hat{\boldsymbol{h}}^f \cdot \boldsymbol{v}_f + \hat{e}^f - \rho^f \frac{\partial g^f}{\partial p_f} \frac{D^f p_f}{Dt} - \rho^f \frac{\partial g^f}{\partial \theta^f} \frac{D^f \theta^f}{Dt}$$
$$- \rho^f \eta^f \frac{D^f \theta^f}{Dt} + n^f \frac{D^f p^f}{Dt} + p_f \frac{D^f n^f}{Dt} - \frac{\boldsymbol{q}_\theta^f \cdot grad\theta^f}{\theta^f} \geq 0. \tag{4.44}$$

Defining the Helmoltz free energy per unit mass of the solid phase as

$$\psi^s = e^s - \theta^s \eta^s \tag{4.45}$$

and combining it with equations 4.36, 4.41, and 4.42 gives the entropy inequality for the solid skeleton as

$$\boldsymbol{\sigma'} : \frac{D^s \boldsymbol{\epsilon}^s}{Dt} + \left[(n^\ell - \chi) + (n^g - (1-\chi))p_g \right] div\boldsymbol{v}_s - \hat{\boldsymbol{h}}^s \cdot \boldsymbol{v}_s + \\ \hat{e}^\alpha - \rho^s \eta^s \frac{D^s \theta^s}{Dt} - \rho^s \frac{D^s \psi^s}{Dt} - \frac{\boldsymbol{q}^s \cdot grad\theta^s}{\theta^s} \geq 0, \tag{4.46}$$

where the strain tensor of the solid phase is the same as that of the solid skeleton, *e.g.* $\boldsymbol{\epsilon}^{skel} = \boldsymbol{\epsilon}^s$. Following the procedure outlined by de Boer[79], Coussy[87] and Wang[105], through combining equations 4.29, 4.44, and 4.46, the entropy inequality for the mixture can be written as

$$\frac{1}{2}\hat{\rho}^\ell \boldsymbol{v}_\ell \cdot \boldsymbol{v}_\ell + \frac{1}{2}\hat{\rho}^g \boldsymbol{v}_g \cdot \boldsymbol{v}_g - \hat{\rho}^\ell \boldsymbol{v}_\ell \cdot \tilde{\boldsymbol{v}}_\ell - \hat{\rho}^g \boldsymbol{v}_g \cdot \tilde{\boldsymbol{v}}_g \\ \left[\left([n^g - (1-\chi)]p_g - (n^\ell - \chi)p_\ell \right) \beta_s^\theta - \rho^s \eta^s - \rho^s \frac{\partial \psi^s}{\partial \theta^s} \right] \frac{D^s \theta^s}{Dt} \\ + \rho^\ell \left[\frac{\partial g^\ell}{\partial \theta^\ell} - \eta^\ell \right] \frac{D^\ell \theta^\ell}{Dt} + \rho^g \left[\frac{\partial g^g}{\partial \theta^g} - \eta^g \right] \frac{D^g \theta^g}{Dt} - \left[\rho^s \frac{\partial \psi^s}{\partial S_\ell} + ns \right] \frac{D^s S_\ell}{Dt} \\ + \left[n^\ell - \rho^\ell \frac{\partial g^\ell}{\partial p_\ell} \right] \frac{D^\ell p_\ell}{Dt} + \left[n^g - \rho^g \frac{\partial g^g}{\partial p_g} \right] \frac{D^g p_g}{Dt} - \boldsymbol{v}_\ell^D \cdot [gradp_\ell - \rho^{\ell R} \boldsymbol{b}^\ell] \\ - \boldsymbol{v}_g^D \cdot [gradp_g - \rho^{gR} \boldsymbol{b}^g] + \left(\boldsymbol{\sigma'} - \frac{\partial \rho^s \psi^s}{\partial \boldsymbol{\epsilon}^{skel}} \right) : \frac{D^s \boldsymbol{\epsilon}^{skel}}{Dt} \\ - \frac{1}{\theta^s} \boldsymbol{q}_\theta^s \cdot grad\theta^s - \frac{1}{\theta^\ell} \boldsymbol{q}_\theta^\ell \cdot grad\theta^\ell - \frac{1}{\theta^g} \boldsymbol{q}_\theta^g \cdot grad\theta^g, \tag{4.47}$$

where $\tilde{\boldsymbol{v}}_f = \boldsymbol{v}_f - \boldsymbol{v}_s$. Using arguments by Coleman and Noll [127] and Coussy[87] that $\frac{D^s \boldsymbol{\epsilon}^{skel}}{Dt}$, $\frac{D^f p_f}{Dt}$, $\frac{D^s S_\ell}{Dt}$, and $\frac{D^s \theta^s}{Dt}$ are independent processes that can be varied separately, it is then required that

$$\left([n^g - (1-\chi)]p_g - (n^\ell - \chi)p_\ell \right) \beta_s^\theta - \rho^s \eta^s - \rho^s \frac{\partial \psi^s}{\partial \theta^s} = 0, \tag{4.48}$$

$$\left[\frac{\partial g^f}{\partial \theta^f} - \eta^f\right] = 0, \quad for \quad f = \ell, g, \tag{4.49}$$

$$\left[\rho^s \frac{\partial \psi^s}{\partial S_\ell} + ns\right] = 0, \tag{4.50}$$

$$\left(\boldsymbol{\sigma}' - \frac{\partial \rho^s \psi^s}{\partial \boldsymbol{\epsilon}^{skel}}\right) = \boldsymbol{0}, \tag{4.51}$$

$$-\boldsymbol{v}_f^D \cdot [gradp_f - \rho^{gR}\boldsymbol{b}^f] \geq 0, \quad for \quad f = \ell, g, \tag{4.52}$$

$$-\frac{1}{\theta^\alpha}\boldsymbol{q}_\theta^\alpha \cdot grad\theta^\alpha \geq 0, \quad for \quad f = \ell, g. \tag{4.53}$$

Therefore, to remain thermodynamically consistent the constitutive models for the mixture must meet the following requirements:

$$\rho^s \eta^s = \left([n^g - (1-\chi)]p_g - (n^\ell - \chi)p_\ell\right)\beta_s^\theta - \rho^s \frac{\partial \psi^s}{\partial \theta^s}, \tag{4.54}$$

$$\eta^f = \left[\frac{\partial g^f}{\partial \theta^f}\right], \quad for \quad f = \ell, g, \tag{4.55}$$

$$\frac{n^f}{\rho^f} = \frac{\partial g^f}{\partial p_f}, \quad for \quad f = \ell, g, \tag{4.56}$$

$$ns = -\rho^s \frac{\partial \psi^s}{S_\ell}, \tag{4.57}$$

$$\boldsymbol{\sigma}' = \rho^s \frac{\partial \psi^s}{\partial \boldsymbol{\epsilon}^{skel}}. \tag{4.58}$$

Applying the conclusion show in equations 4.54-4.58, assuming the temperature of each phase at a point is the same (*e.g.* $\theta = \theta^\alpha$) combining them with equations 4.43 and 4.45 and simplifying gives the balance of energy equation for the combined mixture,

$$\rho^\ell\theta\frac{D^\ell\eta^\ell}{Dt} + \rho^g\theta\frac{D^g\eta^g}{Dt} + \rho^s\theta\frac{D^s\eta^s}{Dt} + \boldsymbol{v}_\ell^D \cdot [gradp_\ell - \rho^{\ell R}\boldsymbol{b}^\ell]$$
$$+\boldsymbol{v}_g^D \cdot [gradp_g - \rho^{gR}\boldsymbol{b}^g] - \frac{1}{2}\hat{\rho}^\ell\boldsymbol{v}_\ell \cdot \boldsymbol{v}_\ell - \frac{1}{2}\hat{\rho}^g\boldsymbol{v}_g \cdot \boldsymbol{v}_g + \hat{\rho}^\ell\boldsymbol{v}_\ell \cdot \tilde{\boldsymbol{v}}_\ell + \hat{\rho}^g\boldsymbol{v}_g \cdot \tilde{\boldsymbol{v}}_g \tag{4.59}$$
$$-\rho^\ell r^\ell - \rho^g r^g - \rho^s r^s + grad\boldsymbol{q}_\theta^\ell + grad\boldsymbol{q}_\theta^g + +grad\boldsymbol{q}_\theta^s + \hat{\rho}^v H_{vap} = 0.$$

Combining the heat sink and flux terms, neglecting body forces, moving material time derivatives to be in reference to the solid skeleton phase and introducing the definition of specific heat, C_p^α, as

$$\rho^\alpha C_p^\alpha \frac{D^\alpha \theta^\alpha}{Dt} = \rho^\alpha \frac{D^\alpha \eta^\alpha}{Dt}, \tag{4.60}$$

allows for the final balance of energy for the mixture to be written as

$$\begin{aligned}
&(\rho C_p)_{eff} \frac{D^s \theta}{Dt} + \rho^{\ell R} C_p^\ell \boldsymbol{v}_\ell^D \cdot grad\theta + \rho^{gR} C_p^g \boldsymbol{v}_g^D \cdot grad\theta + \boldsymbol{v}_\ell^D \cdot gradp_\ell + \boldsymbol{v}_g^D \cdot gradp_g \\
&- \frac{1}{2} \hat{\rho}^\ell \boldsymbol{v}_\ell \cdot \boldsymbol{v}_\ell - \frac{1}{2} \hat{\rho}^g \boldsymbol{v}_g \cdot \boldsymbol{v}_g + \hat{\rho}^\ell \boldsymbol{v}_\ell \cdot \tilde{\boldsymbol{v}}_\ell + \hat{\rho}^g \boldsymbol{v}_g \cdot \tilde{\boldsymbol{v}}_g - \rho^{eff} \boldsymbol{r} + grad\boldsymbol{q}_\theta + \hat{\rho}^v H_{vap} = 0.
\end{aligned} \tag{4.61}$$

where the specific heat, $(\rho C_p)_{eff}$, is defined as

$$(\rho C_p)_{eff} = \rho^s C_p^s (1-n) + n \left[S_\ell \rho^\ell C_p^\ell + S_g \rho^g C_p^g \right], \tag{4.62}$$

the total heat flux, $\boldsymbol{q}_\theta$, is

$$\boldsymbol{q}_\theta = \boldsymbol{q}_\theta^g + \boldsymbol{q}_\theta^\ell + \boldsymbol{q}_\theta^s, \tag{4.63}$$

and the total heat source per unit mass, $\boldsymbol{r}$, is

$$\boldsymbol{r} = \boldsymbol{r}^s + \boldsymbol{r}^\ell + \boldsymbol{r}^g. \tag{4.64}$$

Additionally, the heat flux is assumed to be isotropic and, therefore, can be definted as

$$\boldsymbol{q}_\theta = k_t^{eff} grad\theta \tag{4.65}$$

where k_t^{eff} is the effective mixture conductivity defined as

$$k_t^{eff} = (1-n)k_t^s + n(S_\ell k_t^\ell + S_g k_t^g) \tag{4.66}$$

where k_t^α is the thermal conductivity of the α phase. Furthermore, it is assumed that water

vapor reaches its saturation pressure[128]. Therefore, the Clausius-Capeyron equation can be used to calculate gas pressure, p_g,

$$p_g = p_{gs_0} exp\Big(-\frac{M_m H_{vap}}{R}\Big[\frac{1}{\theta} - \frac{1}{\theta_0}\Big]\Big) \tag{4.67}$$

where M_m is the molar mass of the vapor, H_{vap} is the latent heat of vaporization, R is the ideal gas constant, and p_{gs_0} is the saturated gas pressure at reference temperature, θ_0. Using this calculated gas pressure, the van Genuchten equation can now be used to relate the liquid saturation with the capillary pressure [79], [129], s, which is the difference between the liquid and gas pressures:

$$S_e = \frac{S_\ell - S_r}{S_s - S_r} = \Big(\frac{1}{1 + \big(\frac{s}{a}\big)^{n_{vg}}}\Big)^m, \tag{4.68}$$

$$m = 1 - \frac{1}{n_v g}, \tag{4.69}$$

$$s = p_g = p_\ell, \tag{4.70}$$

where, S_e is the effective degree of saturation, S_r is the residual degree of saturation, and S_s is the saturated degree of saturation, taken to be 1. Literature fails to proved values for constants, a, n_{vg}, m, and S_r for biological tissue, forcing the author to look to fields such as food processing [106] and geomechanics [105] for values. Additionally, Darcy's law will provide the relative velocities of the fluids [104] (the body force term is neglected),

$$\boldsymbol{v}_f^D = -\frac{k_{rel}^f k_{int}^f}{\mu^f} grad p_f \tag{4.71}$$

where μ^f is the viscosity of the fluid phase f. The relative permeability of each fluid, k_{rel}^f, includes the Kozeny-Carman relationship and is defined as

$$k_{rel}^f = \frac{(n)^3}{1 - (n)^2}\frac{1 - (n_0)^2}{(n_0)^3} \tag{4.72}$$

where n and n_0 are the current and initial porosity. The intrinsic permeability, k_{int}^f, of each

fluid is defined as

$$k^f_{int} = k_{0_{int}} \mathcal{Y}(S_\ell) \tag{4.73}$$

where $k_{0_{int}}$ is a material constant and $\mathcal{Y}(S_\ell)$ is a saturation dependent parameter defined for the liquid phase as

$$\mathcal{Y}(S_\ell) = \begin{cases} \left(\frac{S_\ell - S_r}{1 - S_r}\right)^3 & S_\ell > S_r \\ 0 & S_\ell < S_r \end{cases} \tag{4.74}$$

and for the gas phase as

$$\mathcal{Y}(S_\ell) = \begin{cases} 1 - 1.1S_g & S_g > 1/1.11 \\ 0 & S_g < 1/1.1 \end{cases}. \tag{4.75}$$

Lastly, the solid skeleton is assumed to be elastic; thus, the effective skeleton stress, $\boldsymbol{\sigma}'$, can be represented by

$$\boldsymbol{\sigma}' = \boldsymbol{C}\boldsymbol{\epsilon}^{skel} \tag{4.76}$$

where $\boldsymbol{C}$ is the isotropic elasticity tensor that meets the thermodynamic requirements set forth in equation 4.53 and $\boldsymbol{\epsilon}^{skel}$ the strain within the solid skeleton. This chapter examines 3 different constitutive equations: a simple linear elastic case, a bi-linear elastic, and an exponential elastic equation to determine the elasticity tensor, $\boldsymbol{C}$.

4.3.8   FE Implementation

As stated earlier, the field variables to be solved using the finite element method are pore liquid pressure, p_ℓ, the smeared temperature, θ, and the solid skeleton displacement vector, $\boldsymbol{u}$. The balance of mass, linear momentum, and energy equations (Eqs. 4.29, 4.33, and 4.61), were put into weak form and linearized with respect to the desired variables. To avoid element locking, isoparametric quadrilateral elements bi-quadratic in displacement and bi-

linear in temperature and pore pressure were used. A standard backward Euler timestepping scheme was implemented with Newton-Raphson iterations to obtain convergence during each time step. All calculations were conducted using a custom written code in Matlab 2015b. To handle the highly non-linear nature of this problem efficiently, an adaptive time-stepping scheme was performed by altering the time-step size based on the number of Newton-Raphson iterations needed for convergence during the previous step. The FE code was rigorously verified through comparison with published TPM FE results in the geomechanics field [104], [105] and by comparing portions of the code with simulations conducted using the commercial software Comsol Multiphysics.

4.3.9   Experimental Measurements

The experimental results used to evaluate the performance of the FE model were taken from data published within the literature [16], [117], [118] as well as supplemental experiments conducted by the first and third authors following the same procedures outlined in these papers. The temperature measurements were taken within the lumen of a compressed artery using an array of thermocouples. To find water content, a portion of tissue was fused and then weighed. It was then dried completely and weighed again. The percent weight of water is calculated from these measurements. Full experimental details for tissue temperature and water content measurement can be found in the works published by Cezo et al. [15], [117]. To obtain the deformation of the tissue while loaded to 100 N during the tissue fusion process, a custom testing setup affixing Conmed Altrus jaws, to a uniaxial material testing system (MTS; MTS Insight 2 Electromechanical Testing System) was used. The thickness of 8 porcine artery sections was recorded via optical microscope and then each arterial section was placed between the Altrus jaws and a 100 N force was applied using a proportional-integral-derivative control algorithm. Once the 100 N force was reached, the heaters were activated for 3 s. The deformation in the y-direction of the tissue and the force were recorded throughout the loading and heating process. To obtain the Youngs Modulus, E, used in the

finite element simulations, a best fit analysis was conducted using the engineering stress and strain recorded in the tissue after mechanically loading the tissue, but before heating. A more detailed explanation of the MTS attachments and experimental setup can be found Chapter 3.

4.3.10 Tissue Fusion Simulations

Now that the framework for a multiphase TPM FE model has been established, its use in simulating the heating of biological tissue, specifically thermal tissue fusion will be demonstrated. Figures 4.4 and 4.5 show the quarter-symmetry, two-dimensional section representing the center of the tissue clamped within the jaws of a Conmed Altrus tissue fusion device used in the simulations and the applied boundary conditions.
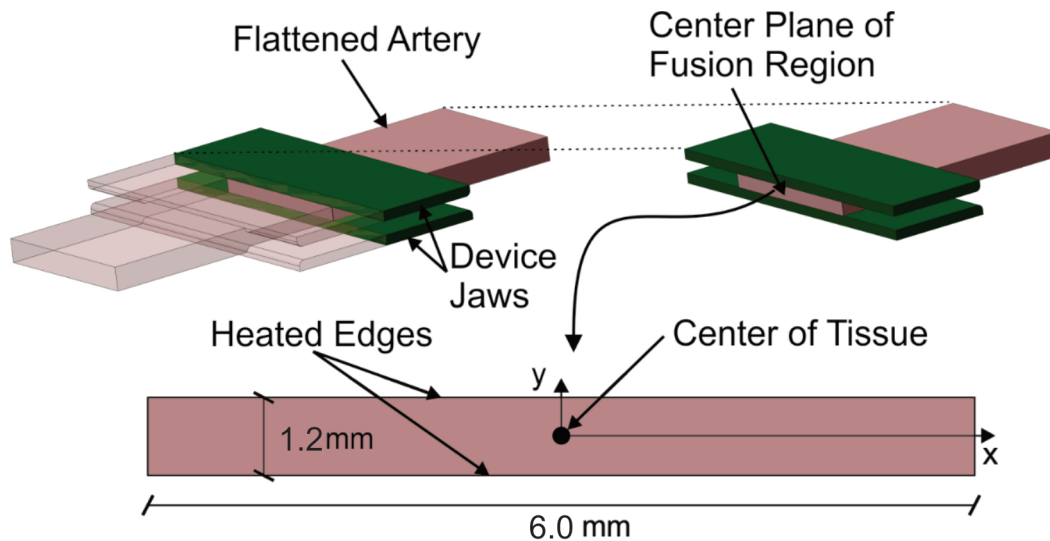
Figure 4.4: Depiction of the tissue clamped within the Conmed Altrus jaws and the 2-D plane to be simulated.

4.3.11 Boundary Conditions

Three different temperature boundary conditions exist within the thermal tissue fusion FE model. The first is the symmetric boundary condition, which sets the heat flux, q_θ, through

the surface equal to 0, (*i.e.* adiabatic),

$$q_\theta = \boldsymbol{q}_\theta \cdot \boldsymbol{n} = 0 \quad on \quad \partial B_\theta^{free}. \tag{4.77}$$

The second thermal boundary condition is a prescribed temperature boundary condition representing the temperature of the jaws, θ^{fixed},

$$\theta(t) = \theta^{fixed}(t) \quad on \quad \partial B_\theta^{fixed}. \tag{4.78}$$

Lastly, on all free edges, free convection is expected to occur. Thus, the normal heat flux, q_θ, is specified as,

$$q_\theta = h_t(\theta - \theta_{amb}) \quad on \quad \partial B_\theta^{free} \tag{4.79}$$

where h_t is the heat transfer coefficient and θ_{amb} is the ambient temperature. Two water species boundary conditions are implemented. The first is an impermeable or symmetric boundary condition preventing flow though the boundary.

$$q_\ell = q_g = 0. \tag{4.80}$$

The second boundary condition consists of the fluid flux, q_f, due to the difference of pore pressure across the boundary,

$$q_f = -\frac{k_{rel}^f k_{int}^f}{\mu^f} \rho^{\alpha R} S_f(p_f - p_{amb}) A \quad for \quad \ell, g \quad on \quad \partial B_p^{free} \tag{4.81}$$

where p_{amb} is the ambient fluid pressure and A is the boundary area. The last boundary conditions are an applied traction, $\boldsymbol{t}$, and a symmetric boundary condition fixing displacements,

$$\boldsymbol{u} \cdot \boldsymbol{n} = 0 \quad on \quad \partial B_u^{fixed}. \tag{4.82}$$
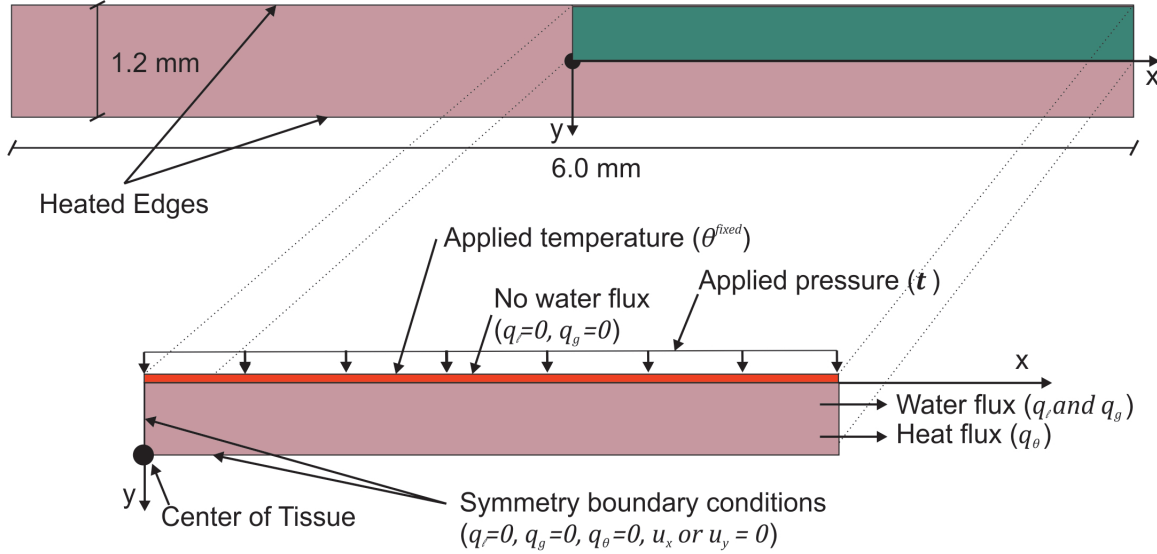
Figure 4.5: Depiction of the quarter-symmetry section of tissue and applied boundary conditions. The device jaws apply temperature and pressure to the top. Symmetry boundary conditions are applied to the bottom and left edges. Heat and water are allowed to flow through the right edge.

4.3.12 Material Properties

Material properties unable to be experimentally measured in the lab were obtained from several sources within the literature. If material properties specifically pertaining to the artery wall were unavailable, properties of tissue similar in composition to the artery wall were used. As it was not possible at this time to find values for the van Genuchten parameters a parametric study of the parameters S_r and n_{vg} was conducted to determine the optimal parameters. To determine the structural mechanical properties, E_{lin}, E_1, E_2, and E_{exp} needed for the constitutive models a non-linear regression analysis using measured experimental stress-strain values was conducted using the commercial statistics software Minitab, All material properties, initial condition. and boundary condition values, along with the source they were found in are listed in Table 4.1.

Table 4.1: Material Properties, Initial Conditions and Boundary Conditions

	Material Property	Value	Description
Universal Constants	R	8.314 N*m/mol K	Ideal Gas Constant
	M_m	0.018 kg/mol	Molar Mass of Water
Solid Skelton Structure	E	1.6 MPa	Linear Elastic Young's Modulus
	ν^{skel}	0.2	Poisson's Ratio
Thermal Constants	α_s	2.5×10^{-4} K^{-1}	Solid Thermal Expansion Coefficient
	β_s^θ	$3*\alpha_s$	Solid Volumetric Thermal Expansion Coefficient
	β_ℓ^θ	4.0×10^{-4} K^{-1}	Water Volumetric Thermal Exp. Coefficient
	C_p^s	145.83 J/(kg K)	Specific Heat of Solid
	C_p^ℓ	4179 J/(kg K)	Specific Heat of Liquid Water
	C_p^g	1850 J/(kg K)	Specific Heat of Water Vapor
	k_t^s	0.5 W/(m K)	Thermal Conductivity of Solid
	k_t^ℓ	0.6 W/(m K)	Thermal Conductivity of Liquid Water
	k_t^g	0.025 W/(m K)	Thermal Conductivity of Water Vapor
	H_{vap}	2.264×10^6 J/kg	Latent Heat of Vaporization of Water
	h_t	25 W/(m^2 K)	Convective Heat Transfer Coefficient
	θ_{amb}	25°C = 298K	Ambient Temperature
Densities	ρ^{sR}	1050 (kg/m^3)	Real Density of Solid
	$\rho^{\ell R}$	$1000/(1+4\beta_\ell^\theta \theta)$	Real Density of Water
	ρ^{gR}	Ideal Gas	
Mass Transport Constants	$k_{o_{int}}^\ell$	5×10^{-14} m^2	Intrinsic Permeability of Liquid Water
	$k_{o_{rel}}^\ell$	Kozemy-Carman Eq.	Relative Permeability of Water
	k_{int}^g	10×10^{-14} m^2	Intrinsic Permeability of Water Vapor
	k_{rel}^g	Kozemy-Carman Eq.	Relative Permeability of Water
	μ_ℓ	5.5×10^{-4} Pa*s	Viscosity of Liquid Water
	μ_g	1.8×10^{-5} Pa*s	Viscosity of Water Vapor
	n_{vg}	1.8	Constant for Clausius-Clapeyron
	a	19.4×10^3 Pa	Constant for Clausius-Clapeyron
	S_r	0.3	Constant for Clausius-Clapeyron
	p_{amb}	1.01×10^5 Pa	Ambient Pressure
Initial Conditions and Model Parameters	p_{g_o}	1.01×10^5 Pa	Initial Water Vapor Pressure
	n_o	0.78	Initial Porosity
	p_{ℓ_o}	1.01×10^5 Pa	Initial Liquid Water Pressure
	θ_{amb}	37 °C = 310K	Initial Ambient Temperature
	S_{ℓ_o}	0.99	Initial Liquid Water Saturation
	θ_{app}	$\begin{cases} = (\theta_{max} - 37)t . t < 2 \\ = \theta_{max} , t > 3 \end{cases}$	Applied Temperature
	θ_{max}	Varies	Maximum Jaw Temperature
	t	2.7×10^6 Pa	Applied Traction
	T	5 s	Total Time
	dt_0	0.0001 (s)	Initial Time Step

4.3.13 Simulations

Seven different simulations were run attempting to predict experimental results of tissue displacement, water content, and internal tissue temperature. The maximum applied temperature, θ_{max}, varied from 120°C to 200°C and simulations were run for 5 s (the same time period as the experiment). The simulation was conducted in three steps: 1) the applied traction matching that of the applied force seen in the experiments was applied during a 2 s step, 2) the temperature was applied during a 1 s step and 3) the temperature held for 2 s. Mesh sensitivity studies were conducted to find the most efficient simulation parameters. This was done by running a simulation, halving the mesh size, rerunning the simulation and comparing the solution vectors. This process was continued until the norm of the difference of the solution vectors was less than 1%. As high temperature gradients and vaporization rates can occur during portions of the simulations, convergence often depended greatly on time step size. Time step size was determined by choosing an initial time step of 0.0001 s and recording the number of Newton-Raphson iterations required for convergence during the current time step. If this value was greater than or less than a certain threshold (7 iterations and 2 iterations respectively), the time step size was halved or doubled for the next step accordingly. Once the simulations were complete the results were compared with experimental measurements.

4.4 Results

Figure 4.6 shows the temperature profile within the tissue at the end of a simulation ($\theta_{max} = 170°C$, $t_{max} = 5s$). The temperature at the tissue center is then compared to published results by Cezo et. al.[130]. The results for the predicted temperature fall within one standard deviation of measured experimental results. The sensitivity analysis of the parameter, n_{vg}, showed less than a 1% difference in the solutions when changed by 20% (results not shown); however, the value selected for the residual degree of saturation parameter, S_r,

impacted the final predicted water content. Figure 4.7 shows the water content by weight throughout the tissue at the end of a simulation ($\theta_{max} = 170°C$, $t_{max} = 5s$) for S_r values of 0.25, 0.3 and 0.35. The water content falls within one standard deviation of the mean measured experimental results in each of the seven comparisons for all values of S_r, and predicts values closest to the measured experimental mean for an S_r of 0.3.

Figure 4.8 compares experimentally measured stress-strain curves in the y-direction of the tissue to the simulated stress-strain curve of the tissue as the load is applied before heating. The experimental model using a linear elastic constitutive model deviates from the measured experimental results (mean standard error (MSE) of 0.33) for the majority of the curve, but ends at the same stress-strain point at the end of loading. The bi-linear constitutive model and the exponential elastic models had a MSE of 0.21 and 0.18 respectively. The bi-linear elastic simulation took an average of 1.1 times longer than the linear elastic simulation whereas the simulation applying an exponential elastic material model took an average of 1.4 times as long as the simulation using a linear elastic material.

Figure 4.9 displays the measured experimental and simulated vertical deformation against time before and during heating of the tissue. Before heating, the tissue deflects as expected for a fully saturated porous medium. During heating, the experimental results show an increase in downward deflection as the temperature increases. The simulation shows a decrease in downward deflection with temperature increase and then an increase in deflection after a steady-state temperature is reached (3 s). Each simulation, predicts a deflection of within 15% of the measured experimental deflection throughout the simulation.
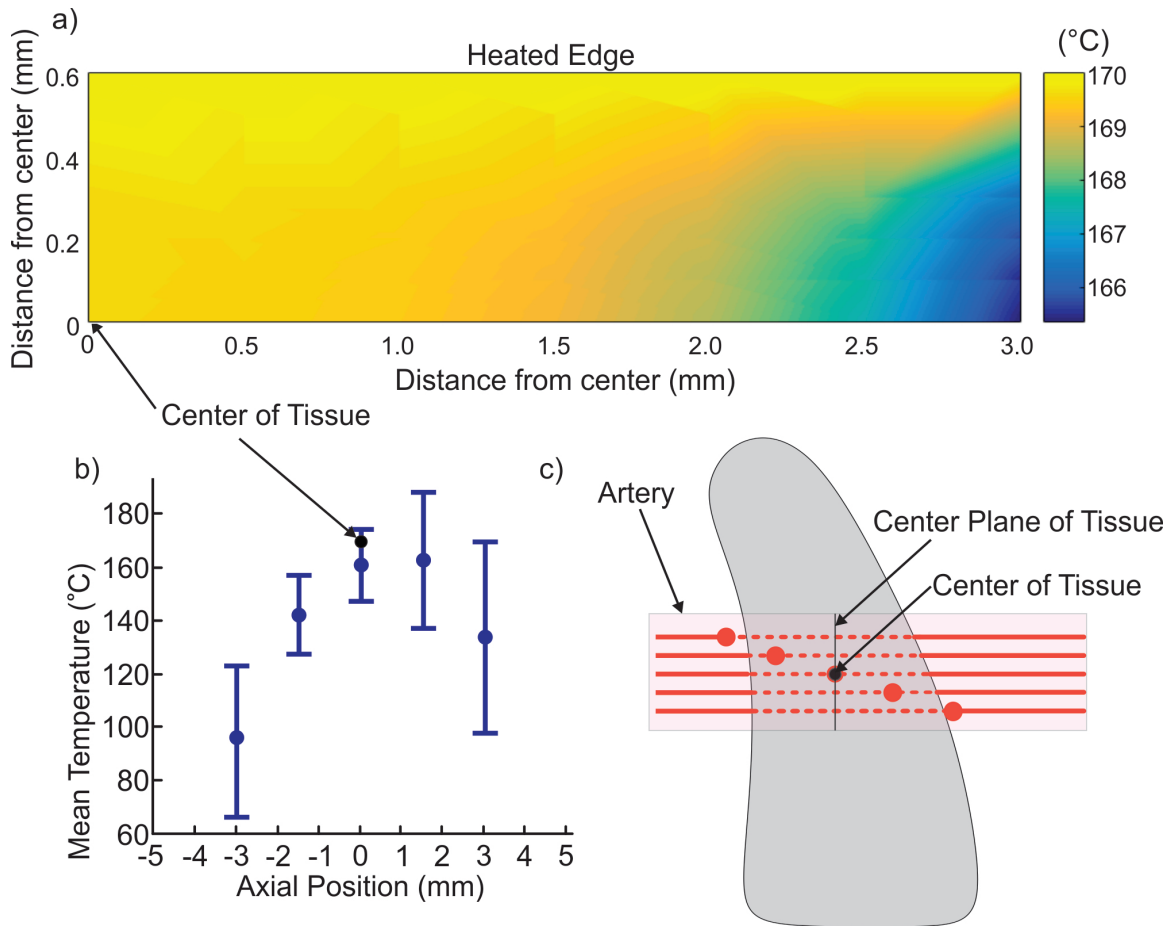
Figure 4.6: a) The temperature (°C) within the tissue for an applied 170 °C and an $S_r = 0.3$ at the end of 5 s. b,c) The temperature at the center of the tissue as it is compared to published experimental results [130]. Only one data point ca be compared as all other experimental points are located too far from the center plane of the tissue.
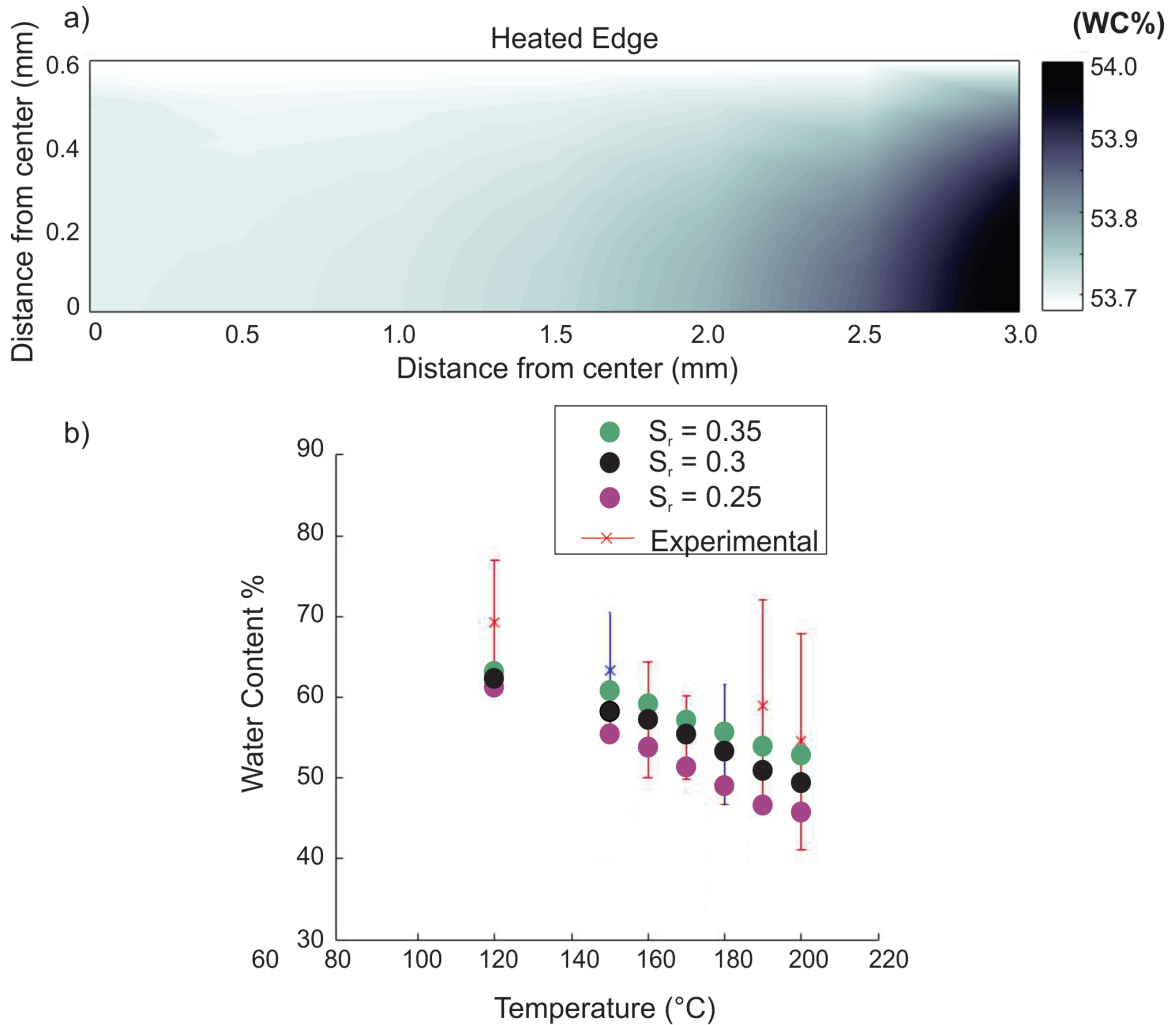
Figure 4.7: Figure 6: a) The water content at 5 s within the center plane of the tissue for a simulation applying 170 °C and an $S_r = 0.3$. b) Dots representing the average water content within the tissue for applied temperatures of 120 - 200 °C for an S_r of 0.25, 0.30 and 0.35 are plotted against measured experimental results. All simulated results of water content fell within one standard deviation (S.D.) of the average experimental results with an S_r of 0.30 producing results nearest the mean of the experimental results. Note: Cezos published results are in red[118], supplemental results obtained following the same procedure are in blue (n=12).
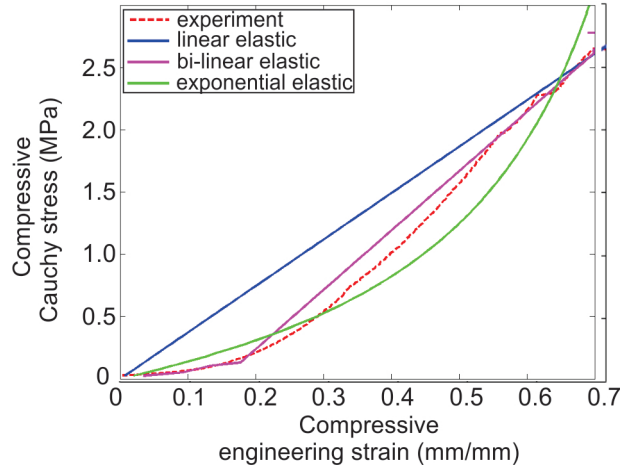
Figure 4.8: The average recorded stress-strain curves for 8 porcine splenic arteries (standard deviation of 0.12 MPa) compared to the simulated stress-strain curves of a linear elastic (MSE = 0.33), bi-linear elastic (MSE = 0.21) and exponential elastic (MSE = 0.18) solid material model before heating.
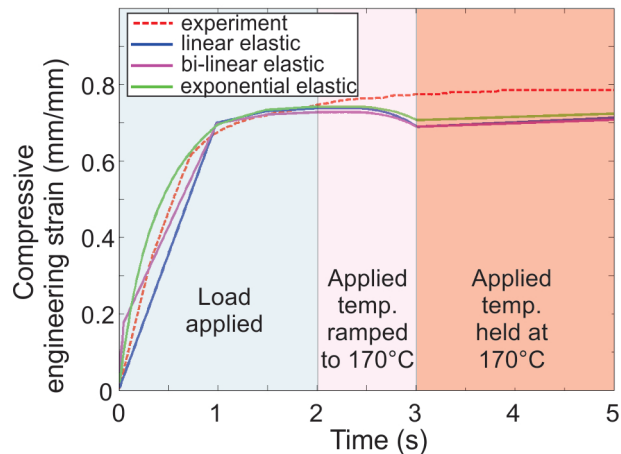
Figure 4.9: The average measured engineering strain (standard deviation of 0.033) for the 8 fused porcine arteries during mechanical loading (0-2 s), while heated up to an applied temperature of 170 °C (2-3 s) and at a constant applied temperature of 170 °(4-5 s).

4.5   Discussion

This chapter provides a method for conducting TPM finite element simulations of biological tissue enabling one to evaluate the physics occurring within the tissue when loaded, thermally and/or mechanically, by an external source. The model incorporates the fluid transport

through the tissue, including phase change between liquid water and water vapor, the heat transfer through the tissue and the deformation of the tissue. Using this method, simulations of thermal tissue fusion were then conducted and compared to experimental results. The simulations were able to predict temperature and water content even though limited by small deformation theory.

4.5.1 Temperature

Figure 4.6 shows the simulated temperature at the end of an applied 170 °C temperature simulation. By this point (5 s) the simulation has reached steady state and the temperature at the center of the tissue is 169 °C which is 6°C higher than the mean published experimental results [117], though still within a standard deviation of the results. This discrepancy is due to the assumption of perfect thermal conduction at the jaw edge. To better represent true device-tissue interaction the conductivity between jaw edge and tissue edge needs to be taken into account. Even with the simplifying assumption of perfect conduction, the simulation predicts the center tissue temperature within one standard deviation of the measured experimental mean.

4.5.2 Water Content

Each of the seven simulations run for all values of the residual degree of saturation, S_r, predicted the average final water content within one standard deviation of the experimentally measured mean [118] with the value of $S_r = 0.3$ predicting final water content values closest to the mean measured experimental value. The value of residual saturation represents the amount of water left bound in the tissue that is impossible to be driven out via a tissue fusion device. Ideally, it would be beneficial to conduct separate experimental measurements to provide the specific van Genuchten parameters; however, these parameters prove particularly difficult to measure in biological tissue and the measurement of them is currently left as future

work. Thus, the sensitivity study presented here provides a baseline for researchers moving forward with this type of analysis.

4.5.3 Deformation

The deformation predicted by the three elastic constitutive models shown in Figures 4.8 and 4.9 shows that although the final displacement before heating is accurately predicted, the model is limited by its linear elastic, small strain assumption. This is seen in Figure 4.8 when the linear elastic stress-strain curve of the tissue deviates significantly from the measured stress-strain curve, and in Figure 4.9 when the small deformation assumption limit the ability of all three models to predict the tissue deflection as the tissue is heated. Despite these limitations, the model still accurately predicts the fluid and thermal transport occurring in the arterial tissue and estimates the final vertical deformation of the tissue to within 15% of the measured experimental mean. A more inclusive TPM FE model utilizing large deformation theory is needed for applications requiring more accurate analysis. While the small deformation theory may be limited, it is still a valuable tool for two reasons. First, simulations assuming small deformations will decrease simulation time significantly when compared to simulations utilizing full non-linear large deformation theory. This is already seen by comparing the computation time between the linear elastic and exponential elastic simulations and would be exacerbated if compared to full large deformation theory. This reduction in computational time would be valuable in applications where a real-time prediction of tissue deformation is desired, but exact accuracy is not necessary such as seen in the field of medical device robotics and automation[131]. Second, the small deformation model presented here is valuable in modeling processes in which large deformation does not occur, such as those seen during ablation[61] or interaction with wearable electronic devices.

4.5.4 Conclusion

Ultimately, a novel method for modeling the physics occurring within biological tissue interacting with external devices has been presented. Despite the weakness of assuming small deformations, the model was still able to predict temperature and water content occurring in tissue during arterial tissue fusion to within a standard deviation of experimentally measured data. To the authors knowledge, while small deformation TPM models have been used to simulate geomechanical processes[105] and food processing [106], [129], this is the first to do so for medical device interaction with biological tissue, providing an initial step toward all-encompassing, predictive models.

4.6 Acknowledgements

Chapter 5: Large Deformation Thermo-Poromechancis Theory

Throughout this chapter, a thermodynamically consistent theory of thermo-poromechanics of porous media including large deformations, following the theory initially seen in the seminal works by de Boer [79] and Coussy [87], will be presented to represent the underlying mechanics occurring within biological tissue when mechanically and thermally loaded. In this chapter, it will be assumed that the tissue being represented will be a partially saturated (also known as unsaturated) porous medium. Meaning the tissue will consist of some solid skeletal matrix and multiple fluid constituents (gas and liquid) occupying the voids between the solid skeletal matrix. It is assumed these voids will be filled with a mixture of liquid and gaseous vapor of the same chemical makeup (*e.g.* liquid water and water vapor). As the chapter progresses, the reader will be taken from an initial description of partially saturated porous media through the initial generic forms of the balance of mass, balance of linear momentum, and balance of energy equations to their final detailed forms, including thermodynamically consistent constitutive models, necessary for implementation in a Galerkin finite element code.

5.1 Initial Definition

To fully describe a partially saturated triphasic porous medium, several definitions must be prescribed and constraints determined. Considering a differential volume, dv, with a differential mass, dm, it can be said that the total differential volume and mass are the sum of the differential volumes, dv_α, and masses, dm_α, of each phase, α ($s = solid, \ell = liquid, g =$

gas),

$$dv = \sum_{\alpha=s,\ell,g} dv_\alpha \tag{5.1}$$

$$dm = \sum_{\alpha=s,\ell,g} m_\alpha. \tag{5.2}$$

Equations 5.1 and 5.2 allow for the definition of the volume fraction, n^α, as

$$n^\alpha = \frac{dv_\alpha}{dv}. \tag{5.3}$$

It is useful to define n as the volume fraction of the pore space or porosity, meaning,

$$n = 1 - n^s = n^\ell + n^g. \tag{5.4}$$

The differential mass of each phase, dm_α, can be written as the product of the true (real) mass density of the α phase, $\rho^{\alpha R}$, and the differential volume of the α phase

$$\rho^{\alpha R}(\boldsymbol{x}, t) = \frac{dm_\alpha}{dv_\alpha} \tag{5.5}$$

where $\boldsymbol{x}$ is the current position. Using this definition, the partial mass density, ρ^α, of the α phase can be defined as

$$\rho^\alpha(\boldsymbol{x}, t) = \frac{dm_\alpha}{dv}, \tag{5.6}$$

or in a more useful form as

$$\rho^\alpha(\boldsymbol{x}, t) = \frac{dm_\alpha}{dv_\alpha} \frac{dv_\alpha}{dv} = \rho^{\alpha R} n^\alpha. \tag{5.7}$$

The total density of the mixture, ρ^{eff}, can be described as

$$\rho^{eff} = \rho^s + \rho^\ell + \rho^g \tag{5.8}$$

which by applying 5.7 can be written as

$$\rho^{eff} = n^s \rho^{sR} + n^\ell \rho^{\ell R} + n^g \rho^{gR}. \tag{5.9}$$

It is also beneficial to define the saturation of a fluid, S_f, as the amount of void volume, dv_{void}, occupied by that fluid,

$$dv_{void} = dv - dv_s, \tag{5.10}$$

$$S_f = \frac{dv_f}{dv_{void}} = \frac{n^f}{n}, \tag{5.11}$$

$$S_\ell + S_g = 1. \tag{5.12}$$

5.2 Kinematics

To gain a full understanding of the physical processes occurring within porous media when loaded, it is necessary to examine the kinematics of a differential volume element and its constituents. From fundamental continuum mechanics, it can be said each phase undergoes a deformation, $\boldsymbol{\chi}_\alpha$, defined as

$$\boldsymbol{x} = \boldsymbol{\chi}_\alpha(\boldsymbol{X_\alpha}, t), \tag{5.13}$$

$$\boldsymbol{X}_\alpha(\boldsymbol{x}, t) = \boldsymbol{\chi}_\alpha^{-1}(\boldsymbol{x}, t), \tag{5.14}$$

where $\boldsymbol{x}$ is the current "smeared" position of the combined 3-phase mixture at time, t, and $\boldsymbol{X}_\alpha$ is the initial location of the α phase as shown in Figure 5.1. The displacement of each phase, $\boldsymbol{u}_\alpha$ or $\boldsymbol{U}_\alpha$, can be described as

$$\boldsymbol{x} = \boldsymbol{X}_\alpha(\boldsymbol{x}, t) + \boldsymbol{u}_\alpha(\boldsymbol{x}, t) \tag{5.15}$$

or

$$\boldsymbol{x}(\boldsymbol{X}_\alpha, t) = \boldsymbol{X}_\alpha + \boldsymbol{U}_\alpha(\boldsymbol{X}_\alpha, t) \tag{5.16}$$
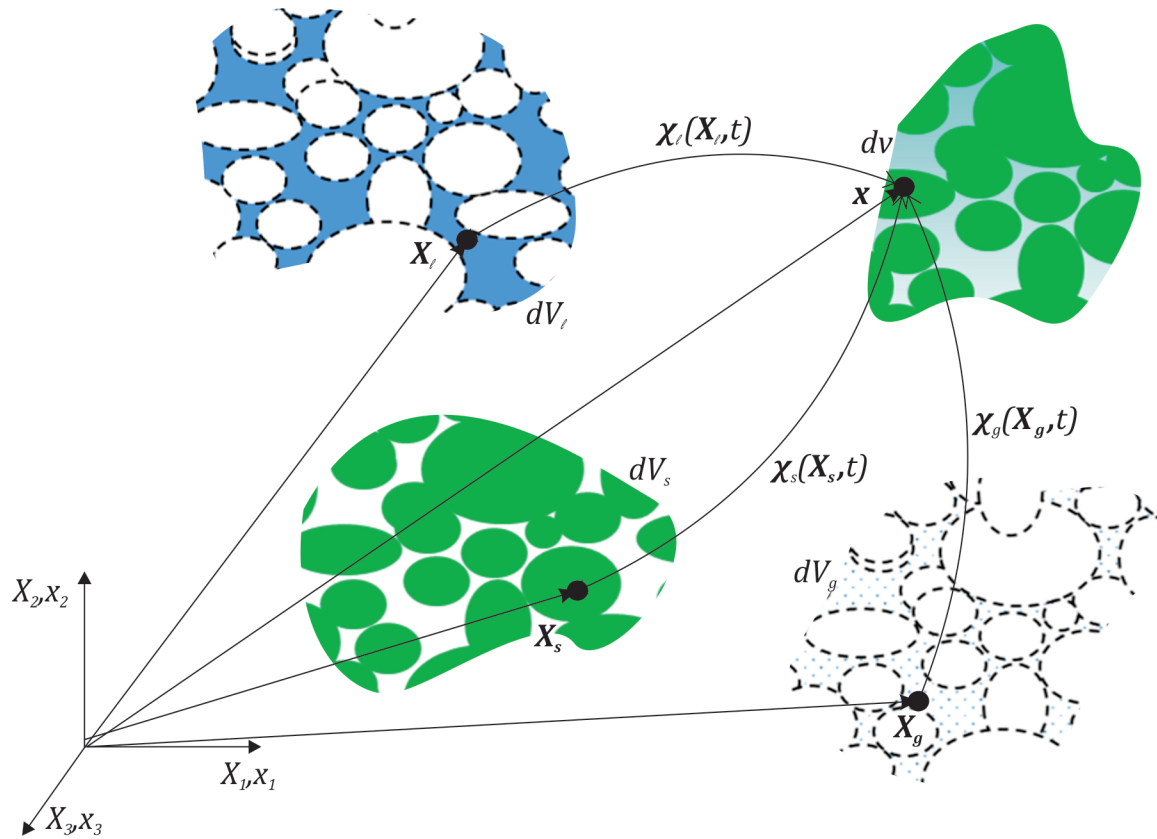
Figure 5.1: A depiction of the deformation of each phase from its initial differential volume dV_α to the final "smeared" differential volume, dv.

thus,

$$\boldsymbol{u}_\alpha = \boldsymbol{U}_\alpha. \tag{5.17}$$

Using 5.13 the deformation gradient, $\boldsymbol{F}_\alpha$, is defined as

$$\boldsymbol{F}_\alpha(\boldsymbol{x}, t) = \frac{\partial \boldsymbol{\chi}_\alpha(\boldsymbol{x}, t)}{\partial (\boldsymbol{X}_\alpha)} = \frac{\partial \boldsymbol{x}}{\partial \boldsymbol{X}_\alpha} \tag{5.18}$$

and its inverse as

$$\boldsymbol{F}_\alpha^{-1} = \frac{\partial \boldsymbol{X}_\alpha}{\partial \boldsymbol{x}}. \tag{5.19}$$

The jacobian, J_α, or determinant of the deformation gradient gives the volume change with respect to the α phase

$$J_\alpha = det(\boldsymbol{F}_\alpha), \tag{5.20}$$

$$J_\alpha = \frac{dv_\alpha}{dV_\alpha}, \tag{5.21}$$

where dV_α is the reference volume of the α phase. Lastly, it is necessary to define the velocity $(\boldsymbol{V}_\alpha, \boldsymbol{v}_\alpha)$ and acceleration $(\boldsymbol{A}_\alpha, \boldsymbol{a}_\alpha)$ of the α phase, which can be defined in terms of the material or reference configuration as

$$\boldsymbol{V}_\alpha(\boldsymbol{X}_\alpha, t) = \frac{\partial \boldsymbol{\chi}_\alpha(\boldsymbol{X}_\alpha, t)}{\partial t} \tag{5.22}$$

and

$$\boldsymbol{A}_\alpha(\boldsymbol{X}_\alpha, t) = \frac{\partial (\boldsymbol{V}_\alpha, t)}{\partial t} = \frac{\partial^2 \boldsymbol{\chi}_\alpha(\boldsymbol{X}_\alpha, t)}{\partial t^2} \tag{5.23}$$

or in the spatial (current) configuration as

$$\boldsymbol{V}_\alpha(\boldsymbol{X}_\alpha, t) = \boldsymbol{V}_\alpha(\boldsymbol{\chi}_\alpha^{-1}(\boldsymbol{x}, t)) = \boldsymbol{v}_\alpha(\boldsymbol{x}, t) \tag{5.24}$$

and

$$\boldsymbol{A}_\alpha(\boldsymbol{X}_\alpha, t) = \boldsymbol{A}_\alpha(\boldsymbol{\chi}_\alpha^{-1}(\boldsymbol{x}, t)) = \boldsymbol{a}_\alpha(\boldsymbol{x}, t). \tag{5.25}$$

The material time derivative describes the time rate of change of a quantity with respect to a defined reference frame. For the α phase the material velocity, $\boldsymbol{V}_\alpha$, and the material acceleration, $\boldsymbol{A}_\alpha$, can be defined as the material time derivative of the deformation with respect to the initial fixed configuration of the α phase,

$$\boldsymbol{V}_\alpha = \frac{D^\alpha \boldsymbol{\chi}_\alpha(\boldsymbol{X}_\alpha, t)}{Dt}, \tag{5.26}$$

$$\boldsymbol{A}_\alpha = \frac{D^\alpha D^\alpha \boldsymbol{\chi}_\alpha(\boldsymbol{X}_\alpha, t)}{Dt Dt}. \tag{5.27}$$

It can then be said the spatial acceleration, $\boldsymbol{a}_\alpha$, is

$$\boldsymbol{a}_\alpha = \frac{D^\alpha}{Dt}\left[\frac{D^\alpha \boldsymbol{\chi}_\alpha(\boldsymbol{X}_\alpha, t)}{Dt}\right] = \frac{\partial \boldsymbol{v}_\alpha(\boldsymbol{x}, t)}{\partial t} + \frac{\partial \boldsymbol{v}_\alpha(\boldsymbol{x}, t)}{\partial \boldsymbol{x}} \cdot \boldsymbol{v}_\alpha(\boldsymbol{x}, t). \tag{5.28}$$

It is also useful to describe how the deformation gradient changes in time. This can be described using material description as

$$\frac{D^\alpha \boldsymbol{F}_\alpha}{Dt} = \frac{\partial\left(\frac{D^\alpha \boldsymbol{x}}{Dt}\right)}{\partial \boldsymbol{X}_\alpha} = \frac{\partial \boldsymbol{v}_\alpha}{\partial \boldsymbol{X}_\alpha} \tag{5.29}$$

or in the spatial realm as

$$\boldsymbol{\ell}_\alpha = \frac{\partial\left(\frac{D^\alpha \boldsymbol{x}}{Dt}\right)}{\partial \boldsymbol{x}} = \frac{\partial \boldsymbol{v}_\alpha}{\partial \boldsymbol{x}} \tag{5.30}$$

such that

$$\boldsymbol{\ell}_\alpha = \frac{D^\alpha \boldsymbol{F}_\alpha}{Dt} \boldsymbol{F}_\alpha^{-1} \tag{5.31}$$

where $\boldsymbol{\ell}_\alpha$ is defined as the spatial velocity gradient of the α phase. Lastly, in the finite deformation realm of continuum mechanics, several different strain measures can be used. In this work, the two most useful strain measures will be the Green-Lagrange strain, $\boldsymbol{E}$, and the Euler-Almansi strain, $\boldsymbol{e}$, which are defined for the α phase as

$$\boldsymbol{E}_\alpha = \frac{1}{2}[\boldsymbol{C}_\alpha - \boldsymbol{I}], \tag{5.32}$$

$$\boldsymbol{e} = \frac{1}{2}[\boldsymbol{I} - \boldsymbol{b}_\alpha^{-1}] \tag{5.33}$$

where $\boldsymbol{C}_\alpha$ is the Right Cauchy-Green tensor,

$$\boldsymbol{C}_\alpha = \boldsymbol{F}_\alpha^T \boldsymbol{F}_\alpha \tag{5.34}$$

and $\boldsymbol{b}_\alpha$ is the Left Cauchy-Green tensor,

$$\boldsymbol{b}_\alpha = \boldsymbol{F}_\alpha \boldsymbol{F}_\alpha^T. \tag{5.35}$$

5.3 Balance Equations

Three governing equations will be used in the finite element formulation for the combined 3-phase mixture: balance of mass, balance of linear momentum, and balance of energy. While these equations can be arranged to solve for several different field variables, it is most useful for this application to set the skeleton displacement, $\boldsymbol{u}$, the liquid pore pressure, p_ℓ, and the average mixture temperature, θ, as the desired field variables. In geomechanics, it is traditional to define the gas as a mixture of dry air and water vapor. Thus, an additional balance equation for dry air is added [105]. However, in this work, the porous media is assumed to be biological tissue; thus, it is assumed all gas is water vapor. The general description for the problem being solved including: traction and prescribed boundary conditions for the balance of linear momentum, prescribed pore pressure and mass flux for the balance of mass of the water species and prescribed temperature and energy flux for the balance of energy can be found in Figure 5.2.
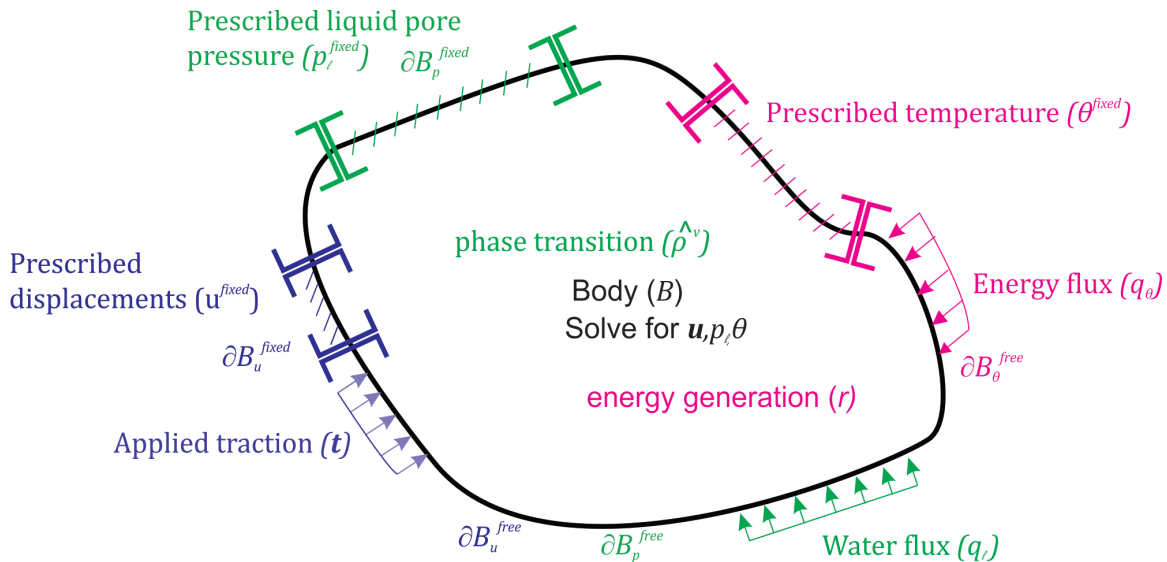
Figure 5.2: A depiction of the TPM problem set up for biological tissue. The field variables are deformation, $\boldsymbol{u}$, liquid pore pressure, p_ℓ, and temperature, θ. Fluxes and prescribed boundary conditions act on surfaces ∂B while heat generation, r, and phase transition, $\hat{\rho}_v$, act throughout the body, B.

5.3.1 Balance of Mass

The mass of the α phase, m_α, within a mixture is defined in the current configuration as

$$m_\alpha = \int_B \rho^\alpha dv \tag{5.36}$$

which can be written in the α reference configuration as

$$m_\alpha = \int_{B_0^\alpha} \rho^\alpha J_\alpha dV_\alpha. \tag{5.37}$$

Thus, the change of mass with respect to time for each phase can be written as

$$\frac{D^\alpha m_\alpha}{Dt} = \int_B \hat{\rho}^\alpha dv. \tag{5.38}$$

As the reference configuration of the α phase, B_0^α, is considered fixed, the material time derivative can be brought inside the integral. Therefore, combing equations 5.37 and 5.38 gives

$$\int_{B_o^\alpha} \frac{D^\alpha}{Dt}(\rho^\alpha J_\alpha) dV_\alpha = \int_B \hat{\rho}^\alpha dv. \tag{5.39}$$

Applying the chain rule gives

$$\int_{B_o^\alpha} \left[\frac{D^\alpha \rho^\alpha}{Dt} J_\alpha + \rho^\alpha \frac{D^\alpha J_\alpha}{Dt} \right] dV_\alpha = \int_B \hat{\rho}^\alpha dv \tag{5.40}$$

where the material time derivative of the jacobian can be expanded as [121]

$$\int_{B_o^\alpha} \left[\frac{D^\alpha \rho^\alpha}{Dt} J_\alpha + \rho^\alpha J_\alpha div \boldsymbol{v}_\alpha \right] dV_\alpha = \int_B \hat{\rho}^\alpha dv. \tag{5.41}$$

Pushing 5.41 forward to the current configuration gives

$$\int_B \left[\frac{D^\alpha \rho^\alpha}{Dt} + \rho^\alpha div \boldsymbol{v}_\alpha \right] dv = \int_B \hat{\rho}^\alpha dv \tag{5.42}$$

which can be localized to

$$\frac{D^\alpha \rho^\alpha}{Dt} + \rho^\alpha div\boldsymbol{v}_\alpha = \hat{\rho}^\alpha. \tag{5.43}$$

Using the arguments laid out by Lewis and Schrefler [103] the material time derivatives of the pressure of the α constituent can be related to the change in its density and temperature as

$$\frac{D^\alpha p_\alpha}{Dt} = \frac{1}{\rho^{\alpha R}}\left[K^\alpha_{bulk}\frac{D^\alpha \rho^{\alpha R}}{Dt} + \beta^\theta_\alpha \frac{D^\alpha \theta^\alpha}{Dt}\right] \tag{5.44}$$

so the material time derivative of the real mass density is

$$\frac{D^\alpha \rho^{\alpha R}}{Dt} = \rho^{\alpha R}\left[\frac{1}{K^\alpha_{bulk}}\frac{D^\alpha p_\alpha}{Dt} - \beta^\theta_\alpha \frac{D^\alpha \theta^\alpha}{Dt}\right] \tag{5.45}$$

where ρ^α is the relative pressure, K^α_{bulk} is the bulk modulus, θ^α is the temperature and β^θ_α is the volumetric thermal expansion coefficient of the α phase. Plugging 5.7 into 5.43 and expanding via the chain rule gives the balance of mass for each phase as

$$\rho^{\alpha R}\frac{D^\alpha n^\alpha}{Dt} + n^\alpha\frac{D^\alpha \rho^{\alpha R}}{Dt} + n^\alpha \rho^{\alpha R} div\boldsymbol{v}_\alpha = \hat{\rho}^\alpha. \tag{5.46}$$

Substituting in 5.45 and dividing by $\rho^{\alpha R}$ gives

$$\frac{D^\alpha n^\alpha}{Dt} + n^\alpha\left[\frac{1}{K^\alpha_{bulk}}\frac{D^\alpha p_\alpha}{Dt} - \beta^\theta_\alpha \frac{D^\alpha \theta^\alpha}{Dt}\right] + n^\alpha div\boldsymbol{v}_\alpha = \frac{\hat{\rho}^\alpha}{\rho^{\alpha R}}. \tag{5.47}$$

Examining the solid phase of equation 5.47, *e.g.* setting $\alpha = s$, provides

$$\frac{D^s n^s}{Dt} + n^s\left[\frac{1}{K^s_{bulk}}\frac{D^s p^s}{Dt} - \beta^\theta_s \frac{D^s \theta^s}{Dt}\right] + n^s div\boldsymbol{v}_s = \frac{\hat{\rho}^s}{\rho^{sR}}. \tag{5.48}$$

It is assumed that the solid material is incompressible thus,

$$\frac{1}{K^s_{bulk}}\frac{D^s p^s}{Dt} = 0 \tag{5.49}$$

and that no solid skeletal mass changes form or is created or destroyed,

$$\frac{\hat{\rho}^s}{\rho^{sR}} = 0. \tag{5.50}$$

Therefore, equation 5.48 can be simplified to

$$\frac{D^s n^s}{Dt} - n^s \beta_s^\theta \frac{D^s \theta^s}{Dt} + n^s div \boldsymbol{v}_s = 0. \tag{5.51}$$

Using the definition of porosity (Eqn. 5.4) allows for

$$\frac{D^s(1-n)}{Dt} - (1-n)\left[\beta_s^\theta \frac{D^s \theta^s}{Dt} + div \boldsymbol{v}_s\right] = 0, \tag{5.52}$$

which can be rearranged to yield the final balance of mass equation for the solid phase as

$$\frac{D^s n}{Dt} + (1-n)\left[\beta_s^\theta \frac{D^s \theta^s}{Dt} + div \boldsymbol{v}_s\right] = 0. \tag{5.53}$$

Now setting α equal to ℓ and examining the balance of mass for the liquid phase, equation 5.47 can be written as

$$\frac{D^\ell n^\ell}{Dt} + n^\ell \left[\frac{1}{K_{bulk}^\ell} \frac{D^\ell p^\ell}{Dt} - \beta_\ell^\theta \frac{D^\ell \theta^\ell}{Dt}\right] + n^\ell div \boldsymbol{v}_\ell = \frac{\hat{\rho}^\ell}{\rho^{\ell R}}. \tag{5.54}$$

In order for the finite element method to be be implemented, a Lagrangian implementation must used; therefore, all equations must refer to the initial solid reference frame. The following equation relating the material time derivative with respect to the α phase to the material time derivative with respect to the solid phase is useful:

$$\frac{D^\alpha(\bullet)}{Dt} = \frac{D^s(\bullet)}{Dt} + grad(\bullet) \cdot \tilde{\boldsymbol{v}}_\alpha, \tag{5.55}$$

where $\tilde{\boldsymbol{v}}_\alpha$ is the relative velocity of the α phase with respect to the solid phase. Applying equation 5.55 to 5.54 gives

$$\frac{n^\ell}{K_{bulk}^\ell}\frac{D^s p^\ell}{Dt} + \frac{n^\ell}{K_{bulk}^\ell} grad(p_\ell) \cdot (\tilde{\boldsymbol{v}}_\ell) + \frac{D^s n^\ell}{Dt} + grad(n^\ell) \cdot \tilde{\boldsymbol{v}}_\ell$$
$$-n^\ell \beta_\ell^\theta \left[\frac{D^s \theta^\ell}{Dt} + grad(\theta) \cdot \tilde{\boldsymbol{v}}_\ell\right] + n^\ell div\boldsymbol{v}_\ell = \frac{\hat{\rho}^\ell}{\rho^{\ell R}}. \tag{5.56}$$

The definition of the chain rule allows one to write

$$div(n^\ell \tilde{\boldsymbol{v}}_\ell) + n^\ell div\boldsymbol{v}_s = grad(n^\ell) \cdot \tilde{\boldsymbol{v}}_\ell + n^\ell div\boldsymbol{v}_\ell, \tag{5.57}$$

where $\tilde{\boldsymbol{v}}_\ell$ is the relative velocity of the liquid with respect to the solid phase (e.g. $\tilde{v}_f = v_f - v_s$). This definition combined with equation 5.57 and plugging in the definition for liquid saturation (Eqn. 5.11) gives the final balance of mass for the liquid phase,

$$\frac{n S_\ell}{K_{bulk}^\ell}\frac{D^s p_\ell}{Dt} + \frac{1}{K_{bulk}^\ell} grad(p_\ell) \cdot (n^\ell \tilde{\boldsymbol{v}}_\ell) + S_\ell \frac{D^s n}{Dt} + n\frac{D^s S_\ell}{Dt}$$
$$+ div(n^\ell \tilde{\boldsymbol{v}}_\ell) + n^\ell div\boldsymbol{v}_s - n S_\ell \beta_\ell^\theta \left[\frac{D^s \theta^\ell}{Dt} + grad(\theta^\ell) \cdot \tilde{\boldsymbol{v}}_\ell\right] = \frac{\hat{\rho}^\ell}{\rho^{\ell R}}. \tag{5.58}$$

Combining the balance of mass equations for the liquid and solid phases (Eqns. 5.53 and 5.58) gives

$$S_\ell \left[(1-n)\left[div\boldsymbol{v}_s - \beta_s^\theta \frac{D^s \theta^s}{Dt}\right]\right] + n\frac{D^s S_\ell}{Dt} + div(n^\ell \tilde{\boldsymbol{v}}_\ell) + n S_\ell div\boldsymbol{v}_s$$
$$-n S_\ell \beta_\ell^\theta \left[\frac{D^s \theta^\ell}{Dt} + grad(\theta^\ell) \cdot \tilde{\boldsymbol{v}}_\ell\right] + \frac{n S_\ell}{K_{bulk}^\ell}\frac{D^s p_\ell}{Dt} + \frac{1}{K_{bulk}^\ell} grad(p_\ell) \cdot (n^\ell \tilde{\boldsymbol{v}}_\ell) = \frac{\hat{\rho}^\ell}{\rho^{\ell R}}, \tag{5.59}$$

which can be further simplified by assuming the temperature-liquid expansion is linear, e.g.

$$\rho^{\ell R} = \rho_0^{\ell R}\left[1 - \beta_\ell^\theta(\theta^\ell - \theta_0^\ell)\right] \tag{5.60}$$

where $\rho_0^{\ell R}$ is the known liquid density at some reference temperature θ_0^ℓ. Additionally, the flow is assumed to be Darcian, meaning that

$$n^\alpha \tilde{\boldsymbol{v}}_\alpha = \boldsymbol{v}_\alpha^D \tag{5.61}$$

where $\boldsymbol{v}_\alpha^D$ is the Darcy velocity of the α phase. Using the definition of the chain rule, one can show that

$$div(\rho^{\ell R}\boldsymbol{v}_\ell^D) = \rho^{\ell R}div\boldsymbol{v}_\ell^D - \rho^{\ell R}\beta_\ell^\theta grad(\theta^\ell) \cdot \boldsymbol{v}_\alpha^D \tag{5.62}$$

and that the final combined solid-liquid balance of mass equation is

$$\frac{\rho^{\ell R}nS_\ell}{K_{bulk}^\ell}\frac{D^sp_\ell}{Dt} + \frac{\rho^{\ell R}}{K_{bulk}^\ell}grad(p_\ell) \cdot (n^\ell \boldsymbol{v}_\ell^D) + S_\ell\rho^{\ell R}div\boldsymbol{v}_s-$$
$$\rho^{\ell R}S_\ell\left[(1-n)\beta_s^\theta\frac{D^s\theta^s}{Dt} + n\beta_\ell^\theta\frac{D^s\theta^\ell}{Dt}\right] + \rho^{\ell R}n\frac{D^sS_\ell}{Dt} + div(\rho^{\ell R}\boldsymbol{v}_\ell^D) = \hat{\rho}^\ell. \tag{5.63}$$

Now examining the balance of mass for the gas phase ($\alpha = g$), several assumptions need to be made. The first assumes that the gas acts as ideal. Therefore, the gas density can be written as

$$\rho^{gR} = \frac{p_g M_g}{\theta^g R} \tag{5.64}$$

where p_g is the gas pressure, M_g is the molar mass of the gas, θ^g is the temperature of the gas, and R is the ideal gas constant. Applying this assumption allows one to write the real density of gas as

$$\frac{D^g\rho^{gR}}{Dt} = \rho^{gR}\left[\frac{1}{p_g}\frac{D^gp_g}{Dt} - \frac{1}{\theta^g}\frac{D^g\theta^g}{Dt}\right]. \tag{5.65}$$

Combining equations 5.65 and 5.43 with $\alpha = g$ gives

$$\frac{D^gn^g}{Dt} + n^gdiv\boldsymbol{v}_g + n^g\left[\frac{1}{p_g}\frac{D^gp_g}{Dt} - \frac{1}{\theta^g}\frac{D^g\theta^g}{Dt}\right] = \frac{\hat{\rho}^g}{\rho^{gR}}. \tag{5.66}$$

Moving the material time derivatives in equation 5.66 to the solid reference frame and applying the definition of saturation (Eqn. 5.11) gives

$$
\begin{aligned}
n\frac{D^s S_g}{Dt} + S_g\frac{D^s n}{Dt} &+ \left[S_g grad(n) + n grad(S_g)\right] \cdot \tilde{\boldsymbol{v}}_g + S_g n div\boldsymbol{v}_s \\
+S_g n \left[\frac{1}{p_g}\left(\frac{D^s p_g}{Dt} + grad(p_g) \cdot \tilde{\boldsymbol{v}}_g\right) - \frac{1}{\theta^g}\left(\frac{D^s \theta^g}{Dt} + grad(\theta^g) \cdot \tilde{\boldsymbol{v}}_g\right)\right] &= \frac{\hat{\rho}^g}{\rho^{gR}},
\end{aligned}
\tag{5.67}
$$

which when combined with the solid balance of mass (Eqn. 5.53) and the definition of Darcy's velocity (Eqn. 5.61) gives

$$
\begin{aligned}
n\frac{D^s S_g}{Dt} + S_g\left[div(\boldsymbol{v}_s) - \beta_s^\theta(1-n)\frac{D^s \theta^s}{Dt}\right] + div\boldsymbol{v}_g^D - S_g n\frac{1}{\theta^g}\frac{D^s \theta^g}{Dt} \\
+ \frac{n^g}{p_g}\frac{D^s p_g}{Dt} + \frac{1}{p_g}grad(p_g) \cdot \boldsymbol{v}_g^D - \frac{1}{\theta^g}grad\theta^g \cdot \boldsymbol{v}_g^D = \frac{\hat{\rho}^g}{\rho^{gR}}.
\end{aligned}
\tag{5.68}
$$

Applying the chain rule on $div(\rho^{gR}\boldsymbol{v}_g^D)$ gives

$$
div(\rho^{gR}\boldsymbol{v}_g^D) = \rho^{gR}div(\boldsymbol{v}_g^D) - \frac{\rho^{gR}}{\theta^g}grad(\theta^g) \cdot div(\rho^{gR}\boldsymbol{v}_g^D) + \frac{\rho^{gR}}{p_g}grad(p_g) \cdot div(\rho^{gR}\boldsymbol{v}_g^D).
\tag{5.69}
$$

From the ideal gas law (Eqn. 5.64) it is seen that

$$
nS_g\frac{D^s \rho^{gR}}{Dt} = -S_g\frac{n}{\theta^g}\frac{D^s \theta^s}{Dt} + \frac{n^g}{p_g}\frac{D^s p_g}{Dt}
\tag{5.70}
$$

which when plugged into equation 5.68 and multiplying be ρ^{gR} gives

$$
\rho^{gR}S_g div\boldsymbol{v}_s - \rho^{gR}S_g\beta_s^\theta(1-n)\frac{D^s \theta^s}{Dt} + n\rho^{gR}\frac{D^s S_g}{Dt} + nS_g\frac{D^s \rho^{gR}}{Dt} + div(\rho^{gR}\boldsymbol{v}_g^D) = \hat{\rho}^g.
\tag{5.71}
$$

Assuming that $\hat{\rho}^g = -\hat{\rho}^\ell$ and that the temperature is the same in all three phases ($\theta = \theta^\alpha$) allows for the combination of the total balance of mass,

$$(S_g\rho^{gR} + S_\ell\rho^{\ell R})div\boldsymbol{v}_s - \left[(1-n)\left[\rho^{\ell R}S_\ell + \rho^{gR}S_g\right] + n\rho^{\ell R}S_\ell\beta_\ell^\theta\right]\frac{D^s\theta}{Dt}$$
$$+div(\rho^{\ell R}\boldsymbol{v}_\ell^D + \rho^{gR}\boldsymbol{v}_g^D) + \rho^{\ell R}n\frac{D^sS_\ell}{Dt} + n\rho^{gR}\frac{D^sS_g}{Dt} + nS_g\frac{D^s\rho^{gR}}{Dt} \quad (5.72)$$
$$+\frac{\rho^{\ell R}nS_\ell}{K_{bulk}^\ell}\frac{D^sp_\ell}{Dt} + \frac{\rho^{\ell R}}{K_{bulk}^\ell}grad(p_\ell)\cdot\boldsymbol{v}_\ell^D = 0.$$

Lastly, the combined balance of mass must be put back in terms of the reference solid configuration. It is useful to remember that [121],

$$div\boldsymbol{v}_s = \frac{1}{J_s}\frac{D^sJ_s}{Dt} \quad (5.73)$$

and

$$div(\bullet) = \frac{\partial(\bullet)}{\partial\boldsymbol{x}} = \frac{\partial(\bullet)}{\partial\boldsymbol{X}_s}\frac{\partial\boldsymbol{X}_s}{\partial\boldsymbol{x}} = GRAD(\bullet) : \boldsymbol{F}_s^{-T}. \quad (5.74)$$

Applying 5.73 and 5.74 the final balance of mass for the combined mixture in the solid reference configuration, B_0^s, is

$$(S_\ell\rho^{\ell R} + S_g\rho^{gR})\frac{D^sJ_s}{Dt} - J_s\left[(1-n)\left[\rho^{\ell R}S_\ell + \rho^{gR}S_g\right] + n\rho^{\ell R}S_\ell\beta_\ell^\theta\right]\frac{D^s\theta}{Dt}$$
$$+J_sGRAD(\rho^{\ell R}\boldsymbol{v}_\ell^D + \rho^{gR}\boldsymbol{v}_g^D) : \boldsymbol{F}_s^{-T} + J_s\left[\rho^{\ell R}n\frac{D^sS_\ell}{Dt} + n\rho^{gR}\frac{D^sS_g}{Dt} + nS_g\frac{D^s\rho^{gR}}{Dt}\right] \quad (5.75)$$
$$+\frac{\rho^{\ell R}JnS_\ell}{K_{bulk}^\ell}\frac{D^sp_\ell}{Dt} + \frac{J\rho^{\ell R}}{K_{bulk}^\ell}GRAD(p_\ell)\cdot\boldsymbol{F}_s^{-T}\cdot\boldsymbol{v}_\ell^D = 0,$$

where Darcy's velocity in the reference configuration is defined as

$$\boldsymbol{v}_f^D = -\boldsymbol{K}\frac{\partial p_f}{\boldsymbol{X}_s} : \boldsymbol{F}^{-T}, \quad (5.76)$$

where $\boldsymbol{K}$ is the permeability tensor of the fluid.

5.3.2 Balance of Linear Momentum

The balance of linear momentum for the α phase can be written as [79]

$$\frac{D^\alpha \boldsymbol{L}^\alpha}{Dt} = \int_B \rho^\alpha \boldsymbol{b}^\alpha dv + \int_{\partial B_u} \boldsymbol{t}^\alpha da + \int_B \boldsymbol{h}^\alpha dv \tag{5.77}$$

where $\frac{D^\alpha \boldsymbol{L}^\alpha}{Dt}$ is the time derivative of linear momentum with respect to the α phase, $\boldsymbol{b}^\alpha$ is the body force, $\boldsymbol{t}^\alpha$ is the per mass traction and $\boldsymbol{h}^\alpha$ is the drag forces of all other phases acting on the α phase. Applying the divergence theorem gives

$$\frac{D^\alpha \boldsymbol{L}^\alpha}{Dt} = \int_B \rho^\alpha \boldsymbol{b}^\alpha dv + \int_B div \boldsymbol{\sigma}^\alpha dv + \int_B \boldsymbol{h}^\alpha dv \tag{5.78}$$

with $\boldsymbol{\sigma}^\alpha$ representing the Cauchy stress in the α phase. Applying the definition provided be de Boer[79] the linear momentum of the α phase, $\boldsymbol{L}^\alpha(t)$, is

$$\boldsymbol{L}^\alpha(t) = \int_B \rho^\alpha(\boldsymbol{x}, t)\boldsymbol{v}_\alpha(\boldsymbol{x}, t)dv. \tag{5.79}$$

Moving equation 5.79 to the α reference frame allows one to bring the material time derivative inside the integral which, with the chain rule, yields

$$\frac{D^\alpha \boldsymbol{L}^\alpha}{Dt} = \int_{B_0^\alpha} \left[\frac{D^\alpha(J_\alpha \rho^\alpha)}{Dt} \boldsymbol{v}_\alpha + \rho^\alpha J_\alpha \frac{D^\alpha \boldsymbol{v}_\alpha}{Dt} \right] dV_\alpha. \tag{5.80}$$

Substituting the definitions of acceleration (Eqn. 5.28) and equation 5.39 gives the time change of linear momentum with respect to the α phase to be

$$\frac{D^\alpha \boldsymbol{L}^\alpha}{Dt} = \int_{B_0^\alpha} \left[J_\alpha \hat{\rho}^\alpha \boldsymbol{v}_\alpha + \rho^\alpha \boldsymbol{a}_\alpha \right] dV_\alpha \tag{5.81}$$

or in the current configuration

$$\frac{D^\alpha \boldsymbol{L}^\alpha}{Dt} = \int_B \left[\hat{\rho}^\alpha \boldsymbol{v}_\alpha + \rho^\alpha \boldsymbol{a}_\alpha \right] dv, \tag{5.82}$$

where J_α is the volumetric deformation of the α phase, $\hat{\rho}^\alpha \boldsymbol{v}_\alpha$ is the change in momentum due to a gain or loss of mass, and $\rho^\alpha \boldsymbol{a}_\alpha$ provides the change in linear momentum due to changing velocity. Combining equations 5.78 and 5.82 and localizing yields

$$\hat{\rho}^\alpha \boldsymbol{v}_\alpha + \rho^\alpha \boldsymbol{a}_\alpha = div(\boldsymbol{\sigma}^\alpha + \rho \boldsymbol{b}^\alpha + \boldsymbol{h}^\alpha). \tag{5.83}$$

To represent the total mixture stress, $\boldsymbol{\sigma}$, the effective stress priciple first presented by Bishop and Blight [132] will be used. The principle states that the total stress, $\boldsymbol{\sigma}$, can be represented by the sum of the partial stress in the solid skeleton, $\boldsymbol{\sigma}'$, and the pressures in the liquid and gas phases, p_ℓ and p_g, respectively. Thus,

$$\sum_{\alpha=s,\ell,g} \boldsymbol{\sigma}^\alpha = \boldsymbol{\sigma} \tag{5.84}$$

and

$$\boldsymbol{\sigma} = \boldsymbol{\sigma}' - \big(p_\ell \chi + p_g(1-\chi)\big)\boldsymbol{I} \tag{5.85}$$

where χ is the effective stress parameter which represents the ratio of the total pore fluid stress provided by each of the liquid and gas phases. This is often taken to be equal to the liquid saturation, S_ℓ[103]. Combining 5.84 and 5.83 yields

$$div(\boldsymbol{\sigma}) + \rho^s \boldsymbol{b}^s + \rho^\ell \boldsymbol{b}^\ell + \rho^g \boldsymbol{b}^g + \boldsymbol{h}^s + \boldsymbol{h}^\ell + \boldsymbol{h}^g = \hat{\rho}^s \boldsymbol{v}_s + \hat{\rho}^\ell \boldsymbol{v}_\ell + \hat{\rho}^g \boldsymbol{v}_g + \rho^s \boldsymbol{a}_s + \rho^\ell \boldsymbol{a}_\ell + + \rho^g \boldsymbol{a}_g. \tag{5.86}$$

Recalling the definition of the effective or combined mixture mass (Eqn. 5.8) and assuming the acceleration of each phase is equal, e.g.,

$$\boldsymbol{a} = \boldsymbol{a}_\alpha, \tag{5.87}$$

assuming gravity is the only body force

$$\boldsymbol{b}^\alpha = \boldsymbol{g}, \tag{5.88}$$

and recognizing that the drag body forces must cancel,

$$\sum_{\alpha=s,\ell,g} \hat{\boldsymbol{h}}^\alpha = 0, \tag{5.89}$$

allows for the local balance of mass in the solid reference configuration to be written as

$$DIV_s(\boldsymbol{P}^s) + J_s\rho^{eff}\boldsymbol{g} = J_s\rho^{eff}\boldsymbol{a} \tag{5.90}$$

where $\boldsymbol{P}^s$ represents the total first Piola-Krchoff stress of the mixture with respect to the solid reference configuration defined by

$$\boldsymbol{P}^s = J_s\boldsymbol{\sigma}\boldsymbol{F}_s^{-1}. \tag{5.91}$$

Substituting 5.85 for the $\boldsymbol{\sigma}$ in equation 5.91 gives

$$\boldsymbol{P}^s = \boldsymbol{P}'_s - J_s\big(\big(p_\ell\chi + p_g(1-\chi)\big)\big)\boldsymbol{F}_s^{-1} \tag{5.92}$$

where $\boldsymbol{P}'_s$ is the effective first Piola-Kirchoff stress defined as

$$\boldsymbol{P}'_s = J_s\boldsymbol{\sigma}'_s\boldsymbol{F}_s^{-1}. \tag{5.93}$$

Recognizing the initial mixture mass ρ_0 is defined as

$$\rho_0 = J_s\rho^{eff} \tag{5.94}$$

the final balance of linear momentum in the solid reference configuratoin (B_0^s) is

$$DIV_s\Big[\boldsymbol{P}_s - J_s\big[p_\ell\chi + p_g(1-\chi)\big]\boldsymbol{F}_s^{-1}\Big] + \rho_0\boldsymbol{g} = \rho_0\boldsymbol{a}. \tag{5.95}$$

5.3.3 Balance of Energy

The first law of thermodynamics provides the balance of energy of each phase in the mixture. It states that the change in time of the internal energy of the mixture with respect to the α phase, $\frac{D^\alpha E^\alpha}{Dt}$, must be equal to the sum of the power acting on the α phase from external forces, P^α_{input}, the heat input to or removed from the the α phase, Q^α_{input}, and the power supplied to the α phase by all other phases, $\bar{E}^\alpha$, e.g.

$$\frac{D^\alpha E^\alpha}{Dt} = P^\alpha_{input} + Q^\alpha_{input} + \bar{E}^\alpha \tag{5.96}$$

where E^α is the total internal energy of the α phase. Examining the time change of total internal energy, $\frac{D^\alpha E^\alpha}{Dt}$, of a body in the current configuration(B) gives

$$\frac{D^\alpha E^\alpha}{Dt} = \frac{D^\alpha}{Dt} \left[\int_B \left(\frac{1}{2}\rho^\alpha \boldsymbol{v}_\alpha \cdot \boldsymbol{v}_\alpha + \rho^\alpha e^\alpha \right) dv \right] \tag{5.97}$$

where $\frac{1}{2}\rho^\alpha \boldsymbol{v}_\alpha \cdot \boldsymbol{v}_\alpha$ represents the kinetic energy of the α phase and e^α is the internal energy of the α phase per unit mass. Moving 5.97 to the solid reference configuration allows for the material time derivative to be brought inside the integral,

$$\frac{D^\alpha E^\alpha}{Dt} = \int_{B_0^s} \frac{D^\alpha}{Dt} \left[\left(\frac{1}{2}\rho^\alpha \boldsymbol{v}_\alpha \cdot \boldsymbol{v}_\alpha + \rho^\alpha e^\alpha \right) J_s \right] dV_s. \tag{5.98}$$

Applying the chain rule to equation 5.98 gives

$$\begin{aligned}
\frac{D^\alpha E^\alpha}{Dt} = \int_{B_0^s} & \left[\frac{D^\alpha \rho^\alpha}{Dt} \frac{1}{2} \boldsymbol{v}_\alpha \cdot \boldsymbol{v}_\alpha J_s + \frac{1}{2} \left[2\rho^\alpha \frac{D^\alpha \boldsymbol{v}_\alpha}{Dt} \cdot \boldsymbol{v}_\alpha J_s \right] \right. \\
& \left. + \frac{1}{2}\rho^\alpha \boldsymbol{v}_\alpha \cdot \boldsymbol{v}_\alpha \frac{D^\alpha J_s}{Dt} + \frac{D^\alpha \rho^\alpha}{Dt} e^\alpha J_s + + \rho^\alpha \frac{D^\alpha e^\alpha}{Dt} J_s + \rho^\alpha e^\alpha \frac{D^\alpha J_s}{Dt} \right] dV_s.
\end{aligned} \tag{5.99}$$

which can be simplified to

$$\frac{D^\alpha E^\alpha}{Dt} = \int_{B_0^s} J_s \left[\frac{D^\alpha \rho^\alpha}{Dt} \left[\frac{1}{2} \boldsymbol{v}_\alpha \cdot \boldsymbol{v}_\alpha \right] + \rho^\alpha \frac{D^\alpha \boldsymbol{v}_\alpha}{Dt} \cdot \boldsymbol{v}_\alpha \right.$$
$$\left. + \rho^\alpha \frac{D^\alpha e^\alpha}{Dt} + \rho^\alpha div(\boldsymbol{v}_\alpha) \left[e^\alpha + \frac{1}{2} \boldsymbol{v}_\alpha \cdot \boldsymbol{v}_\alpha \right] dV_s. \right.$$

(5.100)

Substituting the balance of mass (Eqn. 5.41) for $\rho^\alpha J_s div(\boldsymbol{v_s})$ gives

$$\frac{D^\alpha E^\alpha}{Dt} = \int_{B_0^s} J_s \left[\frac{D^\alpha \rho^\alpha}{Dt} \left[\frac{1}{2} \boldsymbol{v}_\alpha \cdot \boldsymbol{v}_\alpha \right] + \rho^\alpha \frac{D^\alpha \boldsymbol{v}_\alpha}{Dt} \cdot \boldsymbol{v}_\alpha \right.$$
$$\left. + \rho^\alpha \frac{D^\alpha e^\alpha}{Dt} + \left(\hat{\rho}^\alpha - \frac{D^\alpha \rho^\alpha}{Dt} \right) \left[e^\alpha + \frac{1}{2} \boldsymbol{v}_\alpha \cdot \boldsymbol{v}_\alpha \right] dV_s, \right.$$

(5.101)

which can be reduced to

$$\frac{D^\alpha E^\alpha}{Dt} = \int_{B_0^s} J_s \left[\rho^\alpha \frac{D^\alpha \boldsymbol{v}_\alpha}{Dt} \cdot \boldsymbol{v}_\alpha + \rho^\alpha \frac{D^\alpha e^\alpha}{Dt} + \hat{\rho}^\alpha \left[e^\alpha + \frac{1}{2} \boldsymbol{v}_\alpha \cdot \boldsymbol{v}_\alpha \right] \right] dV_s.$$

(5.102)

Moving 5.102 to the current configuration gives the final form for the $\frac{D^\alpha E^\alpha}{Dt}$ term,

$$\frac{D^\alpha E^\alpha}{Dt} = \int_B \left[\rho^\alpha \frac{D^\alpha \boldsymbol{v}_\alpha}{Dt} \cdot \boldsymbol{v}_\alpha + \rho^\alpha \frac{D^\alpha e^\alpha}{Dt} + \hat{\rho}^\alpha \left[e^\alpha + \frac{1}{2} \boldsymbol{v}_\alpha \cdot \boldsymbol{v}_\alpha \right] \right] dv.$$

(5.103)

The power imparted on the α phase by external forces is represented as

$$P_{input}^\alpha = \int_B \boldsymbol{v}_\alpha \cdot (\rho \boldsymbol{b}^\alpha) dv + \int_{\partial B_u} \boldsymbol{v}_\alpha \cdot \boldsymbol{t}^\alpha da$$

(5.104)

where the first term is the dot product of the velocity, $\boldsymbol{v}_\alpha$, and the linear momentum of the body force, $\rho^\alpha \boldsymbol{b}^\alpha$, within body, B, and the second term is the power acting on the α phase of the externally applied forces or traction, $\boldsymbol{t}$, on the surface, ∂B. Application of the divergence theorem and chain rule on the power term yields,

$$P_{input}^\alpha = \int_B \boldsymbol{v}_\alpha \cdot (\rho^\alpha \boldsymbol{b}^\alpha) dv + \int_B div(\boldsymbol{v}_\alpha) : \boldsymbol{\sigma}^\alpha dv + \int_B div(\boldsymbol{\sigma}^\alpha) \cdot \boldsymbol{v}_\alpha dv.$$

(5.105)

Substituting the balance of linear momentum (Eqn. 5.83) into equation 5.105 gives

$$P^\alpha_{input} = \int_B \left(\rho^\alpha \boldsymbol{v}_\alpha \cdot \boldsymbol{a}_\alpha + \hat{\rho}^\alpha \boldsymbol{v}_\alpha \cdot \boldsymbol{v}_\alpha - \boldsymbol{v}_\alpha \cdot \boldsymbol{h} \right) dv + \int_B \boldsymbol{\ell}_\alpha : \boldsymbol{\sigma}^\alpha dv \qquad (5.106)$$

where $\boldsymbol{\ell}_\alpha$ is the spatial velocity gradient defined in equation 5.31. The first integral, represents the power acting acting on the α phase due to linear momentum and the second term represents the stress-power of the α phase. The heat input, Q^α_{input}, for the α phase consists of a source-sink term, r^α, representing heat lost or gained within body, B, and a normal flux term, $\boldsymbol{q}_\theta \cdot \boldsymbol{n}$, representing the heat lost or gained through the surface ∂B_q,

$$Q^\alpha_{input} = \int_B \rho^\alpha r^\alpha dv - \int_{\partial B_q} \boldsymbol{q}^\alpha_\theta \cdot \boldsymbol{n} da. \qquad (5.107)$$

Lastly, the power of each phase acting on the α phase can be written as

$$\bar{E}^\alpha = \int_B \hat{e}^\alpha dv \qquad (5.108)$$

where $\hat{e}^\alpha$ is the per unit volume power of all other phases acting on the α phase. Substituting equations 5.103, 5.106, 5.107, 5.108 into equation 5.96, and applying the divergence theorem gives the expanded balance of energy for the α phase,

$$\int_B \left[\rho^\alpha \frac{D^\alpha \boldsymbol{v}_\alpha}{Dt} \cdot \boldsymbol{v}_\alpha + \rho^\alpha \frac{D^\alpha e^\alpha}{Dt} + \hat{\rho}^\alpha \left[e^\alpha + \frac{1}{2} \boldsymbol{v}_\alpha \cdot \boldsymbol{v}_\alpha \right] \right] dv$$
$$= \int_B \left(\rho \boldsymbol{v}_\alpha \cdot \boldsymbol{a}_\alpha + \hat{\rho}^\alpha \boldsymbol{v}_\alpha \cdot \boldsymbol{v}_\alpha - \boldsymbol{v}_\alpha \cdot \boldsymbol{h}^\alpha \right) dv \qquad (5.109)$$
$$+ \int_B \boldsymbol{\ell}_\alpha : \boldsymbol{\sigma}^\alpha dv + \int_B \left[\rho^\alpha r^\alpha - div \boldsymbol{q}^\alpha \right] dv + \int_B \hat{e}^\alpha dv.$$

Finally, localizing and simplifying equation 5.109 gives

$$\hat{\rho}^\alpha \left[\frac{1}{2} \boldsymbol{v}_\alpha \cdot \boldsymbol{v}_\alpha - e^\alpha \right] - \boldsymbol{v}_\alpha \cdot \boldsymbol{h}^\alpha + \hat{e}^\alpha = \rho^\alpha \frac{D^\alpha e^\alpha}{Dt} - \boldsymbol{\ell}_\alpha : \boldsymbol{\sigma}^\alpha + div(\boldsymbol{q}^\alpha_\theta) - \rho^\alpha r^\alpha. \qquad (5.110)$$

5.4　Closure of Theory

While the balance equations for the mixture have been laid out in Section 5.3, several constitutive equations must be used to develop a fully closed and solvable set of equations. In this section, the second law of thermodynamics will be used to motivate several constitutive equations. Additionally, equations providing the final links between gas pressure and temperature, suction and liquid saturation, and the final form of Darcy's law will be presented. Once established, these equations will be combined with the balance equations to produce the complete thermo-poromechanics (TPM) theory to be implemented via finite element (FE) analysis.

5.4.1　Second Law of Thermodynamics

The second law of thermodynamics states that the total entropy of the α phase must remain constant or increase over time. Thus,

$$\Gamma^\alpha(t) \geq 0 \tag{5.111}$$

where Γ^α is the total α phase entropy rate defined as

$$\Gamma^\alpha(t) = \frac{D^\alpha H^\alpha(t)}{Dt} - \tilde{Q}^\alpha(t) \tag{5.112}$$

where $H^\alpha(t)$ represents the internal entropy of the α phase and $\tilde{Q}^\alpha(t)$ the heat added or removed from the system in time, t. Furthermore, the internal entropy of the system, H^α, can be defined as [79]

$$H^\alpha = \int_B \rho^\alpha(\boldsymbol{x}, t)\eta^\alpha(\boldsymbol{x}, t)dv \tag{5.113}$$

where ρ^α is the mass density of the the α phase and η^α is the entropy per unit mass of the α phase. Now examining the change in internal entropy, $\frac{D^\alpha H^\alpha(t)}{Dt}$, one can write,

$$\frac{D^\alpha H^\alpha(t)}{Dt} = \frac{D^\alpha}{Dt}\int_B \rho^\alpha \eta^\alpha dv \tag{5.114}$$

or moving to the solid reference configuration

$$\frac{D^\alpha H^\alpha(t)}{Dt} = \frac{D^\alpha}{Dt}\int_{B_0^s} J_s \rho^\alpha \eta^\alpha dV_s. \tag{5.115}$$

This, again, allows for the material time derivative to be pulled inside the integral. Applying the chain rule to equation 5.115 and expanding the material time derivative of J_s gives

$$\frac{D^\alpha H^\alpha(t)}{Dt} = \int_{B_0^s} \left[J_s div(\boldsymbol{v}_s)\rho^\alpha \eta^\alpha + J_s \frac{D^\alpha \rho^\alpha}{Dt}\eta^\alpha + J_s \rho^\alpha \frac{D^\alpha \eta^\alpha}{Dt} \right] dV_s. \tag{5.116}$$

Mapping back to the current configuration and substituting the balance of mass (Eqn. 5.43) gives

$$\frac{D^\alpha H^\alpha(t)}{Dt} = \int_B \left[\left(\hat{\rho}^\alpha - \frac{D^\alpha \rho^\alpha}{Dt} \right)\eta^\alpha + \frac{D^\alpha \rho^\alpha}{Dt} + \rho^\alpha \frac{D^\alpha \eta^\alpha}{Dt} \right] dv \tag{5.117}$$

which simplifies to

$$\frac{D^\alpha H^\alpha(t)}{Dt} = \int_B \left[\hat{\rho}^\alpha \eta^\alpha + \rho^\alpha \frac{D^\alpha \eta^\alpha}{Dt} \right] dv. \tag{5.118}$$

Now examining the heat flux term, $\tilde{Q}^\alpha$, it can be seen that it can be defined as [79]

$$\tilde{Q}^\alpha(t) = \int_B \frac{1}{\theta^\alpha}\rho^\alpha r^\alpha dv - \int_{\partial B_q} \frac{1}{\theta^\alpha}\boldsymbol{q}_\theta^\alpha \cdot \boldsymbol{n} da \tag{5.119}$$

where r^α represents a per unit mass source/sink and $\boldsymbol{q}_\theta^\alpha \cdot \boldsymbol{n}$ represents the normal flux of the α phase through the boundary, ∂B_q. Applying the divergence theorem to 5.119 gives

$$\tilde{Q}^\alpha(t) = \int_B \frac{1}{\theta^\alpha}\rho^\alpha r^\alpha dv - \int_B div\left(\frac{1}{\theta^\alpha}\boldsymbol{q}_\theta^\alpha\right) dv \tag{5.120}$$

and the chain rule provides,

$$\tilde{Q}^\alpha(t) = \int_B \frac{1}{\theta^\alpha} \rho^\alpha r^\alpha dv - \int_B \left[-\frac{1}{\theta^\alpha \theta^\alpha} grad(\theta^\alpha) \cdot \boldsymbol{q}_\theta + \frac{1}{\theta^\alpha} div(\boldsymbol{q}_\theta^\alpha) \right] dv. \tag{5.121}$$

Thus, combining equations 5.118 and 5.121 with 5.112 and 5.111 gives

$$\int_B \left[\hat{\rho}^\alpha \eta^\alpha + \rho^\alpha \frac{D^\alpha \eta^\alpha}{Dt} \right] dv - \int_B \frac{1}{\theta^\alpha} \rho^\alpha r^\alpha dv + \int_B \left[-\frac{1}{\theta^\alpha \theta^\alpha} grad(\theta^\alpha) \cdot \boldsymbol{q}_\theta^\alpha + div(\boldsymbol{q}_\theta^\alpha) \right] dv \geq 0 \tag{5.122}$$

which when localized and simplified is

$$\hat{\rho}^\alpha \eta^\alpha \theta^\alpha + \theta^\alpha \rho^\alpha \frac{D^\alpha \eta^\alpha}{Dt} - \rho^\alpha r^\alpha - \frac{1}{\theta^\alpha} grad(\boldsymbol{q}_\theta^\alpha) + div(\boldsymbol{q}_\theta^\alpha) \geq 0. \tag{5.123}$$

5.4.2 Clausius-Duhem Inequality

To obtain a useful form of the second law of thermodynamics, the first and second laws will be combined to generate the Clausius-Duhem inequality which will provide the thermodynamic constraints guiding the final constitutive models. First, it is beneficial to define the Gibb's free energy, g^f, of a fluid as a function of the Helmholtz free energy, ψ^f, the fluid temperature, θ^f, and the fluid entropy per unit mass, η^α,

$$g^f = \psi^f - \theta^f \eta^f; f = g, \ell. \tag{5.124}$$

Thus, the Helmholtz free energy, ψ^f, and the internal energy, e^f, of the fluid can be expressed as

$$\psi^f = g^f + \theta^f \eta^f, \tag{5.125}$$

$$e^f = \psi^f - \frac{p_f}{\rho^{fR}} = g^f + \theta^f \eta^f - \frac{p_f}{\rho^{fR}}. \tag{5.126}$$

Examining the material time derivative of the fluid internal energy with respect to the fluid phase, $\frac{D^f e^f}{Dt}$, one can write,

$$\frac{D^f e^f}{Dt} = \frac{D^f g^f}{Dt} + \frac{D^f (\theta^f \eta^f)}{Dt} - \frac{D^f (\frac{p_f}{\rho^{fR}})}{Dt} \tag{5.127}$$

which is expanded via the chain rule to be

$$\frac{D^f e^f}{Dt} = \frac{D^f g^f}{Dt} + \theta^f \frac{D^f \eta^f}{Dt} + \eta^f \frac{D^f \theta^f}{Dt} - \frac{1}{\rho^{fR}} \frac{D^f p_f}{Dt} + \frac{p_f}{(\rho^{fR})^2} \frac{D^f \rho^{fR}}{Dt}. \tag{5.128}$$

Further examination of the $\frac{D^f \rho^{fR}}{Dt}$ term with equation 5.7 provides,

$$\frac{D^f \rho^{fR}}{Dt} = \frac{1}{n^f} \left[\frac{D^f \rho^f}{Dt} + \rho^{fR} \frac{D^f n^f}{Dt} \right], \tag{5.129}$$

where n^f is the fluid phase volume fraction. Substituting the balance of mass (Eqn. 5.43) into 5.129 gives

$$\frac{D^f \rho^{fR}}{Dt} = -\rho^{fR} div(\boldsymbol{v}_f) + \frac{\hat{\rho}^f}{n^f} - \frac{\rho^{fR}}{n^f} \frac{D^f n^f}{Dt}. \tag{5.130}$$

Multiplying equation 5.128 by the fluid density and combining it with equation 5.130 it becomes

$$\begin{aligned} \rho^f \frac{D^f e^f}{Dt} = \rho^f \frac{D^f g^f}{Dt} &+ \rho^f \theta^f \frac{D^f \eta^f}{Dt} + \rho^f \eta^f \frac{D^f \theta^f}{Dt} + \frac{\rho^f}{\rho^{fR}} \frac{D^f p_f}{Dt} \\ &- \frac{\rho^f p_f}{(\rho^{fR})^2} \left[\frac{\rho^{fR}}{n^f} \frac{D^f n^f}{Dt} + \rho^{fR} div(\boldsymbol{v}_f) - \frac{\hat{\rho}^f}{n^f} \right]. \end{aligned} \tag{5.131}$$

Through rearranging terms and simplifying, equation 5.131 becomes

$$\begin{aligned} \rho^f \theta^f \frac{D^f \eta^f}{Dt} = \rho^f \frac{D^f e^f}{Dt} &- \rho^f \frac{D^f g^f}{Dt} \\ -\rho^f \eta^f \frac{D^f \theta^f}{Dt} + n^f \frac{D^f p^f}{Dt} &- \frac{p_f}{\rho^{fR}} \hat{\rho}^f + n^f p_f div(\boldsymbol{v}_f) + p_f \frac{D^f n^f}{Dt}. \end{aligned} \tag{5.132}$$

Plugging equation 5.132 into 5.122 for $\rho^f \theta^f \frac{D^f \eta^f}{Dt}$ gives the expanded entropy inequality,

$$\theta^f \eta^f \hat{\rho}^f - \rho^f r^f - \frac{1}{\theta^f} grad(\theta^f) \cdot \boldsymbol{q}_\theta^f + div(\boldsymbol{q}_\theta^f) + \rho^f \frac{D^f e^f}{Dt} - \hat{\rho}^f e^f - \rho^f \eta^f \frac{D^f \theta^f}{Dt}$$
$$- \rho^f \frac{D^f g^f}{Dt} + n^f \frac{D^f p_f}{Dt} + n^f p_f div(\boldsymbol{v}_f) - \frac{p_f}{\rho^{fR}} \hat{\rho}^f + p_f \frac{D^f n^f}{Dt} \geq 0. \tag{5.133}$$

Plugging in the first law (Eqn. 5.110) for the $\rho^f \frac{D^f e^f}{Dt}$ term yields,

$$\theta^f \eta^f \hat{\rho}^f - \rho^f r^f - \frac{1}{\theta^f} grad(\theta^f) \cdot \boldsymbol{q}_\theta^f + div(\boldsymbol{q}_\theta^f) - \hat{\rho}^f e^f - \rho^f \eta^f \frac{D^f \theta^f}{Dt}$$
$$- \rho^f \frac{D^f g^f}{Dt} + n^f \frac{D^f p_f}{Dt} + n^f p_f div(\boldsymbol{v}_f) - \frac{p_f}{\rho^{fR}} \hat{\rho}^f + p_f \frac{D^f n^f}{Dt} + \boldsymbol{\ell}_f : \boldsymbol{\sigma}^f - div(\boldsymbol{q}_\theta^f) \tag{5.134}$$
$$+ \rho^f r^f + \hat{e}^f - \boldsymbol{v}_f \cdot \boldsymbol{h}^f + \hat{\rho}^f \left(\frac{1}{2} \boldsymbol{v}_f \cdot \boldsymbol{v}_f - e^f \right) \geq 0.$$

Now, examining the stress power term, $\boldsymbol{\ell}_f : \boldsymbol{\sigma}^f$ and neglecting fluid frictional effects it can be seen that,

$$\boldsymbol{\sigma}^f = n^f p_f \mathbf{1}, \tag{5.135}$$

meaning,

$$\boldsymbol{\ell}_f : \boldsymbol{\sigma}^f = -n^f p_f div(\boldsymbol{v}_f). \tag{5.136}$$

Introducing the definition of enthalpy of a fluid, H^f, as [79]

$$H^f = e^f + \frac{p_f}{\rho^{fR}}, \tag{5.137}$$

it can be written that

$$-\hat{\rho}^f e^f - \frac{p_f}{\rho^{fR}} \hat{\rho}^f = -H^f \hat{\rho}^f, \tag{5.138}$$

and

$$H^f = g^f + \eta^f \theta^f. \tag{5.139}$$

Therefore, the following terms in equation 5.134 become

$$\hat{\rho}^f \eta^f \theta^f = \hat{\rho}^f (H^f - g^f), \tag{5.140}$$

and

$$\hat{\rho}^f \eta^f \theta^f - \hat{\rho}^f e^f - \frac{p_f}{\rho^{fR}} \hat{\rho}^f = \hat{\rho}^f g^f. \tag{5.141}$$

Thermodynamic equilibrium is assumed meaning the free energy of the liquid and gas phases must be equal,

$$g^\ell = g^g. \tag{5.142}$$

Also, the phase transformation from liquid to gas or gas to liquid must be equal and opposite meaning

$$\hat{\rho}^\ell = -\hat{\rho}^g. \tag{5.143}$$

Thus, the combined Clausius-Duhem inequality for all fluid phases can be written as

$$\sum_{f=g,\ell} -\hat{\boldsymbol{h}}^f \cdot \boldsymbol{v}_f + \frac{1}{2}\hat{\rho}^f \boldsymbol{v}_f \cdot \boldsymbol{v}_f + \hat{e}^f - \rho^f \frac{D^f g^f}{Dt}$$
$$-\rho^f \eta^f \frac{D^f \theta^f}{Dt} + n^f \frac{D^f p_f}{Dt} + p_f \frac{D^f n^f}{Dt} - \frac{1}{\theta^f}\boldsymbol{q}_\theta^f \cdot grad(\theta^f) \geq 0, \tag{5.144}$$

where the material time derivative with respect to the α phase of the Gibb's free energy is

$$\frac{D^f g^f}{Dt} = \frac{\partial g^f}{\partial p_f}\frac{D^f p_f}{Dt} - \frac{\partial g^f}{\partial \theta^f}\frac{D^f \theta^f}{Dt}. \tag{5.145}$$

Now looking at the solid phase, the Helmholtz free energy of the solid is [121]

$$\psi^s = e^s - \theta^s \eta^s \tag{5.146}$$

and its material time derivative with respect to the solid phase, $\frac{D^s \psi^s}{Dt}$, is

$$\frac{D^s \psi^s}{Dt} = \frac{D^s e^s}{Dt} - \theta^s \frac{D^s \eta^s}{Dt} - \eta^s \frac{D^s \theta^s}{Dt}. \tag{5.147}$$

Plugging equation 5.147 into the balance of energy for a solid (Eqn. 5.110) and assuming the kinetic energy of the solid is negligible gives

$$\rho^s \theta^s \frac{D^s \eta^s}{Dt} = \boldsymbol{\ell}_s : \boldsymbol{\sigma}^s - \hat{\boldsymbol{h}}^s \cdot \boldsymbol{v}_s - div(\boldsymbol{q}_\theta^s) + \rho^s r^s + \hat{e}^s - \rho^s \eta^s \frac{D^s \theta^s}{Dt} - \rho^s \frac{D^s \psi^s}{Dt}. \tag{5.148}$$

From the effective stress principle (Eqn. 5.85) it is known

$$\boldsymbol{\sigma}^s = \boldsymbol{\sigma}' + \left[n^g - (1-\chi)p_g \right] \mathbf{1} + (n-\chi)p_\ell \mathbf{1}, \tag{5.149}$$

which substituting into the $\boldsymbol{\ell}_s : \boldsymbol{\sigma}^s$ term gives

$$\boldsymbol{\ell}_s : \boldsymbol{\sigma}^s = \boldsymbol{\ell}_s : \boldsymbol{\sigma}' + \boldsymbol{\ell}_s : \left[\left(n^g - (1-\chi) \right) p_g \mathbf{1} + (n-\chi)p_\ell \mathbf{1} \right]. \tag{5.150}$$

Looking more closely at the $\boldsymbol{\ell}_s : \boldsymbol{\sigma}'$ term and using index notation for clarity one can show through symmetry that

$$\ell_{ij}\sigma'_{ij} = \frac{1}{2}(\ell_{ij}\sigma'_{ij} + \ell_{ji}\sigma'_{ji}), \tag{5.151}$$

and

$$\frac{1}{2}(\ell_{ij}\sigma'_{ij} + \ell_{ji}\sigma'_{ji}) = d_{ij}\sigma'_{ij} \tag{5.152}$$

where d_{ij} is the deformation rate tensor of the solid phase. Now recalling that

$$\ell_{ij(s)} = \dot{F}_{iI(s)}F^{-1}_{Ij(s)} \tag{5.153}$$

and

$$\sigma'_{ij} = \frac{1}{J_s}F_{iI(s)}S'_{IJ}F_{Jj(s)} \tag{5.154}$$

it can be shown that

$$d_{ij(s)}\sigma'_{ij(s)} = \frac{1}{2}\left(\dot{F}_{iI(s)}F^{-1}_{Ij(s)} + \dot{F}_{jI(s)}F^{-1}_{Ii} \right)\frac{1}{J_s}F_{iA(s)}S'_{AB}F_{Bj(s)} \tag{5.155}$$

which simplifies to

$$d_{ij(s)}\sigma'_{ij(s)} = \frac{1}{2J_s}\dot{C}_{IJ(s)}S'_{IJ}.$$
(5.156)

Now examining the second part of equation 5.150 which, using the definition of $\boldsymbol{\ell}_\alpha$ (Eqn. 5.31) can be written as

$$\boldsymbol{\ell}_s : \left[\left(n^g - (1-\chi)\right)p_g\mathbf{1} + (n-\chi)\mathbf{1}\right] = div(\boldsymbol{v}_s) : \left[\left(n^g - (1-\chi)\right)p_g\mathbf{1} + (n-\chi)\mathbf{1}\right].$$
(5.157)

Combining equations 5.151, 5.154, and 5.157 gives

$$\boldsymbol{\ell}_s : \boldsymbol{\sigma}^s = \boldsymbol{d}_s : \boldsymbol{\sigma}' + div(\boldsymbol{v}_s) : \left[\left(n^g - (1-\chi)\right)p_g\mathbf{1} + (n-\chi)\mathbf{1}\right].$$
(5.158)

From equation 5.118 it is known that the entropy inequality of the solid phase is

$$\rho^s\theta^s\frac{D^s\eta^s}{Dt} - \rho^s r^s + div(\boldsymbol{q}_\theta^s) - \frac{1}{\theta^s} \cdot grad(\theta^s) \geq 0.$$
(5.159)

Substituting the solid balance of energy (Eqn. 5.148) and equation 5.158 into the solid entropy inequality (Eqn. 5.159) gives

$$\boldsymbol{d}_s : \boldsymbol{\sigma}' + div(\boldsymbol{v}_s) : \left[\left(n^g - (1-\chi)\right)p_g\mathbf{1}\right] + (n-\chi)\mathbf{1}\right] - \hat{\boldsymbol{h}}^s \cdot \boldsymbol{v}_s - div(\boldsymbol{q}_\theta^s) + \rho^s r^s - \hat{e}^s$$
$$-\rho^s\eta^s\frac{D^s\theta^s}{Dt} - \rho^s\frac{D^s\psi^s}{Dt} + div(\boldsymbol{q}_\theta^s) - \rho^s r^s - \frac{1}{\theta^s}\boldsymbol{q}_\theta^s \cdot grad(\theta^s) \geq 0.$$
(5.160)

Examining for a moment the inter-phase linear momentum terms, $\hat{\boldsymbol{h}}^\alpha$, from the balance of linear momentum (Eqn. 5.83) the gas and liquid inter-phase linear momentum terms are

$$\hat{\boldsymbol{h}}^g = div(np_g) + \rho^g(\boldsymbol{a}_g - \boldsymbol{b}^g) + \hat{\rho}^g\boldsymbol{v}_g$$
(5.161)

and

$$\hat{\boldsymbol{h}}^\ell = div(np_\ell) + \rho^\ell(\boldsymbol{a}_\ell - \boldsymbol{b}^\ell) + \hat{\rho}^\ell\boldsymbol{v}_\ell.$$
(5.162)

Using equation 5.89 it must follow that

$$\hat{\boldsymbol{h}}^s = -\hat{\boldsymbol{h}}^g - \hat{\boldsymbol{h}}^\ell, \tag{5.163}$$

therefore,

$$\sum_{\alpha=s,\ell,g} \hat{\boldsymbol{h}}^\alpha \cdot \boldsymbol{v}_\alpha = \hat{\boldsymbol{h}}^\ell \cdot \boldsymbol{v}_\ell + \hat{\boldsymbol{h}}^g \cdot \boldsymbol{v}_g - (\hat{\boldsymbol{h}}^\ell + \hat{\boldsymbol{h}}^g) \cdot \boldsymbol{v}_s. \tag{5.164}$$

Defining the relative velocity of the fluid with respect to the solid as

$$\boldsymbol{v}_f - \boldsymbol{v}_s = \tilde{\boldsymbol{v}}_f \tag{5.165}$$

and substituting equations 5.161 and 5.162 into equation 5.163, it is written as

$$
\begin{aligned}
\sum_{\alpha=s,\ell,g} \hat{\boldsymbol{h}}^\alpha \cdot \boldsymbol{v}_\alpha &= \left[p_\ell grad(n^\ell) + n^\ell grad(p_\ell) + p^\ell(\boldsymbol{a}_\ell + \boldsymbol{b}^\ell) + \hat{\rho}^\ell \boldsymbol{v}_\ell \right] \cdot \tilde{\boldsymbol{v}}_\ell \\
&+ \left[p_g grad(n^g) + n^g grad(p_g) + p^g(\boldsymbol{a}_g + \boldsymbol{b}^g) + \hat{\rho}^g \boldsymbol{v}_g \right] \cdot \tilde{\boldsymbol{v}}_g
\end{aligned}
\tag{5.166}
$$

which can be expanded with the chain rule and definition of Darcy's velocity (Eqn. 5.61) to

$$
\begin{aligned}
\sum_{\alpha=s,\ell,g} \hat{\boldsymbol{h}}^\alpha \cdot \boldsymbol{v}_\alpha &= \boldsymbol{v}_\ell^D \cdot \left[grad(p_\ell) + \rho^{\ell R}(\boldsymbol{a}_\ell - \boldsymbol{b}^\ell) \right] + p_\ell \tilde{\boldsymbol{v}}_\ell \cdot grad(n^\ell) + \hat{\rho}^\ell \boldsymbol{v}_\ell \cdot \boldsymbol{v}_\ell \\
&+ \boldsymbol{v}_g^D \cdot \left[grad(p_g) + \rho^{gR}(\boldsymbol{a}_g - \boldsymbol{b}^g) \right] + p_g \tilde{\boldsymbol{v}}_g \cdot grad(n^g) + \hat{\rho}^g \boldsymbol{v}_g \cdot \boldsymbol{v}_g.
\end{aligned}
\tag{5.167}
$$

Now, through the combination of 5.43, 5.144, 5.160 and 5.167 the total three-phase entropy inequality can be written as

$$
\frac{1}{2}\hat{\rho}^\ell \boldsymbol{v}_\ell \cdot \boldsymbol{v}_\ell + \frac{1}{2}\hat{\rho}^\ell \boldsymbol{v}_g \cdot \boldsymbol{v}_g - \rho^\ell \left[\frac{\partial g^\ell}{\partial p_\ell} \frac{D^\ell p_\ell}{Dt} - \frac{\partial g^\ell}{\partial \theta^\ell} \frac{D^\ell \theta^\ell}{Dt} \right] - \rho^g \left[\frac{\partial g^g}{\partial p_g} \frac{D^\ell p_g}{Dt} - \frac{\partial g^g}{\partial \theta^g} \frac{D^g \theta^g}{Dt} \right]
$$

$$
-\rho^\ell n^\ell \frac{D^\ell \theta^\ell}{Dt} - \rho^g n^g \frac{D^g \theta^g}{Dt} + n^\ell \frac{D^\ell p_\ell}{Dt} + n^g \frac{D^g p_g}{Dt} + p_\ell \frac{D^\ell n^\ell}{Dt} + p_g \frac{D^g n^g}{Dt} + \frac{1}{J_s} \frac{D^s \boldsymbol{C}_s}{Dt} : \boldsymbol{S}'_s
$$

$$
+ \left[[n^g - (1-\chi)]p_g + (1-\chi)p_\ell \right] \left[\beta_s^\theta \frac{D^s \theta^s}{Dt} - \frac{1}{n^s} \frac{D^s n^s}{Dt} \right] - \rho^s \eta^s \frac{D^s \theta^s}{Dt} - \rho^s \frac{D^s \psi^s}{Dt} \quad (5.168)
$$

$$
- \frac{1}{\theta^\ell} \boldsymbol{q}_\theta^\ell \cdot grad(\theta^\ell) - \frac{1}{\theta^g} \boldsymbol{q}_\theta^g \cdot grad(\theta^g) - \frac{1}{\theta^s} \boldsymbol{q}_\theta^s \cdot grad(\theta^s)
$$

$$
- \boldsymbol{v}_\ell^D \cdot \left[grad(p_\ell) + \rho^{\ell R}(\boldsymbol{a}_\ell - \boldsymbol{b}^\ell) \right] + p_\ell \tilde{\boldsymbol{v}}_\ell \cdot grad(n^\ell) + \frac{1}{2}\hat{\rho}^\ell \boldsymbol{v}_\ell \cdot \boldsymbol{v}_\ell
$$

$$
- \boldsymbol{v}_g^D \cdot \left[grad(p_g) + \rho^{gR}(\boldsymbol{a}_g - \boldsymbol{b}^g) \right] + p_g \tilde{\boldsymbol{v}}_g \cdot grad(n^g) + \frac{1}{2}\hat{\rho}^g \boldsymbol{v}_g \cdot \boldsymbol{v}_g \geq 0.
$$

Introducing the suction or capillary pressure, s, as

$$
s = p_g - p_\ell \tag{5.169}
$$

and using it with the definition of saturation (Eqn. 5.11) and equation 5.55 allows one to write

$$
p_\ell \frac{D^\ell n^\ell}{Dt} + p_g \frac{D^g n^g}{Dt} = p_\ell \frac{D^s n^\ell}{Dt} + p_\ell grad(n^\ell) \cdot \tilde{\boldsymbol{v}}_\ell + p_g \frac{D^s n^g}{Dt} + p_\ell grad(n^g) \cdot \tilde{\boldsymbol{v}}_g \tag{5.170}
$$

as

$$
p_\ell \frac{D^\ell n^\ell}{Dt} + p_g \frac{D^g n^g}{Dt} = sn \frac{D^s S_\ell}{Dt} + \left(p_\ell S_\ell + p_g S_g \right) \frac{D^s n}{Dt} + p_\ell grad(n^\ell) \cdot \tilde{\boldsymbol{v}}_\ell + p_\ell grad(n^g) \cdot \tilde{\boldsymbol{v}}_g. \tag{5.171}
$$

Assuming $\chi = S_\ell$ [103], substituting equation 5.171 into equation 5.168 and canceling like terms yields

$$\frac{1}{2}\hat{\rho}^\ell \boldsymbol{v}_\ell \cdot \boldsymbol{v}_\ell + \frac{1}{2}\hat{\rho}^g \boldsymbol{v}_g \cdot \boldsymbol{v}_g - \hat{\rho}^\ell \boldsymbol{v}_\ell \cdot \tilde{\boldsymbol{v}}_\ell - \hat{\rho}^g \boldsymbol{v}_g \cdot \tilde{\boldsymbol{v}}_g$$

$$+\left[\left([n^g - (1-\chi)]p_g - (n^\ell - \chi)\right)\beta_s^\theta - \rho^s\eta^s - \rho^s\frac{\partial\psi^s}{\partial\theta}\right]\frac{D^s\theta^s}{Dt} + \rho^\ell\left[\frac{\partial g^\ell}{\partial\theta^\ell} - \eta^\ell\right]\frac{D^\ell\theta^\ell}{Dt}$$

$$+\rho^g\left[\frac{\partial g^g}{\partial\theta^g} - \eta^g\right]\frac{D^g\theta^g}{Dt} - \left[\rho^s\frac{\partial\psi^s}{\partial S_\ell} + ns\right]\frac{D^s S_\ell}{Dt} + \left[n^\ell - \rho^\ell\frac{\partial g^\ell}{\partial p_\ell}\right]\frac{D^\ell p_\ell}{Dt} + \left[n^g - \rho^g\frac{\partial g^g}{\partial p_g}\right]\frac{D^g p_g}{Dt}$$

$$-\boldsymbol{v}_\ell^D \cdot \left[grad(p_\ell) + \rho^{\ell R}(\boldsymbol{a}_\ell - \boldsymbol{b}^\ell)\right] - \boldsymbol{v}_g^D \cdot \left[grad(p_g) + \rho^{gR}(\boldsymbol{a}_g - \boldsymbol{b}^g)\right]$$

$$+\left[\frac{1}{2J_s}\boldsymbol{S}_s' - \rho^s\frac{\partial\psi^s}{\partial\boldsymbol{C}_s}\right] : \frac{D^s\boldsymbol{C}_s}{Dt} - \frac{1}{\theta^\ell}\boldsymbol{q}_\theta^\ell \cdot grad(\theta^\ell) - \frac{1}{\theta^g}\boldsymbol{q}_\theta^g \cdot grad(\theta^g) - \frac{1}{\theta^s}\boldsymbol{q}_\theta^s \cdot grad(\theta^s) \geq 0. \tag{5.172}$$

Using arguments presented by Coleman and Noll [127] along with Coussy [87] that $\frac{D^s\boldsymbol{C}_s}{Dt}$, $\frac{D^f p_f}{Dt}$, $\frac{D^s S_\ell}{Dt}$, and $\frac{D^\alpha\theta^\alpha}{Dt}$ are independent processes that can be varied separately. It is then necessary that the coefficient of each of those terms must be equal to zero. Thus, it is necessary each constitutive form satisfy the following constraints:

$$\frac{1}{J_s}\boldsymbol{S}_s' - \rho^s\frac{\partial\psi^s}{\partial\boldsymbol{C}_s} = 0, \tag{5.173}$$

$$\left([n^g - (1-\chi)]p_g - (n^\ell - \chi)\right)\beta_s^\theta - \rho^s\eta^s - \rho^s\frac{\partial\psi^s}{\partial\theta} = 0, \tag{5.174}$$

$$\rho^s\frac{\partial\psi^s}{\partial S_\ell} + ns = 0, \tag{5.175}$$

$$\eta^f + \frac{\partial g^f}{\partial\theta^f} = 0, \tag{5.176}$$

$$\frac{n^f}{\rho^f} - \frac{\partial g^f}{\partial p_f} = 0. \tag{5.177}$$

Thus, the following thermodynamics constraints can be drawn,

$$\rho^s\frac{\partial\psi^s}{\partial\boldsymbol{C}_s} = \frac{1}{J_s}\boldsymbol{S}_s', \tag{5.178}$$

$$\rho^s \eta^s = \left(\left[n^g - (1-\chi) \right] p_g - (n^\ell - \chi) \right) \beta_s^\theta - \rho^s \frac{\partial \psi^s}{\partial \theta}, \tag{5.179}$$

$$ns = -\rho^s \frac{\partial \psi^s}{\partial S_\ell}, \tag{5.180}$$

$$\eta^f = -\frac{\partial g^f}{\partial \theta^f}, \tag{5.181}$$

$$\frac{n^f}{\rho^f} = \frac{\partial g^f}{\partial p_f}. \tag{5.182}$$

Applying these constraints allows for equation 5.172 to be simplified to

$$\frac{1}{2}\hat{\rho}^\ell \boldsymbol{v}_\ell \cdot \boldsymbol{v}_\ell + \frac{1}{2}\hat{\rho}^g \boldsymbol{v}_g \cdot \boldsymbol{v}_g - \hat{\rho}^\ell \boldsymbol{v}_\ell \cdot \tilde{\boldsymbol{v}}_\ell - \hat{\rho}^g \boldsymbol{v}_g \cdot \tilde{\boldsymbol{v}}_g$$

$$-\boldsymbol{v}_\ell^D \cdot \left[grad(p_\ell) + \rho^{\ell R}(\boldsymbol{a}_\ell - \boldsymbol{b}^\ell) \right] - \boldsymbol{v}_g^D \cdot \left[grad(p_g) + \rho^{gR}(\boldsymbol{a}_g - \boldsymbol{b}^g) \right] \tag{5.183}$$

$$-\frac{1}{\theta^\ell}\boldsymbol{q}_\theta^\ell \cdot grad(\theta^\ell) - \frac{1}{\theta^g}\boldsymbol{q}_\theta^g \cdot grad(\theta^g) - \frac{1}{\theta^s}\boldsymbol{q}_\theta^s \cdot grad(\theta^s) \geq 0.$$

The preceding arguments will now be used to establish the final usable form of the balance of energy. Recognizing that Gibb's free energy of a fluid is a function of both pressure and time the material time derivative with respect to the fluid phase is

$$\frac{D^f g^f}{Dt} = \frac{\partial g^f}{\partial p_f}\frac{D^f p_f}{Dt} + \frac{\partial g^f}{\partial \theta^f}\frac{D^f \theta^f}{Dt}, \tag{5.184}$$

which can be combined with the definition of fluid internal energy (Eq. 5.127) to be

$$\rho^f \frac{D^f e^f}{Dt} = \left(\rho^f \frac{\partial g^f}{\partial p_f} - n \right)\frac{D^f p_f}{Dt} + \left(\rho^f \frac{\partial g^f}{\partial \theta^f} + \rho^f \eta^f \right)\frac{D^f \theta^f}{Dt}$$

$$+ \rho^f \theta^f \frac{D^f \eta^f}{Dt} + \frac{p_f}{\rho^{fR}}\hat{\rho}^f - n^f p_f div(\boldsymbol{v}_f) - p_f \frac{D^f n^f}{Dt}. \tag{5.185}$$

Plugging in equations 5.181 and 5.182 into 5.185 gives

$$\rho^f \frac{D^f e^f}{Dt} = \rho^f \theta^f \frac{D^f \eta^f}{Dt} + \frac{p_f}{\rho^{fR}}\hat{\rho}^f - n^g p_f div(\boldsymbol{v}_f) - p_f \frac{D^f n^f}{Dt}. \tag{5.186}$$

Now examining the internal energy of the solid skeleton it is seen from equation 5.147 that

$$\frac{D^s e^s}{Dt} = \frac{\partial \psi^s}{\partial \boldsymbol{C}_s}\frac{D^s \boldsymbol{C}_s}{Dt} + \frac{\partial \psi^s}{\partial \theta^s}\frac{D^s \theta^s}{Dt} + \frac{\partial \psi^s}{\partial S_\ell}\frac{D^s S_\ell}{Dt} + \theta^s\frac{D^s \eta^s}{Dt} + \eta^s\frac{D^s \theta^s}{Dt}. \tag{5.187}$$

Finally, substituting 5.158, 5.167, 5.186 and 5.187 into the balance of energy equation 5.110 yields the combined three-phase balance of energy,

$$\rho^s\left[\frac{\partial \psi^s}{\partial \boldsymbol{C}_s}\frac{D^s \boldsymbol{C}_s}{Dt} + \frac{\partial \psi^s}{\partial \theta^s}\frac{D^s \theta^s}{Dt} + \frac{\partial \psi^s}{\partial S_\ell}\frac{D^s S_\ell}{Dt} + \theta^s\frac{D^s \eta^s}{Dt} + \eta^s\frac{D^s \theta^s}{Dt}\right] - \frac{1}{J_s}\boldsymbol{S}'_s\frac{D^s \boldsymbol{C}_s}{Dt}$$

$$-\left([n^g - (1-\chi)]p_g + (n^\ell - \chi)p_\ell\right)div(\boldsymbol{v}_s) + div(\boldsymbol{q}^s_\theta) - \rho^s r^s + \rho^\ell \theta^\ell\frac{D^\ell \eta^\ell}{Dt}$$

$$-n^\ell p_\ell div(\boldsymbol{v}_\ell) + \frac{p_\ell}{\rho^{\ell R}}\hat{\rho}^\ell - p^\ell\frac{D^\ell n^\ell}{Dt} - \rho^\ell r^\ell + div(\boldsymbol{q}^\ell_\theta) + \rho^g \theta^g\frac{D^g \eta^g}{Dt} - n^g p_g div(\boldsymbol{v}_g)$$

$$+\frac{p_g}{\rho^{gR}}\hat{\rho}^g - p_g\frac{D^g n^g}{Dt} - \rho^g r^g + div(\boldsymbol{q}^g_\theta) + p_\ell\tilde{\boldsymbol{v}}_\ell \cdot grad(n^\ell) + p_g\tilde{\boldsymbol{v}}_g \cdot grad(n^g)$$

$$+\boldsymbol{v}^D_\ell \cdot \left[grad(p_\ell) + \rho^{\ell R}(\boldsymbol{a}_\ell - \boldsymbol{b}^\ell)\right] + \boldsymbol{v}^D_g \cdot \left[grad(p_g) + \rho^{gR}(\boldsymbol{a}_g - \boldsymbol{b}^g)\right]$$

$$-\frac{1}{2}\hat{\rho}^\ell \boldsymbol{v}_\ell \cdot \boldsymbol{v}_\ell - \frac{1}{2}\hat{\rho}^g \boldsymbol{v}_g \cdot \boldsymbol{v})g + \hat{\rho}^\ell \boldsymbol{v}_\ell \cdot \tilde{\boldsymbol{v}}_\ell + \hat{\rho}^g \boldsymbol{v}_g \cdot \tilde{\boldsymbol{v}}_g + n^g p_g div(\boldsymbol{v}_g) + n^\ell p_\ell div(\boldsymbol{v}_\ell) = 0. \tag{5.188}$$

To simplify equation 5.188 several measures must be taken. First, all like terms are canceled. Next, the definition of enthalpy (Eqn. 5.139) is used to show that

$$\frac{p_\ell}{\rho^{\ell R}}\hat{\rho}^\ell + \frac{p^g}{\rho^{gR}}\hat{\rho}^g + \hat{\rho}^\ell e^\ell + \hat{\rho}^g e^g = \hat{\rho}^v H_{vap}, \tag{5.189}$$

where $\hat{\rho}^v$ is the rate of mass exchange from vapor to liquid and H_{vap} is the latent heat of vaporization defined as

$$H_{vap} = H_g - H_\ell. \tag{5.190}$$

It can also be seen through using the balance of mass (Eqn. 5.43) that

$$\left([n^g - (1-\chi)]p_g + (n^\ell - \chi)p_\ell\right)div(\boldsymbol{v}_s)$$

$$= \left([n^g - (1-\chi)]p_g + (n^\ell - \chi)p_\ell\right)\left(-\frac{1}{n^s}\frac{D^s n^s}{Dt} + \beta^\theta_s\frac{D^s \theta^s}{Dt}\right). \tag{5.191}$$

which setting χ equal to liquid saturation, S_ℓ, can be simplified to

$$
\begin{aligned}
&\left(\left[n^g - (1-\chi) \right] p_g + (n^\ell - \chi) p_\ell \right) div(\boldsymbol{v}_s) \\
&= (p_\ell S_\ell + p_g S_g) \frac{D^s n}{Dt} + \left(\left[n^g - (1-S_\ell) \right] p_g + (n^\ell - S_\ell) p_\ell \right) \beta_s^\theta \frac{D^s \theta^s}{Dt}.
\end{aligned}
\tag{5.192}
$$

Now it can be shown that

$$
p_\ell \frac{D^\ell n^\ell}{Dt} + p_g \frac{D^g n^g}{Dt} + p_\ell \tilde{\boldsymbol{v}}_\ell \cdot grad(n^\ell) + p_g \tilde{\boldsymbol{v}}_g \cdot grad(n^g) = (p_\ell S_\ell + p_g S_g) \frac{D^s n}{Dt} + ns \frac{D^s S_\ell}{Dt}.
\tag{5.193}
$$

Finally, plugging equations 5.189, 5.192 and 5.193 into equation 5.188 and applying the constraints set forth in equations 5.178-5.180 the balance of energy becomes

$$
\begin{aligned}
&\rho^\ell \theta^\ell \frac{D^\ell \eta^\ell}{Dt} + \rho^g \theta^g \frac{D^g \eta^g}{Dt} + \rho^s \theta^s \frac{D^s \eta^s}{Dt} \\
&+ \boldsymbol{v}_\ell^D \cdot \left[grad(p_\ell) + \rho^{\ell R}(\boldsymbol{a}_\ell - \boldsymbol{b}^\ell) \right] + \boldsymbol{v}_g^D \cdot \left[grad(p_g) + \rho^{gR}(\boldsymbol{a}_g - \boldsymbol{b}^g) \right] \\
&\quad - \frac{1}{2} \hat{\rho}^\ell \boldsymbol{v}_\ell \cdot \boldsymbol{v}_\ell - \frac{1}{2} \hat{\rho}^g \boldsymbol{v}_g \cdot \boldsymbol{v}_g + \hat{\rho}^\ell \boldsymbol{v}_\ell \cdot \tilde{\boldsymbol{v}}_\ell + \hat{\rho}^g \boldsymbol{v}_g \cdot \tilde{\boldsymbol{v}}_g \\
&- \rho^\ell r^\ell - \rho^g r^g - \rho^s r^s + div(\boldsymbol{q}_\theta^\ell) + div(\boldsymbol{q}_\theta^g) + div(\boldsymbol{q}_\theta^s) + \hat{\rho}^v H_{vap} = 0.
\end{aligned}
\tag{5.194}
$$

If necessary, the balance of energy equation can be left in this form; however, it is often beneficial to make several simplifying assumptions. These include defining the material time derivatives of the entropy of the α phase as

$$
\rho^\alpha \theta^\alpha \frac{D^\alpha \eta^\alpha}{Dt} = \rho^\alpha C_p^\alpha \frac{D^\alpha \theta^\alpha}{Dt}
\tag{5.195}
$$

where C_p^α is the heat capacity of the α phase, defining the total heat flux, $\boldsymbol{q}_\theta$, as

$$
\boldsymbol{q}_\theta = \boldsymbol{q}_\theta^s + \boldsymbol{q}_\theta^\ell + \boldsymbol{q}_\theta^g,
\tag{5.196}
$$

defining the total heat generated as

$$
r = r^s + r^\ell + r^g,
\tag{5.197}
$$

defining the combined mass-heat capacity term, ρC_p^{eff}, as

$$\rho C_p^{eff} = \rho^s C_p^s + \rho^\ell C_p^\ell + \rho^g C_p^g, \tag{5.198}$$

and assuming the temperature, θ, of all three phases is the same,

$$\theta = \theta^s = \theta^\ell = \theta^g. \tag{5.199}$$

Plugging the definitions laid out in equations 5.195 - 5.199 into equation 5.194 and moving all material time derivatives to the solid reference frame using equation 5.55 yields the final balance of energy in the current configuration

$$(\rho C_p^{eff})\frac{D^s\theta}{Dt} + \rho^{\ell R}C_p^\ell \boldsymbol{v}_\ell^D \cdot grad(\theta) + \rho^{gR}C_p^g \boldsymbol{v}_g^D \cdot grad(\theta) - \frac{1}{2}\hat{\rho}^\ell \boldsymbol{v}_\ell \cdot \boldsymbol{v}_\ell$$
$$-\frac{1}{2}\hat{\rho}^g \boldsymbol{v}_g \cdot \boldsymbol{v}_g + \hat{\rho}^\ell \boldsymbol{v}_\ell \cdot \tilde{\boldsymbol{v}}_\ell + \hat{\rho}^g \boldsymbol{v}_g \cdot \tilde{\boldsymbol{v}}_g - \rho^{eff}r + div(\boldsymbol{q}_\theta) + \hat{\rho}^v H_{vap} \tag{5.200}$$
$$+\boldsymbol{v}_\ell^D \cdot \left[grad(p_\ell) + \rho^{\ell R}(\boldsymbol{a}_\ell - \boldsymbol{b}^\ell)\right] + \boldsymbol{v}_g^D \cdot \left[grad(p_g) + \rho^{gR}(\boldsymbol{a}_g - \boldsymbol{b}^g)\right] = 0.$$

where $\hat{\rho}^v$ is taken the be equal to the gas change rate

$$\hat{\rho}^v = \hat{\rho}^g = -\hat{\rho}^\ell. \tag{5.201}$$

To implement the balance of energy using the finite element method, one more heat transfer constitutive model must be defined as,

$$\boldsymbol{q}_\theta = -\boldsymbol{K^\theta}grad(\theta) \tag{5.202}$$

where $\boldsymbol{K^\theta}$ is the combined thermal conductivity matrix of the mixture. Lastly, moving the whole balance equation back to the initial solid reference configuration gives

$$
\begin{aligned}
J_s(\rho C_p^{eff})\frac{D^s\theta}{Dt} &+ J_s\rho^{\ell R}C_p^\ell \boldsymbol{v}_\ell^D \cdot GRAD(\theta) \cdot \boldsymbol{F}_s^{-T} + J_s\rho^{gR}C_p^g \boldsymbol{v}_g^D \cdot GRAD(\theta) \cdot \boldsymbol{F}_s^{-T} \\
&- J_s\rho^{eff}r + J_s DIV(-\boldsymbol{K^\theta} \cdot GRAD(\theta) \cdot \boldsymbol{F}_s^{-T}) : \boldsymbol{F}_s^{-T} + J_s H_{vap}\hat{\rho}^v \\
&- J_s\frac{1}{2}\hat{\rho}^\ell \boldsymbol{v}_\ell \cdot \boldsymbol{v}_\ell - J_s\frac{1}{2}\hat{\rho}^g \boldsymbol{v}_g \cdot \boldsymbol{v}_g + J_s\hat{\rho}^\ell \boldsymbol{v}_\ell \cdot \tilde{\boldsymbol{v}}_\ell + J_s\hat{\rho}^g \boldsymbol{v}_g \cdot \tilde{\boldsymbol{v}}_g \quad (5.203) \\
&+ J_s\boldsymbol{v}_\ell^D \cdot \left[GRAD(p_\ell) \cdot \boldsymbol{F}_s^{-T} + \rho^{\ell R}(\boldsymbol{a}^\ell - \boldsymbol{b}^\ell)\right] \\
&+ J_s\boldsymbol{v}_g^D \cdot \left[GRAD(p_g) \cdot \boldsymbol{F}_s^{-T} + \rho^{gR}(\boldsymbol{a}^g - \boldsymbol{b}^g)\right] = 0.
\end{aligned}
$$

where $\hat{\rho}^v$, is defined by 5.63 or in the current configuration as

$$
\begin{aligned}
\hat{\rho}^v = &-\rho^{\ell R}\frac{1}{J_s}\frac{D^s J_s}{Dt} + \rho^{\ell R}S_\ell\left[(1-n)\beta_s^\theta \frac{D^s\theta^s}{Dt}\right. \\
&\left.-n\beta_\ell^\theta \frac{D^s\theta^\ell}{Dt}\right] + \rho^{\ell R}n\frac{D^s S_\ell}{Dt} - GRAD(\rho^{\ell R}\tilde{\boldsymbol{v}}_\ell^D) : F^{-T}
\end{aligned}
\qquad (5.204)
$$

and Darcy's velocity, $\boldsymbol{v}_f^D$, is defined in 5.76.

5.4.3 Other Constitutive Equations

To finalize the full theory, several more assumptions and constitutive equations must still be presented. The first of these assumptions is that all vapor consists of water and that this water vapor reaches is its saturation pressure [128]. This assumptions allows for the Clausius-Clapeyron equation to be used to calculate the gas pressure, p_g,

$$
p_g = p_{gs_0}exp\left(-\frac{M_m H_{vap}}{R}\left[\frac{1}{\theta} - \frac{1}{\theta_0}\right]\right) \qquad (5.205)
$$

where M_m is the molar mass of the vapor, R is the ideal gas constant and p_{gs_0} is the saturated gas pressure at a reference temperature, θ_0. Using the calculated gas pressure, the van Genuchten equation can now be used to relate the liquid saturation with the capillary pressure or suction, s, which is the difference between liquid and gas pressures [79], [87]:

$$S_e = \frac{S_\ell - S_r}{S_s - S_r} = \left(\frac{1}{1 + \left(\frac{s}{a}\right)^{n_{vg}}}\right)^m, \tag{5.206}$$

$$m = 1 - \frac{1}{n}, \tag{5.207}$$

where a, n_{vg}, m, S_r and S_s are constants. Additionally, further examination of Darcy's Law 5.76 is needed. It is assumed that all fluid flow is isotropic meaning that 5.76 can be written as

$$\boldsymbol{v}_f^D = -K_f GRAD(p_f) : \boldsymbol{F}^{-T} \tag{5.208}$$

where K_f is the permeability of the fluid which can be described as

$$K_f = \frac{k_{rel}^f k_{int}^f(S_\ell)}{\mu^f} \tag{5.209}$$

where μ^f is the viscosity of the fluid phase and $k_{int}^f(S_\ell)$ is intrinsic permeability which is a function of liquid saturation, S_ℓ defined as

$$k_{int}^f = k_{0_{int}} \mathscr{Y}(S_\ell) \tag{5.210}$$

where $k_{0_{int}}$ is a material constant and $\mathscr{Y}(S_\ell)$ is a saturation dependent parameter defined for the liquid phase as

$$\mathscr{Y}(S_\ell) = \begin{cases} \left(\frac{S_\ell - S_r}{1 - S_r}\right)^3 & S_\ell > S_r \\ 0 & S_\ell < S_f \end{cases} \tag{5.211}$$

and for the gas phase as

$$\mathscr{Y}(S_\ell) = \begin{cases} 1 - 1.1 S_g & S_g > 1/1.11 \\ 0 & S_g < 1/1.1 \end{cases}. \tag{5.212}$$

The relative permeability of the fluid, k_{rel}^f is defined using the Kozemy-Carmen relationship as

$$k_{rel}^f = \frac{(n)^3}{1-(n)^2}\frac{1-(n_0)^2}{(n_0)^3} \tag{5.213}$$

where n and n_0 are the current and initial porosity of the mixture.

Additionally, the heat transfer is considered isotropic meaning the thermal conductivity matrix seen in 5.202, $\boldsymbol{K}^\theta$, can be reduced to a single term, K^θ. Lastly, for the remainder of this work the solid skeleton will be considered as a Neo-Hookean material, thus, the strain energy function, ψ, is

$$\psi = \frac{\mu_s}{2}(I_1 - 3) + \mu_s lnJ + \frac{\lambda}{2}(lnJ)^2 \tag{5.214}$$

where I_1 is the first invariant of the Right-Cauchy Green tensor, $\boldsymbol{C}_s$, μ_s is the shear modulus and λ is the lame' constant of the solid skeleton. It should be noted, equation 5.214 satisfies the constraints set forth in equation 5.178 such that the second Piola-Kirchoff stress, $\boldsymbol{S}_s$, is

$$\boldsymbol{S}_s = \left[\lambda(lnJ_s) - \mu_s\right]\boldsymbol{C}_s^{-1} + \mu_s\boldsymbol{1}. \tag{5.215}$$

5.5 Finite Element Implementation

5.5.1 Strong and Variational Formulations

To solve the balance equations for the desired field variables, $\boldsymbol{u}$, p_f, and θ the problem must be put into its variational or weak form. First, the solution space for the strong form, $\mathscr{S}$, is defined as

$$\mathcal{S}^u = \big(\boldsymbol{u} : B_0 \times [0,T] \to \mathbb{R}^3, \in H^1, \boldsymbol{u}(t) = \boldsymbol{u}^{fixed}(t) \; on \; \partial B_u^{fixed}, \boldsymbol{u}(\boldsymbol{X}_s, t=0) = \boldsymbol{u}_0(\boldsymbol{X})\big),$$

$$\mathcal{S}^p = \big(p_\ell : B_0 \times [0,T] \to \mathbb{R}^3, \in H^1, p_\ell(t) = p_\ell^{fixed}(t) \; on \; \partial B_p^{fixed}, p_\ell(\boldsymbol{X}_s, t=0) = p_{\ell 0}(\boldsymbol{X})\big),$$

$$\mathcal{S}^\theta = \big((\theta : B_0 \times [0,T] \to \mathbb{R}^3, \in H^1, \theta(t) = \theta^{fixed}(t) \; on \; \partial B_\theta^{fixed}, \theta(\boldsymbol{X}_s, t=0) = \theta_0(\boldsymbol{X})\big)$$

$$(5.216)$$

such that the strong form can be written as:

$$Find \; \boldsymbol{u}(\boldsymbol{X}_s, t) \in \mathcal{S}^u, p_\ell(\boldsymbol{X}, t) \in \mathcal{S}^p and \; \theta(\boldsymbol{X}_s, t) \in \mathcal{S}^\theta \; over \; t \in [0,T] \quad such \; that:$$

$$DIV_s\Big[\boldsymbol{P}'_s - J_s\big[p_\ell \chi + p_g(1-\chi)\big]\boldsymbol{F}_s^{-T}\Big] + \rho_0 \boldsymbol{g} = \rho_o \boldsymbol{a} \in B,$$

$$\boldsymbol{u} = \boldsymbol{u}^{fixed} \quad on \; \partial B_0^u,$$

$$\boldsymbol{P} \cdot \boldsymbol{N} = \boldsymbol{t}_u \quad on \; \partial B_0^t,$$

$$\boldsymbol{u}(\boldsymbol{X}_s, t=0) = \boldsymbol{u}_0(\boldsymbol{X}_s) \in B_0,$$

$$\dot{\boldsymbol{u}}(\boldsymbol{X}_s, t=0) = \dot{\boldsymbol{u}}_0(\boldsymbol{X}_s) \in B_0,$$

$$(S^g \rho^{gR} + S^\ell \rho^{\ell R})\frac{D^s J_s}{Dt} - J_s\Big[(1-n)\big[\rho^{\ell R}S_\ell + \rho^{gR}S_g\big] + n\rho^{\ell R}S_\ell \beta_\ell^\theta\Big]\frac{D^s \theta}{Dt}$$
$$+ \frac{\rho^{\ell R}J_s n S_l}{K_{bulk}^\ell}\frac{D^s p_\ell}{Dt} + \frac{\rho^{\ell R}}{K_{bulk}^\ell}GRAD p_\ell \cdot \boldsymbol{v}_\ell^D \cdot \boldsymbol{F}_s^{-T} + J_s GRAD(\rho^{\ell R}\boldsymbol{v}_\ell^D + \rho^{gR}\boldsymbol{v}_g^D) : \boldsymbol{F}_s^{-T}$$
$$+ J_s\Big[\rho^{\ell R}n\frac{D^s S_\ell}{Dt} + n\rho^{gR}\frac{D^s S_g}{Dt} + nS_g\frac{D^s \rho^{gR}}{Dt}\Big] = 0 \in B,$$

$$p_\ell = p_\ell^{fixed} \quad on \; \partial B_0^p,$$

$$-\rho^{\ell R}S_\ell K_\ell \cdot GRAD(p_\ell) \cdot \boldsymbol{F}_s^{-T} \cdot \boldsymbol{N}_s - \rho^{gR}S_g K_g \cdot GRAD(p_g) \cdot \boldsymbol{F}_s^{-T} \cdot \boldsymbol{N}_s = q_\ell \quad on \; \partial B_0^p,$$

$$p_\ell(\boldsymbol{X}_s, t=0) = p_0(\boldsymbol{x}_s) \in B_0,$$

$$\dot{p}_\ell(\boldsymbol{X}_s, t=0) = \dot{p}_{\ell 0}(\boldsymbol{X}_s) \in B_0,$$

$$J_s(\rho C_p^{eff})\frac{D^s\theta}{Dt} + J_s\rho^{\ell R}C_p^\ell \boldsymbol{v}_\ell^D \cdot GRAD(\theta) \cdot \boldsymbol{F}_s^{-T} + J_s\rho^{gR}C_p^g \boldsymbol{v}_g^D \cdot GRAD(\theta) \cdot \boldsymbol{F}_s^{-T}$$

$$-J_s\rho^{eff}r + J_s DIV(-\boldsymbol{K}^\theta \cdot GRAD(\theta) \cdot \boldsymbol{F}_s^{-T}) : \boldsymbol{F}_s^{-T} + J_s H_{vap}\hat{\rho}^v$$

$$-J_s\frac{1}{2}\hat{\rho}^\ell \boldsymbol{v}_\ell \cdot \boldsymbol{v}_\ell - J_s\frac{1}{2}\hat{\rho}^g \boldsymbol{v}_g \cdot \boldsymbol{v}_g + J_s\hat{\rho}^\ell \boldsymbol{v}_\ell \cdot \tilde{\boldsymbol{v}}_\ell + J + s\hat{\rho}^g \boldsymbol{v}_g \cdot \tilde{\boldsymbol{v}}_g$$

$$+J_s\boldsymbol{v}_\ell^D \cdot \left[GRAD(p_\ell) \cdot \boldsymbol{F}_s^{-T} + \rho^{\ell R}(\boldsymbol{a}^\ell - \boldsymbol{b}^\ell)\right]$$

$$+J_s\boldsymbol{v}_g^D \cdot \left[GRAD(p_g) \cdot \boldsymbol{F}_s^{-T} + \rho^{gR}(\boldsymbol{a}^g - \boldsymbol{b}^g)\right] = 0 \in B_0,$$

$$\theta(\boldsymbol{X}_s,t) = \theta^{fixed}(\boldsymbol{X}_s,t) \quad on\ \partial B_0^\theta,$$

$$h_t\big(\theta(\boldsymbol{X}_s,t) - \theta_{amb}(t)\big) = \boldsymbol{q}_\theta \quad on\ \partial_0^q,$$

$$\theta(\boldsymbol{X},t=0) = \theta_0(\boldsymbol{X}) \in B_0,$$

$$\dot{\theta}(\boldsymbol{X}_s.t=0) = \dot{\theta}_0(\boldsymbol{X}_s) \in B_0.$$

$$(5.217)$$

To solve the balance equations using the finite element method the variational form of the problem must be used. Therefore, it is beneficial to introduce the variational or weighting spaces, $\mathscr{V}^\alpha$, as

$$\mathscr{V}^u = (\boldsymbol{w}^u : B_0 \rightarrow, \boldsymbol{w}^u\ on\ \partial B_0^u),$$

$$\mathscr{V}^p = (w^p : B_0 \rightarrow, w^p\ on\ \partial B_0^p), \qquad (5.218)$$

$$\mathscr{V}^\theta = (w^\theta : B_0 \rightarrow, w^\theta\ on\ \partial B_0^\theta),$$

where $\boldsymbol{w}^u$, w^p, and w^θ are the weighting functions of the displacement, liquid pressure and temperature variables.

Balance of Linear Momentum Variational Form

The variational form of the balance of linear momentum equation, G, is

$$G : \mathscr{S}^u \times \mathscr{S}^p \times \mathscr{S}^\theta \times \mathscr{V}^u \rightarrow \mathbb{R} \qquad (5.219)$$

where in index notation and dropping the (s) subscript

$$G(u_i, p_\ell, \theta, w_i^u) = \int_{B_0} w_i^u \left(\frac{\partial}{\partial X_I} \left[P'_{Ii} - J(p_\ell \chi + p_g(1-\chi)) F_{Ii}^{-1} \right] + \rho_0(g_i + a_i) \right) dV = 0, \quad (5.220)$$

which can be expanded to

$$G(u_i, p_\ell, \theta, w_i^u) = \int_{B_0} w_i^u \frac{\partial P'_{Ii}}{\partial X_I} dV - \int_{B_0} w_i^u \frac{\partial}{\partial X_I} \left[J(p_\ell \chi + p_g(1-\chi)) F_{Ii}^{-1} \right] dV + \int_{B_0} w_i^u \rho_0(g_i - a_i) dV. \quad (5.221)$$

Examining the first two terms and using the definition of the chain rule it can be written that

$$w_i^u \frac{\partial P'_{Ii}}{\partial X_I} = \frac{\partial w_i^u P'_{Ii}}{\partial X_I} - P'_{Ii} \frac{\partial w_i^u}{\partial X_I}, \quad (5.222)$$

and

$$w_i^u \frac{\partial \left(J(p_\ell \chi + p_g(1-\chi)) F_{Ii}^{-1} \right)}{\partial X_I} = \frac{\partial \left(w_i^u J(p_\ell \chi + p_g(1-\chi)) F_{Ii}^{-1} \right)}{\partial X_I} \\ - J(p_\ell \chi + p_g(1-\chi)) F_{Ii}^{-1} \frac{\partial w_i^u}{\partial X_I}. \quad (5.223)$$

Plugging in equations 5.222 and 5.224 into equation 5.221 gives

$$G(u_i, p_\ell, \theta, w_i^u) = \int_{B_0} \left[\frac{\partial (w_i^u P'_{Ii})}{\partial X_I} - P'_{Ii} \frac{\partial w_i^u}{\partial X_I} \right] dV + \int_{B_0} w_i^u \rho_0(g_i - a_i) dV \\ - \int_{B_0} \left[\frac{(w_i^u J(p_\ell \chi + p_g(1-\chi)) F_{Ii}^{-1})}{\partial X_I} - J(p_\ell \chi + p_g(1-\chi)) F_{Ii}^{-1} \frac{\partial w_i^u}{\partial X_I} \right] dV. \quad (5.224)$$

Applying the divergence theorem yields

$$G(u_i, p_\ell, \theta, w_i^u) = \int_{\partial B_0} w_i^u P'_{Ii} N_I dA - \int_{B_0} P'_{Ii} \frac{\partial w_i^u}{\partial X_I} dV + \int_{B_0} w_i^u \rho_0(g_i - a_i) dV \\ - \int_{\partial B_0} w_i^u J(p_\ell \chi + p_g(1-\chi)) F_{Ii}^{-1} N_I dA + \int_{B_0} J(p_\ell \chi + p_g(1-\chi)) F_{Ii}^{-1} \frac{\partial w_i^u}{\partial X_I} dV. \quad (5.225)$$

Going further, the integral over the boundary can be split into a free $(\partial B_{u_0}^{free})$ boundary and one with an applied traction $(\partial B_{u_0}^{trac})$ such that

$$
\begin{aligned}
\int_{\partial B_0} & w_i^u P_{Ii}' N_I dA - \int_{\partial B_0} w_i^u J\big(p_\ell \chi + p_g(1-\chi)\big) F_{Ii}^{-1} N_I dA \\
&= \int_{\partial B_{u_0}^{free}} w_i^u \Big(P_{Ii}' N_I - J\big(p_\ell \chi + p_g(1-\chi)\big) F_{Ii}^{-1} N_I \Big) dA \\
&\quad + \int_{\partial B_{u_0}^{trac}} w_i^u \underbrace{\Big(P_{Ii}' N_I - J\big(p_\ell \chi + p_g(1-\chi)\big) F_{Ii}^{-1} N_I \Big)}_{t_i} dA
\end{aligned}
\tag{5.226}
$$

where t_i is the total applied traction. By definition no load is applied to the free boundary $(\partial B_{u_0}^{free})$ meaning the integral over that boundary is zero. This leaves the final variational balance of linear momentum as

$$
\begin{aligned}
G(u_i, p_\ell, \theta, w_i^u) = & \int_{B_0} \underbrace{P_{Ii}' \frac{\partial w_i^u}{\partial X_I}}_{G_1^{int}} dV - \int_{B_0} \underbrace{J\big(p_\ell \chi + p_g(1-\chi)\big) F_{Ii}^{-1} \frac{\partial w_i^u}{\partial X_I}}_{G_2^{int}} dV \\
& + \int_{B_0} \underbrace{w_i^u \rho_0(a_i)}_{G_3^{int}} dV - \int_{B_0} \underbrace{w_i^u \rho_0(g_i)}_{G_4^{int}} dV - \int_{\partial B_{u_0}^{trac}} \underbrace{w_i^u t_i}_{G_1^{ext}} dA
\end{aligned}
\tag{5.227}
$$

where G^{int} and G^{ext} represent the internal and external portions of the balance of linear momentum.

Balance of Mass Variational Form

The variational form for the balance of mass equation, H, can be written as

$$
H : \mathcal{S}^u \times \mathcal{S}^p \times \mathcal{S}^\theta \times \mathcal{V}^p \to \mathbb{R}
\tag{5.228}
$$

where dropping the (s) subscript for clarity and moving to index notation gives the global balance of mass in the initial configuration to be

$$H(u_i, p_\ell, \theta, w^p) = \int_{B_0} \Big(w^p (S_g \rho^{gR} + S_\ell \rho^{\ell R}) \dot{J} - w^p J \big[(1-n)(\rho^{\ell R} S_\ell + \rho^{gR} S_g) \beta_S^\theta + n \rho^{\ell R} S_\ell \beta_\ell^\theta \big] \dot{\theta}$$

$$+ w^p \frac{\rho^{\ell R} J n S_\ell}{K_{bulk}^\ell} \dot{p}_\ell + w^p \frac{J \rho^{\ell R}}{K_{bulk}^\ell} \frac{\partial p_\ell}{\partial X_I} v_{\ell_i}^D F_{Ii}^{-1} + w^p J \frac{\partial (\rho^{\ell R} v_{\ell_i}^D + \rho^{gR} v_{g_i}^D)}{\partial X_I} F_{Ii}^{-1}$$

$$+ w^p J \big[\rho^{\ell R} n \dot{S}_\ell + n \rho^{gR} \dot{S}_g + n S_g \dot{\rho}^{gR} \big] \Big) dV.$$

$$(5.229)$$

Now with the chain rule it can be seen that

$$\frac{\partial (w^p J F_{Ii}^{-1} [\bullet])}{\partial X_I} = \frac{\partial w^p}{\partial X_I} J F_{Ii}^{-1} [\bullet] + w^p \frac{\partial (J F_{Ii}^{-1})}{\partial X_i} + w^p J F_{Ii}^{-1} \frac{\partial [\bullet]}{\partial X_I}, \qquad (5.230)$$

where $[\bullet]$ represents any function and $w^p \frac{\partial (J F_{Ii}^{-1})}{\partial X_I} [\bullet]$ is zero due to the Piola identity.

Applying 5.230 to 5.229 and applying the divergence theorem gives

$$H(u_i, p_\ell, \theta, w^p) = \int_{B_0} w^p (S_g \rho^{gR} + S_\ell \rho^{\ell R}) \dot{J} dV -$$

$$\int_{B_0} w^p J \big[(1-n)(\rho^{\ell R} S_\ell + \rho^{gR} S_g) \beta_s^\theta + n \rho^{\ell R} S_\ell \beta_\ell^\theta \big] \dot{\theta} dV$$

$$- \int_{B_0} \frac{\partial w^p}{\partial X_I} J F_{Ii}^{-1} \big[\rho^{\ell R} v_{\ell_i}^D + \rho^{gR} v_{g_i}^D \big] dV + \int_{\partial B_0} w^p J F_{Ii}^{-1} \big[\rho^{\ell R} v_{\ell_i}^D + \rho^{gR} v_{g_i}^D \big] N_I dA \qquad (5.231)$$

$$+ \int_{B_0} w^p J \big[\rho^{\ell R} n \dot{S}_\ell + n \rho^{gR} \dot{S}_g + n S_g \dot{\rho}^{gR} \big] dV + \int_{B_0} w^p \bigg[\frac{\rho^{\ell R} J n S_\ell}{K_{bulk}^\ell} \dot{p}_\ell +$$

$$w^p \frac{\rho^{\ell R}}{K_{bulk}^\ell} \frac{\partial p_\ell}{\partial X_I} v_{\ell_i}^D F_{Ii}^{-1} \bigg] dV$$

Again the boundary can be split into a flux ∂B_{p0}^{free} and zero flux ∂B_{p0}^{fixed} portions,

$$\int_{\partial B_0} w^p J F_{Ii}^{-1} \left[\rho^{\ell R} v_{\ell_i}^D + \rho^{gR} v_{g_i}^D \right] N_I dA = \int_{\partial B_{p0}^{free}} w^p \underbrace{J F_{Ii}^{-1} \left[\rho^{\ell R} v_{\ell_i}^D + \rho^{gR} v_{g_i}^D \right] N_I dA}_{q_\ell^{flux}}$$

$$+ \int_{\partial B_{p0}^{fixed}} w^p J F_{Ii}^{-1} \left[\rho^{\ell R} v_{\ell_i}^D + \rho^{gR} v_{g_i}^D \right] N_I dA \tag{5.232}$$

where the integral over the boundary ∂B_{p0}^{fixed} is zero as no fluid flows through. Therefore, applying equation 5.232 gives the final balance of mass variational form as

$$H(u_i, p_\ell, \theta, w^p) = \int_{B_0} \underbrace{w^p (S_g \rho^{gR} + S_\ell \rho^{\ell R}) \dot{J}}_{H_1^{int}} dV$$

$$- \int_{B_0} \underbrace{w^p J \left[(1-n)(\rho^{\ell R} S_\ell + \rho^{gR} S_g) \beta_s^\theta + n \rho^{\ell R} S_\ell \beta_\ell^\theta \right] \dot{\theta}}_{H_2^{int}} dV$$

$$- \int_{B_0} \underbrace{\frac{\partial w^p}{\partial X_I} J F_{Ii}^{-1} \left[\rho^{\ell R} v_{\ell_i}^D + \rho^{gR} v_{g_i}^D \right] dV}_{H_3^{int}} + \int_{B_0} \underbrace{w^p J \left[\rho^{\ell R} n \dot{S}_\ell + n \rho^{gR} \dot{S}_g + n S_g \dot{\rho}^{gR} \right] dV}_{H_4^{int}} \tag{5.233}$$

$$+ \int_{B_0} \underbrace{w^p \left[\frac{\rho^{\ell R} J n S_\ell}{K_{bulk}^\ell} \dot{p}_\ell + \frac{\rho^{\ell R} J}{K_{bulk}^\ell} \frac{\partial p_\ell}{\partial X_I} v_{\ell_i}^D F_{Ii}^{-1} \right] dV}_{H_5^{int}} - \int_{\partial B_{p0}^{free}} \underbrace{w^p q_\ell^{flux} dA}_{H_1^{ext}}$$

Balance of Energy Variational Form

The variational form of the balance of energy, L, can be written as

$$L : \mathcal{S}^u \times \mathcal{S}^p \times \mathcal{S}^\theta \times \mathcal{V}^\theta \to \mathbb{R} \tag{5.234}$$

where again dropping the (s) subscript and moving to index notation gives the integral from in the solid reference configuration as

$$L(u_i, p_\ell, \theta, w^\theta) = \int_{B_0} w^\theta J(\rho C_p^{eff})\dot{\theta}dV + \int_{B_0} w^\theta J\rho^{\ell R}C_p^\ell v_{\ell_i}^D \frac{\partial\theta}{\partial X_I}F_{Ii}^{-1}dV$$

$$+ \int_{B_0} w^\theta J\rho^{gR}C_p^g v_{g_i}^D \frac{\partial\theta}{\partial X_I}F_{Ii}^{-1}dV - \int_{B_0} w^\theta J\rho^{eff}rdV + \int_{B_0} w^\theta J\frac{\partial\left(-K^\theta\frac{\partial\theta}{\partial X_I}F_{Ii}^{-1}\right)}{\partial X_J}F_{Ji}^{-1}dV$$

$$+ \int_{B_0} w^\theta JH_{vap}\left[-\rho^{\ell R}\frac{1}{J}\dot{J} + \rho^{\ell R}S_\ell\left[(1-n)\beta_s^\theta\dot{\theta} - n\beta_\ell^\theta\dot{\theta}\right]\right.$$

$$\left.+\rho^{\ell R}n\dot{S}_\ell - \frac{\partial(\rho^{\ell R}v_{\ell_i}^D)}{\partial X_I}F_{Ii}^{-1}\right]dV + \int_{B_0} w^\theta J\left(\hat{\rho}^\ell v_{\ell_i}\tilde{v}_{\ell_i} + \hat{\rho}^g v_{g_i}\tilde{v}_{g_i} - \frac{1}{2}\hat{\rho}^\ell v_{\ell_i}v_{\ell_i} - \frac{1}{2}\hat{\rho}^g v_{g_i}v_{g_i}\right)dV$$

$$+ \int_{B_0} w^\theta J\left(v_{\ell_i}^D\left[\frac{\partial p_\ell}{\partial X_I}F_{Ii}^{-1} + \rho^{\ell R}(a_i - b_i)\right] + v_{g_i}^D\left[\frac{\partial p_g}{\partial X_I}F_{Ii}^{-1} + \rho^{gR}(a_i - b_i)\right]\right)dV.$$

$$(5.235)$$

Now examining the $\int_{B_0} w^\theta J\frac{\partial\left(-K^\theta\frac{\partial\theta}{\partial X_I}F_{Ii}^{-1}\right)}{\partial X_J}F_{Ji}^{-1}dV$ term one can see

$$\frac{\partial\left(w^\theta J\left(-K^\theta\frac{\partial\theta}{\partial X_I}\right)F_{Ii}^{-1}F_{Ji}^{-1}\right)}{\partial X_J} = \frac{\partial w^\theta}{\partial X_J}J\left(-K^\theta\frac{\partial\theta}{\partial X_I}\right)F_{Ii}^{-1}F_{Ji}^{-1}$$

$$+ w^\theta\frac{\partial(JF_{Ii}^{-1}F_{Ji}^{-1})}{\partial X_J}\left(-K^\theta\frac{\partial\theta}{\partial X_I}\right) + w^\theta J\frac{\partial\left(-K^\theta\frac{\partial\theta}{\partial X_I}F_{Ii}^{-1}\right)}{\partial X_J}F_{Ji}^{-1}$$

$$(5.236)$$

where $w^\theta\frac{\partial(JF_{Ii}^{-1}F_{Ji}^{-1})}{\partial X_J}\left(-K\frac{\partial\theta}{\partial X_I}\right)$ is zero due to the Piola identity. Along these same lines the $div(\rho^{\ell R}\tilde{\boldsymbol{v}}_\ell^D)$ portion of the sixth integral term can be separated to show.

$$\frac{\partial\left(w^\theta JF_{Ii}^{-1}H_{vap}(\rho^{\ell R}v_{\ell_i}^D)\right)}{\partial X_I} = \frac{\partial w^\theta}{\partial X_I}JF_{Ii}^{-1}H_{vap}(\rho^{\ell R}v_{\ell_i}^D) + w^\theta\frac{\partial JF_{Ii}^{-1}H_{vap}}{\partial X_I}(\rho^{\ell R}v_{\ell_i}^D)$$

$$+ w^\theta JF_{Ii}^{-1}H_{vap}\frac{\partial(\rho^{\ell R}v_{\ell_i}^D)}{\partial X_I}.$$

$$(5.237)$$

The second term of equation 5.237 is zero due to the fact H_{vap} is not a function of space and the Piola Identity. Plugging in 5.236 and 5.237 in to 5.235 gives

$$
\begin{aligned}
L(u_i, p_\ell, \theta, w^\theta) = & \int_{B_0} w^\theta J(\rho C_p^{eff}) \dot\theta dV + \int_{B_0} w^\theta J \rho^{\ell R} C_p^\ell v_{\ell_i}^D \frac{\partial \theta}{\partial X_I} F_{Ii}^{-1} dV \\
& + \int_{B_0} w^\theta J \rho^{gR} C_p^g v_{g_i}^D \frac{\partial \theta}{\partial X_I} F_{Ii}^{-1} dV - \int_{B_0} w^\theta J \rho^{eff} dV - \int_{B_0} \frac{\partial w^\theta}{\partial X_J} J\left(-K^\theta \frac{\partial \theta}{\partial X_I}\right) F_{Ii}^{-1} F_{Ji}^{-1} dV \\
& + \int_{B_0} \frac{\partial \left(w^\theta J\left(-K^\theta \frac{\partial \theta}{\partial X_I}\right) F_{Ii}^{-1} F_{Ji}^{-1}\right)}{\partial X_J} dV \\
& + \int_{B_0} w^\theta J H_{vap} \left[-\rho^{\ell R} \frac{1}{J} \dot J + \rho^{\ell R} S_\ell \left[(1-n)\beta_s^\theta \dot\theta - n\beta_\ell^\theta \dot\theta\right] + \rho^{\ell R} n \dot S_\ell\right] dV \\
& - \int_{B_0} \left[\frac{\partial w^\theta J F_{Ii}^{-1} H_{vap}(\rho^{\ell R} v_{\ell_i}^D)}{\partial X_I} - \frac{\partial w^\theta}{\partial X_I} J F_{Ii}^{-1} H_{vap}(\rho^{\ell R} v_{\ell_i}^D)\right] dV \\
& + \int_{B_0} w^\theta J \left(\hat\rho^\ell v_{\ell_i} \tilde v_{\ell_i} + \hat\rho^g v_{g_i} \tilde v_{g_i} - \frac{1}{2}\hat\rho^\ell v_{\ell_i} v_{\ell_i} - \frac{1}{2}\hat\rho^g v_{g_i} v_{g_i}\right) dV \\
& + \int_{B_0} w^\theta J \left(v_{\ell_i}^D \left[\frac{\partial p_\ell}{\partial X_I} F_{Ii}^{-1} + \rho^{\ell R}(a_i - b_i)\right] + v_{g_i}^D \left[\frac{\partial p_g}{\partial X_I} F_{Ii}^{-1} + \rho^{gR}(a_i - b_i)\right]\right) dV.
\end{aligned}
$$

$$(5.238)$$

Applying the divergence theorem and splitting the boundary into a fixed/insulated region $(\partial B_{\theta_0}^{fixed})$ and a flux region $(\partial B_{\theta_0}^{free})$ it is known that

$$
\begin{aligned}
\int_{B_0} = & \frac{\partial \left(w^\theta J\left(-K^\theta \frac{\partial \theta}{\partial X_I}\right) F_{Ii}^{-1} F_{Ji}^{-1}\right)}{\partial X_J} dV - \int_{B_0} \frac{\partial \left(w^\theta J F_{Ii}^{-1} H_{vap}(\rho^{\ell R} v_{\ell_i}^D)\right)}{\partial X_I} dV \\
= & \int_{\partial B_{\theta_0}^{fixed}} \left(w^\theta J\left(-K^\theta \frac{\partial \theta}{\partial X_I}\right) F_{Ii}^{-1} F_{Ji}^{-1} - \left(w^\theta J F_{Ii}^{-1} H_{vap}(\rho^{\ell R} v_{\ell_i}^D)\right)\right) N_I dA \\
& + \int_{\partial B_{\theta_0}^{free}} \underbrace{\left(w^\theta J\left(-K \frac{\partial \theta}{\partial X_I}\right) F_{Ii}^{-1} F_{Ji}^{-1} - \left(w^\theta J F_{Ii}^{-1} H_{vap}(\rho^{\ell R} v_{\ell_i}^D)\right)\right)}_{q_\theta^{flux}} N_I dA.
\end{aligned}
$$

$$(5.239)$$

where the integral over the fixed/insulated surface is zero as no heat is gained or lost and q_θ^{flux} is the heat flux through the free boundary. Applying equation 5.239 gives the final

variational balance of energy as

$$
L(u_i, p_\ell, \theta, w^\theta) = \int_{B_0} w^\theta \underbrace{J(\rho C_p^{eff})\dot{\theta}}_{L_1^{int}} \, dV + \int_{B_0} w^\theta \underbrace{J\rho^{\ell R} C_p^\ell v_{\ell_i}^D \frac{\partial \theta}{\partial X_I} F_{Ii}^{-1}}_{L_2^{int}} \, dV
$$

$$
+ \int_{B_0} w^\theta \underbrace{J\rho^{gR} C_p^g v_{g_i}^D \frac{\partial \theta}{\partial X_I} F_{Ii}^{-1}}_{L_3^{int}} \, dV - \int_{B_0} w^\theta \underbrace{J\rho^{eff} r}_{L_4^{int}} \, dV - \int_{B_0} \underbrace{\frac{\partial w^\theta}{\partial X_J} J\left(-K^\theta \frac{\partial \theta}{\partial X_I}\right) F_{Ii}^{-1} F_{Ji}^{-1}}_{L_5^{int}} \, dV
$$

$$
- \int_{B_0} w^\theta \underbrace{JH_{vap}\left[\rho^{\ell R}\frac{1}{J}\dot{J} - \rho^{\ell R} S_\ell\left((1-n)\beta_s^\theta - n\beta_\ell^\theta\right)\dot{\theta} + \rho^{\ell R} n \dot{S}_\ell + \frac{\partial w^\theta}{\partial X_I} F_{Ii}^{-1}(\rho^{\ell R} v_{\ell_i}^D)\right]}_{L_6^{int}} \, dV
$$

$$
+ \int_{B_0} w^\theta \underbrace{J\left(\hat{\rho}^\ell v_{\ell_i} \tilde{v}_{\ell_i} + \hat{\rho}^g v_{g_i} \tilde{v}_{g_i} - \frac{1}{2}\hat{\rho}^\ell v_{\ell_i} v_{\ell_i} - \frac{1}{2}\hat{\rho}^g v_{g_i} v_{g_i}\right)}_{L_7^{int}} \, dV
$$

$$
+ \int_{B_0} w^\theta \underbrace{J\left(v_{\ell_i}^D\left[\frac{\partial p_\ell}{\partial X_I} F_{Ii}^{-1} + \rho^{\ell R}(a_i - b_i)\right] + v_{g_i}^D\left[\frac{\partial p_g}{\partial X_I} F_{Ii}^{-1} + \rho^{gR}(a_i - b_i)\right]\right)}_{L_8^{int}} \, dV
$$

$$
- \int_{\partial B_{\theta_0}^{free}} w^\theta \underbrace{q_\theta^{flux}}_{L_1^{ext}} \, dA.
$$

$$
(5.240)
$$

Chapter 6: Large Deformation Thermo-Poromechanics Linearization and Implementation via the Galerkin Finite Element Method

Now that the weak form of the thermo-poromechanics problem has been established in Chapter 5 the method of implementing and solving the balance equations using the Galerkin Finite Element Method will be introduced in this chapter. First the combined generalized trapezoid rule, Newton-Raphson solution algorithm will be presented and then the linearization of each balance equation needed by the algorithm will be shown in detail. Lastly, the matrix forms of the balance equations will be presented and test case simulations put forth.

6.1 Generalized Trapezoid Rule and Newton Raphson Implementations

To solve the given set of partial differential equations given by the variational forms of balance of mass, linear momentum and energy (Eqns. 5.227, 5.232, and 5.240) using the finite element method, the generalized trapezoid time-stepping method is used to solve the equations in the time domain:

$$
\begin{aligned}
u_{i_{n+1}} &= u_{i_n} + \Delta t(1-\alpha)\dot{u}_{i_n} + \alpha\Delta t\dot{u}_{i_{n+1}}, \\
p_{\ell_{n+1}} &= p_{\ell_n} + \Delta t(1-\alpha)\dot{p}_{\ell_n} + \alpha\Delta t\dot{p}_{\ell_{n+1}}, \\
\theta_{n+1} &= \theta_n + \Delta t(1-\alpha)\dot{\theta}_n + \alpha\Delta t\dot{\theta}_{n+1},
\end{aligned}
\tag{6.1}
$$

where n represents the current time step, α the time parameter ($\alpha = 1$ corresponds to the Backward Euler Method, $\alpha = 0$, the Forward Euler Method). The Newton-Raphson method is used to solve for the desired variables at each time step.

In generalized vector form corresponding to the nodal degrees of freedom, the balance equations can be written as

$$0 = \boldsymbol{R} = \boldsymbol{F}^{int}(\boldsymbol{D}, \boldsymbol{V}) - \boldsymbol{F}^{ext}(\boldsymbol{D}, \boldsymbol{V}) \tag{6.2}$$

where

$$\boldsymbol{F}^{int} = \begin{bmatrix} \boldsymbol{G}^{int} \\ \boldsymbol{H}^{int} \\ \boldsymbol{L}^{int} \end{bmatrix} \quad, \quad \boldsymbol{F}^{ext} = \begin{bmatrix} \boldsymbol{G}^{ext} \\ \boldsymbol{H}^{ext} \\ \boldsymbol{L}^{ext} \end{bmatrix} \tag{6.3}$$

and

$$\boldsymbol{D} = \begin{bmatrix} u_i \\ p_\ell \\ \theta \end{bmatrix} \quad, \quad \boldsymbol{V} = \begin{bmatrix} \dot{u}_i \\ \dot{p}_\ell \\ \dot{\theta} \end{bmatrix}. \tag{6.4}$$

To get into a Newton-Raphson form it is necessary to apply a small perturbation of $\delta \boldsymbol{V}$. The Taylor expansion of Equation 6.2 about a velocity perturbation ($\delta \boldsymbol{V}$) gives

$$\boldsymbol{R}^{k+1} = 0 = \boldsymbol{R}^k + \frac{\partial \boldsymbol{R}}{\partial \boldsymbol{V}} \delta \boldsymbol{V} + H.O.T. \tag{6.5}$$

where k is the Newton-Raphson iteration number and $\frac{\partial \boldsymbol{R}}{\partial \boldsymbol{V}}$ is the tangent stiffness matrix given as

$$\frac{\partial \boldsymbol{R}}{\partial \boldsymbol{V}} = \begin{bmatrix} \frac{\partial \boldsymbol{G}}{\partial \dot{u}} & \frac{\partial \boldsymbol{G}}{\partial \dot{p}_\ell} & \frac{\partial \boldsymbol{G}}{\partial \dot{\theta}} \\ \frac{\partial \boldsymbol{H}}{\partial \dot{u}} & \frac{\partial \boldsymbol{H}}{\partial \dot{p}_\ell} & \frac{\partial \boldsymbol{H}}{\partial \dot{\theta}} \\ \frac{\partial \boldsymbol{L}}{\partial \dot{u}} & \frac{\partial \boldsymbol{L}}{\partial \dot{p}_\ell} & \frac{\partial \boldsymbol{L}}{\partial \dot{\theta}} \end{bmatrix} \tag{6.6}$$

Thus the change in velocity, $\delta \boldsymbol{V}$, can be solved for using equation 6.6 by

$$\delta \boldsymbol{V} = \left(\frac{\partial \boldsymbol{R}}{\partial \boldsymbol{V}} \right)^{-1} \boldsymbol{R}^k. \tag{6.7}$$

Then $\boldsymbol{V}$ and $\boldsymbol{D}$ solved with

$$\boldsymbol{V}^{k+1} = \boldsymbol{V}^k + \delta\boldsymbol{V}, \tag{6.8}$$

and

$$\boldsymbol{D}^{k+1} = \boldsymbol{D}^k + \alpha\Delta t\boldsymbol{V}^{k+1}. \tag{6.9}$$

The linearized form of the time change of the balance equations is

$$\mathscr{L}A_{n+1} = A^o_{n+1} + \delta A_{n+1} = 0. \; A = G, H, L. \tag{6.10}$$

where δA represents a perturbation in the change in A balance equation with respect to time due to a small perturbation in the change of field variables with respect to time $(\dot{\boldsymbol{u}}, \dot{p}_\ell, \dot{\theta})$, thus,

$$\delta\dot{A} = \frac{\partial A}{\partial \dot{u}_i}\delta\dot{u}_i + \frac{\partial A}{\partial \dot{p}_\ell}\delta\dot{p}_\ell + \frac{\partial A}{\partial \dot{\theta}}\delta\dot{\theta}. \tag{6.11}$$

Additionally, it is useful to realize that

$$\begin{aligned} \frac{\partial u_i}{\partial \dot{u}_i} &= \alpha\Delta t \\ \frac{\partial p_\ell}{\partial \dot{p}_\ell} &= \alpha\Delta t \\ \frac{\partial \theta}{\partial \dot{\theta}} &= \alpha\Delta t. \end{aligned} \tag{6.12}$$

Figure 6.1 shows Newton-Raphson process.
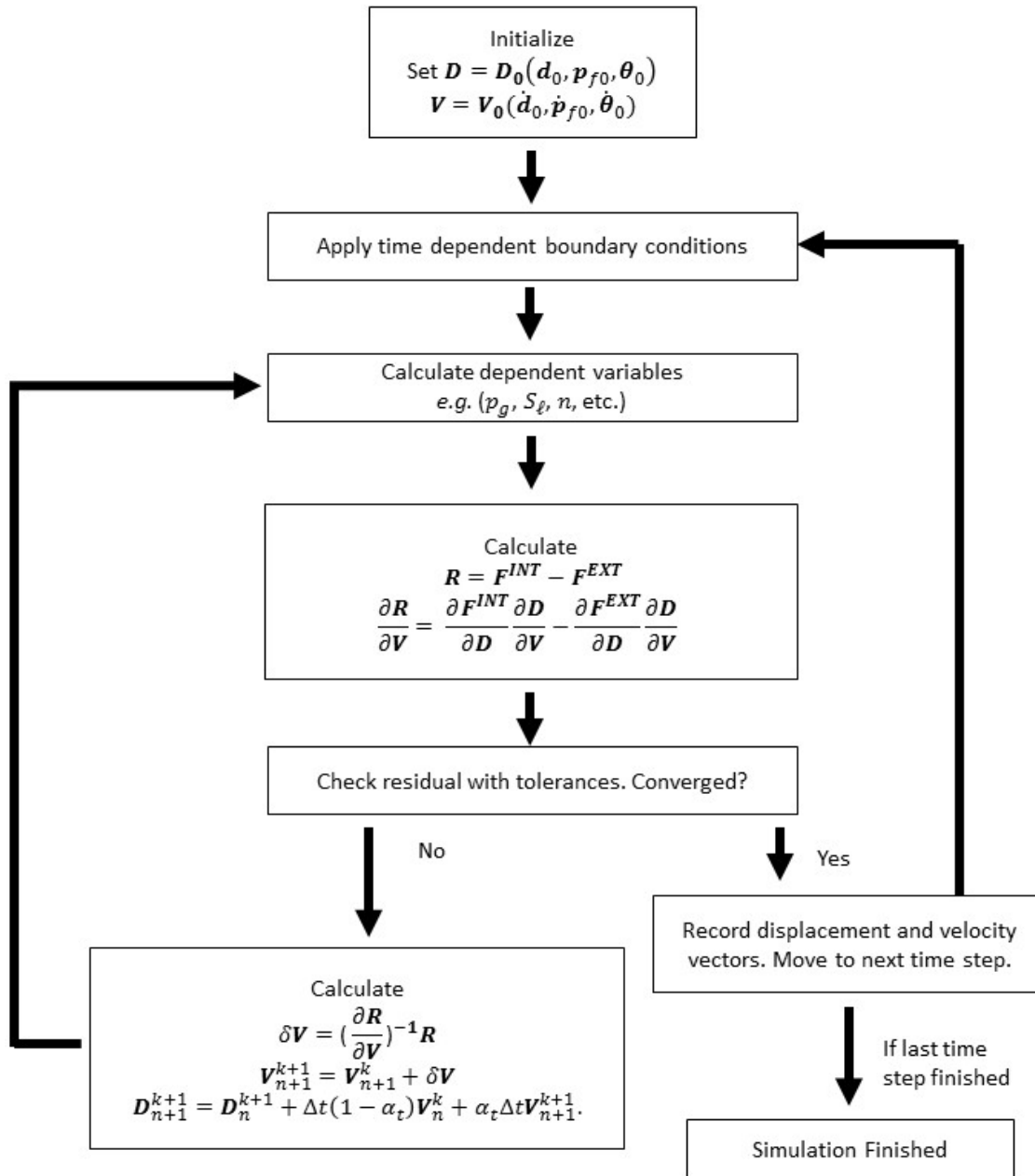
Figure 6.1: Flow chart for generalized trapezoid, Newton-Raphson algorithm.

6.2 Linearization of Balance of Linear Momentum (G)

To find the tangent stiffness $\left(\frac{\partial \boldsymbol{R}}{\partial \boldsymbol{V}}\right)$ it is necessary to find the linearized terms as shown in equations 6.10 and 6.11. This next section will step through the linearization process of each term. For clarity, index notation will be used.

δG_1^{int}

The δG_1^{int} term is not a function of p_ℓ or θ thus

$$\delta G_1^{int} = \frac{\partial G_1^{int}}{\partial \dot{u}_j} \delta \dot{u}_j. \tag{6.13}$$

To get an expanded form it is beneficial to find the partial derivative of G_1^{int} with respect to u_j as

$$\frac{\partial G_1^{int}}{\partial u_j} = \frac{\partial \left(\frac{\partial w_i^u}{\partial X_I} F_{iA} S'_{AI}\right)}{\partial u_j} \tag{6.14}$$

or, expanding,

$$\frac{\partial G_1^{int}}{\partial u_j} = \frac{\partial \left(\frac{\partial w_i^u}{\partial X_I}\right)}{\partial u_j} F_{iA} S'_{AI} + \frac{\partial w_i^u}{\partial X_I} \frac{\partial (F_{iA} S'_{AI})}{\partial u_j}. \tag{6.15}$$

As weighting functions are not a function of field variables 6.15 can be simplified to

$$\frac{\partial G_1^{int}}{\partial u_j} = \frac{\partial w_i^u}{\partial X_I} \frac{\partial (F_{iA} S'_{AI})}{\partial u_j}. \tag{6.16}$$

For numerical implementation via the finite element method it is beneficial to write equation 6.16 as

$$\frac{\partial w_i^u}{\partial X_I} \frac{\partial (F_{iA} S'_{AI})}{\partial u_j} = \frac{\partial (F_{iA} S'_{AI})}{\partial F_{bB}} \frac{\partial F_{bB}}{\partial u_j} \tag{6.17}$$

where

$$\frac{\partial F_{bB}}{\partial u_j} = \frac{\partial \left(\delta_{bB}^{kron} + \frac{\partial u_b}{\partial X_B}\right)}{\partial u_j} = \delta_{bj}^{kron} \frac{\partial u_j}{\partial X_B} = \frac{\partial \delta \dot{u}_b}{\partial X_B} \alpha \Delta t \tag{6.18}$$

where δ^{kron} is the Kronecker delta. Now examining $\frac{\partial(F_{iA}S'_{AI})}{\partial F_{bB}}$ yields

$$\frac{\partial(F_{iA}S'_{AI})}{\partial F_{bB}} = \frac{\partial F_{iA}}{\partial F_{bB}}S'_{AI} + F_{iA}\frac{\partial S'_{AI}}{\partial F_{bB}} \tag{6.19}$$

where

$$\frac{\partial F_{iA}}{\partial F_{bB}} = \delta^{kron}_{ib}\delta^{kron}_{AB} \tag{6.20}$$

and

$$\frac{S'_{AI}}{\partial F_{bB}} = \frac{\partial(\mu_s\delta^{kron}_{AI} + [\lambda lnJ - \mu_s]C^{-1}_{AI})}{\partial F_{bB}}. \tag{6.21}$$

Expanding 6.21 gives

$$\frac{S'_{AI}}{\partial F_{bB}} = \lambda\frac{\partial(lnJ)}{\partial F_{bB}}C^{-1}_{AI} + [\lambda lnJ - \mu_s]\frac{\partial C^{-1}_{AI}}{\partial F_{bB}} \tag{6.22}$$

where

$$\frac{\partial(lnJ)}{\partial F_{bB}} = \frac{1}{J}\frac{\partial J}{\partial F_{bB}} = F^{-1}_{Bb}. \tag{6.23}$$

Expansion of $\frac{\partial C^{-1}_{AI}}{\partial F_{bB}}$ gives

$$\frac{\partial C^{-1}_{AI}}{\partial F_{bB}} = -C^{-1}_{AM}\frac{\partial C_{MN}}{\partial F_{bB}}C^{-1}_{NI} \tag{6.24}$$

where

$$\frac{\partial C_{MN}}{\partial F_{bB}} = \frac{\partial F_{kM}F_{kN}}{\partial F_{bB}} = \delta^{kron}_{kb}\delta^{kron}_{MB}F_{kN} + F_{bM}\delta^{kron}_{kb}\delta^{kron}_{NB}. \tag{6.25}$$

Therefore the final linearization of G^{int}_1 gives

$$\delta G^{int}_1 = \frac{\partial w^u_i}{\partial X_I}\Big[\delta^{kron}_{bi}S_{AI} + \big(\lambda F^{-1}_{Ab}F^{-1}_{Ii} - (\lambda lnJ - \mu_s)(F^{-1}_{Ai}F^{-1}_{Ib} + \delta^{kron}_{bi}C^{-1}_{AI})\big)\Big]\frac{\partial\delta\dot{u}_b}{\partial X_A}\alpha\Delta t. \tag{6.26}$$

δG_2^{int}

The linearization of G_2^{int} can be written as

$$\delta G_2^{int} = \frac{\partial G_2^{int}}{\partial \dot{u}_j}\delta \dot{u}_j + \frac{\partial G_2^{int}}{\partial \dot{p}_\ell}\delta \dot{p}_\ell + \frac{\partial G_2^{int}}{\partial \dot{\theta}}\delta \dot{\theta}. \tag{6.27}$$

Examining the first term it can be seen that

$$\frac{\partial G_2^{int}}{\partial u_j} = \frac{\partial}{\partial u_j}\left(J\big(p_\ell\chi + p_g(1-\chi)\big)F_{Ii}^{-1}\frac{\partial w_i^u}{\partial X_I}\right). \tag{6.28}$$

Applying the chain rule and assuming χ is not a function of u_j and rearranging yields

$$\frac{\partial G_2^{int}}{\partial u_j} = \frac{\partial w_i^u}{\partial X_I}\big(p_\ell\chi + p_g(1+\chi)\big)\left[\frac{\partial J}{\partial F_{aA}}F_{Ii}^{-1} + J\frac{\partial F_{Ii}^{-1}}{\partial F_{aA}}\right]\frac{\partial u_a}{\partial X_A} \tag{6.29}$$

where

$$\frac{\partial J}{\partial F_{aA}} = JF_{Aa}^{-1} \tag{6.30}$$

and

$$\frac{\partial F_{Ii}^{-1}}{\partial F_{aA}} = -F_{Ib}^{-1}\frac{\partial F_{bB}}{\partial F_{aA}}F_{Bi}^{-1} \tag{6.31}$$

where $\frac{\partial F_{bB}}{\partial F_{aA}}$ is defined by equation 6.20. Combining 6.11, 6.29, 6.30, and 6.31 gives the final G_2^{int} perturbation with respect to displacement,

$$\frac{\partial G_2^{int}}{\partial \dot{u}_j}\delta \dot{u}_j = \frac{\partial w_i^u}{\partial X_I}\big(p_\ell\chi + p_g(1-\chi)\big)J[F_{Ii}^{-1}F_{Aa}^{-1} - F_{Ia}^{-1}F_{Ai}^{-1}]\frac{\partial(\delta \dot{u}_a)}{\partial X_A}\alpha\Delta t. \tag{6.32}$$

Now examining the second term of equation 6.27 one finds

$$\frac{\partial G_2^{int}}{\partial p_\ell} = \frac{\partial}{\partial p_\ell}\left(\frac{\partial w_i^u}{\partial X_I}J\big(p_\ell\chi + p_g(1-\chi)\big)F_{Ii}^{-1}\right) \tag{6.33}$$

which can be simplified to

$$\frac{\partial G_2^{int}}{\partial p_\ell} = \frac{\partial w_i^u}{\partial X_I} J F_{Ii}^{-1} \left[\frac{\partial p_\ell}{\partial p_\ell} \chi - s \frac{\partial \chi}{\partial p_\ell} \right]. \tag{6.34}$$

Applying 6.11 to 6.34 and combining with equation 6.27 gives

$$\frac{\partial G_2^{int}}{\partial \dot{p}_\ell} \delta \dot{p}_\ell = \frac{\partial w_i^u}{\partial X_I} J F_{Ii}^{-1} \left[\chi - s \frac{\partial \chi}{\partial p_\ell} \right] \delta \dot{p}_\ell \alpha \Delta t \tag{6.35}$$

where $\frac{\partial \chi}{\partial p_\ell}$ is defined in 9.1. Examining the third term of 6.27 gives

$$\frac{\partial G_2^{int}}{\partial \theta} = \frac{\partial}{\partial \theta} \left(\frac{\partial w_i^u}{\partial X_I} J \left(p_\ell \chi + p_g (1 - \chi) \right) F_{Ii}^{-1} \right). \tag{6.36}$$

Simplifying 6.36 and applying equation 6.11 gives

$$\frac{\partial G_2^{int}}{\partial \dot{\theta}} \delta \dot{\theta} = \frac{\partial w_i^u}{\partial X_I} J F_{Ii}^{-1} \left[\frac{\partial p_\ell}{\partial \theta} \chi + \frac{\partial p_g}{\partial \theta} (1 - \chi) - s \frac{\partial \chi}{\partial \theta} \right] \delta \dot{\theta} \alpha \Delta t \tag{6.37}$$

where $\frac{\partial p_\ell}{\partial \theta}$, $\frac{\partial p_g}{\partial \theta}$, and $\frac{\partial \chi}{\partial \theta}$ are defined in 9.5, 9.6 and 9.7.

δG_3^{int}, δG_4^{int} and δG_1^{ext}

It is assumed that the acceleration, a_i, gravity, g_i, and traction, t_i, are not a function of the field variables, u_i, p_ℓ and θ; therefore,

$$\delta G_3^{int} = 0, \tag{6.38}$$

$$\delta G_4^{int} = 0 \tag{6.39}$$

$$\delta G_1^{ext} = 0 \tag{6.40}$$

6.3   Linearization of Balance of Mass (H)

δH_1^{int}

The linearization of H_1^{int} can be written as

$$\delta H_1^{int} = \frac{\partial H_1^{int}}{\partial \dot{u}_j}\delta \dot{u}_j + \frac{\partial H_1^{int}}{\partial \dot{p}_\ell}\delta \dot{p}_\ell + \frac{\partial H_1^{int}}{\partial \dot{\theta}}\delta \dot{\theta}. \tag{6.41}$$

Examining the first term of 6.41 yields

$$\frac{\partial H_1^{int}}{\partial \dot{u}_j} = \frac{\partial}{\partial \dot{u}_j}\left(w^p (S_g \rho^{gR} + S_\ell \rho^{\ell R})\dot{J} \right) \tag{6.42}$$

which as S_ℓ, S_g, ρ^{gR}, and $\rho^{\ell R}$ are not a function of deformation (u_j) can be written as

$$\frac{\partial H_1^{int}}{\partial \dot{u}_j} = w^p (S_g \rho^{gR} + S_\ell \rho^{\ell R})\frac{\partial \dot{J}}{\partial \dot{u}_j} \tag{6.43}$$

where using the chain rule

$$\frac{\partial \dot{J}}{\partial u_j} = \frac{\partial (JF_{Ii}^{-1})}{\partial F_{aA}}\frac{\partial F_{aA}}{\partial \dot{u}_j}\dot{F}_{iI} + JF_{Ii}^{-1}\frac{\partial \dot{F}_{iI}}{\partial \dot{u}_i} \tag{6.44}$$

which with equations 6.20 and 6.30 can be simplified to

$$\frac{\partial \dot{J}}{\partial u_j} = JF_{Aa}^{-1}F_{Ii}^{-1}\dot{F}_{iI}\frac{\partial u_a}{X_A}\frac{\partial \dot{u}_j}{\partial u_a} - JF_{Ia}^{-1}F_{Ai}^{-1}\dot{F}_{iI}\frac{\partial u_a}{X_A}\frac{\partial \dot{u}_j}{\partial u_a} + JF_{Ii}\frac{\partial \dot{u}_i}{\partial X_I}. \tag{6.45}$$

Thus, the final combination of 6.45 with 6.43 gives that

$$\frac{\partial H_1^{int}}{\partial \dot{u}_j}\delta \dot{u}_j = w^p (\rho^{gR}S^g + \rho^{\ell R}S^\ell)J\left[F_{Aa}^{-1}F_{Ii}^{-1}\dot{F}_{iI} - F_{Ia}^{-1}F_{Ai}^{-1}\dot{F}_{iI} \right]\frac{\partial \delta \dot{u}_a}{\partial X_A}\alpha \Delta t + F_{Ii}^{-1}\frac{\partial \delta \dot{u}_i}{\partial X_I}. \tag{6.46}$$

The second term of 6.41 is

$$\frac{\partial H_1^{int}}{\partial \dot{p}_\ell} \delta \dot{p}_\ell = \frac{\partial}{\partial \dot{p}_\ell} \left(w^p \left(S_g \rho^{gR} + S_\ell \rho^{\ell R} \right) \dot{J} \right). \tag{6.47}$$

which through recognizing that $\frac{\partial S_g}{\partial p_\ell} = -\frac{\partial S_\ell}{\partial p_\ell}$ and assuming that $\frac{\partial \rho^{lR}}{\partial p_\ell}$ is negligible allows for the final linearized term

$$\frac{\partial H_1^{int}}{\partial \dot{p}_\ell} \delta \dot{p}_\ell = w^p \dot{J} \left(\rho^{\ell R} - \rho^{gR} \right) \frac{\partial S_\ell}{\partial p_\ell} \delta \dot{p}_\ell \alpha \Delta t \tag{6.48}$$

where $\frac{\partial S_\ell}{\partial p_\ell}$ is defined in equations 9.4. The third term of 6.41 with 6.11 is

$$\frac{\partial H_1^{int}}{\partial \dot{\theta}} \delta \dot{\theta} = \frac{\partial (w^p (S_g \rho^{gR} + S_\ell \rho^{\ell R}) \dot{J})}{\partial \theta} \delta \dot{\theta} \alpha \Delta t \tag{6.49}$$

which can be simplified to

$$\frac{\partial H_1^{int}}{\partial \dot{\theta}} \delta \dot{\theta} = w^p \left(\frac{\partial \rho^{gR}}{\partial \theta} S_g + \rho^{gR} \frac{\partial S_g}{\partial \theta} + \frac{\partial \rho^{\ell R}}{\partial \theta} S_\ell + \rho^{\ell R} \frac{\partial S_\ell}{\partial \theta} \right) \dot{J} \delta \dot{\theta} \alpha \Delta t \tag{6.50}$$

where $\frac{\partial \rho^{gR}}{\partial \theta}$, $\frac{\partial \rho^{\ell R}}{\partial \theta}$, $\frac{\partial S_\ell}{\partial \theta}$, and $\frac{\partial S_g}{\partial \theta}$ are defined in 9.14, 9.12, 9.10, and 9.15.

δH_2^{int}

The linearization of δH_2^{int} can be written as

$$\delta H_2^{int} = \frac{\partial H_2^{int}}{\partial \dot{u}_j} \delta \dot{u}_j + \frac{\partial H_2^{int}}{\partial \dot{p}_\ell} \delta \dot{p}_\ell + \frac{\partial H_2^{int}}{\partial \dot{\theta}} \delta \dot{\theta}. \tag{6.51}$$

An examination of the first term yields

$$\frac{H_2^{int}}{\partial u_j} = \frac{\partial}{\partial u_j} \left(w^p J \left[(1-n)(\rho^{\ell R} S_\ell + \rho^{gR} S_g) \beta_S^\theta + n \rho^{\ell R} S_\ell \beta_\ell^\theta \right] \dot{\theta} \right) \tag{6.52}$$

which can be written as

$$\frac{H_2^{int}}{\partial u_j} = w^p \frac{\partial J}{\partial u_j} \beta_{s\ell g}^\theta + w^p J \frac{\beta_{s\ell g}^\theta}{\partial u_j} \tag{6.53}$$

with

$$\beta_{s\ell g}^\theta = \left[(1-n)(\rho^{\ell R} S_\ell + \rho^{gR} S_g)\beta_s^\theta + n\rho^{\ell R} S_\ell \beta_\ell^\theta\right]\dot{\theta}. \tag{6.54}$$

Examining the second term of equation 6.53 it can be seen that

$$\frac{\partial \beta_{s\ell g}^\theta}{\partial u_j} = \frac{\partial(1-n)}{\partial u_j}(\rho^{\ell R} S_\ell + \rho^{gR} S_g)\beta_s^\theta \dot{\theta} + \frac{\partial n}{\partial u_j}\rho^{\ell R} S_\ell \beta_\ell^\theta \dot{\theta}. \tag{6.55}$$

Recalling that $n_s = 1 - n$ allows for 6.55 to be written as

$$\frac{\partial \beta_{s\ell g}^\theta}{\partial u_j} = \frac{\partial(n_s)}{\partial u_j}(\rho^{\ell R} S_\ell + \rho^{gR} S_g)\beta_s^\theta \dot{\theta} - \frac{\partial n_s}{\partial u_j}\rho^{\ell R} S_\ell \beta_\ell^\theta \dot{\theta}. \tag{6.56}$$

where

$$\frac{\partial n_s}{\partial u_j} = n_{s0}\frac{\partial(\frac{1}{J})}{\partial u_j} = n_{s0}(-\frac{1}{J})F_{Ij}^{-1}\frac{\partial u_j}{\partial X_I}. \tag{6.57}$$

Combining equations 6.52 - 6.57 and arranging dummy indices gives

$$\frac{\partial H_2^{int}}{\partial \dot{u}_j}\delta\dot{u}_j = w^p J \left[F_{Ii}^{-1}\beta_{s\ell g}^\theta - \frac{(1-n_0)}{J}F_{Ii}^{-1}(\rho^{\ell R} S_\ell + \rho^{gR} S_g)\beta_s^\theta \dot{\theta} \right. \\ \left. + \frac{(1-n_0)}{J}F_{Ii}^{-1}\rho^{\ell R} S_\ell \beta_\ell^\theta \dot{\theta} \right]\frac{\partial \delta\dot{u}_i}{\partial X_I}\alpha\Delta t. \tag{6.58}$$

Expanding the second term of 6.51 yields

$$\frac{\partial H_2^{int}}{\partial \dot{p}_\ell}\delta\dot{p}_\ell = \frac{\partial}{\partial p_\ell}(w^p J[(1-n)(\rho^{\ell R} S_\ell + \rho^{gR} S_g)\beta_s^\theta + n\rho^{\ell R} S_\ell \beta_\ell^\theta]\dot{\theta})\delta\dot{p}_\ell \alpha\Delta t \tag{6.59}$$

which applying $S_g = 1 - S_\ell$ and simplifying can be written as

$$\frac{\partial H_2^{int}}{\partial \dot{p}_\ell}\delta\dot{p}_\ell = w^p J(\beta_s^\theta(1-n)(\rho^{\ell R} - \rho^{gR}) + n\rho^{\ell R}\beta_\ell^\theta)\dot{\theta}\frac{\partial S_\ell}{\partial p_\ell}\delta\dot{p}_\ell \alpha\Delta t \tag{6.60}$$

where $\frac{\partial S_\ell}{\partial p_\ell}$ is defined in 9.4. Expanding the third term of 6.51 gives

$$\frac{\partial H_2^{int}}{\partial \dot{\theta}} \delta \dot{\theta} = \frac{\partial}{\partial \theta} \left(w^p J[(1-n)(\rho^{\ell R} S_\ell + \rho^{gR} S_g) \beta_s^\theta + n \rho^{\ell R} S_\ell \beta_\ell^\theta \right) \dot{\theta} \delta \dot{\theta} \alpha \Delta t$$
$$+ \left(w^p J[(1-n)(\rho^{\ell R} S_\ell + \rho^{gR} S_g) \beta_s^\theta + n \rho^{\ell R} S_\ell \beta_\ell^\theta \right) \delta \dot{\theta}. \tag{6.61}$$

which by assuming that β_ℓ^θ and β_s^θ are constant with respect to temperature can be expanded to yield

$$\frac{\partial H_2^{int}}{\partial \dot{\theta}} \delta \dot{\theta} = w^p J(1-n) \beta_s^\theta \dot{\theta} \left(\frac{\partial (\rho^{\ell R} S_\ell)}{\partial \theta} + \frac{\partial (\rho^{gR} S_g)}{\partial \theta} \right) \delta \dot{\theta} \alpha \Delta t$$
$$+ w^p J n \beta_\ell^\theta \dot{\theta} \frac{\partial (\rho^{\ell R} S_\ell)}{\partial \theta} \delta \dot{\theta} \alpha \Delta t + \left(w^p J[(1-n)(\rho^{\ell R} S_\ell + \rho^{gR} S_g) \beta_s^\theta + n \rho^{\ell R} S_\ell \beta_\ell^\theta \right) \delta \dot{\theta} \tag{6.62}$$

which is expanded via chain rule to

$$\frac{\partial H_2^{int}}{\partial \dot{\theta}} \delta \dot{\theta} = w^p J(1-n) \beta_s^\theta \dot{\theta} \left(\frac{\partial \rho^{\ell R}}{\partial \theta} S_\ell + \rho^{\ell R} \frac{\partial S_\ell}{\partial \theta} + \frac{\partial \rho^{gR}}{\partial \theta} S_g + \rho^{gR} \frac{\partial S_g}{\partial \theta} \right) \delta \dot{\theta} \alpha \Delta t$$
$$+ w^p J n \beta_\ell^\theta \dot{\theta} \left(\frac{\partial \rho^{\ell R}}{\partial \theta} S_\ell + \rho^{\ell R} \frac{\partial S_\ell}{\partial \theta} \right) \delta \dot{\theta} \alpha \Delta t \tag{6.63}$$
$$+ \left(w^p J[(1-n)(\rho^{\ell R} S_\ell + \rho^{gR} S_g) \beta_s^\theta + n \rho^{\ell R} S_\ell \beta_\ell^\theta \right) \delta \dot{\theta}$$

where $\frac{\partial (\rho^{\ell R})}{\partial \theta}$, $\frac{\partial S_\ell}{\partial \theta}$, $\frac{\partial (\rho^{gR})}{\partial \theta}$, and $\frac{\partial S_g}{\partial \theta}$ are defined in 9.12, 9.10, 9.14, and 9.15, respectively.

δH_3^{int}

The linearization of H_3^{int} can be written as

$$\delta H_3^{int} = \frac{\partial H_3^{int}}{\partial \dot{u}_j} \delta \dot{u}_j + \frac{\partial H_3^{int}}{\partial \dot{p}_\ell} \delta \dot{p}_\ell + \frac{\partial H_3^{int}}{\partial \dot{\theta}} \delta \dot{\theta}. \tag{6.64}$$

The first term leads to

$$\frac{\partial H_3^{int}}{\partial u_j} = \frac{\partial}{\partial F_{aA}} \left(\frac{\partial w^p}{\partial X_i} J F_{Ii}^{-1} \left[\rho^{\ell R} v_{\ell_i}^D + \rho^{gR} v_{g_i}^D \right] \right) \frac{\partial F_{aA}}{\partial u_j} \tag{6.65}$$

which can be expanded and simplified using 6.18 to be

$$\frac{\partial H_3^{int}}{\partial u_j} = \frac{\partial w^p}{\partial X_I} \left(\frac{\partial (JF_{Ii}^{-1})}{\partial F_{aA}} [\rho^{\ell R} v_{\ell_i}^D + \rho^{gR} v_{g_i}^D] + JF_{Ii}^{-1} \frac{\partial}{\partial F_{aA}} [\rho^{\ell R} v_{\ell_i}^D + \rho^{gR} v_{g_i}^D] \right) \frac{\partial u_a}{\partial X_A}. \tag{6.66}$$

Applying equations 6.30 and 6.31 to the first portion of equation 6.66 gives

$$\frac{\partial (JF_{Ii}^{-1})}{\partial F_{aA}} [\rho^{\ell R} v_{\ell_i}^D + \rho^{gR} v_{g_i}^D] = J \left[\left(F_{Aa}^{-1} F_{Ii}^{-1} - F_{Ia}^{-1} F_{Ai}^{-1} \right) [\rho^{\ell R} v_{\ell_i}^D + \rho^{gR} v_{g_i}^D] \right]. \tag{6.67}$$

Inserting 6.67 in 6.66 and rearranging gives the final linearization for H_3^{int} with respect to u_j as

$$\frac{\partial H_3^{int}}{\partial \dot{u}_j} \delta \dot{u}_j = \frac{\partial w^p}{\partial X_I} J \left[\left(F_{Aa}^{-1} F_{Ii}^{-1} - F_{Ia}^{-1} F_{Ai}^{-1} \right) [\rho^{\ell R} v_{\ell_i}^D + \rho^{gR} v_{g_i}^D] \right.$$
$$\left. + F_{Ii}^{-1} \left(\rho^{\ell R} \frac{\partial v_{\ell_i}^D}{\partial F_{aA}} + \rho^{gR} \frac{\partial v_{g_i}^D}{\partial F_{aA}} \right) \right] \frac{\partial \delta \dot{u}_a}{\partial X_A} \alpha \Delta t \tag{6.68}$$

where $\frac{\partial v_{g_i}^D}{\partial F_{aA}}$ and $\frac{\partial v_{\ell_i}^D}{\partial F_{aA}}$ are defined by 9.18. Now from the second part of 6.64 it can be seen that

$$\frac{\partial H_3^{int}}{\partial p_\ell} = \frac{\partial}{\partial p_\ell} \left(\frac{\partial w^p}{\partial X_I} JF_{Ii}^{-1} [\rho^{\ell R} v_{\ell_i}^D + \rho^{gR} v_{g_i}^D] \right). \tag{6.69}$$

Assuming $\rho^{\ell R}$, and ρ^{gR} are not a function of liquid pressure, p_ℓ equation 6.69 becomes

$$\frac{\partial H_3^{int}}{\partial p_\ell} = \frac{\partial w^p}{\partial X_I} JF_{Ii}^{-1} \rho^{\ell R} \frac{\partial v_{\ell_i}^D}{\partial p_\ell} \tag{6.70}$$

where $\frac{\partial v_{\ell_i}^D}{\partial p_\ell}$ and is defined in 9.25. This allows for 6.70 to be written in final form as

$$\frac{\partial H_3^{int}}{\partial \dot{p}_\ell} \delta \dot{p}_\ell = \frac{\partial w^p}{\partial X_I} JF_{Ii}^{-1} \rho^{\ell R} \frac{k_{rel}^\ell}{\mu_\ell} F_{Ji}^{-1} \left(\frac{\partial k_{int}^\ell}{\partial p_\ell} \frac{\partial p_\ell}{\partial X_J} \right) \delta \dot{p}_\ell \alpha \Delta t$$
$$+ \frac{\partial w^p}{\partial X_I} JF_{Ii}^{-1} \rho^{\ell R} \frac{k_{rel}^\ell}{\mu_\ell} F_{Ji}^{-1} \left(k_{int}^\ell \frac{\partial \delta \dot{p}_\ell}{\partial X_J} \right) \alpha \Delta t + \frac{\partial w^p}{\partial X_I} JF_{Ii}^{-1} \rho^{gR} \frac{k_{rel}^\ell}{\mu_\ell} F_{Ji}^{-1} \left(\frac{\partial k_{int}^g}{\partial p_g} \frac{\partial p_g}{\partial X_J} \right) \delta \dot{p}_g \alpha \Delta t \tag{6.71}$$

where $\frac{\partial k_{int}^{\ell}}{\partial p_{\ell}}$ and $\frac{\partial k_{int}^{g}}{\partial p_g}$ are defined in 9.27 and 9.27. Along these same lines the final portion of 6.64 leads to

$$\frac{\partial H_3^{int}}{\partial \theta} = \frac{\partial}{\partial \theta} \left(\frac{\partial w^p}{\partial X_I} J F_{Ii}^{-1} \left[\rho^{\ell R} v_{\ell_i}^D + \rho^{g R} v_{g_i}^D \right] \right), \tag{6.72}$$

which can be expanded to

$$\frac{\partial H_3^{int}}{\partial \theta} = \frac{\partial w^p}{\partial X_I} J F_{Ii}^{-1} \left[\frac{\partial \rho^{\ell R}}{\partial \theta} v_{\ell_i}^D + \rho^{\ell R} \frac{\partial v_{\ell_i}^D}{\partial \theta} + \frac{\partial \rho^{g R}}{\partial \theta} v_{g_i}^D + \rho^{g R} \frac{\partial v_{g_i}^D}{\partial \theta} \right]. \tag{6.73}$$

This leads to the final version of

$$\frac{\partial H_3^{int}}{\partial \dot{\theta}} \delta \dot{\theta} = \frac{\partial w^p}{\partial X_I} J F_{Ii}^{-1} \left[\frac{\partial \rho^{\ell R}}{\partial \theta} v_{\ell_i}^D + \rho^{\ell R} \frac{\partial v_{\ell_i}^D}{\partial \theta} + \frac{\partial \rho^{g R}}{\partial \theta} v_{g_i}^D + \rho^{g R} \frac{\partial v_{g_i}^D}{\partial \theta} \right] \delta \dot{\theta} \alpha \Delta t \tag{6.74}$$

where $\frac{\partial \rho^{\ell R}}{\partial \theta}$, $\frac{\partial v_{\ell_i}^D}{\partial \theta}$, $\frac{\partial \rho^{g R}}{\partial \theta}$, and $\frac{\partial v_{g_i}^D}{\partial \theta}$ are defined in 9.12, 9.33, 9.14, and 9.37.

δH_4^{int}

Moving on to δH_4^{int} it can be seen that

$$\delta H_4^{int} = \frac{\partial H_4^{int}}{\partial \dot{u}_j} \delta \dot{u}_j + \frac{\partial H_4^{int}}{\partial \dot{p}_{\ell}} \delta \dot{p}_{\ell} + \frac{\partial H_4^{int}}{\partial \dot{\theta}} \delta \dot{\theta}. \tag{6.75}$$

Looking at the first portion of equation 6.75 one can write

$$\frac{\partial H_4^{int}}{\partial u_j} = \frac{\partial}{\partial F_{aA}} \left(w^p J [\rho^{\ell R} n \dot{S}_{\ell} + n \rho^{g R} \dot{S}_g + n S_g \dot{\rho}^{g R}] \right) \frac{\partial F_{aA}}{\partial u_j} \tag{6.76}$$

which, assuming $\rho^{\ell R}, \rho^{g R}, \dot{S}_{\ell}$, and $\dot{S}_g$ are not of function of deformation, can be simplified to

$$\frac{\partial H_4^{int}}{\partial \dot{u}_j} \delta \dot{u}_j = w^p \left(\frac{\partial J}{\partial F_{aA}} n + J \frac{\partial n}{\partial F_{aA}} \right) (\rho^{\ell R} \dot{S}_{\ell} + \rho^{g R} \dot{S}_g + S_g \dot{\rho}^{g R}) \frac{\partial \dot{u}_a}{\partial X_A} \alpha \Delta t. \tag{6.77}$$

where $\frac{\partial n}{\partial F_{aA}}$ is defined in 9.23 and $\frac{\partial J}{\partial F_{aA}}$ in 6.30. Examining the second term of 6.75 allows for

$$\frac{\partial H_4^{int}}{\partial \dot{p}_\ell} = \frac{\partial}{\partial \dot{p}_\ell}\left(w^p J[\rho^{\ell R} n \dot{S}_\ell + n\rho^{gR}\dot{S}_g + nS_g\dot{\rho}^{gR}]\right) \tag{6.78}$$

which, assuming that only $\dot{S}_g$ and $\dot{S}_\ell$ are a function of $\dot{p}_\ell$ and recognizing that $\dot{S}_\ell = -\dot{S}_g$, can be expanded to

$$\frac{\partial H_4^{int}}{\partial \dot{p}_\ell} = w^p Jn(\rho^{\ell R} - \rho^{gR})\frac{\partial \dot{S}_\ell}{\partial \dot{p}_\ell} \tag{6.79}$$

leading to the final linearized form

$$\frac{\partial H_4^{int}}{\partial \dot{p}_\ell}\delta\dot{p}_\ell = w^p Jn(\rho^{\ell R} - \rho^{gR})\frac{\partial \dot{S}_\ell}{\partial \dot{p}_\ell}\delta\dot{p}_\ell \tag{6.80}$$

where $\frac{\partial \dot{S}_\ell}{\partial \dot{p}_\ell}$ is given in 9.41.

The final portion of 6.75 can be expanded with the chain rule as

$$\begin{aligned}\frac{\partial H_4^{int}}{\partial \dot{\theta}}\dot{\theta} = w^p Jn\left(\frac{\partial \rho^{\ell R}}{\partial \theta}\dot{S}_\ell + \frac{\partial \rho^{gR}}{\partial \theta}\dot{S}_g \right. \\ \left. +\dot{\rho}^{gR}\frac{\partial S_g}{\partial \theta}\right)\delta\dot{\theta}\alpha\Delta t + w^p Jn\left((\rho^{\ell R} - \rho^{gR})\frac{\partial \dot{S}\ell}{\partial \dot{\theta}} + S_g\frac{\partial \dot{\rho}^{gR}}{\partial \dot{\theta}}\right)\delta\dot{\theta}\end{aligned} \tag{6.81}$$

where $\frac{\partial \rho^{\ell R}}{\partial \theta}$, $\frac{\partial \rho^{gR}}{\partial \theta}$, $\frac{\partial S_g}{\partial \theta}$, $\frac{\partial \dot{S}_\ell}{\partial \dot{\theta}}$, and $\frac{\dot{\rho}^{gR}}{\partial \theta}$ are defined in 9.12, 9.14, 9.15, 9.41, and 9.14 respectively.

δH_5^{int}

Moving on, δH_5^{int} it can be seen that

$$\delta H_5^{int} = \frac{\partial H_5^{int}}{\partial \dot{u}_j}\delta\dot{u}_j + \frac{\partial H_5^{int}}{\partial \dot{p}_\ell}\delta\dot{p}_\ell + \frac{\partial H_5^{int}}{\partial \dot{\theta}}\delta\dot{\theta} \tag{6.82}$$

Examining the first term of equation 6.82 one can see the first term leads to

$$\frac{\partial H_5^{int}}{\partial u_j} = \frac{\partial}{\partial F_{aA}}\left(w^p\left(\frac{\rho^{\ell R} JnS_\ell}{K_{bulk}^\ell}\dot{p}_\ell + \frac{J\rho^{\ell R}}{K_{bulk}^\ell}\frac{\partial p_\ell}{\partial X_I}v_{\ell_i}^D F_{Ii}^{-1}\right)\right)\frac{\partial F_{aA}}{\partial u_j} \tag{6.83}$$

which can be expanded through the chain rule to be

$$\frac{\partial H_5^{int}}{\partial u_j} = w^p\rho^{\ell R}\left(\frac{\partial J}{\partial F_{aA}}\left(\frac{nS_\ell}{K_{bulk}^\ell}\dot{p}_\ell + \frac{1}{K_{bulk}^\ell}\frac{\partial p_\ell}{\partial X_I}v_{\ell_i}^D F_{Ii}^{-1}\right) + J\frac{\partial n}{\partial F_{aA}}\frac{S_\ell}{K_\ell}\dot{p}_\ell\right.$$
$$\left. + \frac{J}{K_{bulk}^\ell}\frac{\partial p_\ell}{\partial X_I}\frac{\partial v_{\ell_i}^D}{\partial F_{aA}}F_{Ii}^{-1} + \frac{J}{K_{bulk}^\ell}\frac{\partial p_\ell}{\partial X_I}v_{\ell_i}^D\frac{\partial F_{Ii}^{-1}}{\partial F_{aA}}\right)\frac{\partial F_{aA}}{\partial u_j}. \tag{6.84}$$

Applying equations 6.20 and 6.30 allows for the first term of equation 6.82 to be written as

$$\frac{\partial H_5^{int}}{\partial \dot{u})j}\delta\dot{u}_j = w^p\rho^{\ell R}J\left(F_{Aa}^{-1}\left(\frac{nS_\ell}{K_{bulk}^\ell}\dot{p}_\ell + \frac{1}{K_{bulk}^\ell}\frac{\partial p_\ell}{\partial X_I}v_{\ell_i}^D F_{Ii}^{-1}\right)\right.$$
$$\left. + \frac{J}{K_{bulk}^\ell}\frac{\partial p_\ell}{\partial X_I}\frac{\partial v_{\ell_i}^D}{\partial F_{aA}}F_{Ii}^{-1} + \frac{1}{K_{bulk}^\ell}\frac{\partial p_\ell}{\partial X_I}v_{\ell_i}^D F_{Ia}^{-1}F_{Ai}^{-1}\right)\frac{\partial\delta\dot{u}_a}{\partial X_A}\alpha\Delta t \tag{6.85}$$

where $\frac{\partial v_{\ell_i}^D}{\partial F_{aA}}$ is defined in equation 9.18.

The second term of equation 6.82 can be written as

$$\frac{\partial H_5^{int}}{\partial \dot{p}_\ell}\delta\dot{p}_\ell = \frac{\partial}{\partial \dot{p}_\ell}\left(w^p\rho^{\ell R}\left(\frac{JnS_\ell}{K_{bulk}^\ell}\dot{p}_\ell + \frac{J}{K_{bulk}^\ell}\frac{\partial p_\ell}{\partial X_I}v_{\ell_i}^D F_{Ii}^{-1}\right)\right)\delta\dot{p}_\ell \tag{6.86}$$

which can be expanded to

$$\frac{\partial H_5^{int}}{\partial \dot{p}_\ell}\delta\dot{p}_\ell = w^p\rho^{\ell R}\frac{J}{K_{bulk}^\ell}\left(nS_\ell\delta\dot{p}_\ell + n\frac{\partial S_\ell}{\partial p_\ell}\dot{p}_\ell\alpha\Delta t\delta\dot{p}_\ell\right.$$
$$\left. + \frac{\partial\delta\dot{p}_\ell}{\partial X_I}v_{\ell_i}^D F_{Ii}^{-1}\alpha\Delta t + \frac{\partial p_\ell}{\partial X_I}\frac{\partial v_{\ell_i}^D}{\partial p_\ell}F_{Ii}^{-1}\alpha\Delta\delta\dot{p}_\ell\right) \tag{6.87}$$

where $\frac{\partial S_\ell}{\partial p_\ell}$ and $\frac{\partial v_{\ell_i}^D}{\partial p_\ell}$ are defined in equations 9.4 and 9.25.

Finally, the third term of equation 6.82 can be written as

$$\frac{\partial H_5^{int}}{\partial \dot{\theta}}\delta\dot{\theta} = \frac{\partial}{\partial\dot{\theta}}\left(w^p\rho^{\ell R}\left(\frac{JnS_\ell}{K_{bulk}^\ell}\dot{p}_\ell + \frac{J}{K_{bulk}^\ell}\frac{\partial p_\ell}{\partial X_I}v_{\ell_i}^D F_{Ii}^{-1}\right)\right)\delta\dot{\theta} \tag{6.88}$$

which can be expanded and simplified to

$$\frac{\partial H_5^{int}}{\partial\dot{\theta}}\delta\dot{p}_\ell = w^p\frac{J\rho^{\ell R}}{K_{bulk}^\ell}\left(n\frac{\partial S_\ell}{\partial\theta}\dot{p}_\ell + \frac{\partial p_\ell}{\partial X_I}\frac{v_{\ell_i}^D}{\partial\theta}F_{Ii}^{-1}\right)\alpha\Delta t\dot{\theta} \tag{6.89}$$

where $\frac{\partial S_\ell}{\partial\theta}$ and $\frac{\partial v_{\ell_i}^D}{\partial\theta}$ are defined in equation 9.10 and 9.33.

δH_1^{ext}

Moving on to δH_1^{ext} it can be seen that

$$\delta H_1^{ext} = \frac{\partial H_1^{ext}}{\partial\dot{u}_j}\delta\dot{u}_j + \frac{\partial H_1^{ext}}{\partial\dot{p}_\ell}\delta\dot{p}_\ell + \frac{\partial H_1^{ext}}{\partial\dot{\theta}}\delta\dot{\theta} \tag{6.90}$$

which from equation 5.232 can be written as

$$\delta H_1^{ext} = w^p\left(\frac{\partial q_\ell^{flux}}{\partial\dot{u}_j}\delta\dot{u}_j + \frac{\partial q_\ell^{flux}}{\partial\dot{p}_\ell}\delta\dot{p}_\ell + \frac{\partial q_\ell^{flux}}{\partial\dot{\theta}}\delta\dot{\theta}\right) \tag{6.91}$$

where q_ℓ^{flux} is the flux of the liquid and vapor through the boundary. Therefore, these derivatives can vary based on the type of boundary condition used. For the simulations in this thesis q_ℓ^{flux} is defined in 7.5 with its derivatives in 9.45, 9.48 and 9.50.

6.4 Linearization of Balance of Energy (L)

δL_1^{int}

The linearization of L_1^{int} can be written as

$$\delta L_1^{int} = \frac{\partial L_1^{int}}{\partial \dot{u}_j}\delta \dot{u}_j + \frac{\partial L_1^{int}}{\partial \dot{p}_\ell}\delta \dot{p}_\ell + \frac{\partial L_1^{int}}{\partial \dot{\theta}}\delta \dot{\theta}. \tag{6.92}$$

Examining the first term it can be seen that

$$\frac{\partial L_1^{int}}{\partial u_j} = \frac{\partial}{\partial u_j}\left(w^\theta J (\rho C_p)^{eff} \dot{\theta} \right) \tag{6.93}$$

which can be expanded to

$$\frac{\partial L_1^{int}}{\partial u_j} = w^\theta \left(\frac{\partial J}{\partial F_{aA}}(\rho C_p)^{eff}\dot{\theta} + J\frac{\partial (\rho C_p)^{eff}}{\partial F_{aA}}\dot{\theta} \right)\frac{\partial F_{aA}}{\partial u_j}. \tag{6.94}$$

where $\frac{\partial (\rho C_p)^{eff}}{\partial F_{aA}}$ can be written as

$$\frac{\partial (\rho C_p)^{eff}}{\partial F_{aA}} = \frac{\partial}{\partial F_{aA}}\left((1-n)\rho^{sR}C_p^s + n\big(S_\ell \rho^{\ell R}C_p^\ell + S_g\rho^{gR}C_p^g\big) \right) \tag{6.95}$$

which can be simplified to

$$\frac{\partial (\rho C_p)^{eff}}{\partial F_{aA}} = \left(\big(S_\ell \rho^{\ell R}C_p^\ell + S_g\rho^{gR}C_p^g\big) - \rho^{sR}C_p^s \right)\frac{\partial n}{\partial F_{aA}}. \tag{6.96}$$

Finally, combining equations 6.94, 6.96 and 6.30 gives the final form

$$\frac{\partial L_1^{int}}{\partial \dot{u}_j}\delta \dot{u}_j = w^\theta J\dot{\theta}\left(F_{Aa}^{-1}(\rho C_p)^{eff} + \left(\big(S_\ell \rho^{\ell R}C_p^\ell + S_g\rho^{gR}C_p^g\big) - \rho^{sR}C_p^s \right)\frac{\partial n}{\partial F_{aA}} \right)\frac{\partial (\delta \dot{u}_a)}{\partial X_A}\alpha \Delta t \tag{6.97}$$

where $\frac{\partial n}{\partial F_{aA}}$ is defined in 9.23. Now looking at the second term of 6.92 it is seen that

$$\frac{\partial L_1^{int}}{\partial p_\ell} = \frac{\partial}{\partial p_\ell}\left(w^\theta J(\rho C_p)^{eff}\dot\theta\right) \tag{6.98}$$

which applying the chain rule is

$$\frac{\partial L_1^{int}}{\partial p_\ell} = w^\theta J\dot\theta\frac{\partial(\rho C_p)^{eff}}{\partial p_\ell} \tag{6.99}$$

where $\frac{\partial(\rho C_p)^{eff}}{\partial p_\ell}$ can be expanded as

$$\frac{\partial(\rho C_p)^{eff}}{\partial p_\ell} = \frac{\partial}{\partial p_\ell}\left((1-n)\rho^{sR}C_p^s + n\left(S_\ell\rho^{\ell R}C_p^\ell + S_g\rho^{gR}C_p^g\right)\right) \tag{6.100}$$

which can simplified with the fact that $S_g = 1 - S_\ell$ to

$$\frac{\partial(\rho C_p)^{eff}}{\partial p_\ell} = n\left(\rho^{\ell R}C_p^\ell - \rho^{gR}C_p^g\right)\frac{\partial S_\ell}{\partial p_\ell}. \tag{6.101}$$

Lastly, combining equation 6.101 with equations 6.92 and 6.99 gives the linearization

$$\frac{\partial L_1^{int}}{\partial \dot p_\ell}\delta\dot p_\ell = w^\theta J\dot\theta\left(n\left(\rho^{\ell R}C_p^\ell - \rho^{gR}C_p^g\right)\frac{\partial S_\ell}{\partial p_\ell}\right)\delta\dot p_\ell\alpha\Delta t \tag{6.102}$$

where $\frac{\partial S_\ell}{\partial p_\ell}$ is given in 9.4.

From the third term of equation 6.92

$$\frac{\partial L_1^{int}}{\partial \dot\theta}\delta\dot\theta = \frac{\partial}{\partial\theta}\left(w^\theta J(\rho C_p)^{eff}\right)\dot\theta\delta\dot\theta\alpha\Delta t + \left(w^\theta J(\rho C_p)^{eff}\right)\delta\dot\theta. \tag{6.103}$$

A closer examination of the first term of 6.103 gives

$$\frac{\partial(\rho C_p)^{eff}}{\partial\theta} = \frac{\partial}{\partial\theta}\left((1-n)\rho^{sR}C_p^s + n\left(S_\ell\rho^{\ell R}C_p^\ell + S_g\rho^{gR}C_p^g\right)\right) \tag{6.104}$$

which can be expanded to

$$\frac{\partial(\rho C_p)^{eff}}{\partial\theta} = (1-n)\frac{\partial\rho^{sR}}{\partial\theta}C_p^s + n\left(S_\ell\frac{\partial\rho^{\ell R}}{\partial\theta}C_p^\ell + S_g\frac{\partial\rho^{gR}}{\partial\theta}C_p^g\right) + n\left(\rho^{\ell R}C_p^\ell - \rho^{gR}C_p^g\right)\frac{\partial S_\ell}{\partial\theta}. \quad (6.105)$$

Thus, equation 6.103 can be written as

$$\frac{\partial L_1^{int}}{\partial\dot\theta}\delta\dot\theta = \left[w^\theta J\dot\theta\left((1-n)\frac{\partial\rho^{sR}}{\partial\theta}C_p^s + n\left(S_\ell\frac{\partial\rho^{\ell R}}{\partial\theta}C_p^\ell\right.\right.\right.$$
$$\left.\left.\left. +S_g\frac{\partial\rho^{gR}}{\partial\theta}C_p^g\right) + n\left(\rho^{\ell R}C_p^\ell - \rho^{gR}C_p^g\right)\frac{\partial S_\ell}{\partial\theta}\right)\right]\delta\dot\theta\alpha\Delta t + \left(w^\theta J(\rho C_p)^{eff}\right)\delta\dot\theta \quad (6.106)$$

where $\frac{\partial\rho^{\ell R}}{\partial\theta}$, $\frac{\partial\rho^{gR}}{\partial\theta}$ and $\frac{\partial S_\ell}{\partial\theta}$ are found in 9.12, 9.14 and 9.10.

δL_2^{int}

The linearization of L_2^{int} can be written as

$$\delta L_2^{int} = \frac{\partial L_2^{int}}{\partial\dot u_j}\delta\dot u_j + \frac{\partial L_2^{int}}{\partial\dot p_\ell}\delta\dot p_\ell + \frac{\partial L_2^{int}}{\partial\dot\theta}\delta\dot\theta. \quad (6.107)$$

Examination of the first term of 6.107 gives

$$\frac{\partial L_2^{int}}{\partial u_j} = \frac{\partial}{\partial u_j}\left(w^\theta J\rho^{\ell R}C_p^\ell v_{\ell_i}^D\frac{\partial\theta}{\partial X_I}F_{Ii}^{-1}\right) \quad (6.108)$$

or expanding

$$\frac{\partial L_2^{int}}{\partial u_j} = \frac{\partial}{\partial F_{aA}}\left(w^\theta J\rho^{\ell R}C_p^\ell v_{\ell_i}^D\frac{\partial\theta}{\partial X_I}F_{Ii}^{-1}\right)\frac{\partial F_{aA}}{\partial u_j} \quad (6.109)$$

which can be rearranged to be

$$\frac{\partial L_2^{int}}{\partial u_j} = w^\theta\rho^{\ell R}C_p^\ell\frac{\partial\theta}{\partial X_I}\left(\frac{\partial J}{\partial F_{aA}}v_{\ell_i}^D F_{Ii}^{-1} + J\frac{\partial v_{\ell_i}^D}{\partial F_{aA}}F_{Ii}^{-1} + Jv_{\ell_i}^D\frac{\partial F_{Ii}^{-1}}{\partial F_{aA}}\right)\frac{\partial F_{aA}}{\partial u_j} \quad (6.110)$$

which applying 6.30, 6.18 and 6.20 allows for

$$\frac{\partial L_2^{int}}{\partial \dot{u}_j} \delta \dot{u}_j = w^\theta J \rho^{\ell R} C_p^\ell \frac{\partial \theta}{\partial X_I} \left(F_{Aa}^{-1} v_{\ell_i}^D F_{Ii}^{-1} + \frac{\partial v_{\ell_i}^D}{\partial F_{aA}} F_{Ii}^{-1} - v_{\ell_i}^D F_{Ia}^{-1} F_{Ai}^{-1} \right) \frac{\partial (\delta \dot{u}_a)}{\partial X_A} \alpha \Delta t \quad (6.111)$$

where $\frac{\partial v_{\ell_i}^D}{\partial F_{aA}}$ is defined in 9.18. The second term of 6.107 leads to the conclusion that

$$\frac{\partial L_2^{int}}{\partial p_\ell} = \frac{\partial}{\partial p_\ell} \left(w^\theta J \rho^{\ell R} C_p^\ell v_{\ell i}^D \frac{\partial \theta}{\partial X_I} F_{Ii}^{-1} \right). \quad (6.112)$$

Expanding via the chain rule gives

$$\frac{\partial L_2^{int}}{\partial p_\ell} = w^\theta J \rho^{\ell R} C_p^\ell \frac{\partial \theta}{\partial X_I} F_{Ii}^{-1} \frac{\partial v_{\ell_i}^D}{\partial p_\ell} \quad (6.113)$$

which allows for the following,

$$\frac{\partial L_2^{int}}{\partial \dot{p}_\ell} \delta \dot{p}_\ell = w^\theta J \rho^{\ell R} C_p^\ell \frac{\partial \theta}{\partial X_I} F_{Ii}^{-1} \frac{\partial v_{\ell_i}^D}{\partial p_\ell} \delta \dot{p}_\ell \alpha \Delta t \quad (6.114)$$

where $\frac{\partial v_{\ell_i}}{\partial p_\ell}$ is found in 9.25. Finally, the third term of 6.107 can be written as

$$\frac{\partial L_2^{int}}{\partial \dot{\theta}} \delta \dot{\theta} = w^\theta J \rho^{\ell R} C_p^\ell v_{\ell_i}^D F_{Ii}^{-1} \frac{\partial \delta \dot{\theta}}{\partial X_I} \alpha \Delta t + w^\theta J C_p^\ell \frac{\partial \theta}{\partial X_I} F_{Ii}^{-1} \frac{\partial}{\partial \theta} \left(\rho^{\ell R} v_{\ell_i}^D \right) \delta \dot{\theta} \alpha \Delta t \quad (6.115)$$

which can be expanded to its final form as

$$\frac{\partial L_2^{int}}{\partial \dot{\theta}} \delta \dot{\theta} = w^\theta J \rho^{\ell R} C_p^\ell v_{\ell_i}^D F_{Ii}^{-1} \frac{\partial \delta \dot{\theta}}{\partial X_I} \alpha \Delta t + w^\theta J C_p^\ell \frac{\partial \theta}{\partial X_I} F_{Ii}^{-1} \left(\frac{\partial \rho^{\ell R}}{\partial \theta} v_{\ell_i}^D + \rho^{\ell R} \frac{\partial v_{\ell_i}^D}{\partial \theta} \right) \delta \dot{\theta} \alpha \Delta t \quad (6.116)$$

where $\frac{\partial \rho^{\ell R}}{\partial \theta}$ and $\frac{\partial v_{\ell_i}^D}{\partial \theta}$ are defined in 9.12 and 9.33.

$\boldsymbol{\delta L_3^{int}}$

The linearization of L_3^{int} can be written as

$$\delta L_3^{int} = \frac{\partial L_3^{int}}{\partial \dot{u}_j} \delta \dot{u}_j + \frac{\partial L_3^{int}}{\partial \dot{p}_\ell} \delta \dot{p}_\ell + \frac{\partial L_3^{int}}{\partial \dot{\theta}} \delta \dot{\theta}. \tag{6.117}$$

Examination of the first term of 6.117 gives

$$\frac{\partial L_3^{int}}{\partial u_j} = \frac{\partial}{\partial u_j} \left(w^\theta J \rho^{gR} C_p^g v_{g_i}^D \frac{\partial \theta}{\partial X_I} F_{Ii}^{-1} \right) \tag{6.118}$$

which can be expanded to

$$\frac{\partial L_3^{int}}{\partial u_j} = w^\theta \rho^{gR} C_p^g \frac{\partial \theta}{\partial X_I} \left(\frac{\partial J}{\partial F_{aA}} v_{g_i}^D F_{Ii}^{-1} + J \frac{\partial v_{g_i}^D}{\partial F_{aA}} F_{Ii}^{-1} + J v_{g_i}^D \frac{\partial F_{Ii}^{-1}}{\partial F_{aA}} \right) \frac{\partial F_{aA}}{\partial u_j}. \tag{6.119}$$

This allows for the final form to be written as

$$\frac{\partial L_3^{int}}{\partial \dot{u}_j} \delta \dot{u}_j = w^\theta J \rho^{gR} C_p^g \frac{\partial \theta}{\partial X_I} \left(F_{Aa}^{-1} v_{g_i}^D F_{Ii}^{-1} + \frac{\partial v_{g_i}^D}{\partial F_{aA}} F_{Ii}^{-1} - v_{g_i}^D F_{Ia}^{-1} F_{Ai}^{-1} \right) \frac{\partial (\delta \dot{u}_a)}{\partial X_A} \alpha \Delta t \tag{6.120}$$

where $\frac{\partial v_{g_i}^D}{\partial F_{aA}}$ is defined in 9.18.

The second term of equation 6.117 leads to

$$\frac{\partial L_3^{int}}{\partial p_\ell} = \frac{\partial}{\partial p_\ell} \left(w^\theta J \rho^{gR} C_p^g \frac{\partial \theta}{\partial X_I} F_{Ii}^{-1} \right). \tag{6.121}$$

However, none of the terms are dependent on the liquid pressure thus

$$\frac{\partial L_3^{int}}{\partial \dot{p}_\ell} \delta \dot{p}_\ell = 0. \tag{6.122}$$

Finally, the third term of 6.117 can be written as

$$\frac{\partial L_3^{int}}{\partial \dot{\theta}} \delta \dot{\theta} = w^\theta J \rho^{gR} C_p^g v_{g_i}^D F_{Ii}^{-1} \frac{\partial \delta \dot{\theta}}{\partial X_I} \alpha \Delta t + w^\theta J C_p^g \frac{\partial \theta}{\partial X_I} F_{Ii}^{-1} \frac{\partial}{\partial \theta} \left(\rho^{gR} v_{g_i}^D \right) \delta \dot{\theta} \alpha \Delta t \tag{6.123}$$

which can be expanded to its final form as

$$\frac{\partial L_3^{int}}{\partial \dot\theta}\delta\dot\theta = w^\theta J\rho^{gR}C_p^g v_{g_i}^D F_{Ii}^{-1}\frac{\partial \delta\dot\theta}{\partial X_I}\alpha\Delta t + w^\theta JC_p^g\frac{\partial\theta}{\partial X_I}F_{Ii}^{-1}\Big(\frac{\partial\rho^{gR}}{\partial\theta}v_{g_i}^D + \rho^{gR}\frac{\partial v_{g_i}^D}{\partial\theta}\Big)\delta\dot\theta\alpha\Delta t \quad (6.124)$$

where $\frac{\partial\rho^{gR}}{\partial\theta}$ and $\frac{\partial v_{g_i}^D}{\partial\theta}$ are defined in 9.14 and 9.37.

δL_4^{int}

The linearization of L_4^{int} can be expanded to

$$\delta L_4^{int} = \frac{\partial L_4^{int}}{\partial \dot u_j}\delta\dot u_j + \frac{\partial L_4^{int}}{\partial \dot p_\ell}\delta\dot p_\ell + \frac{\partial L_4^{int}}{\partial \dot\theta}\delta\dot\theta. \quad (6.125)$$

Examining the first term of equation 6.125 yields

$$\frac{\partial L_4^{int}}{\partial u_j} = \frac{\partial}{\partial u_j}\Big(w^\theta J\rho^{eff}r\Big) \quad (6.126)$$

this can then be expanded to be

$$\frac{\partial L_4^{int}}{\partial u_j} = \frac{\partial}{\partial F_{aA}}\Big(w^\theta J\rho^{eff}r\Big)\frac{\partial F_{aA}}{\partial u_j}. \quad (6.127)$$

Applying the chain rule gives

$$\frac{\partial L_4^{int}}{\partial u_j} = w^\theta\Big(\frac{J}{F_{aA}}\rho^{eff}r + J\frac{\partial\rho^{eff}}{\partial F_{aA}}r + J\rho^{eff}\frac{\partial r}{\partial F_{aA}}\Big)\frac{\partial F_{aA}}{\partial u_j}. \quad (6.128)$$

Examining the $\frac{\partial\rho^{eff}}{\partial F_{aA}}$ term and expanding via equation 5.9 gives

$$\frac{\partial\rho^{eff}}{\partial F_{aA}} = \frac{\partial}{\partial F_{aA}}\big((1-n)\rho^{sR} + n(S_\ell\rho^{\ell R} + S_g\rho^{gR})\big). \quad (6.129)$$

which can be expanded to

$$\frac{\partial \rho^{eff}}{\partial F_{aA}} = \left((S_\ell \rho^{\ell R} + S_g \rho^{gR}) - \rho^{sR}\right)\frac{\partial n}{\partial F_{aA}}. \tag{6.130}$$

Substituting equations 6.130 and 6.30 into 6.128 and combining with 6.125 yields

$$\frac{\partial L_4^{int}}{\partial \dot{u}_j}\delta \dot{u}_j = w^\theta J\left(F_{Aa}^{-1}\rho^{eff}r + \left((S_\ell \rho^{\ell R} + S_g \rho^{gR}) - \rho^{sR}\right)\frac{\partial n}{\partial F_{aA}}r + \rho^{eff}\frac{\partial r}{\partial F_{aA}}\right)\frac{\partial \delta \dot{u}_a}{\partial X_A}\alpha \Delta t \tag{6.131}$$

where $\frac{\partial n}{\partial F_{aA}}$ is defined in 9.23 and $\frac{\partial r}{\partial F_{aA}}$ is dependent on the source-sink term r. In this work r is not taken to be a function of the deformation. Looking at the second term of equation 6.125 yields

$$\frac{\partial L_4^{int}}{\partial p_\ell} = \frac{\partial}{\partial p_\ell}\left(w^\theta J\rho^{eff}r\right) \tag{6.132}$$

which as r, J, and w^θ are not considered a function of p_ℓ can be expanded to

$$\frac{\partial L_4^{int}}{\partial p_\ell} = w^\theta Jr\frac{\partial \rho^{eff}}{\partial p_\ell} \tag{6.133}$$

where using $S_\ell = (1 - S_g)$, $\frac{\partial \rho^{eff}}{\partial p_\ell}$ can be written as

$$\frac{\partial \rho^{eff}}{\partial p_\ell} = n(\rho^{\ell R} - \rho^{gR})\frac{\partial S_\ell}{\partial p_\ell}. \tag{6.134}$$

This allows the second term of 6.125 to be written as

$$\frac{\partial L_4^{int}}{\partial \dot{p}_\ell}\delta \dot{p}_\ell = w^\theta Jrn(\rho^{\ell R} - \rho^{gR})\frac{\partial S_\ell}{\partial p_\ell}\delta \dot{p}_\ell \alpha \Delta t \tag{6.135}$$

where $\frac{\partial S_\ell}{\partial p_\ell}$ is defined in 9.4. Lastly, examining the second term of equation 6.125 yields

$$\frac{\partial L_4^{int}}{\partial \theta} = \frac{\partial}{\partial \theta}\left(w^\theta J\rho^{eff}r\right) \tag{6.136}$$

which can be simplifying using the assumptions w^θ, J and r are not a function of temperature to

$$\frac{\partial L_4^{int}}{\partial \theta} = w^\theta J r \frac{\partial \rho^{eff}}{\partial \theta} \tag{6.137}$$

where $\frac{\partial \rho^{eff}}{\partial \theta}$ is defined as

$$\frac{\partial \rho^{eff}}{\partial \theta} = n\Big(\frac{\partial \rho^{\ell R}}{\partial \theta} S_\ell + \rho^{\ell R}\frac{\partial S_\ell}{\partial \theta} + \frac{\partial \rho^{gR}}{\partial \theta} S_g + \frac{\partial S_g}{\partial \theta}\Big). \tag{6.138}$$

Combining 6.138 with equations 6.137 allows for the third term of 6.125 to be

$$\frac{\partial L_4^{int}}{\partial \dot\theta}\delta\dot\theta = w^\theta J r n\Big(\frac{\partial \rho^{\ell R}}{\partial \theta} S_\ell + \rho^{\ell R}\frac{\partial S_\ell}{\partial \theta} + \frac{\partial \rho^{gR}}{\partial \theta} S_g + \frac{\partial S_g}{\partial \theta}\Big)\delta\dot\theta\alpha\Delta t \tag{6.139}$$

where $\frac{\partial \rho^{\ell R}}{\partial \theta}$, $\frac{\partial S_\ell}{\partial \theta}$, $\frac{\partial \rho^{gR}}{\partial \theta}$ and $\frac{\partial S_g}{\partial \theta}$ are defined in equations 9.12, 9.10, 9.14 and 9.15 respectively.

δL_5^{int}

The linearization of L_5^{int} can be expanded to

$$\delta L_5^{int} = \frac{\partial L_5^{int}}{\partial \dot u_j}\delta \dot u_j + \frac{\partial L_5^{int}}{\partial \dot p_\ell}\delta \dot p_\ell + \frac{\partial L_5^{int}}{\partial \dot\theta}\delta\dot\theta. \tag{6.140}$$

Examining the first term of equation 6.140 yields

$$\frac{\partial L_5^{int}}{\partial u_j} = \frac{\partial}{\partial u_j}\Big(\frac{\partial w^\theta}{\partial X_J}J\Big(-K^\theta\frac{\partial\theta}{\partial X_I}\Big)F_{Ii}^{-1}F_{Ji}^{-1}\Big) \tag{6.141}$$

where expansion via the chain rule is

$$\frac{\partial L_5^{int}}{\partial u_j} = \frac{\partial w^\theta}{\partial X_J}\frac{\partial\theta}{\partial X_I}\Big(\frac{\partial J}{\partial F_{aA}}(-K^\theta)F_{Ii}^{-1}F_{Ji}^{-1}$$
$$+J\frac{\partial(-K^\theta)}{\partial F_{aA}}F_{Ii}^{-1}F_{Ji}^{-1} + J(-K^\theta)\frac{\partial F_{Ii}^{-1}}{\partial F_{aA}}F_{Ji}^{-1} + J(-K^\theta)F_{Ii}^{-1}\frac{\partial F_{Ji}^{-1}}{\partial F_{aA}}\Big)\frac{\partial F_{aA}}{\partial u_j} \tag{6.142}$$

which applying 6.30, 6.18 and 6.20 allows for

$$\frac{\partial L_5^{int}}{\partial u_j} = \frac{\partial w^\theta}{\partial X_J}\frac{\partial \theta}{\partial X_I}J\left(F_{Aa}^{-1}(-K^\theta)F_{Ii}^{-1}F_{Ji}^{-1}\right.$$
$$\left.-\frac{\partial(K^\theta)}{\partial F_{aA}}F_{Ii}^{-1}F_{Ji}^{-1} - (-K^\theta)F_{Ia}^{-1}F_{Ai}^{-1}F_{Ji}^{-1} - (-K^\theta)F_{Ii}^{-1}F_{Ai}^{-1}F_{Ja}^{-1}\right)\frac{\partial F_{aA}}{\partial u_j} \tag{6.143}$$

where $\frac{\partial(K^\theta)}{\partial F_{aA}}$ is

$$\frac{\partial(K^\theta)}{\partial F_{aA}} = \frac{\partial}{\partial F_{aA}}\left((1-n)K_s^\theta + n(S_\ell K_\ell^\theta + S_g K_g^\theta)\right) \tag{6.144}$$

which can be written as

$$\frac{\partial(-K^\theta)}{\partial F_{aA}} = \frac{\partial n}{\partial F_{aA}}\left(S_\ell K_\ell^\theta + S_g K_g^\theta - K_s^\theta\right) \tag{6.145}$$

which allows for the combination of 6.140, 6.143 and 6.145 to give final linearization of H_5^{int} as

$$\frac{\partial L_5^{int}}{\partial \dot{u}_j}\delta \dot{u}_j = \frac{\partial w^\theta}{\partial X_J}\frac{\partial \theta}{\partial X_I}J\left(F_{Aa}^{-1}(-K^\theta)F_{Ii}^{-1}F_{Ji}^{-1} - \frac{\partial n}{\partial F_{aA}}\left(S_\ell K_\ell^\theta + S_g K_g^\theta\right.\right.$$
$$\left.\left.-K_s^\theta\right)F_{Ii}^{-1}F_{Ji}^{-1} - (-K^\theta)F_{Ia}^{-1}F_{Ai}^{-1}F_{Ji}^{-1} - (-K^\theta)F_{Ii}^{-1}F_{Ai}^{-1}F_{Ja}^{-1}\right)\frac{\partial(\delta \dot{u}_a)}{\partial X_A}\alpha\Delta t \tag{6.146}$$

where $\frac{\partial(n)}{\partial F_{aA}}$ is found in 9.23. Examining the first term of equation 6.140 yields

$$\frac{\partial L_5^{int}}{\partial p_\ell} = \frac{\partial}{\partial p_\ell}\left(\frac{\partial w^\theta}{\partial X_J}J\left(-K^\theta\frac{\partial \theta}{\partial X_I}\right)F_{Ii}^{-1}F_{Ji}^{-1}\right) \tag{6.147}$$

which can be written as

$$\frac{\partial L_5^{int}}{\partial p_\ell} = -\frac{\partial w^\theta}{\partial X_J}J\frac{\partial \theta}{\partial X_I}F_{Ii}^{-1}F_{Ji}^{-1}\frac{\partial K^\theta}{\partial p_\ell} \tag{6.148}$$

where $\frac{\partial K^\theta}{\partial p_\ell}$ can be expanded

$$\frac{\partial K^\theta}{\partial p_\ell} = \frac{\partial}{\partial p_\ell}\left((1-n)K_s^\theta + n(S_\ell K_\ell^\theta + S_g K_g^\theta)\right). \tag{6.149}$$

Equation 6.149 can be simplified as

$$\frac{\partial K^\theta}{\partial p_\ell} = n(K_\ell^\theta - K_g^\theta)\frac{\partial S_\ell}{,}\partial p_\ell \tag{6.150}$$

allowing for the final form of the linearization of L_5^{int} with respect to liquid pressure to be written as

$$\frac{\partial L_5^{int}}{\partial \dot{p}_\ell}\delta \dot{p}_\ell = -\frac{\partial w^\theta}{\partial X_J}J\frac{\partial \theta}{\partial X_I}F_{Ii}^{-1}F_{Ji}^{-1}n(K_\ell^\theta - K_g^\theta)\frac{\partial S_\ell}{\partial p_\ell}\delta \dot{p}_\ell \alpha \Delta t \tag{6.151}$$

where $\frac{\partial S_\ell}{\partial p_\ell}$ is defined in 9.4.

Lastly, the third part of equation 6.140 can be written as

$$\frac{\partial L_5^{int}}{\partial \dot{\theta}}\delta \dot{\theta} = \frac{\partial w^\theta}{\partial X_J}JF_{Ii}^{-1}F_{Ji}^{-1}(-K^\theta)\frac{\partial \delta \dot{\theta}}{\partial X_I}\alpha \Delta t - \frac{\partial w^\theta}{\partial X_j}JF_{Ii}^{-1}F_{Ji}^{-1}\frac{\partial \theta}{\partial X_I}\frac{\partial K^\theta}{\partial \theta}\delta \dot{\theta}\alpha \Delta t \tag{6.152}$$

where $\frac{\partial K^\theta}{\partial \theta}$ can be written as

$$\frac{\partial K^\theta}{\partial \theta} = \frac{\partial}{\partial \theta}\left((1-n)K_s^\theta + n(S_\ell K_\ell^\theta + S_g K_g^\theta)\right) \tag{6.153}$$

which can be written as

$$\frac{\partial K^\theta}{\partial \theta} = n(K_\ell^\theta - K_g^\theta)\frac{\partial S_\ell}{\partial \theta}. \tag{6.154}$$

This allows for 6.152 to be written as

$$\begin{aligned}\frac{\partial L_5^{int}}{\partial \dot{\theta}}\delta \dot{\theta} &= \frac{\partial w^\theta}{\partial X_J}JF_{Ii}^{-1}F_{Ji}^{-1}(-K^\theta)\frac{\partial \delta \dot{\theta}}{\partial X_I}\alpha \Delta t \\ &- \frac{\partial w^\theta}{\partial X_J}JF_{Ii}^{-1}F_{Ji}^{-1}\frac{\partial \theta}{\partial X_I}n(K_\ell^\theta - K_g^\theta)\frac{\partial S_\ell}{\partial \theta}\delta \dot{\theta}\alpha \Delta t\end{aligned} \tag{6.155}$$

where $\frac{\partial S_\ell}{\partial \theta}$ is defined in 9.10.

δL_6^{int}

The linearization of L_6^{int} can be expanded to

$$\delta L_6^{int} = \frac{\partial L_6^{int}}{\partial \dot{u}_j} \delta \dot{u}_j + \frac{\partial L_6^{int}}{\partial \dot{p}_\ell} \delta \dot{p}_\ell + \frac{\partial L_6^{int}}{\partial \dot{\theta}} \delta \dot{\theta}. \tag{6.156}$$

Using the first term of 6.156 it can be seen

$$\frac{\partial L_6^{int}}{\partial u_j} = \frac{\partial}{\partial F_{aA}} \left[w^\theta H_{vap} \dot{J} - w^\theta J H_{vap} \rho^{\ell R} S_\ell \Big((1-n)\beta_s^\theta - n\beta_\ell^\theta \Big) \dot{\theta} \right. \\ \left. + w^\theta J H_{vap} \rho^{\ell R} n \dot{S}_\ell + J H_{vap} \frac{\partial w^\theta}{\partial X_I} (\rho^{\ell R} v_{\ell_i}^D) F_{Ii}^{-1} \right] \frac{\partial F_{aA}}{\partial u_j} \tag{6.157}$$

which can be expanded to

$$\frac{\partial L_6^{int}}{\partial u_j} = w^\theta H_{vap} \frac{\partial \dot{J}}{\partial \dot{u}} + \left[-w^\theta H_{vap} \Big(\frac{\partial J}{\partial F_{aA}} \rho^{\ell R} S_\ell ((1-n)\beta_s^\theta - n\beta_\ell^\theta)\dot{\theta} \right. \\ - J\rho^{\ell R} S_\ell (\beta_s^\theta + \beta_\ell^\theta)\dot{\theta} \frac{\partial n}{\partial F_{aA}} \Big) + w^\theta \Big(\frac{\partial J}{\partial F_{aA}} \rho^{\ell R} n \dot{S}_\ell + J\rho^{\ell R} \dot{S}_\ell \frac{\partial n}{\partial F_{aA}} \Big) \\ \left. + \frac{\partial w^\theta}{\partial X_I} H_{vap} F_{Ii}^{-1} \Big(\frac{\partial J}{\partial F_{aA}} \rho^{\ell R} v_{\ell_i}^D + J\rho^{\ell R} \frac{\partial v_{\ell_i}^D}{\partial F_{aA}} \Big) \right] \frac{\partial F_{aA}}{\partial u_j}. \tag{6.158}$$

Applying the equations 6.45 and 6.30 and combining like terms gives

$$\frac{\partial L_6^{int}}{\partial u_j} = w^\theta H_{vap} J \left[\Big(F_{Aa}^{-1} F_{Ii}^{-1} \dot{F}_{iI} - F_{Ai}^{-1} F_{Ia}^{-1} \dot{F}_{iI} \Big) \frac{\partial F_{aA}}{\partial u_j} + F_{Ii}^{-1} \frac{\partial \dot{F}_{iI}}{\partial u_j} \right. \\ + \left(F_{Aa}^{-1} \rho^{\ell R} \Big(S_\ell ((1-n)\beta_s^\theta - n\beta_\ell^\theta)\dot{\theta} + \dot{S}_\ell n \Big) - \rho^{\ell R} \Big(S_\ell (\beta_s^\theta + \beta_\ell^\theta)\dot{\theta} - \dot{S}_\ell \Big) \frac{\partial n}{\partial F_{aA}} \right) \frac{\partial F_{aA}}{\partial u_j} \right] \tag{6.159} \\ \left. + \frac{\partial w^\theta}{\partial X_I} J H_{vap} \rho^{\ell R} F_{Ii}^{-1} \Big(F_{aA}^{-1} v_{\ell_i}^D + \frac{\partial v_{\ell_i}^D}{\partial F_{aA}} \Big) \frac{\partial F_{aA}}{\partial u_j}. \right.$$

which can be inserted into the first term of equation 6.156 to yield

$$\frac{\partial L_6^{int}}{\partial u_j} = w^\theta H_{vap} J \Bigg[\left(F_{Aa}^{-1} F_{Ii}^{-1} \dot{F}_{iI} - F_{Ai}^{-1} F_{Ia}^{-1} \dot{F}_{iI} \right) \frac{\partial \delta \dot{u}_a}{\partial X_A} \alpha \Delta t + F_{Ii}^{-1} \frac{\partial \delta \dot{u}_j}{\partial X_I}$$
$$+ \left(F_{Aa}^{-1} \rho^{\ell R} \left(S_\ell ((1-n)\beta_s^\theta - n\beta_\ell^\theta)\dot{\theta} + \dot{S}_\ell n \right) \right.$$
$$\left. - \rho^{\ell R} \left(S_\ell (\beta_s^\theta + \beta_\ell^\theta)\dot{\theta} - \dot{S}_\ell \right) \frac{\partial n}{\partial F_{aA}} \right) \frac{\partial \delta \dot{u}_a}{\partial X_A} \alpha \Delta t \Bigg]$$
$$+ \frac{\partial w^\theta}{\partial X_I} J H_{vap} \rho^{\ell R} F_{Ii}^{-1} \left(F_{aA}^{-1} v_{\ell_i}^D + \frac{\partial v_{\ell_i}^D}{\partial F_{aA}} \right) \frac{\partial \delta \dot{u}_a}{\partial X_A} \alpha \Delta t. \tag{6.160}$$

Now examining the second term of 6.156 it can be seen that

$$\frac{\partial L_6^{int}}{\partial \dot{p}_\ell} \delta \dot{p}_\ell = \frac{\partial}{\partial p_\ell} \left(w^\theta \dot{J} H_{vap} - w^\theta J H_{vap} \rho^{\ell R} S_\ell ((1-n)\beta_s^\theta - n\beta_\ell^\theta)\dot{\theta} \right.$$
$$\left. + J H_{vap} \frac{\partial w^\theta}{\partial X_I} \rho^{\ell R} v_{\ell_i}^D F_{Ii}^{-1} \right) \delta \dot{p}_\ell \alpha \Delta t + w^\theta J H_{vap} \rho^{\ell R} n \frac{\partial \dot{S}_\ell}{\partial \dot{p}_\ell} \delta \dot{p}_\ell \tag{6.161}$$

Simplifying equation 6.161 gives

$$\frac{\partial L_6^{int}}{\partial \dot{p}_\ell} \delta \dot{p}_\ell = \left(- w^\theta \dot{J} H_{vap} \rho^{\ell R} \frac{\partial S_\ell}{\partial p_\ell} ((1-n)\beta_s^\theta - n\beta_\ell^\theta)\dot{\theta} \right.$$
$$+ J H_{vap} \frac{\partial w^\theta}{\partial X_I} \rho^{\ell R} \frac{\partial v_{\ell_i}^D}{\partial p_\ell} F_{Ii}^{-1} \Bigg) \delta \dot{p}_\ell \alpha \Delta t + w^\theta J H_{vap} \rho^{\ell R} n \frac{\partial \dot{S}_\ell}{\partial \dot{p}_\ell} \delta \dot{p}_\ell \tag{6.162}$$

with $\frac{\partial S_\ell}{\partial p_\ell}$, $\frac{\partial v_{\ell_i}^D}{\partial p_\ell}$, and $\frac{\partial \dot{S}_\ell}{\partial \dot{p}_\ell}$ defined in 9.4, 9.25 and 9.41. Examining the final term of equation 6.156 allows one to write

$$\frac{\partial L_6^{int}}{\partial \dot{\theta}} \delta \dot{\theta} = \frac{\partial}{\partial \theta} \left(w^\theta H_{vap} \dot{J} \right) \delta \dot{\theta} \alpha \Delta t + \frac{\partial}{\partial \theta} \left(w^\theta J H_{vap} \rho^{\ell R} S_\ell ((1-n)\beta_s^\theta - n\beta_\ell^\theta) \right) \dot{\theta} \delta \dot{\theta} \alpha \Delta t$$
$$+ \left(w^\theta J H_{vap} \rho^{\ell R} S_\ell ((1-n)\beta_s^\theta - n\beta_\ell^\theta) \right) \delta \dot{\theta} + w^\theta J H_{vap} \frac{\partial \rho^{\ell R}}{\partial \theta} \dot{S}_\ell n \delta \dot{\theta} \alpha \Delta t \tag{6.163}$$
$$+ w^\theta J H_{vap} \rho^{\ell R} \frac{\partial S_\ell}{\partial \theta} \delta \dot{\theta} + \frac{\partial}{\partial \theta} \left(J H_{vap} \frac{\partial w^\theta}{\partial X_I} \rho^{\ell R} v_{\ell_i}^D F_{Ii}^{-1} \right) \delta \dot{\theta} \alpha \Delta t.$$

which expanding via chain rule and simplifying gives,

$$
\frac{\partial L_6^{int}}{\partial \dot{\theta}} \delta \dot{\theta} = \left[w^\theta J H_{vap} \left(\dot{\theta} \left((1-n)\beta_s^\theta - n\beta_\ell^\theta \right) \left[\frac{\partial \rho^{\ell R}}{\partial \theta} S_\ell + \rho^{\ell R} \frac{\partial S_\ell}{\partial \theta} + \frac{\partial \rho^{\ell R}}{\partial \theta} \dot{S}_\ell n \right] \right) \right.
$$
$$
\left. + J H_{vap} \frac{\partial w^\theta}{\partial X_I} F_{Ii}^{-1} \left(\frac{\partial \rho^{\ell R}}{\partial \theta} v_{\ell_i}^D + \rho^{\ell R} \frac{\partial v_{\ell_i}^D}{\partial \theta} \right) \right] \delta \dot{\theta} \alpha \Delta t \qquad (6.164)
$$
$$
+ w^\theta J H_{vap} \rho^{\ell R} \left[\left(S_\ell \left((1-n)\beta_s^\theta - n\beta_\ell^\theta \right) \right) + \frac{\partial S_\ell}{\partial \theta} \right] \delta \dot{\theta}
$$

where $\frac{\partial \rho^{\ell R}}{\partial \theta}$, $\frac{\partial S_\ell}{\partial \theta}$ and $\frac{\partial v_{\ell_i}^D}{\partial \theta}$ are defined in 9.12, 9.10 and 9.33.

δL_7^{int}

For this linearization and finite element implementation inertial effects are considered insignificant and neglected thus,

$$
\delta L_7^{int} = 0. \qquad (6.165)
$$

δL_8^{int}

The linearization of L_8^{int} can be expanded to

$$
\delta L_8^{int} = \frac{\partial L_8^{int}}{\partial \dot{u}_j} \delta \dot{u}_j + \frac{\partial L_8^{int}}{\partial \dot{p}_\ell} \delta \dot{p}_\ell + \frac{\partial L_8^{int}}{\partial \dot{\theta}} \delta \dot{\theta}. \qquad (6.166)
$$

The first term of equation 6.166 leads to

$$
\frac{\partial L_8^{int}}{\partial u_j} = \frac{\partial}{\partial F_{aA}} \left[w^\theta J \left(v_{\ell_i}^D \left[\frac{\partial p_\ell}{\partial X_I} F_{Ii}^{-1} + \rho^{\ell R} (a_i - b_i) \right] + v_{g_i}^D \left[\frac{\partial p_g}{\partial X_I} F_{Ii}^{-1} + \rho^{gR} (a_i - b_i) \right] \right) \right] \frac{\partial F_{aA}}{\partial u_j}. \qquad (6.167)
$$

This equation can be expanded via the chain rule and simplified using the assumptions a_i and b_i are constants to

$$
\begin{aligned}
\frac{\partial L_8^{int}}{\partial u_j} = w^\theta \Bigg[& \frac{\partial J}{\partial F_{aA}} \Big(v_{\ell_i}^D \big[\frac{\partial p_\ell}{\partial X_I} F_{Ii}^{-1} + \rho^{\ell R}(a_i - b_i) \big] + v_{g_i}^D \big[\frac{\partial p_g}{\partial X_I} F_{Ii}^{-1} + \rho^{gR}(a_i - b_i) \big] \Big) \\
& + J \Big[\Big(\frac{\partial v_{\ell_i}^D}{\partial F_{aA}} F_{Ii}^{-1} + v_{\ell_i}^D \frac{\partial F_{Ii}^{-1}}{\partial F_{aA}} \Big) \frac{\partial p_\ell}{\partial X_I} + \Big(\frac{\partial v_{g_i}^D}{\partial F_{aA}} F_{Ii}^{-1} + v_{g_i}^D \frac{\partial F_{Ii}^{-1}}{\partial F_{aA}} \Big) \frac{\partial p_g}{\partial X_I} \Big) \Big] \Bigg] \frac{\partial F_{aA}}{\partial u_j}.
\end{aligned}
\tag{6.168}
$$

Through applying 6.30 and 6.20 the final linearization of L_8^{int} can be described as

$$
\begin{aligned}
\frac{\partial L_8^{int}}{\partial \dot{u}_j} \delta \dot{u}_j = w^\theta J \Bigg[& F_{Aa}^{-1} \Big(v_{\ell_i}^D \big[\frac{\partial p_\ell}{\partial X_I} F_{Ii}^{-1} + \rho^{\ell R}(a_i - b_i) \big] + v_{g_i}^D \big[\frac{\partial p_g}{\partial X_I} F_{Ii}^{-1} + \rho^{gR}(a_i - b_i) \big] \Big) \\
& + \Big[\Big(\frac{\partial v_{\ell_i}^D}{\partial F_{aA}} F_{Ii}^{-1} - v_{\ell_i} F_{Ia}^{-1} F_{Ai}^{-1} \Big) \frac{\partial p_\ell}{\partial X_I} + \Big(\frac{\partial v_{g_i}^D}{\partial F_{aA}} F_{Ii}^{-1} - v_{g_i}^D F_{Ia}^{-1} F_{Ai}^{-1} \Big) \frac{\partial p_g}{\partial X_I} \Big) \Big] \frac{\partial \delta \dot{u}_a}{\partial X_A} \alpha \Delta t.
\end{aligned}
\tag{6.169}
$$

where $\frac{\partial v_{f_i}^D}{\partial F_{aA}}$ is defined in 9.18. The second term of equation 6.166 allows for

$$
\frac{\partial L_8^{int}}{\partial p_\ell} = \frac{\partial}{\partial p_\ell} \Big[w^\theta J \Big(v_{\ell_i}^D \big[\frac{\partial p_\ell}{\partial X_I} F_{Ii}^{-1} + \rho^{\ell R}(a_i - b_i) \big] + v_{g_i}^D \big[\frac{\partial p_g}{\partial X_I} F_{Ii}^{-1} + \rho^{gR}(a_i - b_i) \big] \Big) \Big]
\tag{6.170}
$$

which using the chain rule and assuming a_i and b_i are not dependent on p_ℓ can be written as

$$
\begin{aligned}
\frac{\partial L_8^{int}}{\partial p_\ell} = w^\theta J F_{Ii}^{-1} \Bigg[& \frac{\partial v_{\ell_i}^D}{\partial p_\ell} \Big(\frac{\partial p_\ell}{\partial X_I} + \rho^{\ell R}(a_i - b_i) \Big) + v_{\ell_i}^D \frac{\partial p_\ell}{\partial X_I} \\
& + \frac{\partial v_{g_i}^D}{\partial p_\ell} \Big(\frac{\partial p_g}{\partial X_I} + \rho^{gR}(a_i - b_i) \Big) \Bigg]
\end{aligned}
\tag{6.171}
$$

allowing for the final linearization of L_8^{int} with respect to liquid pressure to be written as

$$
\begin{aligned}
\frac{\partial L_8^{int}}{\partial \dot{p}_\ell} \delta \dot{p}_\ell = w^\theta J \Bigg[& \frac{\partial v_{\ell_i}^D}{\partial p_\ell} \Big(\frac{\partial p_\ell}{\partial X_I} F_{Ii}^{-1} + \rho^{\ell R}(a_i - b_i) \Big) \delta \dot{p}_\ell + v_{\ell_i}^D \frac{\partial \delta \dot{p}_\ell}{\partial X_I} \\
& + \frac{\partial v_{g_i}^D}{\partial p_\ell} \Big(\frac{\partial p_g}{\partial X_I} + \rho^{gR}(a_i - b_i) \Big) \Bigg] \alpha \Delta t
\end{aligned}
\tag{6.172}
$$

where $\frac{\partial v_{\ell_i}^D}{\partial p_\ell}$ and $\frac{\partial v_{g_i}^D}{\partial p_\ell}$ are defined in 9.25 and 9.29. Finally, the third term allows for

$$\frac{\partial L_8^{int}}{\partial \theta} = \frac{\partial}{\partial \theta}\left[w^\theta J\left(v_{\ell_i}^D\left[\frac{\partial p_\ell}{\partial X_I}F_{Ii}^{-1} + \rho^{\ell R}(a_i - b_i)\right] + v_{g_i}^D\left[\frac{\partial p_g}{\partial X_I}F_{Ii}^{-1} + \rho^{gR}(a_i - b_i)\right]\right)\right] \quad (6.173)$$

which can be written as

$$\frac{\partial L_8^{int}}{\partial \theta} = w^\theta J\left[\frac{\partial v_{\ell_i}^D}{\partial \theta}\left(\frac{\partial p_\ell}{\partial X_I}F_{Ii}^{-1} + \rho^{\ell R}(a_i - b_i)\right) + \frac{\partial \rho^{\ell R}}{\partial \theta}(a_i - b_i)\right.$$
$$\left. + \frac{\partial v_{g_i}^D}{\partial \theta}\left(\frac{\partial p_g}{\partial X_i}F_{Ii}^{-1} + \rho^{gR}(a_i - b_i)\right) + v_{g_i}^D\frac{\partial p_g}{\partial \theta}\frac{\partial \theta}{\partial X_I}F_{Ii}^{-1} + \frac{\partial \rho^{gR}}{\partial \theta}(a_i - b_i)\right]. \quad (6.174)$$

Combining equation 6.174 and equation 6.166 allows for the final linearization of L_8^{int} with respect to temperature,

$$\frac{\partial L_8^{int}}{\partial \dot\theta}\delta\dot\theta = w^\theta J\left[\frac{\partial v_{\ell_i}^D}{\partial \theta}\left(\frac{\partial p_\ell}{\partial X_I}F_{Ii}^{-1} + \rho^{\ell R}(a_i - b_i)\right)\delta\dot\theta + \frac{\partial \rho^{\ell R}}{\partial \theta}(a_i - b_i)\delta\dot\theta\right.$$
$$\left. + \frac{\partial v_{g_i}^D}{\partial \theta}\left(\frac{\partial p_g}{\partial X_i}F_{Ii}^{-1} + \rho^{gR}(a_i - b_i)\right)\delta\dot\theta + v_{g_i}^D\frac{\partial p_g}{\partial \theta}\frac{\partial \delta\dot\theta}{\partial X_I}F_{Ii}^{-1} + \frac{\partial \rho^{gR}}{\partial \theta}(a_i - b_i)\delta\dot\theta\right]\alpha\Delta t \quad (6.175)$$

where $\frac{\partial v_{\ell_i}^D}{\partial \theta}$, $\frac{\partial v_{g_i}^D}{\partial \theta}$, $\frac{\partial \rho^{\ell R}}{\partial \theta}$, $\frac{\partial \rho^{gR}}{\partial \theta}$ and $\frac{\partial p_g}{\partial \theta}$ are defined in equations 9.33, 9.12, 9.37, 9.14, and 9.6.

δL_1^{ext}

It be seen that the linearization of δL_1^{ext} can be written as

$$\delta L_1^{ext} = \frac{\partial L_1^{ext}}{\partial \dot u_j}\delta\dot u_j + \frac{\partial L_1^{ext}}{\partial \dot p_\ell}\delta\dot p_\ell + \frac{\partial L_1^{ext}}{\partial \dot\theta}\delta\dot\theta \quad (6.176)$$

which from equation 5.240 can be written as

$$\delta L_1^{ext} = w^p\left(\frac{\partial q_\theta^{flux}}{\partial \dot u_j}\delta\dot u_j + \frac{\partial q_\theta^{flux}}{\partial \dot p_\ell}\delta\dot p_\ell + \frac{\partial q_\theta^{flux}}{\partial \dot\theta}\delta\dot\theta\right) \quad (6.177)$$

where q_θ^{flux} is energy flux through the boundary. Therefore, these derivatives can vary based on the type of boundary condition used. For the simulations in this thesis q_θ^{flux} is defined in

7.3 with its derivatives in 9.53, 9.55 and 9.57.

6.5   Finite Element Discretization

Galerkin's method will now be used to implement and solve the weak form of the equations via a finite element approximation. Volumetric locking can occur for incompressible and nearly incompressible materials for linear elements [28], as is the case for porous media loaded quickly, especially when permeability is low. To prevent this locking problem, isoparametric quadrilateral elements (Fig. 6.2) that use biquadratic interpolation in displacement and bilinear interpolation in pore pressure and temperature are used.
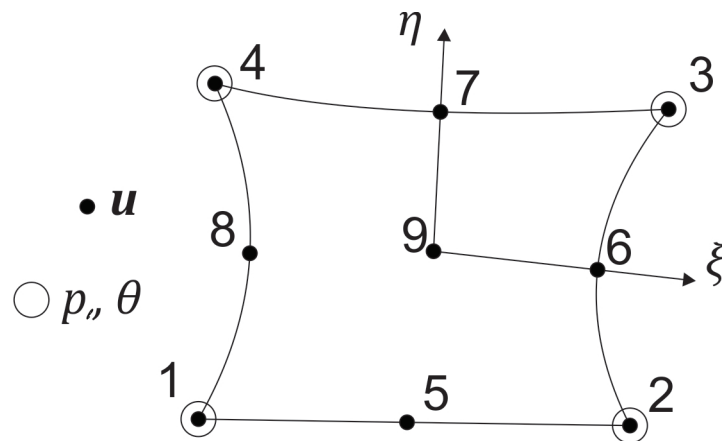
Figure 6.2: An isoparametric quadrilateral element that is biquadratic in displacement and bilinear in temperature and pressure. There are two degrees of freedom at each biquadratic node(u_x and u_y) and an additional two degrees of freedom (liquid pore pressure and temperature) at each bilinear node.

There are two degrees of freedom for spatial displacements at each quadratic node and two additional degrees of freedom (liquid pore pressure and temperature) at each linear node,

thus, the displacement and velocity vectors for each element are written as

$$\boldsymbol{d}_u^e = \left[u_{x1},\ u_{y1},\ u_{x_2},\ u_{y_2},\ \dots u_{x9}\ u_{y9}\right]^T \tag{6.178}$$

$$\boldsymbol{p}_\ell^e = \left[p_{\ell_1},\ p_{\ell_2},\ p_{\ell_3},\ p_{\ell_4}\right]^T \tag{6.179}$$

$$\boldsymbol{\theta}^e = \left[\theta_1,\ \theta_2,\ \theta_3,\ \theta_4\right]^T \tag{6.180}$$

and

$$\boldsymbol{v}_u^e = \left[\dot{u}_{x1},\ \dot{u}_{y1},\ \dot{u}_{x_2},\ \dot{u}_{y_2},\ \dots \dot{u}_{x9},\ \dot{u}_{y9}\right]^T \tag{6.181}$$

$$\dot{\boldsymbol{p}}_\ell^e = \left[\dot{p}_{\ell_1}.\ \dot{p}_{\ell_2},\ \dot{p}_{\ell_3},\ \dot{p}_{\ell_4}\right]^T \tag{6.182}$$

$$\dot{\boldsymbol{\theta}}^e = \left[\dot{\theta}_1,\ \dot{\theta}_2,\ \dot{\theta}_3,\ \dot{\theta}_4\right]^T. \tag{6.183}$$

The trial and weighting functions can then be written as

$$\boldsymbol{u}^e = \boldsymbol{N}^{u,e} \cdot \boldsymbol{d}^e, \tag{6.184}$$

$$\boldsymbol{w}^u = \boldsymbol{N}^{u,e} \cdot \boldsymbol{c}^e, \tag{6.185}$$

$$p_\ell^e = \boldsymbol{N}^{p,e} \cdot \boldsymbol{p}_\ell^e, \tag{6.186}$$

$$w^p = \boldsymbol{N}^{p,e} \cdot \boldsymbol{\alpha}^e, \tag{6.187}$$

$$\theta_\ell^e = \boldsymbol{N}^{\theta,e} \cdot \boldsymbol{\theta}^e, \tag{6.188}$$

$$w^\theta = \boldsymbol{N}^{\theta,e} \cdot \boldsymbol{\beta}^e, \tag{6.189}$$

where $\boldsymbol{d}^e$, $\boldsymbol{p}_\ell^e$, and $\boldsymbol{\theta}^e$ are the nodal displacements, liquid pore pressures and temperatures and $\boldsymbol{c}^e$, $\boldsymbol{\alpha}^\alpha$, and $\boldsymbol{\beta}^e$ are vectors made up of the nodal values of the weighting functions $\boldsymbol{w}^u$, w^p, and w^θ. $\boldsymbol{N}^{e,p}$ is the displacement shape function matrix defined as

$$\boldsymbol{N}^{u,e} = \begin{bmatrix} N_1^u & 0 & N_2^u & 0 & \dots & N_9^u & 0 \\ 0 & N_1^u & 0 & N_2^u & \dots & 0 & N_9^u \end{bmatrix}, \tag{6.190}$$

and $\boldsymbol{N}^{p,e}$ and $\boldsymbol{N}^{\theta,e}$ are the liquid pore pressure and temperature matrices defined as

$$\boldsymbol{N}^{p,e} = \boldsymbol{N}^{\theta,e} = \begin{bmatrix} N_1^l & N_2^l & N_3^l & N_4^l \end{bmatrix}. \tag{6.191}$$

It is also beneficial to define the gradients with respect to the reference configuration of the displacement ($\frac{\partial \boldsymbol{u}}{\partial \boldsymbol{X}}$), liquid pore pressure ($\frac{\partial p_\ell}{\partial \boldsymbol{x}}$), and temperatures ($\frac{\partial \theta}{\partial \boldsymbol{x}}$) as

$$\frac{\partial \boldsymbol{u}}{\partial \boldsymbol{X}} = \boldsymbol{B}^{u,e} \boldsymbol{d}^e, \tag{6.192}$$

$$\frac{\partial p_\ell}{\partial \boldsymbol{X}} = \boldsymbol{B}^{p,e} \boldsymbol{p}_\ell^e, \tag{6.193}$$

$$\frac{\partial \theta}{\partial \boldsymbol{X}} = \boldsymbol{B}^{\theta,e} \boldsymbol{\theta}^e, \tag{6.194}$$

where

$$\boldsymbol{B}^{u,e} = \begin{bmatrix} \frac{\partial N_1^u}{\partial X_1} & 0 & \frac{\partial N_2^u}{\partial X_1} & 0 & \dots & \frac{\partial N_9^u}{\partial X_1} & 0 \\ \frac{\partial N_1^u}{\partial X_2} & 0 & \frac{\partial N_2^u}{\partial X_2} & 0 & \dots & \frac{\partial N_9^u}{\partial X_2} & 0 \\ 0 & \frac{\partial N_1^u}{\partial X_1} & 0 & \frac{\partial N_2^u}{\partial X_1} & \dots & 0 & \frac{\partial N_9^u}{\partial X_1} \\ 0 & \frac{\partial N_1^u}{\partial X_2} & 0 & \frac{\partial N_2^u}{\partial X_2} & \dots & 0 & \frac{\partial N_9^u}{\partial X_2} \end{bmatrix}, \tag{6.195}$$

and

$$\boldsymbol{B}^{p,e} = \boldsymbol{B}^{\theta,e} = \begin{bmatrix} \frac{\partial N_1^l}{\partial X_1} & \frac{\partial N_2^l}{\partial X_1} & \frac{\partial N_3^l}{\partial X_1} & \frac{\partial N_4^l}{\partial X_1} \\ \frac{\partial N_1^l}{\partial X_2} & \frac{\partial N_2^l}{\partial X_2} & \frac{\partial N_3^l}{\partial X_2} & \frac{\partial N_4^l}{\partial X_2} \end{bmatrix}. \tag{6.196}$$

Following these same lines the gradients of the shape functions with respect to the initial solid reference configuration, $\frac{\partial \boldsymbol{w}^u}{\partial \boldsymbol{X}}$, $\frac{\partial \boldsymbol{w}^p}{\partial \boldsymbol{X}}$, and $\frac{\partial \boldsymbol{w}^\theta}{\partial \boldsymbol{X}}$ can be written as

$$\frac{\partial \boldsymbol{w}^u}{\partial \boldsymbol{X}} = \boldsymbol{B}^{u,e} \cdot \boldsymbol{c}^e, \tag{6.197}$$

$$\frac{\partial w^p}{\partial \boldsymbol{X}} = \boldsymbol{B}^{p,e} \cdot \boldsymbol{\alpha}^e, \tag{6.198}$$

$$\frac{\partial w^\theta}{\partial \boldsymbol{X}} = \boldsymbol{B}^{\theta,e} \cdot \boldsymbol{\beta}^e. \tag{6.199}$$

Lastly, it is beneficial to recall that the deformation gradient, $\boldsymbol{F}$, can be written as

$$\boldsymbol{F} = \boldsymbol{I} + \boldsymbol{B}^{u,e} \boldsymbol{d}^e \tag{6.200}$$

and its determinate as

$$J = det\boldsymbol{F} \tag{6.201}$$

where I is the identity matrix in Voight-like notation defined as

$$\boldsymbol{I} = \begin{bmatrix} 1 \\ 0 \\ 0 \\ 1 \end{bmatrix}. \tag{6.202}$$

6.6 Matrix forms of the balance equations

Using the definitions of the finite element descretization laid out in section 6.5 the weak forms of the balance equations (Eqns. 5.227, 5.232 and 5.240) can now be written in the matrix form in which they will be written into computer code.

6.6.1 Balance of Linear Momentum Matrix Form

Applying the definitions in section 6.5 to the weak form of the final balance of linear momentum equation (Eqn. 5.227) allows for

$$\boldsymbol{G} = \boldsymbol{A}\boldsymbol{A}^{n_{el}}(\boldsymbol{c}^e)^T \cdot \left[\int_{B_0} \boldsymbol{B}^{u,e^T} \boldsymbol{P}' dV - \int_{B_0} \boldsymbol{B}^{u,e^T} J\big(p_\ell \chi + p_g(1-\chi)\big) \boldsymbol{F}^{-T} dV + \right.$$
$$\left. \int_{B_0} \boldsymbol{N}^{u,e^T} \rho_0 \boldsymbol{a} dV - \int_{B_0} \boldsymbol{N}^{u,e^T} \rho_0 \boldsymbol{b} - \int_{\partial B_{u_0}^{trac}} \boldsymbol{N}^{u,e^T} \boldsymbol{t} dA \right] \tag{6.203}$$

where $\boldsymbol{A}\boldsymbol{A}^{n_{el}}$ is an element assembly operator. The First Piola Kirchoff effective stress tensor $\boldsymbol{P}'$, is defined as

$$\boldsymbol{P}' = \boldsymbol{F}\boldsymbol{S}' \tag{6.204}$$

where $\boldsymbol{S}'$ is the Second Piola Kirchoff stress that is a defined for this paper in equations 5.215 and is a function of the Jacobian, J, and the deformation gradient, $\boldsymbol{F}$, which are defined in matrix form in equations 6.200 and 6.201.

6.6.2 Balance of Mass Matrix Form

Following the same assumptions put forth in section 6.6.1 the matrix form of the balance of mass equation can be written as

$$\boldsymbol{H} = \boldsymbol{A}\boldsymbol{A}^{n_{el}}(\boldsymbol{\alpha}^e)^T \cdot \left[\int_{B_0} \boldsymbol{N}^{p,e^T} (S_g \rho^{gR} + S_\ell \rho^{\ell R}) \dot{J} dV \right.$$
$$- \int_{B_0} \boldsymbol{N}^{p,e^T} J\big[(1-n)(\rho^{\ell R} S_\ell + \rho^{gR} S_g)\beta_s^\theta + n\rho^{\ell R} S_\ell \beta_\ell^\theta\big] \dot{\theta} dV$$
$$- \int_{B_0} \boldsymbol{B}^{p,e^T} J\boldsymbol{F}^{-1} \cdot \big[\rho^{\ell R} \boldsymbol{v}_\ell^D + \rho^{gR} \boldsymbol{v}_g^D\big] dV \tag{6.205}$$
$$+ \int_{B_0} \boldsymbol{N}^{p,e^T} J\big[\rho^{\ell R} n\dot{S}_\ell + n\rho^{gR}\dot{S}_g + nS_g\dot{\rho}^{gR}\big] dV$$
$$\left. + \int_{B_0} \boldsymbol{N}^{p,e^T} \left[\frac{\rho^{\ell R} JnS_\ell}{K_{bulk}^\ell}\dot{p}_\ell + \frac{J\rho^{\ell R}}{K_{bulk}^\ell}\frac{\partial p_\ell}{\partial \boldsymbol{X}} \cdot \boldsymbol{v}_\ell^D \cdot \boldsymbol{F}^{-T}\right] dV - \int_{\partial B_{p_0}^{free}} \boldsymbol{N}^{u,e^T} \boldsymbol{q}_\ell^{flux} dA \right]$$

where $\boldsymbol{F}^{-T}$, J, $\boldsymbol{v}_\ell^D$, and $\boldsymbol{v}_g^D$ are defined in 6.200, 6.201 and 5.76.

6.6.3 Balance of Energy Matrix Form

Again, following the same assumptions put forth in section 6.6.1 the matrix form of the balance of mass equation can be written as

$$
\begin{aligned}
\boldsymbol{L} = \boldsymbol{A}\boldsymbol{A}^{n_{el}}(\boldsymbol{\beta}^e)^T \cdot \Bigg[& \int_{B_0} \boldsymbol{N}^{\theta,e^T} J(\rho C_p^{eff})\dot{\theta}dV + \int_{B_0} \boldsymbol{N}^{\theta,e^T} J\rho^{\ell R}\boldsymbol{v}_\ell^D \cdot \frac{\partial\theta}{\partial\boldsymbol{X}} \cdot \boldsymbol{F}^{-T}dV \\
& + \int_{B_0} \boldsymbol{N}^{\theta,e^T} J\rho^{gR}v_{g_i}^D \frac{\partial\theta}{\partial\boldsymbol{X}} \cdot \boldsymbol{F}^{-T}dV - \int_{B_0} w^\theta J\rho^{eff}rdV \\
& - \int_{B_0} \boldsymbol{B}^{\theta,e^T} J\big(-K\frac{\partial\theta}{\partial\boldsymbol{X}}\big) \cdot \boldsymbol{F}^{-T} \cdot \boldsymbol{F}^{-T}dV \\
- \int_{B_0} \boldsymbol{N}^{\theta,e^T}\Big[\rho^{\ell R}\frac{1}{J}\dot{J} & - \rho^{\ell R}S_\ell\big((1-n)\beta_s^\theta - n\beta_\ell^\theta\big)\dot{\theta} + \rho^{\ell R}n\dot{S}_\ell + \frac{\partial w^\theta}{\partial\boldsymbol{X}} \cdot \boldsymbol{F}^{-T} \cdot (\rho^{\ell R}v_{\ell_i}^D)\Big]dV \\
& + \int_{B_0} \boldsymbol{N}^{\theta,e^T} J\big(\hat{\rho}^\ell\boldsymbol{v}_\ell \cdot \tilde{\boldsymbol{v}}_\ell + \hat{\rho}^g\boldsymbol{v}_g \cdot \tilde{\boldsymbol{v}}_g - \frac{1}{2}\hat{\rho}^\ell\boldsymbol{v}_\ell \cdot \boldsymbol{v}_\ell - \frac{1}{2}\hat{\rho}^g\boldsymbol{v}_g \cdot \boldsymbol{v}_g\big)dV \\
+ \int_{B_0} \boldsymbol{N}^{\theta,e^T} J\Big(v_{\ell_i}^D & \cdot \big[\frac{\partial p_\ell}{\partial\boldsymbol{X}} \cdot \boldsymbol{F}^{-T} + \rho^{\ell R}(a_i - b_i)\big] + v_{g_i}^D \cdot \big[\frac{\partial p_g}{\partial\boldsymbol{X}} \cdot \boldsymbol{F}^{-T} + \rho^{gR}(a_i - b_i)\big]\Big)dV \\
& - \int_{\partial B_{\theta_0}^{free}} \boldsymbol{N}^{\theta,e^T}\boldsymbol{q}_\theta^{flux}dA \Bigg].
\end{aligned}
$$

$$(6.206)$$

where $\boldsymbol{F}^{-T}$, J, $\boldsymbol{v}_\ell^D$, $\boldsymbol{v}_g^D$, $\frac{\partial\theta}{\partial\boldsymbol{X}}$, $\frac{\partial p_g}{\partial\boldsymbol{X}}$, and $\frac{\partial p_g}{\partial\boldsymbol{X}}$ are defined in equations 6.200, 6.201, 5.76, 6.199 and 6.198.

6.7 Matrix form of Linearizations

Recalling from equation 6.8 that the tangent stiffness matrix for each iteration must be put into the form of

$$
\boldsymbol{0} = \boldsymbol{R}^k = \big(\frac{\partial\boldsymbol{R}}{\partial\boldsymbol{V}}\big)\delta\boldsymbol{V} \tag{6.207}
$$

it is necessary to put each linearized term into matrix form. Which can be shown as

$$
\left(\frac{\partial \boldsymbol{R}}{\partial \boldsymbol{V}}\right)\delta \boldsymbol{V} =
\begin{bmatrix}
\frac{\partial \boldsymbol{G}}{\partial \dot{\boldsymbol{u}}} & \frac{\partial \boldsymbol{G}}{\partial \dot{\boldsymbol{p}}_\ell} & \frac{\partial \boldsymbol{G}}{\partial \dot{\boldsymbol{\theta}}} \\
\frac{\partial \boldsymbol{H}}{\partial \dot{\boldsymbol{u}}} & \frac{\partial \boldsymbol{H}}{\partial \dot{\boldsymbol{p}}_\ell} & \frac{\partial \boldsymbol{H}}{\partial \dot{\boldsymbol{\theta}}} \\
\frac{\partial \boldsymbol{L}}{\partial \dot{\boldsymbol{u}}} & \frac{\partial \boldsymbol{L}}{\partial \dot{\boldsymbol{p}}_\ell} & \frac{\partial \boldsymbol{L}}{\partial \dot{\boldsymbol{\theta}}}
\end{bmatrix}
\begin{bmatrix}
\delta \dot{\boldsymbol{u}} \\
\delta \dot{\boldsymbol{p}}_\ell \\
\delta \dot{\boldsymbol{\theta}}
\end{bmatrix}
\tag{6.208}
$$

where each of the matrix terms can be broken down further for the balance of linear momentum as

$$
\frac{\partial \boldsymbol{G}}{\partial \dot{\boldsymbol{u}}} = \frac{\partial \boldsymbol{G}_1^{int}}{\partial \dot{\boldsymbol{u}}} + \frac{\partial \boldsymbol{G}_2^{int}}{\partial \dot{\boldsymbol{u}}} - \frac{\partial \boldsymbol{G}_1^{ext}}{\partial \dot{\boldsymbol{u}}},
\tag{6.209}
$$

$$
\frac{\partial \boldsymbol{G}}{\partial \dot{\boldsymbol{p}}_\ell} = \frac{\partial \boldsymbol{G}_1^{int}}{\partial \dot{\boldsymbol{p}}_\ell} + \frac{\partial \boldsymbol{G}_2^{int}}{\partial \dot{\boldsymbol{p}}_\ell} - \frac{\partial \boldsymbol{G}_1^{ext}}{\partial \dot{\boldsymbol{p}}_\ell},
\tag{6.210}
$$

$$
\frac{\partial \boldsymbol{G}}{\partial \dot{\boldsymbol{\theta}}} = \frac{\partial \boldsymbol{G}_1^{int}}{\partial \dot{\boldsymbol{\theta}}} + \frac{\partial \boldsymbol{G}_2^{int}}{\partial \dot{\boldsymbol{\theta}}} - \frac{\partial \boldsymbol{G}_1^{ext}}{\partial \dot{\boldsymbol{\theta}}},
\tag{6.211}
$$

for the balance of mass as

$$
\frac{\partial \boldsymbol{H}}{\partial \dot{\boldsymbol{u}}} = \frac{\partial \boldsymbol{H}_1^{int}}{\partial \dot{\boldsymbol{u}}} + \frac{\partial \boldsymbol{H}_2^{int}}{\partial \dot{\boldsymbol{u}}} + \frac{\partial \boldsymbol{H}_3^{int}}{\partial \dot{\boldsymbol{u}}} + \frac{\partial \boldsymbol{H}_4^{int}}{\partial \dot{\boldsymbol{u}}} + \frac{\partial \boldsymbol{H}_5^{int}}{\partial \dot{\boldsymbol{u}}} - \frac{\partial \boldsymbol{H}_1^{ext}}{\partial \dot{\boldsymbol{u}}},
\tag{6.212}
$$

$$
\frac{\partial \boldsymbol{H}}{\partial \dot{\boldsymbol{p}}_\ell} = \frac{\partial \boldsymbol{H}_1^{int}}{\partial \dot{\boldsymbol{p}}_\ell} + \frac{\partial \boldsymbol{H}_2^{int}}{\partial \dot{\boldsymbol{p}}_\ell} + \frac{\partial \boldsymbol{H}_3^{int}}{\partial \dot{\boldsymbol{p}}_\ell} + + \frac{\partial \boldsymbol{H}_4^{int}}{\partial \dot{\boldsymbol{p}}_\ell} + \frac{\partial \boldsymbol{H}_5^{int}}{\partial \dot{\boldsymbol{p}}_\ell} - \frac{\partial \boldsymbol{H}_1^{ext}}{\partial \dot{\boldsymbol{p}}_\ell},
\tag{6.213}
$$

$$
\frac{\partial \boldsymbol{H}}{\partial \dot{\boldsymbol{\theta}}} = \frac{\partial \boldsymbol{H}_1^{int}}{\partial \dot{\boldsymbol{\theta}}} + \frac{\partial \boldsymbol{H}_2^{int}}{\partial \dot{\boldsymbol{\theta}}} \frac{\partial \boldsymbol{H}_3^{int}}{\partial \dot{\boldsymbol{\theta}}} + \frac{\partial \boldsymbol{H}_4^{int}}{\partial \dot{\boldsymbol{\theta}}} + \frac{\partial \boldsymbol{H}_5^{int}}{\partial \dot{\boldsymbol{\theta}}} - \frac{\partial \boldsymbol{H}_1^{ext}}{\partial \dot{\boldsymbol{\theta}}}
\tag{6.214}
$$

and for the balance of energy as

$$
\frac{\partial \boldsymbol{L}}{\partial \dot{\boldsymbol{u}}} = \frac{\partial \boldsymbol{L}_1^{int}}{\partial \dot{\boldsymbol{u}}} + \frac{\partial \boldsymbol{L}_2^{int}}{\partial \dot{\boldsymbol{u}}} + \frac{\partial \boldsymbol{L}_3^{int}}{\partial \dot{\boldsymbol{u}}} + \frac{\partial \boldsymbol{L}_4^{int}}{\partial \dot{\boldsymbol{u}}} + \frac{\partial \boldsymbol{L}_5^{int}}{\partial \dot{\boldsymbol{u}}} + \frac{\partial \boldsymbol{L}_6^{int}}{\partial \dot{\boldsymbol{u}}} + \frac{\partial \boldsymbol{L}_7^{int}}{\partial \dot{\boldsymbol{u}}} + \frac{\partial \boldsymbol{L}_8^{int}}{\partial \dot{\boldsymbol{u}}} - \frac{\partial \boldsymbol{L}_1^{ext}}{\partial \dot{\boldsymbol{u}}}, \tag{6.215}
$$

$$
\frac{\partial \boldsymbol{L}}{\partial \dot{\boldsymbol{p}}_\ell} = \frac{\partial \boldsymbol{L}_1^{int}}{\partial \dot{\boldsymbol{p}}_\ell} + \frac{\partial \boldsymbol{L}_2^{int}}{\partial \dot{\boldsymbol{p}}_\ell} + \frac{\partial \boldsymbol{L}_3^{int}}{\partial \dot{\boldsymbol{p}}_\ell} + + \frac{\partial \boldsymbol{L}_4^{int}}{\partial \dot{\boldsymbol{p}}_\ell} + \frac{\partial \boldsymbol{L}_5^{int}}{\partial \dot{\boldsymbol{p}}_\ell} + \frac{\partial \boldsymbol{L}_6^{int}}{\partial \dot{\boldsymbol{p}}_\ell} + \frac{\partial \boldsymbol{L}_7^{int}}{\partial \dot{\boldsymbol{p}}_\ell} + + \frac{\partial \boldsymbol{L}_8^{int}}{\partial \dot{\boldsymbol{p}}_\ell} - \frac{\partial \boldsymbol{L}_1^{ext}}{\partial \dot{\boldsymbol{p}}_\ell}, \tag{6.216}
$$

$$
\frac{\partial \boldsymbol{L}}{\partial \dot{\boldsymbol{\theta}}} = \frac{\partial \boldsymbol{L}_1^{int}}{\partial \dot{\boldsymbol{\theta}}} + \frac{\partial \boldsymbol{L}_2^{int}}{\partial \dot{\boldsymbol{\theta}}} \frac{\partial \boldsymbol{L}_3^{int}}{\partial \dot{\boldsymbol{\theta}}} + \frac{\partial \boldsymbol{L}_4^{int}}{\partial \dot{\boldsymbol{\theta}}} + \frac{\partial \boldsymbol{L}_5^{int}}{\partial \dot{\boldsymbol{\theta}}} + \frac{\partial \boldsymbol{L}_6^{int}}{\partial \dot{\boldsymbol{\theta}}} + \frac{\partial \boldsymbol{L}_7^{int}}{\partial \dot{\boldsymbol{\theta}}} + \frac{\partial \boldsymbol{L}_8^{int}}{\partial \dot{\boldsymbol{\theta}}} - \frac{\partial \boldsymbol{L}_1^{ext}}{\partial \dot{\boldsymbol{\theta}}}. \tag{6.217}
$$

The following sections provides these terms.

6.7.1 Matrix form of δG_1^{int}

Recalling the final form of δG_1^{int} shown in equation 6.26 it can be seen that the matrix form of the equation can be written as

$$\frac{\partial \boldsymbol{G}_1^{int}}{\partial \dot{\boldsymbol{u}}} = \boldsymbol{A}\boldsymbol{A}^{n_{el}}(\boldsymbol{c}^e)^T \cdot \left[\int_{B_o} \boldsymbol{B}^{u,e^T}[\boldsymbol{\mathscr{C}}]\boldsymbol{B}^{u,e}\alpha\Delta t dV \right] \tag{6.218}$$

where $\boldsymbol{\mathscr{C}}$ is the 4-d matrix put into Voight-Kelvin notation to have the dimensions of $n_{sdof} \times n_{sdof}$, where n_{sdof} is the number of displacement degrees of freedom per element. $\boldsymbol{\mathscr{C}}$ is defined as

$$\boldsymbol{\mathscr{C}} = \left[\boldsymbol{I} \otimes \boldsymbol{S} + \left(\lambda \boldsymbol{F}^{-1} \otimes \boldsymbol{F}^{-T} - (\lambda ln J - \mu_s)(\boldsymbol{F}^{-1} \otimes \boldsymbol{F}^{-T} + \boldsymbol{I} \otimes \boldsymbol{C}^{-T}) \right) \right] \tag{6.219}$$

where $\boldsymbol{C}$ is the Right-Cauchy Green tensor defined in 5.34 and the deformation gradient, $\boldsymbol{F}$, and its determinant, J, are defined in 6.200 and 6.201.

6.7.2 Matrix form of δG_2^{int}

Recalling equation 6.32 it can be written that

$$\frac{\partial \boldsymbol{G}_2^{int}}{\partial \dot{\boldsymbol{u}}} = \boldsymbol{A}\boldsymbol{A}^{n_{el}}(\boldsymbol{c}^e)^T \cdot \left[\int_{B_o} \boldsymbol{B}^{u,e^T}[\boldsymbol{\mathscr{P}}]\boldsymbol{B}^{u,e}\alpha\Delta t dV \right] \tag{6.220}$$

where $\boldsymbol{\mathscr{P}}$ is a 4-d matrix put in Voight-like notation resulting in an $n_{sdof} \times n_{sdof}$ matrix defined as

$$\boldsymbol{\mathscr{P}} = \left(p_\ell^e \chi + p_g(1 - \chi) \right) J \left[\boldsymbol{F}^{-1} \otimes \boldsymbol{F}^{-T} - \boldsymbol{F}^{-1} \otimes \boldsymbol{F}^{-T} \right] \tag{6.221}$$

where p_ℓ^e, J, and $\boldsymbol{F}$ are defined in equations 6.186, 6.201, and 6.200.

Now recalling equation 6.35 it can be seen that

$$\frac{\partial \boldsymbol{G}_2^{int}}{\partial \dot{\boldsymbol{p}}_\ell} = \boldsymbol{A}\boldsymbol{A}^{n_{el}}(\boldsymbol{c}^e)^T \cdot \left[\int_{B_o} \boldsymbol{B}^{u,e^T} \left[J\boldsymbol{F}^{-T}\left[\chi - s^e\frac{\partial \chi}{\partial p_\ell}\right]\boldsymbol{N}^{p,e}\alpha\Delta t dV \right] \right. \tag{6.222}$$

where s^e is the suction at the element level defined as

$$s^e = p_g^e - p_\ell^e \tag{6.223}$$

where p_ℓ^e is defined in 6.186 and p_g^e is defined as

$$p_g^e = \boldsymbol{N}^{p,e}\boldsymbol{p}_g \tag{6.224}$$

with $\boldsymbol{p}_g$ being a vector of the gas pressures at the nodes. Lastly, recalling equation 6.37 it can be written that

$$\frac{\partial \boldsymbol{G}_2^{int}}{\partial \dot{\boldsymbol{\theta}}} = \boldsymbol{A}\boldsymbol{A}^{n_{el}}(\boldsymbol{c}^e)^T \cdot \left[\int_{B_o} \boldsymbol{B}^{u,e^T} \left[J\boldsymbol{F}^{-T}\left[\frac{\partial p_\ell^e}{\partial \theta}\chi + \frac{\partial p_g^e}{\partial \theta}(1-\chi) - s^e\frac{\partial \chi}{\partial \theta}\right]\right]\boldsymbol{N}^{\theta,e}\alpha\Delta t dV \right]. \tag{6.225}$$

6.7.3 Matrix form of δH_1^{int}

From equation 6.46 it can be seen that

$$\frac{\partial \boldsymbol{H}_1^{int}}{\partial \dot{\boldsymbol{u}}} = \boldsymbol{A}\boldsymbol{A}^{n_{el}}(\boldsymbol{\alpha}^e)^T \cdot \left[\int_{B_o} \boldsymbol{N}^{p,e^T}(S_g\rho^{gR} + S_\ell\rho^{\ell R})J\left(\boldsymbol{\mathscr{F}}\boldsymbol{B}^{u,e}\alpha\Delta t + \boldsymbol{F}^{-T}\boldsymbol{B}^{u,e}\right)dV \right] \tag{6.226}$$

where $\boldsymbol{\mathscr{F}}$ is a 4-d matrix put in Voight-like notation resulting in an $n_{sdof} \times n_{sdof}$ matrix defined as

$$\boldsymbol{\mathscr{F}} = \boldsymbol{F}^{-1} \otimes \boldsymbol{F}^{-T}\dot{\boldsymbol{F}} - \boldsymbol{F}^{-T} \otimes \boldsymbol{F}^{-1}\dot{\boldsymbol{F}} \tag{6.227}$$

where $\dot{\boldsymbol{F}}$ is defined in matrix form as

$$\dot{\boldsymbol{F}} = \boldsymbol{B}^{u,e}\boldsymbol{v}^e. \tag{6.228}$$

From equation 6.48 it is seen that

$$\frac{\partial \boldsymbol{H}_1^{int}}{\partial \dot{\boldsymbol{p}}_\ell} = \boldsymbol{A}\boldsymbol{A}^{n_{el}}(\boldsymbol{\alpha}^e)^T \cdot \left[\int_{B_o} \boldsymbol{N}^{p,e^T}(\rho^{\ell R} - \rho^{gR}) \dot{J} \frac{\partial S_\ell}{\partial p_\ell} \boldsymbol{N}^{p,e}\alpha\Delta t dV \right]. \tag{6.229}$$

From equation 6.50 it is seen that

$$\frac{\partial \boldsymbol{H}_1^{int}}{\partial \dot{\boldsymbol{\theta}}} = \boldsymbol{A}\boldsymbol{A}^{n_{el}}(\boldsymbol{\alpha}^e)^T \cdot \left[\int_{B_o} \boldsymbol{N}^{p,e^T} \dot{J} \Big(\frac{\partial \rho^{gR}}{\partial \theta} S_g + \rho^{gR}\frac{\partial S_g}{\partial \theta} + \frac{\partial \rho^{\ell R}}{\partial \theta} S_\ell + \rho^{\ell R}\frac{\partial S_\ell}{\partial \theta} \Big) \boldsymbol{N}^{\theta,e}\alpha\Delta t dV \right]. \tag{6.230}$$

6.7.4 Matrix form of δH_2^{int}

Equation 6.58 can be written in matrix form as

$$\frac{\partial \boldsymbol{H}_2^{int}}{\partial \dot{\boldsymbol{u}}} = \boldsymbol{A}\boldsymbol{A}^{n_{el}}(\boldsymbol{\alpha}^e)^T \cdot \left[\int_{B_o} \boldsymbol{N}^{p,e^T} J \Big(\boldsymbol{F}^{-T}\beta_{s\ell g}^\theta - \frac{(1-n_0)}{J}\boldsymbol{F}^{-T}(\rho^{\ell R}S_\ell \right.$$
$$\left. + \rho^{gR}S_g)\beta_s^\theta\dot{\theta}^e + \frac{(1-n_0)}{J}\boldsymbol{F}^{-T}\rho^{\ell R}S_\ell\beta_\ell^\theta\dot{\theta}^e \Big) \boldsymbol{B}^{u,e} dV \right]. \tag{6.231}$$

Equation 6.71 can be written in matrix form as

$$\frac{\partial \boldsymbol{H}_2^{int}}{\partial \dot{\boldsymbol{p}}_\ell} = \boldsymbol{A}\boldsymbol{A}^{n_{el}}(\boldsymbol{\alpha}^e)^T \cdot \left[\int_{B_o} \boldsymbol{N}^{p,e^T} J \big(\beta_s^\theta(1-n)(\rho^{\ell R} - \rho^{gR}) + n\rho^{\ell R}\beta_\ell^\theta \big)\dot{\theta}^e \frac{\partial S_\ell}{\partial p_\ell}\boldsymbol{N}^{p,e}\alpha\Delta t dV \right]. \tag{6.232}$$

Lastly, equation 6.61 can be written in matrix form as

$$\frac{\partial \boldsymbol{H}_2^{int}}{\partial \dot{\boldsymbol{\theta}}} = \boldsymbol{A}\boldsymbol{A}^{n_{el}}(\boldsymbol{\alpha}^e)^T \cdot \left[\int_{B_o} \boldsymbol{N}^{p,e^T} J \Big((1-n)\beta_s^\theta\dot{\theta}^e \Big(\frac{\partial \rho^{gR}}{\partial \theta}S_g + \rho^{gR}\frac{\partial S_g}{\partial \theta} \right.$$
$$+ \frac{\partial \rho^{\ell R}}{\partial \theta}S_\ell + \rho^{\ell R}\frac{\partial S_\ell}{\partial \theta} \Big)\boldsymbol{N}^{\theta,e}\alpha\Delta t + n\beta_\ell^\theta \Big(\frac{\partial \rho^{\ell R}}{\partial \theta} + \rho^{\ell R}\frac{\partial S_\ell}{\partial \theta} \Big)\boldsymbol{N}^{\theta,e}\alpha\Delta t \tag{6.233}$$
$$\left. + \Big((1-n)\big(\rho^{\ell R}S_\ell + \rho^{gR}S_g \big)\beta_s^\theta + n\rho^{\ell R}S_\ell\beta_\ell^\theta \Big)\boldsymbol{N}^{\theta,e} \Big) dV \right].$$

6.7.5 Matrix form of δH_3^{int}

Equation 6.68 can be written in matrix form as

$$\frac{\partial \boldsymbol{H}_3^{int}}{\partial \dot{\boldsymbol{u}}} = \boldsymbol{A}\boldsymbol{A}^{n_{el}}(\boldsymbol{\alpha}^e)^T \cdot \left[\int_{B_o} \boldsymbol{B}^{p,e^T} J \Big[\Big(\boldsymbol{F}^{-1} \otimes \boldsymbol{F}^{-T} - \boldsymbol{F}^{-T} \otimes \boldsymbol{F}^{-1} \Big) \cdot \big[\rho^{\ell R} \boldsymbol{v}_\ell^D \right.$$
$$\left. + \rho^{gR} \boldsymbol{v}_g^D \big] + \boldsymbol{F}^{-T} \cdot \Big(\rho^{\ell R} \frac{\partial \boldsymbol{v}_\ell^D}{\partial \boldsymbol{F}} + \rho^{gR} \frac{\partial \boldsymbol{v}_g^D}{\partial \boldsymbol{F}} \Big) \Big] \boldsymbol{B}^{u,e} \alpha \Delta t dV \right]. \tag{6.234}$$

Equation 6.71 can be written in matrix form as

$$\frac{\partial \boldsymbol{H}_3^{int}}{\partial \dot{\boldsymbol{p}}_\ell} = \boldsymbol{A}\boldsymbol{A}^{n_{el}}(\boldsymbol{\alpha}^e)^T \cdot \left[\int_{B_o} \boldsymbol{B}^{p,e^T} J \boldsymbol{F}^{-1} \cdot \Big(\rho^{\ell R} \frac{k_{rel}^\ell}{\mu_\ell} \boldsymbol{F}^{-T} \Big[\frac{\partial k_{int}^\ell}{\partial p_\ell} \frac{\partial p_\ell^e}{\partial \boldsymbol{X}} \Big] \boldsymbol{N}^{p,e} \alpha \Delta t \right.$$
$$\left. + \rho^{\ell R} \frac{k_{rel}^\ell}{\mu_\ell} \boldsymbol{F}^{-T} k_{int}^\ell \boldsymbol{B}^{p,e} \Big) dV \right]. \tag{6.235}$$

Lastly, equation 6.74 can be written in matrix form as

$$\frac{\partial \boldsymbol{H}_3^{int}}{\partial \dot{\boldsymbol{\theta}}} = \boldsymbol{A}\boldsymbol{A}^{n_{el}}(\boldsymbol{\alpha}^e)^T \cdot \left[\int_{B_o} \boldsymbol{B}^{p,e^T} J \boldsymbol{F}^{-1} \cdot \Big[\frac{\partial \rho^{\ell R}}{\partial \theta} \boldsymbol{v}_\ell^D + \rho^{\ell R} \frac{\partial \boldsymbol{v}_\ell^D}{\partial \theta} \right.$$
$$\left. + \frac{\partial \rho^{gR}}{\partial \theta} \boldsymbol{v}_g^D + \rho^{gR} \frac{\partial \boldsymbol{v}_g^D}{\partial \theta} \Big] \boldsymbol{N}^{\theta,u} \alpha \Delta t dV \right]. \tag{6.236}$$

6.7.6 Matrix form of δH_4^{int}

Equation 6.77 can be written in matrix form as

$$\frac{\partial \boldsymbol{H}_4^{int}}{\partial \dot{\boldsymbol{u}}} = \boldsymbol{A}\boldsymbol{A}^{n_{el}}(\boldsymbol{\alpha}^e)^T \cdot \left[\int_{B_o} \boldsymbol{N}^{p,e^T} \Big(\frac{\partial J}{\partial \boldsymbol{F}} n + J \frac{\partial n}{\partial \boldsymbol{F}} \Big) \big(\rho^{\ell R} \dot{S}_\ell + \rho^{gR} \dot{S}_g + S_g \dot{\rho}^{gR} \big) \boldsymbol{B}^{u,e} \alpha \Delta t dV \right]. \tag{6.237}$$

Equation 6.80 can be written in matrix form as

$$\frac{\partial \boldsymbol{H}_4^{int}}{\partial \dot{\boldsymbol{p}}_\ell} = \boldsymbol{A}\boldsymbol{A}^{n_{el}}(\boldsymbol{\alpha}^e)^T \cdot \left[\int_{B_o} \boldsymbol{N}^{p,e^T} Jn(\rho^{\ell R} - \rho^{gR})\frac{\partial \dot{S}_\ell}{\partial \dot{p}_\ell}\boldsymbol{N}^{p,e}dV \right]. \tag{6.238}$$

Lastly, equation 6.81 can be written in matrix form as

$$\begin{aligned}
\frac{\partial \boldsymbol{H}_4^{int}}{\partial \dot{\boldsymbol{\theta}}} = \boldsymbol{A}\boldsymbol{A}^{n_{el}}(\boldsymbol{\alpha}^e)^T \cdot &\left[\int_{B_o} \boldsymbol{N}^{p,e^T} Jn\left[\left(\frac{\partial \rho^{\ell R}}{\partial \theta}\dot{S}_\ell + \frac{\partial \rho^{gR}}{\partial \theta}\dot{S}_g + \dot{\rho}^{gR}\frac{\partial S_g}{\partial \theta}\right)\boldsymbol{N}^{\theta,e}\alpha\Delta t \right. \right. \\
&\left. \left. + \left((\rho^{\ell R} - \rho^{gR})\frac{\partial \dot{S})\ell}{\partial \dot{\theta}} + S_g\frac{\partial \dot{\rho}^{gR}}{\partial \dot{\theta}}\boldsymbol{N}^{\theta,e}\right]dV \right].
\end{aligned} \tag{6.239}$$

6.7.7 Matrix form of δH_5^{int}

Equation 6.85 can be written in matrix form as

$$\begin{aligned}
\frac{\partial \boldsymbol{H}_5^{int}}{\partial \dot{\boldsymbol{u}}} = \boldsymbol{A}\boldsymbol{A}^{n_{el}}(\boldsymbol{\alpha}^e)^T \cdot &\left[\int_{B_o} \boldsymbol{N}^{p,e^T} J\left(\boldsymbol{F}^{-1}\left(\frac{nS_\ell\rho^{\ell R}}{K_{bulk}^\ell}\ddot{p}_\ell^e + \frac{\rho^{\ell R}}{K_{bulk}^\ell}\frac{\partial p_\ell^e}{\partial \boldsymbol{X}}\cdot \boldsymbol{v}_\ell^D \cdot \boldsymbol{F}^{-T}\right) \right. \right. \\
&\left. \left. + \frac{J\rho^{\ell R}}{K_{bulk}^\ell}\frac{\partial p_\ell^e}{\partial \boldsymbol{X}}\cdot\frac{\partial \boldsymbol{v}_\ell^D}{\partial \boldsymbol{F}}\cdot \boldsymbol{F}^{-T} + \frac{\rho^{\ell R}}{K_{bulk}^\ell}\frac{\partial p_\ell^e}{\partial \boldsymbol{X}}\cdot \boldsymbol{v}_\ell^D \cdot \boldsymbol{F}^{-1} \otimes \boldsymbol{F}^{-T}\right)\boldsymbol{B}^{u,e}\alpha\Delta tdV \right].
\end{aligned} \tag{6.240}$$

Equation 6.87 can be written in matrix form as

$$\begin{aligned}
\frac{\partial \boldsymbol{H}_5^{int}}{\partial \dot{\boldsymbol{p}}_\ell} = \boldsymbol{A}\boldsymbol{A}^{n_{el}}(\boldsymbol{\alpha}^e)^T \cdot &\left[\int_{B_o} \boldsymbol{N}^{p,e^T} \frac{J\rho^{\ell R}}{K_{bulk}^\ell}\left(nS_\ell\boldsymbol{N}^{p,e} + n\frac{\partial S_\ell}{\partial p_\ell}\dot{p}_\ell^e\boldsymbol{N}^{p,e}\alpha\Delta t \right. \right. \\
&\left. \left. + \boldsymbol{v}_\ell^D \cdot \boldsymbol{F}^{-T}\boldsymbol{B}^{p,e}\alpha\Delta t + \frac{\partial p_\ell^e}{\partial \boldsymbol{X}}\cdot\frac{\partial \boldsymbol{v}_\ell^D}{\partial p_\ell}\cdot \boldsymbol{F}^{-T}\boldsymbol{N}^{p,e}\alpha\Delta tdV \right].
\end{aligned} \tag{6.241}$$

Lastly, equation 6.89 can be written in matrix form as

$$\frac{\partial \boldsymbol{H}_5^{int}}{\partial \dot{\boldsymbol{\theta}}} = \boldsymbol{A}\boldsymbol{A}^{n_{el}}(\boldsymbol{\alpha}^e)^T \cdot \left[\int_{B_o} \boldsymbol{N}^{p,e^T} \frac{J\rho^{\ell R}}{K_{bulk}^\ell}\left(n\frac{\partial S_\ell}{\partial \theta}\dot{p}_\ell^e + \frac{\partial p_\ell^e}{\partial \boldsymbol{X}}\cdot\frac{\partial \boldsymbol{v}_\ell^D}{\partial \theta}\cdot \boldsymbol{F}^{-T}\right)\boldsymbol{N}^{\theta,e}\right]dV \right]. \tag{6.242}$$

6.7.8 Matrix form of δL_1^{int}

Equation 6.97 can be written in matrix form as

$$\frac{\partial \boldsymbol{L}_1^{int}}{\partial \dot{\boldsymbol{u}}} = \boldsymbol{A}\boldsymbol{A}^{n_{el}}(\boldsymbol{\beta}^e)^T \cdot \left[\int_{B_o} \boldsymbol{N}^{\theta,e^T} J\dot{\theta}^e \left(\boldsymbol{F}^{-T}(\rho C_p)^{eff} \right. \right.$$
$$\left. \left. + \left((S_\ell \rho^{\ell R} C_p^\ell S_g \rho^{gR} C_p^g) - \rho^{sR} C_p^s \right) \frac{\partial n}{\partial \boldsymbol{F}} \right) \boldsymbol{B}^{u,e} \alpha \Delta t dV \right]. \tag{6.243}$$

Equation 6.102 can be written in matrix form as

$$\frac{\partial \boldsymbol{L}_1^{int}}{\partial \dot{\boldsymbol{p}}_\ell} = \boldsymbol{A}\boldsymbol{A}^{n_{el}}(\boldsymbol{\alpha}^e)^T \cdot \left[\int_{B_o} \boldsymbol{N}^{\theta,e^T} J\dot{\theta}^e \left(n(\rho^{\ell R} C_p^\ell - \rho^{gR} C_p^g) \frac{\partial S_\ell}{\partial p_\ell} \right) \boldsymbol{N}^{p,e} \alpha \Delta t dV \right]. \tag{6.244}$$

Lastly, equation 6.106 can be written in matrix form as

$$\frac{\partial \boldsymbol{L}_1^{int}}{\partial \dot{\boldsymbol{\theta}}} = \boldsymbol{A}\boldsymbol{A}^{n_{el}}(\boldsymbol{\alpha}^e)^T \cdot \left[\int_{B_o} \boldsymbol{N}^{\theta,e^T} J \left[\dot{\theta}^e \left((1-n) \frac{\partial \rho^{sR}}{\partial \theta} C_p^s + n(S_\ell \frac{\partial \rho^{\ell R}}{\partial \theta} C_p^\ell \right. \right. \right.$$
$$\left. \left. \left. + S_g \frac{\partial \rho^{gR}}{\partial \theta} C_p^g + n(\rho^{\ell R} C_p^\ell - \rho^{gR} C_p^g) \frac{\partial S_\ell}{\partial \theta} \right) \boldsymbol{N}^{\theta,e} \alpha \Delta t + (\rho C_p)^{eff} \boldsymbol{N}^{\theta,e} \right] dV \right]. \tag{6.245}$$

6.7.9 Matrix form of δL_2^{int}

Equation 6.111 can be written in matrix form as

$$\frac{\partial \boldsymbol{L}_2^{int}}{\partial \dot{\boldsymbol{u}}} = \boldsymbol{A}\boldsymbol{A}^{n_{el}}(\boldsymbol{\beta}^e)^T \cdot \left[\int_{B_o} \boldsymbol{N}^{\theta,e^T} J\rho^{\ell R} C_p^\ell \frac{\partial \theta^e}{\partial \boldsymbol{X}} \cdot \left(\boldsymbol{F}^{-1} \otimes \boldsymbol{v}_\ell^D \cdot \boldsymbol{F}^{-T} \right. \right.$$
$$\left. \left. + \frac{\partial \boldsymbol{v}_\ell^D}{\partial \boldsymbol{F}} \boldsymbol{F}^{-T} - \boldsymbol{v}_\ell^D \cdot \boldsymbol{F}^{-T} \otimes \boldsymbol{F}^{-1} \right) \boldsymbol{B}^{u,e} \alpha \Delta t dV \right]. \tag{6.246}$$

Equation 6.114 can be written in matrix form as

$$\frac{\partial \boldsymbol{L}_2^{int}}{\partial \dot{\boldsymbol{p}}_\ell} = \boldsymbol{A}\boldsymbol{A}^{n_{el}}(\boldsymbol{\alpha}^e)^T \cdot \left[\int_{B_o} \boldsymbol{N}^{\theta,e^T} J\rho^{\ell R} C_p^\ell \frac{\partial \theta^e}{\partial \boldsymbol{X}} \cdot \boldsymbol{F}^{-T} \cdot \frac{\partial \boldsymbol{v}_\ell^D}{\partial p_\ell} \boldsymbol{N}^{p,e} \alpha \Delta t dV \right]. \tag{6.247}$$

Lastly, equation 6.124 can be written in matrix form as

$$\frac{\partial \boldsymbol{L}_2^{int}}{\partial \dot{\boldsymbol{\theta}}} = \boldsymbol{A}\boldsymbol{A}^{n_{el}}(\boldsymbol{\alpha}^e)^T \cdot \left[\int_{B_o} \boldsymbol{N}^{\theta,e^T} J C_p^\ell \boldsymbol{F}^{-T} \cdot \left(\boldsymbol{v}_\ell^D \rho^{\ell R} \boldsymbol{B}^{\theta,e} \right. \right.$$
$$\left. \left. + \frac{\partial \theta^e}{\partial \boldsymbol{X}} \cdot (\frac{\partial \rho^{\ell R}}{\partial \theta} \boldsymbol{v}_\ell^D + \rho^{\ell R}\frac{\partial \boldsymbol{v}_\ell^D}{\partial \theta}) \boldsymbol{N}^{\theta,e} \right) \alpha \Delta t dV \right]. \tag{6.248}$$

6.7.10 Matrix form of δL_3^{int}

Equation 6.119 can be written in matrix form as

$$\frac{\partial \boldsymbol{L}_3^{int}}{\partial \dot{\boldsymbol{u}}} = \boldsymbol{A}\boldsymbol{A}^{n_{el}}(\boldsymbol{\beta}^e)^T \cdot \left[\int_{B_o} \boldsymbol{N}^{\theta,e^T} J \rho^{gR} C_p^g \frac{\partial \theta^e}{\partial \boldsymbol{X}} \cdot \left(\boldsymbol{F}^{-T} \otimes \boldsymbol{v}_g^D \cdot \boldsymbol{F}^{-1} \right. \right.$$
$$\left. \left. + \frac{\partial \boldsymbol{v}_g^D}{\partial \boldsymbol{F}} \boldsymbol{F}^{-T} - \boldsymbol{v}_g^D \cdot \boldsymbol{F}^{-1} \otimes \boldsymbol{F}^{-T} \right) \boldsymbol{B}^{u,e} \alpha \Delta t dV \right]. \tag{6.249}$$

Equation 6.122 can be written in matrix form as

$$\frac{\partial \boldsymbol{L}_3^{int}}{\partial \dot{\boldsymbol{p}}_\ell} = \boldsymbol{0}. \tag{6.250}$$

Lastly, equation 6.123 can be written in matrix form as

$$\frac{\partial \boldsymbol{L}_3^{int}}{\partial \dot{\boldsymbol{\theta}}} = \boldsymbol{A}\boldsymbol{A}^{n_{el}}(\boldsymbol{\alpha}^e)^T \cdot \left[\int_{B_o} \boldsymbol{N}^{\theta,e^T} J C_p^g \boldsymbol{F}^{-T} \cdot \left(\boldsymbol{v}_g^D \rho^{gR} \boldsymbol{B}^{\theta,e} \right. \right.$$
$$\left. \left. + \frac{\partial \theta^e}{\partial \boldsymbol{X}} \cdot (\frac{\partial \rho^{gR}}{\partial \theta} \boldsymbol{v}_\ell^D + \rho^{gR}\frac{\partial \boldsymbol{v}_g^D}{\partial \theta}) \boldsymbol{N}^{\theta,e} \right) \alpha \Delta t dV \right]. \tag{6.251}$$

6.7.11   Matrix form of δL_4^{int}

Equation 6.131 can be written in matrix form as

$$
\frac{\partial \boldsymbol{L}_4^{int}}{\partial \dot{\boldsymbol{u}}} = \boldsymbol{A}\boldsymbol{A}^{n_{el}}(\boldsymbol{\beta}^e)^T \cdot \left[\int_{B_o} \boldsymbol{N}^{\theta,e^T} J\left(\boldsymbol{F}^{-T}\rho^{eff}r + \left(\left(S_\ell\rho^{\ell R} + S_g\rho^{gR} \right) \right. \right. \right.
$$
$$
\left. \left. \left. -\rho^{sR} \right)\frac{\partial n}{\partial \boldsymbol{F}} + \rho^{eff}\frac{\partial r}{\partial \boldsymbol{F}} \right) \boldsymbol{B}^{u,e}\alpha\Delta t dV \right]. \tag{6.252}
$$

Equation 6.135 can be written in matrix form as

$$
\frac{\partial \boldsymbol{L}_4^{int}}{\partial \dot{\boldsymbol{p}}_\ell} = \boldsymbol{A}\boldsymbol{A}^{n_{el}}(\boldsymbol{\alpha}^e)^T \cdot \left[\int_{B_o} \boldsymbol{N}^{\theta,e^T} Jrn(\rho^{\ell R} - \rho^{gR})\frac{\partial S_\ell}{\partial p_\ell}\boldsymbol{N}^{p,e}\alpha\Delta t dV \right]. \tag{6.253}
$$

Lastly, equation 6.139 can be written in matrix form as

$$
\frac{\partial \boldsymbol{L}_4^{int}}{\partial \dot{\boldsymbol{\theta}}} = \boldsymbol{A}\boldsymbol{A}^{n_{el}}(\boldsymbol{\alpha}^e)^T \cdot \left[\int_{B_o} \boldsymbol{N}^{\theta,e^T} Jrn\left(\frac{\partial \rho^{\ell R}}{\partial \theta}S_\ell\rho^{\ell R}\frac{\partial S_\ell}{\partial \theta} \right. \right.
$$
$$
\left. \left. +\frac{\partial \rho^{gR}}{\partial \theta}S_g + \rho^{gR}\frac{\partial S_g}{\partial \theta} \right) \boldsymbol{N}^{\theta,e}\alpha\Delta t dV \right]. \tag{6.254}
$$

6.7.12   Matrix form of δL_5^{int}

Equation 6.146 can be written in matrix form as

$$
\frac{\partial \boldsymbol{L}_5^{int}}{\partial \dot{\boldsymbol{u}}} = \boldsymbol{A}\boldsymbol{A}^{n_{el}}(\boldsymbol{\beta}^e)^T \cdot \left[\int_{B_o} \boldsymbol{B}^{\theta,e^T} J\frac{\partial \theta^e}{\partial \boldsymbol{X}} \cdot \left(\boldsymbol{\mathscr{K}} \right)\boldsymbol{B}^{u,e}\alpha\Delta t dV \right]. \tag{6.255}
$$

where $\boldsymbol{\mathscr{K}}$ is defined as

$$
\boldsymbol{\mathscr{K}} = \boldsymbol{F}^{-T}(-K^\theta)\otimes\boldsymbol{F}^{-T}\cdot\boldsymbol{F}^{-1} - \frac{\partial n}{\partial \boldsymbol{F}}(S_\ell K_\ell^\theta + S_g K_g^\theta - K_s^\theta)\otimes\boldsymbol{F}^{-1}\cdot\boldsymbol{F}^{-T}
$$
$$
-(-K^\theta)\boldsymbol{F}^{-1}\otimes\boldsymbol{F}^{-T}\cdot\boldsymbol{F}^{-T} - (-K^\theta)\boldsymbol{F}^{-T}\cdot\boldsymbol{F}^{-T}\otimes\boldsymbol{F}^{-1} \tag{6.256}
$$

Equation 6.151 can be written in matrix form as

$$\frac{\partial \boldsymbol{L}_5^{int}}{\partial \dot{\boldsymbol{p}}_\ell} = \boldsymbol{A}\boldsymbol{A}^{n_{el}}(\boldsymbol{\alpha}^e)^T \cdot \left[\int_{B_o} -\boldsymbol{B}^{\theta,e^T} J \frac{\partial \theta}{\partial \boldsymbol{X}} \cdot \boldsymbol{F}^{-1} \cdot \boldsymbol{F}^{-T} n (K_\ell^\theta - K_g^\theta) \frac{\partial S_\ell}{\partial p_\ell} \boldsymbol{N}^{p,e} \alpha \Delta t dV \right]. \quad (6.257)$$

Lastly, equation 6.155 can be written in matrix form as

$$\frac{\partial \boldsymbol{L}_5^{int}}{\partial \dot{\boldsymbol{\theta}}} = \boldsymbol{A}\boldsymbol{A}^{n_{el}}(\boldsymbol{\alpha}^e)^T \cdot \left[\int_{B_o} \boldsymbol{B}^{\theta,e^T} J \left(\boldsymbol{F}^{-1} \cdot \boldsymbol{F}^{-T}(-K^\theta) \boldsymbol{B}^{\theta,e} \right. \right.$$
$$\left. \left. -\left(\boldsymbol{F}^{-1} \cdot \boldsymbol{F}^{-T} \cdot \frac{\partial \theta^e}{\partial \boldsymbol{X}} n (K_\ell^\theta - K_g^\theta) \frac{\partial S_\ell}{\partial \theta} \boldsymbol{N}^{\theta,e} \right) \alpha \Delta t dV \right]. \right. \quad (6.258)$$

6.7.13 Matrix form of δL_6^{int}

Equation 6.160 can be written in matrix form as

$$\frac{\partial \boldsymbol{L}_6^{int}}{\partial \dot{\boldsymbol{u}}} = \boldsymbol{A}\boldsymbol{A}^{n_{el}}(\boldsymbol{\alpha}^e)^T \cdot \left[\int_{B_o} + H_{vap} J \left(\boldsymbol{N}^{\theta,e^T} \left[\boldsymbol{\mathscr{A}} + \boldsymbol{F}^{-T} + \boldsymbol{\mathscr{B}} \right] \boldsymbol{B}^{u,e} \right. \right.$$
$$\left. \left. + \boldsymbol{B}^{\theta,e^T} \rho^{\ell R} \boldsymbol{\mathscr{D}} \boldsymbol{B}^{u,e} \right) \alpha \Delta t dV \right]. \quad (6.259)$$

where $\boldsymbol{\mathscr{A}}$ is defined as

$$\boldsymbol{\mathscr{A}} = \boldsymbol{F}^{-T} \otimes \boldsymbol{F}^{-T} \cdot \boldsymbol{F}^{-1} - \boldsymbol{F}^{-T} \cdot \boldsymbol{F}^{-1} \otimes \boldsymbol{F}^{-T}, \quad (6.260)$$

$\boldsymbol{\mathscr{B}}$ is defined as

$$\boldsymbol{\mathscr{B}} = \boldsymbol{F}^{-T} \rho^{\ell R} \left(S_\ell \big((1-n)\beta_s^\theta - n\beta_\ell^\theta \big) \dot{\theta}^e + \dot{S}_\ell n \right) - \rho^{\ell R} \left(S_\ell (\beta_\ell^\theta + beta_s^\theta) \dot{\theta}^e - \dot{S}_\ell \right) \frac{\partial n}{\partial \boldsymbol{F}}, \quad (6.261)$$

and $\boldsymbol{\mathscr{D}}$ is defined as

$$\boldsymbol{\mathscr{D}} = \boldsymbol{F}^{-T} \cdot \left(\boldsymbol{F}^{-T} \otimes \boldsymbol{v}_\ell^D + \frac{\partial \boldsymbol{v}_\ell^D}{\partial \boldsymbol{F}} \right). \quad (6.262)$$

Equation 6.162 can be written in matrix form as

$$
\frac{\partial \boldsymbol{L}_6^{int}}{\partial \dot{\boldsymbol{p}}_\ell} = \boldsymbol{A}\boldsymbol{A}^{n_{el}}(\boldsymbol{\alpha}^e)^T \cdot \left[\int_{B_o} \left[\left(- \boldsymbol{N}^{\theta,e^T} \dot{J} H_{vap} \rho^{\ell R} S_\ell \big((1-n)\beta_s^\theta - n\beta_\ell^\theta \big) \dot{\theta}^e \right. \right. \right.
$$
$$
\left. \left. \left. + \boldsymbol{B}^{\theta,e^T} \rho^{\ell R} J H_{vap} \boldsymbol{v}_\ell^D \cdot \boldsymbol{F}^{-1} \right) \boldsymbol{N}^{p,e} \alpha \Delta t + \boldsymbol{N}^{\theta,e^T} J H_{vap} \rho^{\ell R} n \frac{\partial \dot{S}_\ell}{\partial \dot{p}_\ell} \boldsymbol{N}^{\theta,e} \right] dV \right].
$$

(6.263)

Lastly, equation 6.164 can be written in matrix form as

$$
\frac{\partial \boldsymbol{L}_6^{int}}{\partial \dot{\boldsymbol{\theta}}} = \boldsymbol{A}\boldsymbol{A}^{n_{el}}(\boldsymbol{\alpha}^e)^T \cdot \left[\int_{B_o} \left[\boldsymbol{N}^{\theta,e^T} J H_{vap} \left(\dot{\theta}^e \big((1-n)\beta_s^\theta - n\beta_\ell^\theta \big) \left[\frac{\partial \rho^{\ell R}}{\partial \theta} S_\ell + \rho^{\ell R} \frac{\partial S_\ell}{\partial \theta} \right. \right. \right. \right.
$$
$$
\left. \left. + \frac{\partial \rho^{\ell R}}{\partial \theta} \dot{S}_\ell n \right] \right) + \boldsymbol{B}^{\theta,e^T} J H_{vap} \boldsymbol{F}^{-T} \cdot \left(\frac{\partial \rho^{\ell R}}{\partial \theta} \boldsymbol{v}_\ell^D \rho^{\ell R} \frac{\partial \boldsymbol{v}_\ell^D}{\partial \theta} \right) \boldsymbol{N}^{\theta,e} \alpha \Delta t
$$
$$
\left. + \boldsymbol{N}^{\theta,e^T} J H_{vap} \rho^{\ell R} \left[\big(S_\ell \big((1-n)\beta_s^\theta - n\beta_\ell^\theta \big) \big) + \frac{\partial S_\ell}{\partial \theta} \right] \boldsymbol{N}^{\theta,e} \right] dV \right].
$$

(6.264)

6.7.14 Matrix form of δL_8^{int}

Equation 6.169 can be written in matrix form as

$$
\frac{\partial \boldsymbol{L}_8^{int}}{\partial \dot{\boldsymbol{u}}} = \boldsymbol{A}\boldsymbol{A}^{n_{el}}(\boldsymbol{\beta}^e)^T \cdot \left[\int_{B_o} \boldsymbol{N}^{\theta,e^T} J \left(\boldsymbol{F}^{-T} \cdot \left(\boldsymbol{v}_\ell^D \left[\frac{\partial p_\ell}{\partial \boldsymbol{X}} \cdot \boldsymbol{F}^{-1} + \rho^{\ell R}(\boldsymbol{a} - \boldsymbol{b}) \right] \right. \right. \right.
$$
$$
\left. + \boldsymbol{v}_g^D \left[\frac{\partial p_g}{\partial \boldsymbol{X}} \cdot \boldsymbol{F}^{-1} + \rho^{gR}(\boldsymbol{a} - \boldsymbol{b}) \right] \right) + \left[\left(\frac{\partial \boldsymbol{v}_\ell^D}{\partial \boldsymbol{F}} \cdot \boldsymbol{F}^{-1} - \boldsymbol{v}_\ell^D \cdot \boldsymbol{F}^{-T} \otimes \boldsymbol{F}^{-1} \right) \cdot \frac{\partial p_\ell}{\partial \boldsymbol{X}} \right.
$$
$$
\left. \left. \left. + \left(\frac{\partial \boldsymbol{v}_g^D}{\partial \boldsymbol{F}} \cdot \boldsymbol{F}^{-1} - \boldsymbol{v}_g^D \cdot \boldsymbol{F}^{-T} \otimes \boldsymbol{F}^{-1} \right) \cdot \frac{\partial p_g}{\partial \boldsymbol{X}} \right] \right) \boldsymbol{B}^{u,e} \alpha \Delta t dV \right].
$$

(6.265)

Equation 6.172 can be written in matrix form as

$$
\frac{\partial \boldsymbol{L}_4^{int}}{\partial \dot{\boldsymbol{p}}_\ell} = \boldsymbol{A}\boldsymbol{A}^{n_{el}}(\boldsymbol{\beta}^e)^T \cdot \left[\int_{B_o} \boldsymbol{N}^{\theta,e^T} J \left[\left(\frac{\partial \boldsymbol{v}_\ell^D}{\partial p_\ell} \cdot \left(\frac{\partial p_\ell}{\partial \boldsymbol{X}} \cdot \boldsymbol{F}^{-1} + \rho^{\ell R}(\boldsymbol{a} - \boldsymbol{b}) \right) \right. \right. \right.
$$
$$
\left. \left. \left. + \frac{\partial \boldsymbol{v}_g^D}{\partial p_g} \cdot \left(\frac{\partial p_g}{\partial \boldsymbol{X}} \cdot \boldsymbol{F}^{-1} + \rho^{gR}(\boldsymbol{a} - \boldsymbol{b}) \right) \right) \boldsymbol{N}^{p,e} + \boldsymbol{F}^{-T} \cdot \boldsymbol{v}_\ell^D \boldsymbol{B}^{p,e} \right] \alpha \Delta t dV \right].
$$

(6.266)

Lastly, equation 6.175 can be written in matrix form as

$$
\frac{\partial \boldsymbol{L}_8^{int}}{\partial \dot{\boldsymbol{\theta}}} = \boldsymbol{A}\boldsymbol{A}^{n_{el}}(\boldsymbol{\beta}^e)^T \cdot \left[\int_{B_o} \boldsymbol{N}^{\theta,e^T} J \left[\left(\frac{\partial \boldsymbol{v}_\ell^D}{\partial \theta} \left(\frac{\partial p_\ell}{\partial \boldsymbol{X}} \cdot \boldsymbol{F}^{-1} + \rho^{\ell R}(\boldsymbol{a} - \boldsymbol{b}) \right) \right. \right. \right.
$$
$$
\left. + \frac{\partial \boldsymbol{v}_g^D}{\partial \theta} \left(\frac{\partial p_g}{\partial \boldsymbol{X}} \cdot \boldsymbol{F}^{-1} + \rho^{gR}(\boldsymbol{a} - \boldsymbol{b}) \right) + \frac{\partial \rho^{\ell R}}{\partial \theta}(\boldsymbol{a} - \boldsymbol{b}) + \frac{\partial \rho^{gR}}{\partial \theta}(\boldsymbol{a} - \boldsymbol{b}) \right) \boldsymbol{N}^{\theta,e} +
$$
$$
\left. \left. \boldsymbol{v}_g^D \frac{\partial p_g}{\partial \boldsymbol{X}} \cdot \boldsymbol{F}^{-1} \boldsymbol{B}^{\theta.e} \right] \alpha \Delta t dV \right]. \tag{6.267}
$$

6.8 Finite Element Model Verification

To verify that the theory has been correctly implemented via the finite element method several test problems were developed, these include purely mechanical deformation, biphasic poromechanics and lastly, triphasic thermo-poromechanics. To verify the correct implementation the simulated results were compared, when possible, with simulations run in the commercial software Abaqus. For the large-deformation full TPM case, no analytic solutions or commercial software capable of solving the case exist. Therefore, the large and small deformation simulations were compared. It should be noted that all tests presented in this section were used to verify cases with material parameters and geometries representing situations close to those seen in arterial tissue fusion. For a complete verification of the code, especially pertaining to cases involving vastly different materials and parameters, such as seen in geomechanics, additional verification is needed.

6.8.1 Neo-Hookean Solid Material Verification

Two tests were proposed to verify the the solid portion of the large deformation of the code was working correctly. The first is a simple compression test shown in Figure 6.3. The simulation applies a top traction (t) of 7 MPa to a 3 mm x 3 mm block of hyperelastic material with a Young's Modulus (E) of 5 MPa and a poisson's ratio (ν) of 0.3. Simulations were run in the custom matlab code for both the small and large deformation cases and are compared to Abaqus' results with the non-linear geometry option on.

Figure 6.3: The first simulation run to test the Neo-Hookean solid portion of the custom written Matlab code. A traction (t) of 7 MPa is applied to a solid section of tissue with a Young's Modulus of (E) of 5MPa and a poisson's ratio (ν) of 0.3. The bottom edge is fixed in the y-direction and the left edge fixed in the x-direction.

Figure 6.4 shows the stress in the vertical direction vs the vertical displacement of the top edge for the three simulations (Abaqus, small deformation Matlab, and large deformation Matlab). Notice that the Abaqus and large deformation Matlab simulations match. The horizontal and vertical displacements of the upper right most node for the 3 displacements, again the large deformation Matlab and Abaqus simulations nearly match.
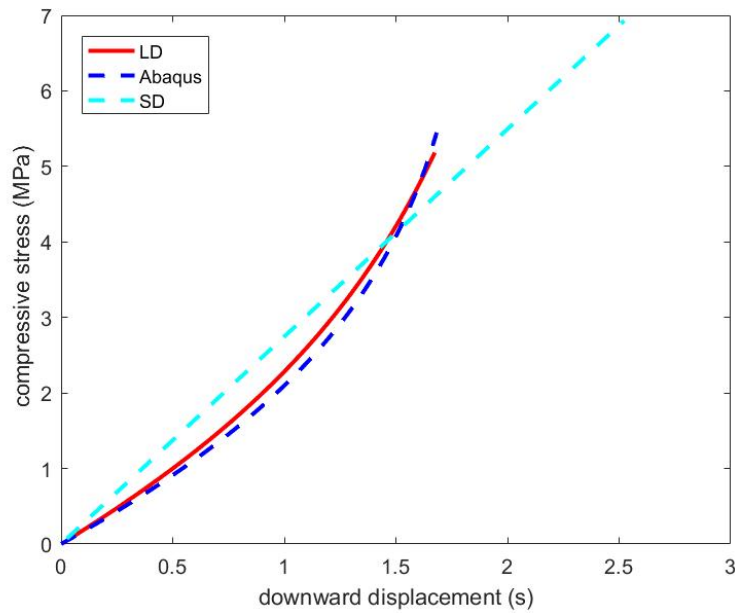
Figure 6.4: The stress in the y-direction vs top displacement for the Abaqus (Abaqus), the large deformation (LD), and the linear small deformation (SD) of the problem shown in figure 6.3. Notice the Abaqus and large deformation results nearly match.
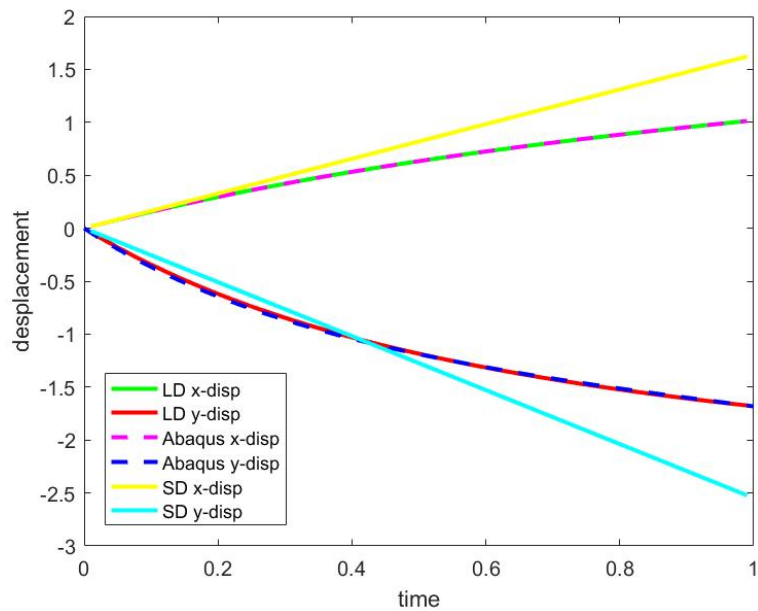
Figure 6.5: The x and y displacement for the top-rightmost node in the Abaqus (Abaqus), the large deformation (LD), and the linear small deformation (SD) of the problem shown in figure 6.3. Notice the Abaqus and large deformation results nearly match.

6.8.2   Biphasic Material Model Verification

To verify the biphasic poromechanics of the material a single test was run consisting of a 3 mm x 3 mm porous solid skeleton (Fig. 6.6). The pore space was considered to be filled solely with water. A traction of 1.2 MPa was applied to the top surface, ramping over 1 s and then held for an additional 1 s. All surfaces except the right edge are considered impermeable with the right edge pore pressure set to that of the ambient surroundings. Again, the bottom and left edges are fixed in the y and x directions, respectively. This problem was then simulated using the large and small deformation Matlab codes as well as Abaqus (with non-linear geometry on). Table 6.1 lists all of the material properties used for the test.
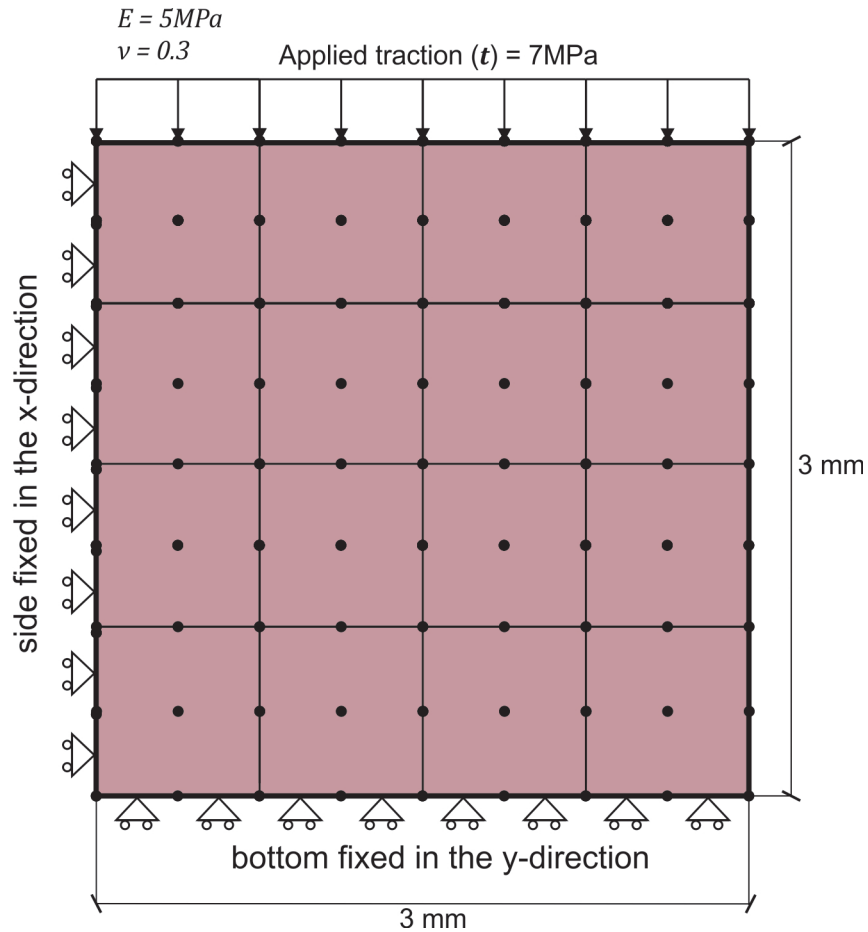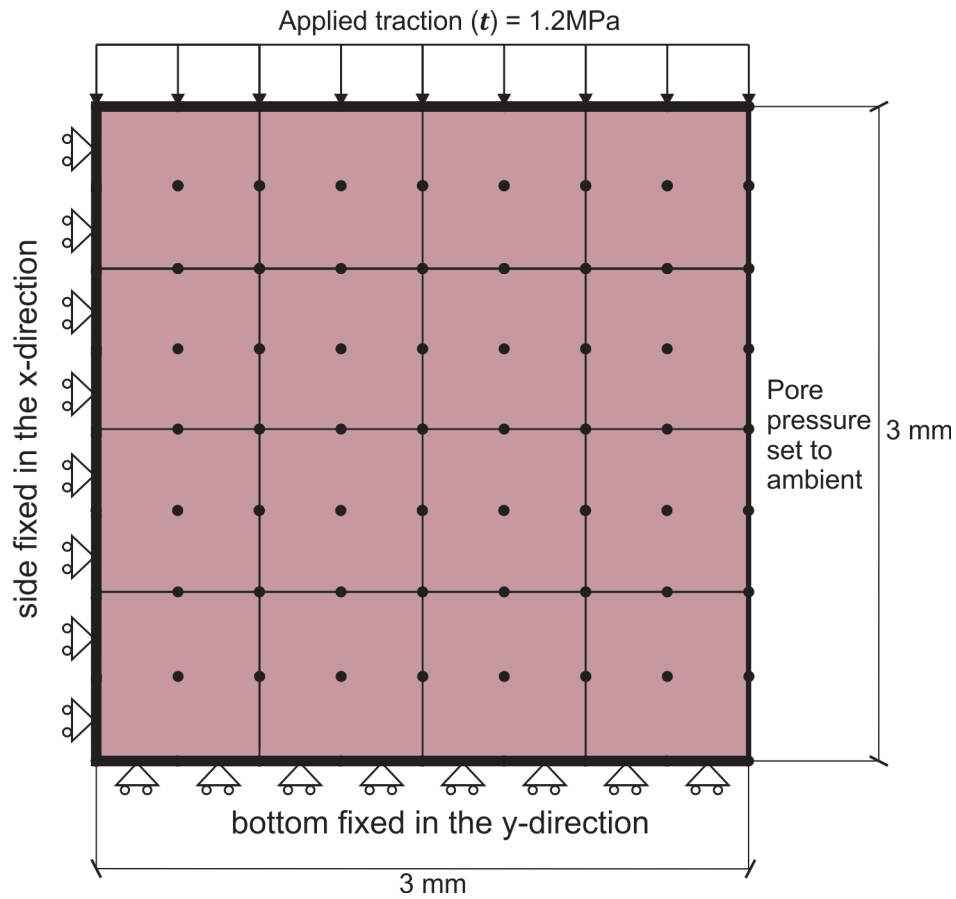
Figure 6.6: The first simulation run to test the biphasic portion of the custom written Matlab code. A traction (t) of 1.2 MPa is applied to a porous section of tissue. The bottom edge is fixed in the y-direction and the left edge fixed in the x-direction. The top, left, and bottom sides are set to be impermeable while the pore pressure along the right edge is set to the ambient pressure.

	Material Property	Value	Description
Solid Skelton Structure	E	5.00 MPa	Linear Elastic Young's Modulus
	ν^{skel}	0.3	Poisson's Ratio
Densities	ρ^{sR}	1050 (kg/m^3)	Real Density of Solid
	$\rho^{\ell R}$	1000 (kg/m^3)	Real Density of Water
Mass Transport Constants	$k_{o\,rel}^{\ell}$	Kozemy-Carmen Eq.	Relative Permeability of Water
	μ_ℓ	3x10^{-9} MPa*s	Viscosity of Liquid Water
		5x10^{-14} m^2	Intrinsic Permeability of Liquid Water
		1.01x10^5 Pa	Ambient Pressure
Initial Conditions and Model Parameters	n_o	0.78	Initial Porosity
	t	1.2 MPa	Applied Traction
	T	2 s	Total Time
	dt_0	0.001 (s)	Initial Time Step

Table 6.1: Material Properties for the Biphasic Test Simulation

Figure 6.8 shows the deformed shape and the pore pressure within the tissue of the Abaqus simulation and the large deformation matlab code at t = 2.0 s in the simulation. It should be noted that obtaining convergence was challenging as the top right hand element experienced severe distortion. The Abaqus simulation especially had difficulty and thus only a 1.2 MPa load could be applied to the medium. The x and y displacements of the top-rightmost node for the three different (Abaqus, large deformation, and small deformation) elements are presented in Figure 6.8. To further explore tissue deformation in this case, remeshing capabilities would need to be explored.

Figure 6.7: The predicted pore pressure throughout the tissue at the end of a 1.2 MPa, 2 s simulation in the large deformation matlab code (left) and by Abaqus (right).
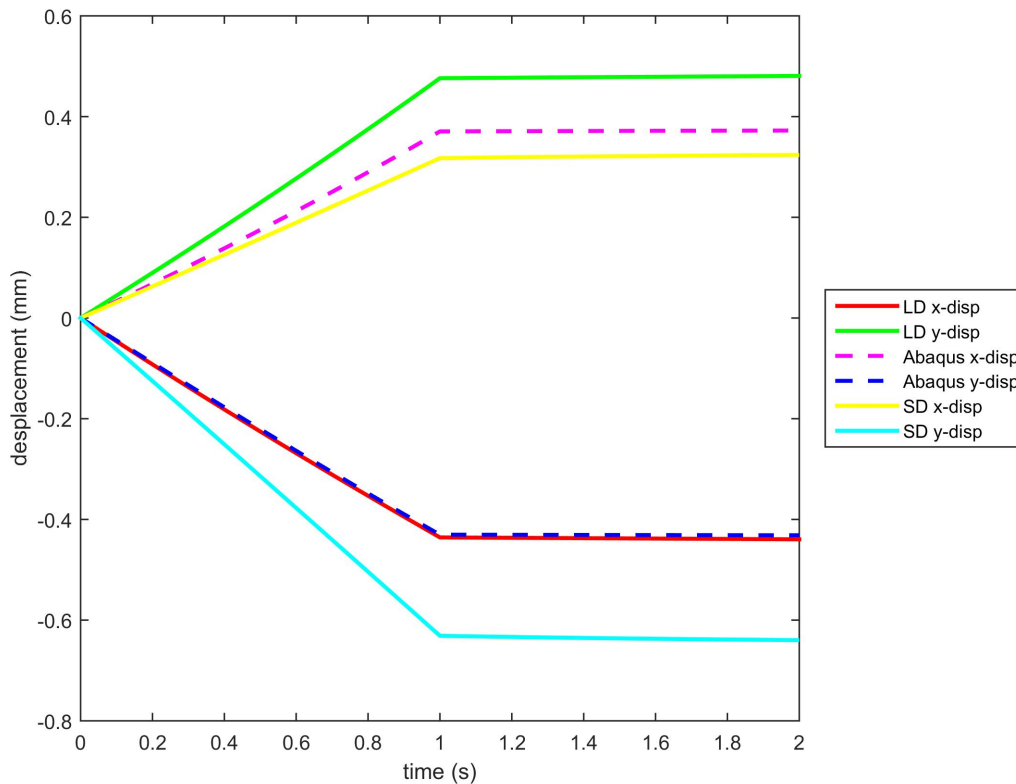
Figure 6.8: The predicted x and y displacement of the top-right node of the biphasic simulation for the large deformation(LD) matlab, small deformation (SD) Matlab, and Abaqus simulations. Note the x-displacements do not match due to the 3-d nature of the Abaqus simulation.

6.8.3 Biphasic TPM Material Model Verification

To verify the biphasic poromechanics of the material including heat transfer a test was run consisting of a 3 mm x 3 mm porous solid skeleton (Fig. 6.9). The pore space was considered to be filled solely with water. A traction of 1.2 MPa was applied to the top surface, ramping over 1 s, after the maximum applied traction was reached, the top boundary temperature was then linearly ramped to 170°C over the 1 s, the temperature and traction were then held for an additional 1 s. All surfaces except the right edge are considered impermeable with the right edge pore pressure set to that of the ambient surroundings. The bottom and left edges are fixed in the y and x directions, respectively, and a free convective heat

flux boundary condition was implemented on the right boundary. This problem was then simulated using the large and small deformation Matlab codes as well as Abaqus (with non-linear geometry on). Table 6.2 lists all of the material properties used for the test. Although the temperature reached above boiling point, a phase change of the pore fluid was not included as the capabilities of Abaqus to conduct TPM analysis are limited (bilinear 3-d elements are the only type available).
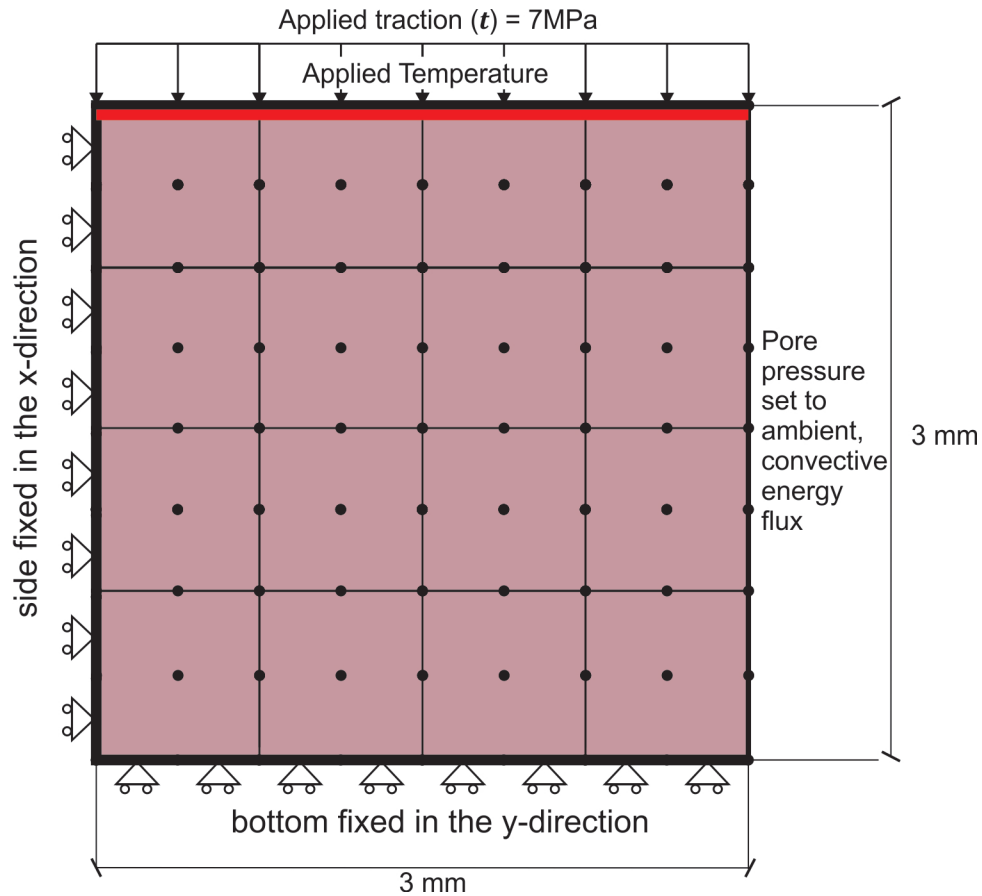
Figure 6.9: The first simulation run to test the biphasic portion of the custom written Matlab code. A traction (t) of 1.2 MPa is applied to a porous section of tissue. The bottom edge is fixed in the y-direction and the left edge fixed in the x-direction. The top, left, and bottom sides are set to be impermeable while along the right edge the pore pressure is set to the ambient pressure and a free convection boundary condition is applied.

	Material Property	Value	Description
Solid Skelton Structure	E	5 MPa	Linear Elastic Young's Modulus
	ν^{skel}	0.3	Poisson's Ratio
Thermal Constants	α_s	2.5x10^{-4} K^{-1}	Solid Thermal Expansion Coefficient
	β_s^θ	3*α_s	Solid Volumetric Thermal Expansion Coefficient
	β_ℓ^θ	4.0x10^{-4} K^{-1}	Water Volumetric Thermal Exp. Coefficient
	C_p^s	145.83 J/(kg K)	Specific Heat of Solid
	C_p^ℓ	4179 J(kg K)	Specific Heat of Liquid Water
	k_t^s	0.5 W/(m K)	Thermal Conductivity of Solid
	k_t^ℓ	0.6 W/(m K)	Thermal Conductivity of Liquid Water
	h_t	25 W/(m^2 K)	Convective Heat Transfer Coefficient
	θ_{amb}	25°C = 298K	Ambient Temperature
Densities	ρ^{sR}	1050 (kg/m^3)	Real Density of Solid
	$\rho^{\ell R}$	1000/(1+4$\beta_\ell^\theta\theta$)	Real Density of Water
Mass Transport Constants	$k_{o_{int}}^\ell$	5x10^{-12} mm^2	Intrinsic Permeability of Liquid Water
	$k_{o_{rel}}^\ell$	Kozemy-Carman Eq.	Relative Permeability of Water
	μ_ℓ	5.5x10^{-10} MPa*s	Viscosity of Liquid Water
	p_{amb}	1.01x10^5 Pa	Ambient Pressure
Initial Conditions and Model Parameters	p_{g_o}	1.01x10^5 Pa	Initial Water Vapor Pressure
	n_o	0.78	Initial Porosity
	p_{ℓ_o}	1.01x10^5 Pa	Initial Liquid Water Pressure
	θ_{amb}	37 °C = 310K	Initial Ambient Temperature
	S_{ℓ_o}	0.99	Initial Liquid Water Saturation
	θ_{app}	$t\begin{cases} = \dfrac{t}{.5}*(\theta_{max}-37)t. \, t < 1 \\ = \theta_{max}, t > 2 \end{cases}$	Applied Temperature
	θ_{max}	170°C	Maximum Jaw Temperature
	t	1.2x10^6 Pa	Applied Traction
	T	3 s	Total Time
	dt_0	0.0001 (s)	Initial Time Step

Table 6.2: Material Properties for the Biphasic TPM Test Simulation

The deformations and internal pore pressures between the Abaqus and large deformation Matlab simulations were not significantly different from those seen in the biphasic test (Fig. 6.8). Figure 6.10 shows the predicted temperature at 3 s for the large deformation biphasic simulations.
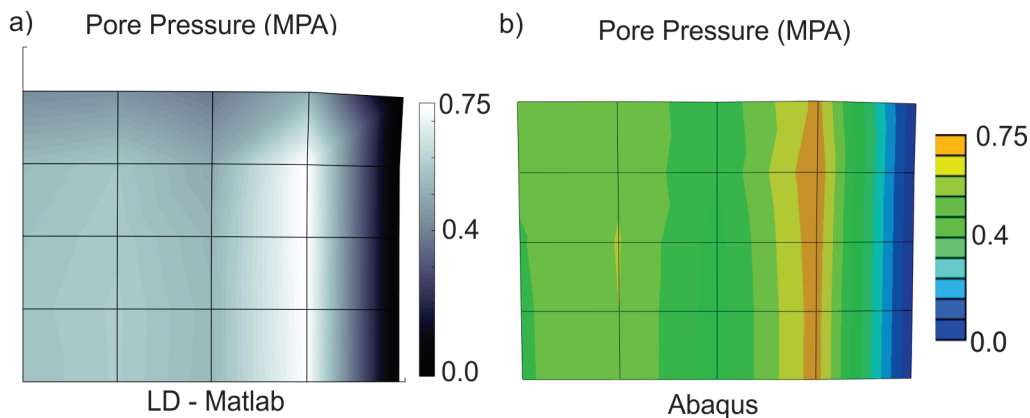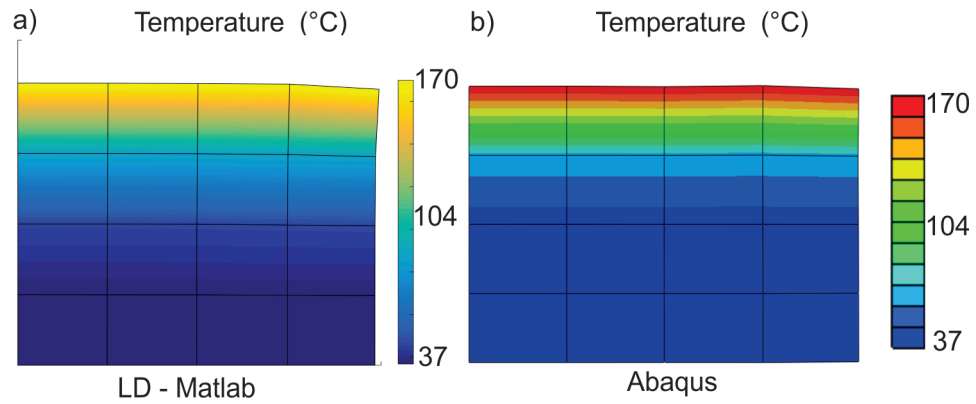
Figure 6.10: The predicted temperature throughout the tissue at the end of a 1.2 MPa, 3 s simulation in the large deformation matlab code (left) and by Abaqus (right).

Chapter 7: Simulating Arterial Tissue Fusion with a Large Deformation Thermo-poromechanics Finite Element Model

Now that Chapters 5 and 6 have established a large deformation TPM finite element model this chapter will make use of that model to simulate the tissue fusion process. The ability to provide surgeons and medical device designers with accurate simulations of the tissue fusion process would provide invaluable insight into the physics of tissue fusion, leading to safer more effective fusion devices and potentially aiding in ground breaking medical procedures such as tissue anastamosis.

As seen in experimental results presented in Chapter 4, tissue undergoes large deformations during the tissue fusion process. Thus, to accurately model tissue fusion a large deformation finite element model must be used. This chapter first presents the tissue fusion model setup and the simulations run using the large deformation TPM model. It then presents the results of these simulations and demonstrates their ability to predict the final temperature and water content of the tissue to within one standard deviation of the experimental results. Lastly, it demonstrates the ability to predict the deformation of the tissue to within 5% of measured experimental results, showing improvement over the small deformation TPM model.

7.1   Tissue Fusion Simulations

The large deformation tissue fusion simulations conducted follow those laid out in Chapter 4. The geometry and overview of the simulations is presented again here for completeness.

A quarter symmetry, two dimensional section of tissue is used to represent a flattened (not yet compressed) piece of tissue clamped within the jaws of a Conmed Altrus tissue fusion device (Figs. 7.1 and 7.2).
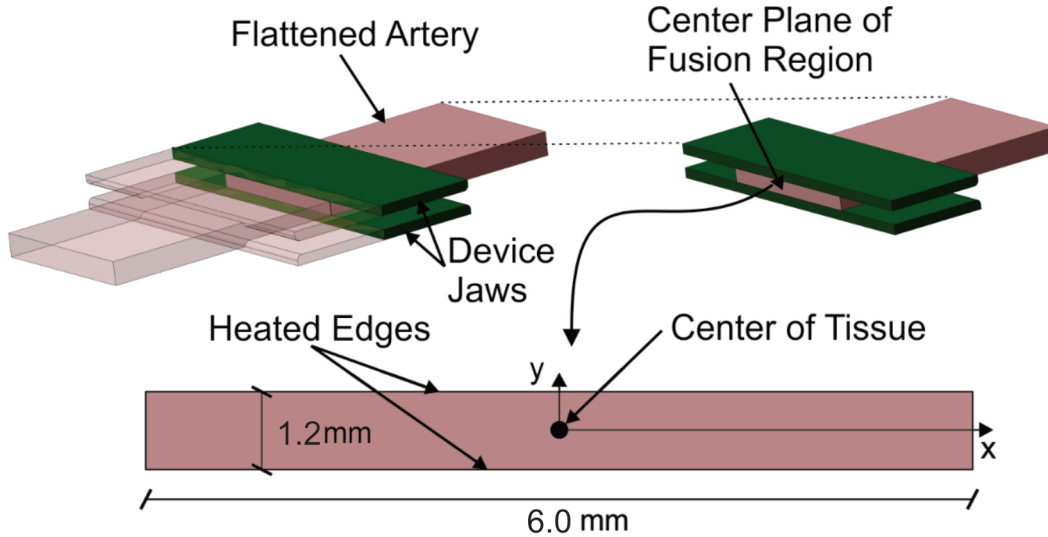
Figure 7.1: Depiction of the tissue clamped within the Conmed Altrus jaws and the 2-D plane to be simulated.

7.1.1 Boundary Conditions

Three different temperature boundary conditions exist within the thermal tissue fusion FE model. The first is the symmetric boundary condition, which sets the heat flux, $\boldsymbol{q}_\theta$, through the surface equal to 0, (*i.e.* adiabatic),

$$q_\theta = \boldsymbol{q}_\theta \cdot \boldsymbol{n} = 0 \quad on \quad \partial B_\theta^{free}. \tag{7.1}$$

The second thermal boundary condition is a prescribed temperature boundary condition representing the temperature of the jaws, θ^{fixed},

$$\theta(t) = \theta^{fixed}(t) \quad on \quad \partial B_\theta^{fixed}. \tag{7.2}$$

Lastly, on all free edges, free convection is expected to occur. Thus, the normal heat flux, q_θ, is specified as,

$$q_\theta = h_t(\theta - \theta_{amb}) \quad on \quad \partial B_\theta^{free} \tag{7.3}$$

where h_t is the heat transfer coefficient and θ_{amb} is the ambient temperature. Two water species boundary conditions are implemented. The first is an impermeable or symmetric boundary condition preventing flow though the boundary.

$$q_\ell = q_g = 0. \tag{7.4}$$

The second boundary condition consists of fluid flux on the right boundary, this is the a function of the permeability of the tissue and the difference between internal pore fluid pressure and the ambient fluid pressure, p_{amb},

$$q_f = -\frac{k_{rel}^f k_{int}^f}{\mu^f} \rho^{\alpha R} S_f (p_f - p_{amb}) A \quad for \quad \ell, g \quad on \quad \partial B_p^{free}. \tag{7.5}$$

The last boundary conditions are an applied traction, $\boldsymbol{t}$, and a symmetric boundary condition fixing displacements,

$$\boldsymbol{u} \cdot \boldsymbol{n} = 0 \quad on \quad \partial B_u^{fixed}. \tag{7.6}$$

7.1.2 Material Properties

The majority of material properties were found either in literature or were experimentally measured in the lab. Often, material properties specific to the artery wall were not able to be found or a wide range of properties was found. In these cases properties of tissue most similar in composition to the artery wall were used. To determine the structural mechanical properties for the Neo-Hookean constitutive model (E, ν) a nonlinear regression analysis was first used to get a "ballpark" value of these properties, they were then adjusted manually until

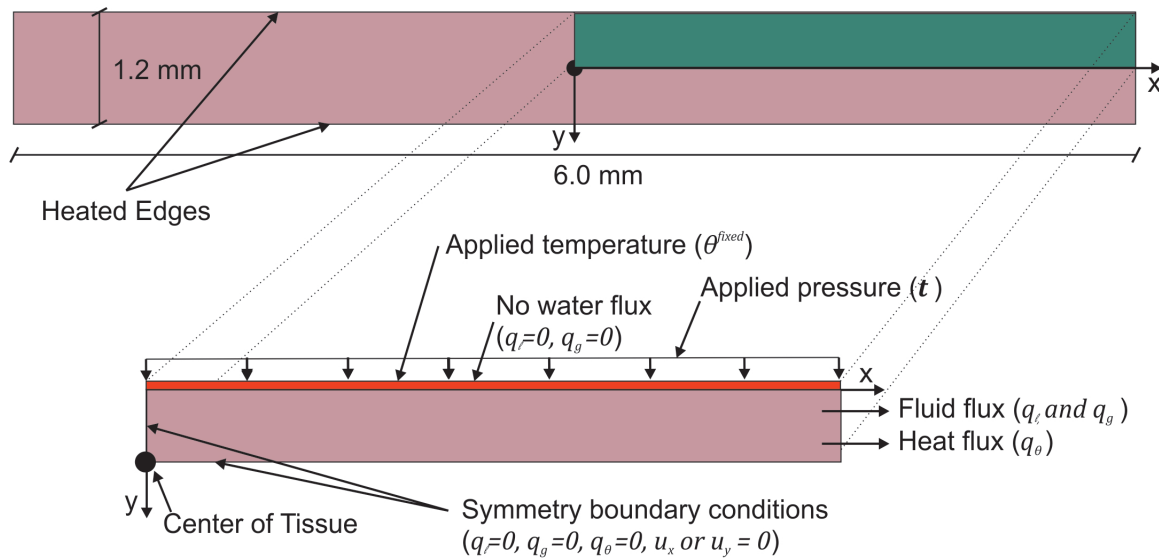Figure 7.2: The quarter-symmetry section of tissue and applied boundary conditions. The device jaws apply temperature and pressure to the top. Symmetry boundary conditions are applied to the bottom and left edges. Heat and water are allowed to flow through the right edge.

a best fit was found. A summary of all material properties, initial condition and boundary condition values used in the simulations are included in Table 7.1.

	Material Property	Value	Description
Universal Constants	R	8.314 N*m/mol K	Ideal Gas Constant
	M_m	0.018 kg/mol	Molar Mass of Water
Solid Skelton Structure	E	1.6 MPa	Linear Elastic Young's Modulus
	ν^{skel}	0.2	Poisson's Ratio
Thermal Constants	α_s	2.5x10⁻⁴ K⁻¹	Solid Thermal Expansion Coefficient
	β_s^θ	3*α_s	Solid Volumetric Thermal Expansion Coefficient
	β_ℓ^θ	4.0x10⁻⁴ K⁻¹	Water Volumetric Thermal Exp. Coefficient
	C_p^s	145.83 J/(kg K)	Specific Heat of Solid
	C_p^ℓ	4179 J(kg K)	Specific Heat of Liquid Water
	C_p^g	1850 J/(kg K)	Specific Heat of Water Vapor
	k_t^s	0.5 W/(m K)	Thermal Conductivity of Solid
	k_t^ℓ	0.6 W/(m K)	Thermal Conductivity of Liquid Water
	k_t^g	0.025 W/(m K)	Thermal Conductivity of Water Vapor
	H_{vap}	2.264x10⁶ J/kg	Latent Heat of Vaporization of Water
	h_t	25 W/(m² K)	Convective Heat Transfer Coefficient
	θ_{amb}	25°C = 298K	Ambient Temperature
Densities	ρ^{sR}	1050 (kg/m³)	Real Density of Solid
	$\rho^{\ell R}$	1000/(1+4$\beta_\ell^\theta \theta$)	Real Density of Water
	ρ^{gR}	Ideal Gas	
Mass Transport Constants	$k_{o\,int}^\ell$	5x10⁻¹⁴ m²	Intrinsic Permeability of Liquid Water
	$k_{o\,rel}^\ell$	Kozemy-Carman Eq.	Relative Permeability of Water
	k_{int}^g	10x10⁻¹⁴ m²	Intrinsic Permeability of Water Vapor
	k_{rel}^g	Kozemy-Carman Eq.	Relative Permeability of Water
	μ_ℓ	5.5x10⁻⁴ Pa*s	Viscosity of Liquid Water
	μ_g	1.8x10⁻⁵ Pa*s	Viscosity of Water Vapor
	n_{vg}	1.8	Constant for Clausius-Clapeyron
	a	19.4x10³ Pa	Constant for Clausius-Clapeyron
	S_r	0.3	Constant for Clausius-Clapeyron
	p_{amb}	1.01x10⁵ Pa	Ambient Pressure
Initial Conditions and Model Parameters	p_{g_o}	1.01x10⁵ Pa	Initial Water Vapor Pressure
	n_o	0.78	Initial Porosity
	p_{ℓ_o}	1.01x10⁵ Pa	Initial Liquid Water Pressure
	θ_{amb}	37 °C = 310K	Initial Ambient Temperature
	S_{ℓ_o}	0.99	Initial Liquid Water Saturation
	θ_{app}	$\begin{cases} = (\theta_{max}-37)t, t<2 \\ = \theta_{max}, t>3 \end{cases}$	Applied Temperature
	θ_{max}	Varies	Maximum Jaw Temperature
	t	2.7x10⁶ Pa	Applied Traction
	T	5 s	Total Time
	dt_0	0.0001 (s)	Initial Time Step

Table 7.1: Material Properties for the Tissue Fusion Simulations

7.1.3 Simulations Run

Seven different simulations were run attempting to predict experimental results of tissue displacement, water content, and temperature. Each simulation was run for 5 s (the same time period as the experiments), with the traction (matching that of experimentally measured loads) compressing the tissue applied over the first 2 seconds. A ramping temperature boundary condition was then applied over for the next second (θ_{max} varied from 120°C to 200 °C) with the traction held constant. Finally, the traction and temperature were held for the final 2 seconds of the simulations. Mesh sensitivity studies were conducted, by running a simulation, halving the mesh size, rerunning the simulation and comparing solution vectors. This was to be done until the solution vectors differed by 0.05 mm x 0.1 mm. A variable time stepping scheme was used, at any time step if the model failed to converge in 34 iterations, the time step was halved and attempted again. To keep computational times reasonable a a minimum time step of $1x10^-5$ s was used. Once the simulations were complete the results were compared with experimental results and the small deformation TPM finite element simulations.

7.2 Results

Figure 7.3 displays the final simulation temperature profile within the tissue ($\theta_{max} = 170°C$, $t_{max} = 5s$, $S_r = 0.3$) and the comparison of the temperature at the center of the tissue with published results [15] and the small deformation model results. The results for both small and large deformation simulate final temperatures fall within one standard deviation of the measured experimental results and fall within 1% of each other. Figure 7.4 shows the water content throughout the tissue at the end of a simulation ($\theta_{max} = 170°C, t_{max} = 5s, S_r = 0.3$) and compares them against the results shown in Chapter 4. The water content falls within one standard deviation of the mean measured experimental results for both the small and large deformation simulations. Again, the small and large deformation simulations predicted

water content fall within 5% of each other.
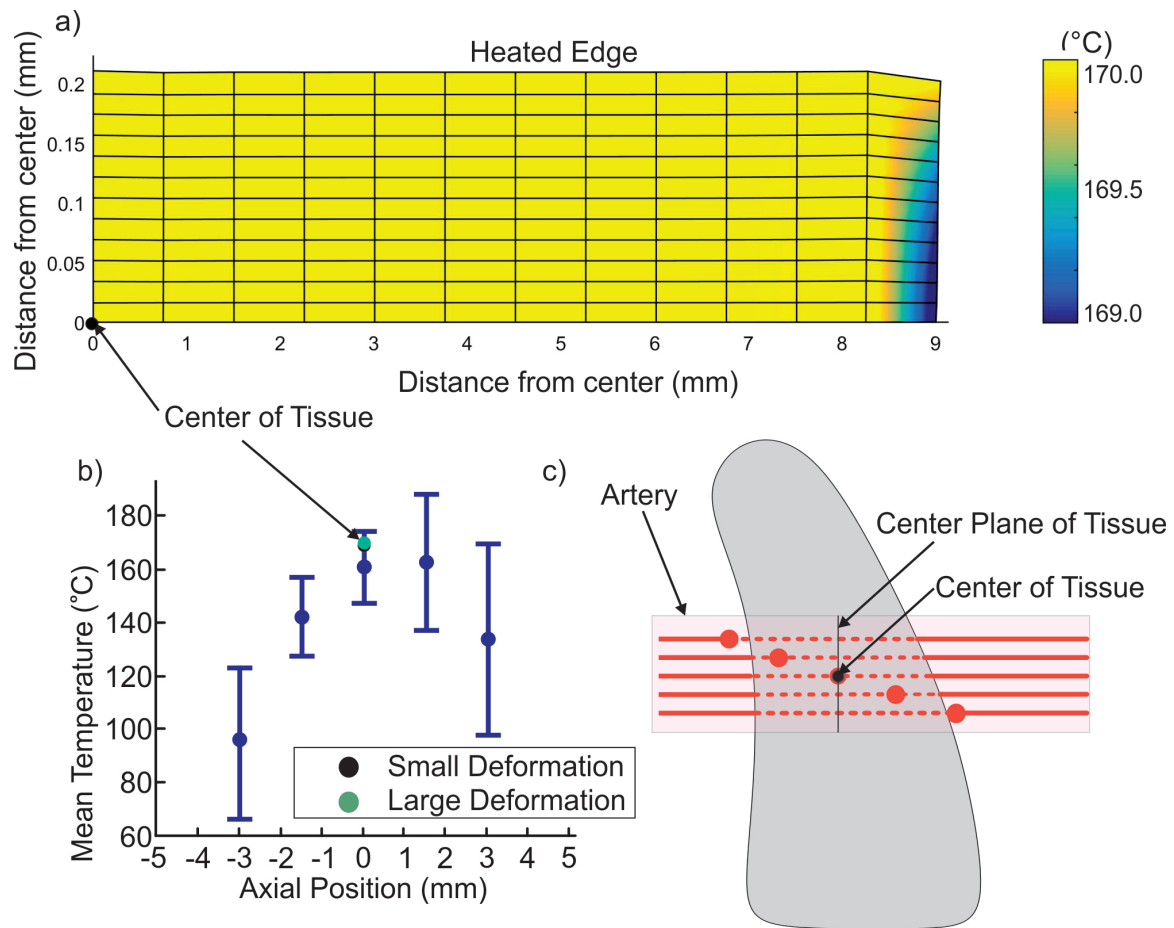
Figure 7.3: a) The temperature (°C) within the tissue for and applied temperature of 170°C and $S_r = 0.3$ at the end of 5 s for the large deformation model. b,c) The temperature at the center of the tissue predicted by small and large deformation models. Notice, there is almost no predicted difference.
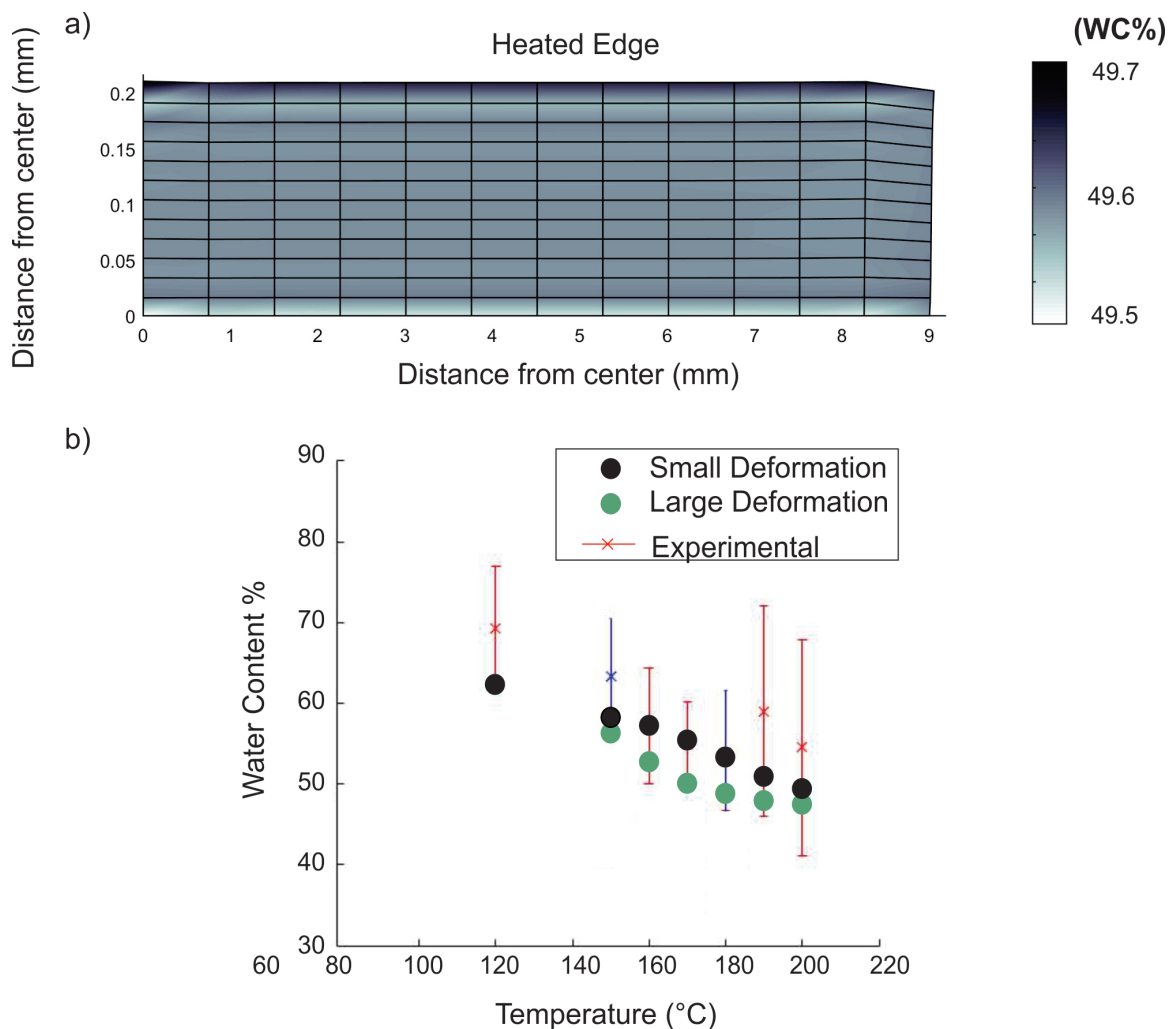
Figure 7.4: a) The water content within the tissue for and applied temperature of 170°C and $S_r = 0.3$ at the end of 5 s for the large deformation model. b,c) The water content predicted at the end of each temperature simulation for both small and large deformation models. Notice the water content is slightly less than in the large deformation model.

Figure 7.5 compares the measured applied traction-displacement curves in the y-direction of tissue before the temperature was applied (t = 0-2 s) for the elastic small deformation models, the large deformation model and experimental results. The large deformation model was better able to capture the geometric effects and had a mean square error of 0.12. Additionally, when the simulations were run with the same mesh size, the large deformation simulation took roughly 5 times longer to run.

Figure 7.6 compares the simulated tissue deformation of the top of the tissue for the large
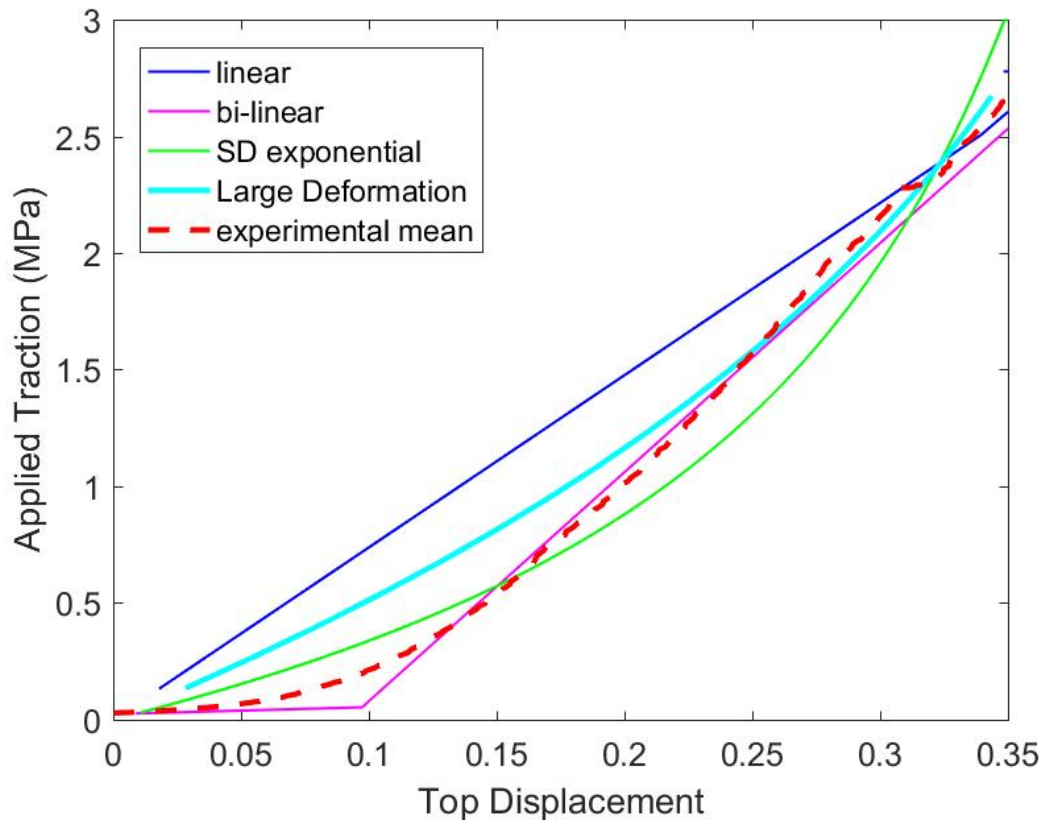
Figure 7.5: The average recorded applied traction -displacement curve for 8-porcine arteries compared to the simulated displacement curves of a small deformation porous bi-linear elastic and large deformation porous Neo-Hookean model.

deformation model and the small deformation linear elastic, bi-linear elastic and exponential elastic to experimentally measured results. All simulations were able to match within 15% the measured experimental results. The large deformation model doing so within 5% of the final results.

7.3   Discussion

This chapter applies the large deformation thermo-poromechanics theory and models shown in Chapters 5 and 6 to simulate direct heat tissue fusion. The simulations compute the fluid transport, thermal transport, and deformation occurring within the artery wall during the
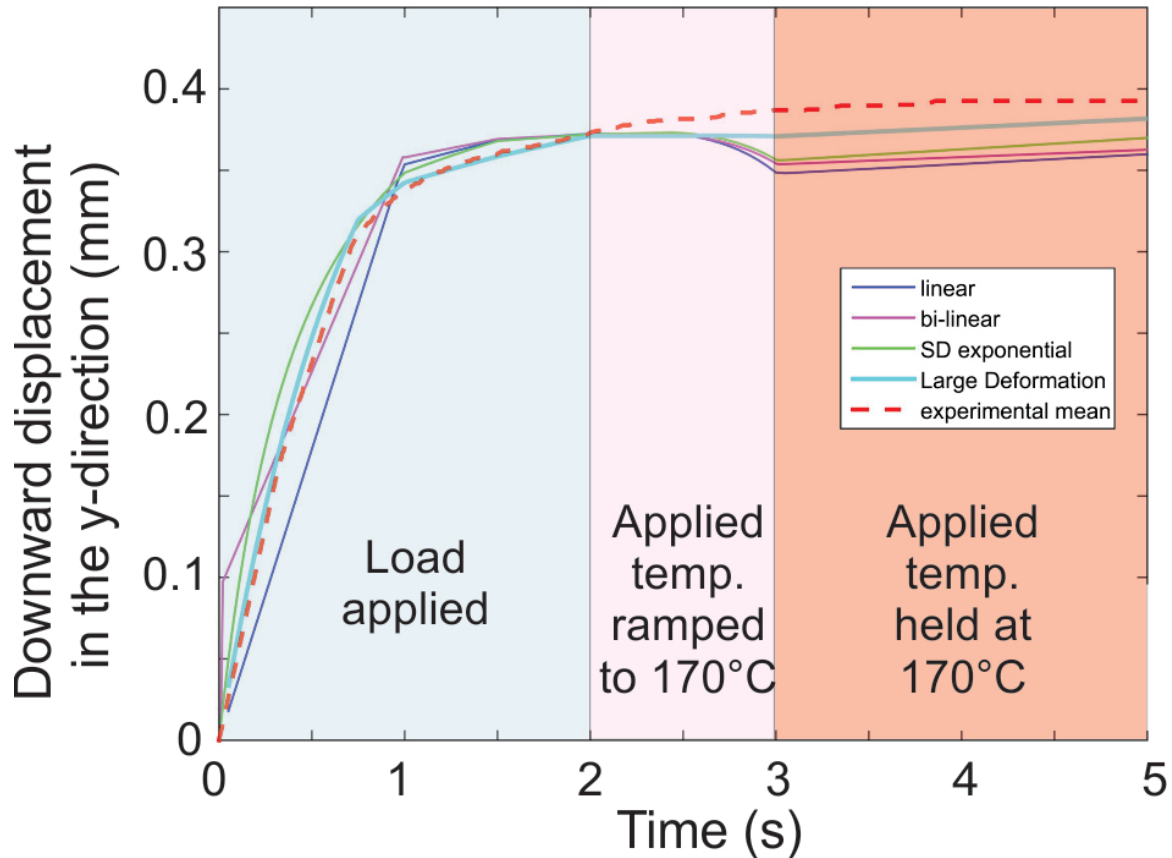
Figure 7.6: The average measured displacement (standard deviation of 0.033) for the 8 fused porcine arteries and the predicted displacement for a small deformation porous linear elastic, bi-linear elastic, exponential elastic and a large deformation Neo-Hookean model during mechanical loading (0-2 s), while heated up to an applied temperature of 170 °C (2-3 s) and at a constant applied temperature of 170 °(4-5 s).

tissue fusion problem. The results of the direct heat tissue fusion problem are able to predict final tissue temperature and water content to within one standard deviation of measured experimental results and final tissue deformation to with 5% of the final measured experimental results. The large deformation model shows improvement over the small deformation model in predicting the displacement of the tissue as it is able to account for non-linear geometric effects.

7.3.1 Temperature

As seen in Figure 7.3 the large deformation simulation and the small deformation simulation predict the final temperature to within one standard deviation of the final results. The predicted temperature at 5 s is 6°C higher than the measured temperature for both simulations, a discrepancy caused by the assumption of perfect thermal conduction. It should be noted that taking into account non-linear geometric effects resulted in a slightly higher temperature at the edge of the tissue. This is likely because the final deformed area of the convection surface is about 1/3 smaller at the end of the large deformation simulation than at the end of the small deformation simulation.

7.3.2 Water Content

Each of the seven simulations run for all values of the average tissue water content fall within one standard deviation of the mean measured experimental values. The large deformation simulations predict a slightly lower water content than that predicted by the small deformation model. This is likely due to the fact the large deformation model takes into account the changing area the fluid is allowed to flow out of and that it more accurately takes into account volumetric and geometric changes. While the results are slightly different between the small and large deformation models, they do not differ nearly as significantly as the final water content results do when the residual degree of saturation (S_r) is changed as seen in Chapter 4. This again provides strong evidence in measuring the exact values of these parameters experimentally. Additionally, experimental results are only available for the beginning and end of the tissue fusion process. Thus, to verify the flow of fluid seen during the fusion process, additional experiments measuring water content in real time are necessary and would provide valuable insight into the physics of the fusion process.

7.3.3 Deformation

The largest difference between the large and small deformation models can be seen in the predicted tissue displacement of each simulation. Though the bi-linear and exponential elastic models are able to predict the tissue deformation to within 15%. They lack the ability to account for non-linear geometric effects. The large deformation model has no such limitations and is therefore able to better capture the final tissue deformation. While the simulation nearly matches the experimental results for the first 2.0 s, it still only manages to capture the top displacement to within 5% of the final measured displacement. This is likely due to several assumptions. First, the permeability of the tissue is assumed to be only a function of the change in volume and saturation of the pore space. It does not take into account any damage that may be occurring within the tissue allowing for greater pore fluid flow. Again, the need for accurately measured material properties presents itself again. Despite these limitations the model still managed to predict tissue deformation well, providing valuable information to those trying to improve and expand the tissue fusion process.

7.3.4 Conclusion

Finally, a novel method for modeling the physics occurring during the thermal tissue fusion process has been presented in this chapter. The large deformation TPM FE model developed in Chapters 5 and 6 was used to predict the final tissue temperature and water content to within a standard deviation and the final deformation to within 5% of measured experimental results. In this study, the model showed what may be construed as incremental improvements over using a small deformation TPM FE model. However, the geometry simulated here does not enable the large deformation TPM model to display its full capabilities. As the desire for modeling exact surgical procedures (such as simulating a full 3-d tube as the artery) becomes more prevalent, the ability to take into account not only large strains, but also large rotations

becomes essential. Thus, the large deformation simulations presented in this work provide an essential step to achieving this goal and ultimately provide a necessary building block for all encompassing predictive surgical models.

Chapter 8: Discussion

Imagine, for a moment, a world where a surgeon visits with a patient, inputs some parameters into a simulation program and presses enter. Quickly, on the screen a simulation of the surgical procedure appears, and the program tunes the surgical tools to the optimal settings, allowing for the surgeon to efficiently and effectively perform the best possible surgery. While this vision may be many years in the future, the groundwork must be laid now. To accomplish this goal of real-time, patient specific surgeries, in depth, multiphase models representing the physics occurring within biological tissue are necessary.

This work presents two models to aid in the advancement of this goal. The first is a thermo-mechanical damage finite element model that demonstrates the ability to predict arterial cutting with a laparoscopic tissue fusion device. The second is a fully coupled triphasic thermo-poromechanics finite element model that demonstrates the ability to predict arterial tissue temperature, water content and deformation during the tissue fusion process.

8.1 Aim 1 - Modeling Tissue Cutting

The work presented in this thesis was done to attack a void in the multiphysical modeling of biological tissue, in particular the fusion and cutting of arterial tissue with laparoscopic fusion devices. Chapter 3 attempts to fill this void by providing, to the author's knowledge, the first thermo-mechanical model of the arterial fusion and cutting process. Once the ability to determine the structural and thermal state of the tissue under different loading conditions was demonstrated, experimental work needed to be conducted to determine the conditions (isochoric strain energy and temperature) at which an artery is cut.

From this experimental work a novel damage parameter was then developed and implemented via the finite element method. This parameter displayed the ability to predict cutting outcomes with an 83% success rate, but was limited by its empirical nature. Still, the work presented in Chapter 3 provides a valuable thermo-mechanical FE model of tissue fusion and cutting, insight into the internal tissue conditions at which an artery is cut, and a method for evaluating tissue fusion device design; thus, providing a valuable tool for aiding the development of safer more effective devices.

8.2   Aim 2 - Small Deformation Thermo-poromechanics Modeling

While Aim 1 (Chap. 3) provided important insight into the internal tissue conditions, it also shed light on the limitations of treating biological tissue as a homogeneous material. As arterial tissue, like most biological tissue, consists of an extracellular matrix and internal water, modeling the true internal physics of the tissue fusion process requires a multiphysics approach. During the tissue fusion process water inside the tissue is heated, vaporized and pushed out of the tissue. To represent this, Chapter 4 presents a small deformation triphasic thermo-poromechanics theory and its implementation using the finite element method.

The TPM finite element model solves the balance of mass, balance of linear momentum and balance of energy equations to provide the tissue water content, liquid and gas pore pressures, fluid fluxes, temperature, and deformation. When used to simulate the tissue fusion process the model demonstrated an ability to predict arterial tissue water content and temperature to within one standard deviation of measured experimental results. Additionally, despite its small deformation limitation, the model predicted final tissue deformation to within 15% of measured experimental results. The ability to quickly and accurately predict tissue conditions has potential to be a valuable tool in applications where a quick, reasonably accurate, estimate of tissue response is useful, such as needed when autonomously controlling

surgical robots [131].

8.3   Aim 3 - Large deformation Thermo-poromechanics Modeling

While Chapter 4 solved the problem of treating biological tissue as a porous media, it still failed to account for the large deformations occurring during the tissue fusion process. Chapters 5, 6, and 7 attempt to address this issue. Chapter 5 starts from first principles to extend the small deformation TPM theory of Chapter 4 to a fully coupled large deformation TPM theory. The linearization of this theory and its implementation in a custom written finite element code is then presented in Chapter 6. Lastly, Chapter 7 displays this FE model's capability to simulate the tissue fusion process.

The large deformation FE model, as did the small deformation model, demonstrated the ability to predict the final temperature and water content in the tissue to within one standard deviation of the mean of experimental results. The true value of the large deformation model is displayed by its ability to simulate the tissue deformation to within 5% of measured experimental results. To the author's knowledge this is the first implementation and application of a fully coupled large deformation unsaturated TPM finite element model.

8.4   Implications on Future Research

Porous media undergoes thermal and mechanical loading in a wide variety of situations. These include the deformation of soil near geothermal sources [28], [104], biological tissue when exposed to surgical devices or natural thermal sources [29] and porous high explosives [133]. During all of these situations large deformations of the porous medium can occur, yet models incorporating this large deformation theory are significantly lacking in modern

literature. The large deformation thermo-poromechanics model presented in this thesis attacks this void in the literature. Providing a platform for which simulation efforts in the previously mentioned fields can be based.

While the model presented here provides the foundation for these large deformation TPM modeling efforts, several points of necessary advancement are apparent. First, currently the model has only been implemented in a 2-d finite element code and has only been verified for conditions close to those seen during the tissue fusion process. To provide true value to the scientific community, this 2-d FE code needs to be implemented in 3-d, verified for a broad spectrum of conditions and optimized. Only once this is accomplished can the goal of predicting full surgical procedures be realized.

It addition to this work, a good deal of complimentary experimental/theoretical work needs to be done to provide the correct material parameters and constitutive theories to the model. Part of the beauty of the large deformation theory is that the deformation gradient ($\boldsymbol{F}$) of the smeared medium is directly calculated, thus, the door is open to a great range of solid skeleton constitutive models. Adding these models to the TPM theory would greatly improve the model's ability to represent a wide variety of materials. Lastly, as seen in Chapters 4-7, more accurate constitutive models relating the porosity, saturation, and permeability are needed. These often prove challenging to measure experimentally; therefore, literature is limited in provided accurate values for these parameters. A combined theoretical-experimental effort would be invaluable in providing accurate constitutive models.

Examining the broader picture, the efforts presented in this thesis provide a first step towards complete, accurate, multi-physical modeling of porous media. While a great deal of work still needs to be done, with ever increasing computational and experimental capabilities, it is not impossible to imagine a world where full direct simulations of specific surgeries are conducted regularly.

Bibliography

[1]   J. Breasted, *The edwin smith surgical papyrus*, 1930.

[2]   S. Paget, *Ambroise par and his times: 1510-1590*. G.P. Putnam's Sons, 1897, 404 pp.

[3]   S. G. Farah, D. T. Azar, C. Gurdal, and J. Wong, "Laser in situ keratomileusis: Literature review of a developing technique," *Journal of Cataract & Refractive Surgery*, vol. 24, no. 7, pp. 989–1006, Jul. 1998.

[4]   H. Lubatschowski, A. Heisterkamp, F. Will, J. Serbin, T. Bauer, C. Fallnich, H. Welling, W. Mueller, B. Schwab, A. I. Singh, and W. Ertmer, "Ultrafast laser pulses for medical applications," vol. 4633, 2002, pp. 38–49.

[5]   S. Dessole, G. Rubattu, G. Capobianco, S. Caredda, and P. L. Cherchi, "Utility of bipolar electrocautery scissors for abdominal hysterectomy," *American Journal of Obstetrics and Gynecology*, vol. 183, no. 2, pp. 396–399, Aug. 2000.

[6]   J. A. Rand and T. A. Gaffey, "Effect of electrocautery on fresh human articular cartilage," *Arthroscopy: The Journal of Arthroscopic & Related Surgery: Official Publication of the Arthroscopy Association of North America and the International Arthroscopy Association*, vol. 1, no. 4, pp. 242–246, 1985.

[7]   I. A. Chang and U. D. Nguyen, "Thermal modeling of lesion growth with radiofrequency ablation devices," *Biomedical engineering online*, vol. 3, no. 1, p. 27, 2004.

[8]   S. R and P. R, "The role of vessel sealing technologies in laparoscopic surgery.," *Surgical technology international*, vol. 17, pp. 208–212, Dec. 2007.

[9]   T. C. Gasser, C. A. J. Schulze-Bauer, and G. A. Holzapfel, "A three-dimensional finite element model for arterial clamping," *Journal of Biomechanical Engineering*, vol. 124, no. 4, pp. 355–363, Jul. 30, 2002.

[10] K. Entezari, P. Hoffmann, M. Goris, A. Peltier, and R. Van Velthoven, "A review of currently available vessel sealing systems," *Minimally Invasive Therapy & Allied Technologies*, vol. 16, no. 1, pp. 52–57, Jan. 1, 2007.

[11] J. Landman, K. Kerbl, J. Rehman, C. Andreoni, P. A. Humphrey, W. Collyer, E. Olweny, C. Sundaram, and R. V. Clayman, "Evaluation of a vessel sealing system, bipolar electrosurgery, harmonic scalpel, titanium clips, endoscopic gastrointestinal anastomosis vascular staples and sutures for arterial and venous ligation in a porcine model," *The Journal of Urology*, vol. 169, no. 2, pp. 697–700, Feb. 2003.

[12] J. S. Kennedy, P. L. Stranahan, K. D. Taylor, and J. G. Chandler, "High-burst-strength, feedback-controlled bipolar vessel sealing," *Surgical endoscopy*, vol. 12, no. 6, pp. 876–878, 1998.

[13] R. F. Sing, B. T. Heniford, K. L. Harold, H. Pollinger, B. D. Matthews, and K. W. Kercher, "Comparison of ultrasonic energy, bipolar thermal energy, and vascular clips for the hemostasis of small-, medium-, and large-sized arteries," *Surgical Endoscopy*, vol. 17, no. 8, pp. 1228–1230, Aug. 1, 2003.

[14] L. S. Bass and M. R. Treat, "Laser tissue welding: A comprehensive review of current and future clinical applications," *Lasers in Surgery and Medicine*, vol. 17, no. 4, pp. 315–349, 1995, WOS:A1995TL19300001.

[15] J. D. Cezo, E. Kramer, K. D. Taylor, V. Ferguson, and M. E. Rentschler, "Temperature measurement methods during direct heat arterial tissue fusion," *IEEE Transactions on Biomedical Engineering*, vol. 60, no. 9, pp. 2552–2558, Sep. 2013.

[16] D. P. Fankell, E. Kramer, J. Cezo, K. D. Taylor, V. L. Ferguson, and M. E. Rentschler, "A novel parameter for predicting arterial fusion and cutting in finite element models," *Annals of Biomedical Engineering*, Mar. 16, 2016.

[17] C. W. Wallwiener, T. K. Rajab, W. Zubke, K. B. Isaacson, M. Enderle, D. Schller, and M. Wallwiener, "Thermal conduction, compression, and electrical currentan evaluation of major parameters of electrosurgical vessel sealing in a porcine in vitro model," *Journal of Minimally Invasive Gynecology*, vol. 15, no. 5, pp. 605–610, Sep. 2008.

[18] E. A. Kramer, N. S. Anderson, K. D. Taylor, V. L. Ferguson, and M. E. Rentschler, "The role of glycosaminoglycans in tissue adhesion during energy-based vessel sealing," vol. 9326, 2015, 93260B–93260B–6.

[19] J. Cezo, E. Kramer, K. Taylor, V. Ferguson, and M. Rentschler, "Tissue fusion bursting pressure and the role of tissue water content," in *Proceedings of the SPIE - The International Society for Optical Engineering*, ser. Proc. SPIE, Int. Soc. Opt. Eng. (USA), vol. 8584, SPIE - The International Society for Optical Engineering, 2013, pp. 85840M–85840M–9.

[20] J. D. Humphrey, *Cardiovascular solid mechanics: Cells, tissues, and organs*, J. D. Humphrey, Ed. Humphrey, Jay D.; Department of Biomedical Engineering, Texas A and M University, College Station, TX, 77843-3120, USA, 2002.

[21] M. H. Holmes and V. C. Mow, "The nonlinear characteristics of soft gels and hydrated connective tissues in ultrafiltration," *Journal of Biomechanics*, vol. 23, no. 11, pp. 1145–1156, 1990.

[22] N. Karajan, "Multiphasic intervertebral disc mechanics: Theory and application," *Arch Computat Methods Eng*, vol. 19, no. 2, pp. 261–339, May 2012.

[23] C. W. J. Oomens, D. H. van Campen, and H. J. Grootenboer, "A mixture approach to the mechanics of skin," *Journal of Biomechanics*, vol. 20, no. 9, pp. 877–885, 1987.

[24] S. L. Butler, S. S. Kohles, R. J. Thielke, C. Chen, and D. R. V. Jr, "Interstitial fluid flow in tendons or ligaments: A porous medium finite element simulation," *Medical and Biological Engineering and Computing*, vol. 35, no. 6, pp. 742–746, Nov. 1997.

[25] O. Amft and P. Lukowicz, "From backpacks to smartphones: Past, present, and future of wearable computers," *IEEE Pervasive Computing*, vol. 8, no. 3, pp. 8–13, Jul. 2009.

[26] K. Bourzac. (). TR10: Implantable electronics, MIT Technology Review.

[27] R. C. G. Martin, C. R. Scoggins, and K. M. McMasters, "Safety and efficacy of microwave ablation of hepatic tumors: A prospective review of a 5-year experience," *Annals of Surgical Oncology*, vol. 17, no. 1, pp. 171–178, Aug. 26, 2009.

[28] W. Sun, "A stabilized finite element formulation for monolithic thermo-hydro-mechanical simulations at finite strain," *International Journal for Numerical Methods in Engineering*, vol. 103, no. 11, pp. 798–839, Sep. 14, 2015.

[29] A. K. Datta and V. Rakesh, *An introduction to modeling of transport processes: Applications to biomedical systems*, ser. Cambridge texts in biomedical engineering. Cambridge, UK: Cambridge University Press, 2010, 1 online resource (xxviii, 503 pages).

[30] N. T. Wright and J. D. Humphrey, "Denaturation of collagen via heating: An irreversible rate process," *Annual Review of Biomedical Engineering*, vol. 4, pp. 109–128, 2002.

[31] L. W. Murray, L. Su, G. E. Kopchok, and R. A. White, "Crosslinking of extracellular matrix proteins: A preliminary report on a possible mechanism of argon laser welding," *Lasers in Surgery and Medicine*, vol. 9, no. 5, pp. 490–496, 1989.

[32] M. C. Oz, L. S. Bass, H. W. Popp, R. S. Chuck, J. P. Johnson, S. L. Trokel, and M. R. Treat, "In vitro comparison of thulium-holmium-chromium:YAG and argon ion lasers for welding of biliary tissue," *Lasers in Surgery and Medicine*, vol. 9, no. 3, pp. 248–253, Jan. 1, 1989.

[33] J. D. Cezo, E. A. Kramer, J. A. Schoen, V. L. Ferguson, K. D. Taylor, and M. E. Rentschler, "Tissue storage ex vivo significantly increases vascular fusion bursting pressure," *Surgical Endoscopy*, vol. 29, no. 7, pp. 1999–2005, Jul. 2015.

[34] D. C. Auth, "Introduction: Angioplasty with high speed rotary ablation," in *Restenosis after Intervention with New Mechanical Devices*, ser. Developments in Cardiovascular Medicine 131, P. W. Serruys, B. H. Strauss, and S. B. K. III, Eds., DOI: 10.1007/978-94-011-2650-2_17, Springer Netherlands, 1992, pp. 275–288.

[35] B. Majaron, P. Plestenjak, and M. Luka, "Thermo-mechanical laser ablation of soft biological tissue: Modeling the micro-explosions," *Applied Physics B*, vol. 69, no. 1, pp. 71–80, Jul. 1999.

[36] Y. Fung, *Biomechanics. mechanical properties of living tissues*. New York, NY, USA: Springer-Verlag, 1981, xii+433.

[37] Y. C. Fung, K. Fronek, and P. Patitucci, "Pseudoelasticity of arteries and the choice of its mathematical expression," *American Journal of Physiology - Heart and Circulatory Physiology*, vol. 237, no. 5, H620–H631, Nov. 1, 1979.

[38] J. D. Humphrey, "An evaluation of pseudoelastic descriptors used in arterial mechanics," *Journal of Biomechanical Engineering*, vol. 121, no. 2, pp. 259–262, Apr. 1, 1999.

[39] G. A. Holzapfel, M. Stadler, and C. A. Schulze-Bauer, "A layer-specific three dimensional model for the simulation of balloon angioplasty using magnetic resonance imaging and mechanical testing," *Annals of Biomedical Engineering*, vol. 30, no. 6, pp. 753–767, 2002.

[40] D. Balzani, J. Schrder, and D. Gross, "Numerical simulation of residual stresses in arterial walls," *Computational Materials Science*, Proceedings of the 15th International Workshop on Computational Mechanics of Materials The 15th International Workshop on Computational Mechanics of Materials, vol. 39, no. 1, pp. 117–123, Mar. 2007.

[41] N. Famaey, G. Sommer, J. Vander Sloten, and G. A. Holzapfel, "Arterial clamping: Finite element simulation and in vivo validation," *Journal of the Mechanical Behavior of Biomedical Materials*, vol. 12, pp. 107–118, Aug. 2012.

[42] G. A. Holzapfel, "Structural and numerical models for the (visco)elastic response of arterial walls with residual stresses," in *Biomechanics of Soft Tissue in Cardiovascu-

lar Systems, G. A. Holzapfel and R. W. Ogden, Eds., WOS:000183595000004, 2003, pp. 109–184.

[43] J. Schrder, D. Balzani, and D. Gross, "Aspects of modeling and computer simulation of soft tissues: Applications to arterial walls," *Materialwissenschaft und Werkstofftechnik*, vol. 36, no. 12, pp. 795–801, Dec. 1, 2005.

[44] M. A. Zulliger, A. Rachev, and N. Stergiopulos, "A constitutive formulation of arterial mechanics including vascular smooth muscle tone," *American Journal of Physiology - Heart and Circulatory Physiology*, vol. 287, no. 3, H1335–H1343, Sep. 1, 2004.

[45] N. Famaey, E. Kuhl, G. A. Holzapfel, and J. Vander Sloten, "Cardiovascular tissue damage: An experimental and computational framework," in *Computer Models in Biomechanics*, Springer, 2013, pp. 129–148.

[46] D. Yang, M. C. Converse, D. M. Mahvi, and J. G. Webster, "Measurement and analysis of tissue temperature during microwave liver ablation," *IEEE Transactions on Biomedical Engineering*, vol. 54, no. 1, pp. 150–155, Jan. 2007.

[47] S. H. Farkoush, N. Abolfathi, H. Mehmanesh, and S. Najarian, "Design and finite element analysis of a novel smart clamper for aortic cross-clamping in minimally invasive surgery," *Minimally Invasive Therapy & Allied Technologies*, vol. 25, no. 1, pp. 15–21, Jan. 2, 2016.

[48] D. Balzani, "Simulation of deformation, damage and residual stresses in arterial walls," *Advanced Engineering Materials*, vol. 10, no. 4, pp. 315–321, Apr. 1, 2008.

[49] B. Calvo, E. Pea, M. A. Martinez, and M. Doblar, "An uncoupled directional damage model for fibred biological soft tissues. formulation and computational aspects," *International Journal for Numerical Methods in Engineering*, vol. 69, no. 10, pp. 2036–2057, Mar. 5, 2007.

[50] X. Li, "Finite-element analysis for immiscible two-phase fluid flow in deforming porous media and an unconditionally stable staggered solution," *Communications in Applied Numerical Methods*, vol. 6, no. 2, pp. 125–135, Feb. 1, 1990.

[51] E. Pena, V. Alastrue, A. Laborda, M. A. Martinez, and M. Doblare, "A constitutive formulation of vascular tissue mechanics including viscoelasticity and softening behaviour," *Journal of Biomechanics*, vol. 43, no. 5, pp. 984–989, Mar. 22, 2010, WOS:000276711700025.

[52] K. Y. Volokh, "Prediction of arterial failure based on a microstructural bi-layer fiber-matrix model with softening," *Journal of Biomechanics*, vol. 41, no. 2, pp. 447–453, 2008.

[53] H. H. Pennes, "Analysis of tissue and arterial blood temperatures in the resting human forearm," *Journal of applied physiology*, vol. 85, no. 1, pp. 5–34, 1948.

[54] E. H. Wissler, "Comments on the new bioheat equation proposed by weinbaum and jiji," *Journal of Biomechanical Engineering*, vol. 109, no. 3, pp. 226–233, Aug. 1, 1987.

[55] S. Weinbaum and L. M. Jiji, "A new simplified bioheat equation for the effect of blood flow on local average tissue temperature," *Journal of Biomechanical Engineering*, vol. 107, no. 2, pp. 131–139, May 1985.

[56] E. H. Wissler, "Pennes' 1948 paper revisited," *Journal of Applied Physiology*, vol. 85, no. 1, pp. 35–41, Jul. 1998, WOS:000074689200004.

[57] A. R. A. Khaled and K. Vafai, "The role of porous media in modeling flow and heat transfer in biological tissues," *International Journal of Heat and Mass Transfer*, vol. 46, no. 26, pp. 4989–5003, Dec. 2003.

[58] Y. Xuan and W. Roetzel, "Bioheat equation of the human thermal system," *Chemical Engineering & Technology*, vol. 20, no. 4, pp. 268–276, May 1997.

[59] A. Nakayama and F. Kuwahara, "A general bioheat transfer model based on the theory of porous media," *International Journal of Heat and Mass Transfer*, vol. 51, no. 11, pp. 3190–3199, Jun. 2008.

[60] K. R. Diller and L. J. Hayes, "A finite element model of burn injury in blood-perfused skin," *Journal of Biomechanical Engineering*, vol. 105, no. 3, pp. 300–307, Aug. 1983.

[61] E. J. Berjano, "Theoretical modeling for radiofrequency ablation: State-of-the-art and challenges for the future," *Biomed Eng Online*, vol. 5, p. 24, Apr. 2006.

[62] S. Tungjitkusolmun, T. Staelin, D. Haemmerich, J.-Z. Tsai, H. Cao, J. Webster, J. Lee F.T., D. Mahvi, and V. Vorperian, "Three-dimensional finite-element analyses for radio-frequency hepatic tumor ablation," *IEEE Transactions on Biomedical Engineering*, vol. 49, no. 1, pp. 3–9, Jan. 2002.

[63] Y. He, M. Shirazaki, H. Liu, R. Himeno, and Z. Sun, "A numerical coupling model to analyze the blood flow, temperature, and oxygen transport in human breast tumor under laser irradiation," *Computers in Biology and Medicine*, vol. 36, no. 12, pp. 1336–1350, Dec. 2006.

[64] R. K. Chen, M. W. Chastagner, R. E. Dodde, and A. J. Shih, "Electrosurgical vessel sealing tissue temperature: Experimental measurement and finite element modeling," *IEEE Transactions on Biomedical Engineering*, vol. 60, no. 2, pp. 453–460, Feb. 2013.

[65] J. A. Pearce, "Numerical models of laser fusion of intestinal tissues," in *Annual International Conference of the IEEE Engineering in Medicine and Biology Society, 2009. EMBC 2009*, Sep. 2009, pp. 4303–4306.

[66] J. A. Pearce, "Models for thermal damage in tissues: Processes and applications," *Critical Reviews in Biomedical Engineering*, vol. 38, no. 1, pp. 1–20, 2010.

[67] J. A. Pearce and S. Thomsen, "Kinetic models of laser-tissue fusion processes," *Biomedical Sciences Instrumentation*, vol. 29, pp. 355–360, 1993.

[68] X. Y. Wu and Y. Zhou, "Finite element analysis of diffusional drug release from complex matrix systems. II. factors influencing release kinetics," *Journal of Controlled Release*, vol. 51, no. 1, pp. 57–71, Jan. 23, 1998, WOS:000071940000006.

[69] C. Nicholson, "Diffusion and related transport mechanisms in brain tissue," *Reports on Progress in Physics*, vol. 64, pp. 815–884, Jul. 2001.

[70] H. Darcy, *Les fontaines publiques de la ville de Dijon: exposition et application ...* Victor Dalmont, 1856, 664 pp.

[71] V. C. Mow, M. H. Holmes, and W. Michael Lai, "Fluid transport and mechanical properties of articular cartilage: A review," *Journal of Biomechanics*, vol. 17, no. 5, pp. 377–394, 1984.

[72] S. J. Ferguson, K. Ito, and L.-P. Nolte, "Fluid flow and convective transport of solutes within the intervertebral disc," *Journal of Biomechanics*, Spinal Biomechanics, vol. 37, no. 2, pp. 213–221, Feb. 2004.

[73] G. Jayaraman, "Water transport in the arterial walla theoretical study," *Journal of Biomechanics*, vol. 16, no. 10, pp. 833–840, 1983.

[74] H. C. Brinkman, "On the permeability of media consisting of closely packed porous particles," *Applied Scientific Research*, vol. 1, no. 1, pp. 81–86, 1949.

[75] R. de Boer, "Highlights in the historical development of the porous media theory: Toward a consistent macroscopic theory," *Applied Mechanics Reviews*, vol. 49, no. 4, pp. 201–262, Apr. 1, 1996.

[76] M. A. Biot, "General theory of threedimensional consolidation," *Journal of Applied Physics*, vol. 12, no. 2, pp. 155–164, Feb. 1, 1941.

[77] M. A. Biot, "Theory of elasticity and consolidation for a porous anisotropic solid," *Journal of Applied Physics*, vol. 26, no. 2, pp. 182–185, Feb. 1, 1955.

[78] M. A. Biot, "Theory of finite deformations of porous solids," *Indiana University Mathematics Journal*, vol. 21, no. 7, pp. 597–620, 1972.

[79] R. De Boer, *Trends in continuum mechanics of porous media*. Dordrecht: Springer Netherlands, 2005.

[80] R. de Boer, *Theory of porous media: Highlights in the historical development and current state*. Springer Berlin Heidelberg, 2000.

[81] J. W. Nunziato and E. K. Walsh, "On ideal multiphase mixtures with chemical reactions and diffusion," *Archive for Rational Mechanics and Analysis*, vol. 73, no. 4, pp. 285–311, Dec. 1980.

[82] S. L. Passman, J. W. Nunziato, and E. K. Walsh, "A theory of multiphase mixtures," in *Rational Thermodynamics*, DOI: 10.1007/978-1-4612-5206-1_15, Springer New York, 1984, pp. 286–325.

[83] S. C. Cowin and J. W. Nunziato, "Linear elastic materials with voids," *Journal of Elasticity*, vol. 13, no. 2, pp. 125–147, Jul. 1983.

[84] O. Coussy, "A general theory of thermoporoelastoplasticity for saturated porous materials," *Transport in Porous Media*, vol. 4, no. 3, pp. 281–293, Jun. 1989.

[85] R. d. Boer and S. J. Kowalski, "Thermodynamics of fluid-saturated porous media with a phase change," *Acta Mechanica*, vol. 109, no. 1, pp. 167–189, Mar. 1995.

[86] S. J. Kowalski, "Toward a thermodynamics and mechanics of drying processes," *Chemical Engineering Science*, vol. 55, no. 7, pp. 1289–1304, Apr. 2000.

[87] O. Coussy, "Poromechanics of freezing materials," *Journal of the Mechanics and Physics of Solids*, vol. 53, no. 8, pp. 1689–1718, Aug. 2005.

[88] O. Coussy, *Mechanics and physics of porous solids*. John Wiley & Sons, Jun. 28, 2011, 149 pp.

[89] V. C. Mow, S. C. Kuei, W. M. Lai, and C. G. Armstrong, "Biphasic creep and stress relaxation of articular cartilage in compression: Theory and experiments," *Journal of Biomechanical Engineering*, vol. 102, no. 1, pp. 73–84, Feb. 1, 1980.

[90] J. M. Huyghe and J. D. Janssen, "Quadriphasic mechanics of swelling incompressible porous media," *International Journal of Engineering Science*, vol. 35, no. 8, pp. 793–802, Jun. 1997.

[91] J. M. Huyghe and D. H. Van Campen, "Finite deformation theory of hierarchically arranged porous solidsII. constitutive behaviour," *International Journal of Engineering Science*, vol. 33, no. 13, pp. 1873–1886, Oct. 1995.

[92] B. R. Simon, "Multiphase poroelastic finite element models for soft tissue structures," *Applied Mechanics Reviews*, vol. 45, no. 6, pp. 191–218, Jun. 1, 1992.

[93] H. Snijders, J. M. Huyghe, and J. D. Janssen, "Triphasic finite element model for swelling porous media," *International Journal for Numerical Methods in Fluids*, vol. 20, no. 8, pp. 1039–1046, Apr. 30, 1995.

[94] W. Ehlers and B. Markert, "A linear viscoelastic biphasic model for soft tissues based on the theory of porous media," *Journal of Biomechanical Engineering*, vol. 123, no. 5, p. 418, 2001.

[95] B. R. Simon, J. P. Liable, D. Pflaster, Y. Yuan, and M. H. Krag, "A poroelastic finite element formulation including transport and swelling in soft tissue structures," *Journal of Biomechanical Engineering-Transactions of the Asme*, vol. 118, no. 1, pp. 1–9, Feb. 1996, WOS:A1996TY35500001.

[96] R. L. Spilker and J. K. Suh, "Special issue: Frontiers in computational mechanics formulation and evaluation of a finite element model for the biphasic model of hydrated soft tissues," *Computers & Structures*, vol. 35, no. 4, pp. 425–439, Jan. 1, 1990.

[97] Z. Jin, *Computational modelling of biomechanics and biotribology in the musculoskeletal system: Biomaterials and tissues*. Elsevier, May 2014.

[98] D. Chapelle, J.-F. Gerbeau, J. Sainte-Marie, and I. E. Vignon-Clementel, "A poroelastic model valid in large strains with applications to perfusion in cardiac modeling," *Comput Mech*, vol. 46, no. 1, pp. 91–101, Dec. 2009.

[99] R. A. Regueiro, B. Zhang, and S. L. Wozniak, "Large deformation dynamic three-dimensional coupled finite element analysis of soft biological tissues treated as biphasic porous media," *Computer Modeling in Engineering and Sciences*, vol. 98, no. 1, pp. 1–39, 2014.

[100] X. Li, O. C. Zienkiewicz, and Y. M. Xie, "A numerical model for immiscible two-phase fluid flow in a porous medium and its time domain solution," *International Journal for Numerical Methods in Engineering*, vol. 30, no. 6, pp. 1195–1212, Oct. 20, 1990.

[101] B. A. Schrefler, X. Zhan, and L. Simoni, "A coupled model for water flow, airflow and heat flow in deformable porous media," *International Journal of Numerical Methods for Heat & Fluid Flow*, vol. 5, no. 6, pp. 531–547, Aug. 1995.

[102] B. A. Schrefler and Z. Xiaoyong, "A fully coupled model for water flow and airflow in deformable porous media," *Water Resources Research*, vol. 29, no. 1, pp. 155–167, Jan. 1, 1993.

[103] R. W. Lewis and B. A. Schrefler, *The finite element method in the static and dynamic deformation and consolidation of porous media, 2nd edition*. Wiley, Jan. 1999, 508 pp.

[104] W. Wang, R. A. Regueiro, and J. S. McCartney, "Coupled axisymmetric thermo-poro-mechanical finite element analysis of energy foundation centrifuge experiments in partially saturated silt," *Geotechnical and Geological Engineering*, vol. 33, no. 2, pp. 373–388, Jul. 19, 2014.

[105] W. Wang, "Coupled thermo-poro-mechanical axisymmetric finite element modeling of soil-structure interaction in partially saturated soils," PhD thesis, University of Colorado - Boulder, Boulder, CO, 2014.

[106] A. Dhall and A. K. Datta, "Transport in deformable food materials: A poromechanics approach," *Chemical Engineering Science*, Novel Gas Conversion Symposium- Lyon 2010, C1-C4 Catalytic Processes for the Production of Chemicals and Fuels, vol. 66, no. 24, Dec. 2011.

[107] R. I. Borja, "On the mechanical energy and effective stress in saturated and unsaturated porous continua," *International Journal of Solids and Structures*, vol. 43, no. 6, pp. 1764–1786, Mar. 2006.

[108] X. Song and R. I. Borja, "Mathematical framework for unsaturated flow in the finite deformation range," *International Journal for Numerical Methods in Engineering*, vol. 97, no. 9, pp. 658–682, Mar. 2, 2014.

[109] D. Ebrahimi, "Three-dimensional finite element implementation for a dynamic solid-fluid mixture at finite strain," PhD thesis, University of Colorado - Boulder, 2007.

[110] G. Sommer and G. A. Holzapfel, "3d constitutive modeling of the biaxial mechanical response of intact and layer-dissected human carotid arteries," *Journal of the Mechanical Behavior of Biomedical Materials*, vol. 5, no. 1, pp. 116–128, Jan. 2012.

[111] H. Y. Chen, J. A. Navia, and G. S. Kassab, "A simulation of vesselclamp interaction: Transient closure dynamics," *Annals of Biomedical Engineering*, vol. 37, no. 9, pp. 1772–1780, Sep. 1, 2009.

[112] N. Anderson, E. Kramer, J. Cezo, V. Ferguson, and M. E. Rentschler, "Tissue bond strength as a function of applied fusion pressure1," *Journal of Medical Devices*, vol. 8, no. 3, pp. 030 925–030 925, Jul. 21, 2014.

[113] R. K. Chen, M. W. Chastagner, J. D. Geiger, and A. J. Shih, "Bipolar electrosurgical vessel-sealing device with compressive force monitoring," *Journal of Biomechanical Engineering*, vol. 136, no. 6, pp. 061 001–061 001, Apr. 18, 2014.

[114] B. Person, D. A. Vivas, D. Ruiz, M. Talcott, J. E. Coad, and S. D. Wexner, "Comparison of four energy-based vascular sealing and cutting instruments: A porcine model," *Surgical Endoscopy*, vol. 22, no. 2, pp. 534–538, Feb. 2008.

[115] D. Li and A. M. Robertson, "A structural multi-mechanism damage model for cerebral arterial tissue," *Journal of Biomechanical Engineering*, vol. 131, no. 10, pp. 101 013–101 013, Sep. 17, 2009.

[116] S. S. Chen, N. T. Wright, and J. D. Humphrey, "Heat-induced changes in the mechanics of a collagenous tissue: Isothermal free shrinkage," *J Biomech Eng*, vol. 119, no. 4, pp. 372–378, Nov. 1997.

[117] J. D. Cezo, A. C. Passernig, V. L. Ferguson, K. D. Taylor, and M. E. Rentschler, "Evaluating temperature and duration in arterial tissue fusion to maximize bond strength," *Journal of the Mechanical Behavior of Biomedical Materials*, vol. 30, pp. 41–49, Feb. 2014, WOS:000331493900004.

[118] J. Cezo, "Thermal tissue fusion of arteries: Methods, mechanisms, and mechanics," PhD thesis, University of Colorado - Boulder, Boulder, CO, 2013.

[119] Y. Cengel and A. Ghajar, *Heat and mass transfer: Fundamentals and applications*, 4 edition. New York: McGraw-Hill Science Engineering Math, Feb. 2010.

[120] F. A. Duck, *Physical properties of tissues: A comprehensive reference book*. Academic Press, Oct. 22, 2013, 357 pp.

[121] G. A. Holzapfel, *Nonlinear solid mechanics: A continuum approach for engineering*. 2000.

[122] G. A. Holzapfel and R. W. Ogden, "Modelling the layer-specific three-dimensional residual stresses in arteries, with an application to the human aorta," *Journal of The Royal Society Interface*, vol. 7, no. 46, pp. 787–799, May 6, 2010.

[123] B. D. Stemper, N. Yoganandan, M. R. Stineman, T. A. Gennarelli, J. L. Baisden, and F. A. Pintar, "Mechanics of fresh, refrigerated, and frozen arterial tissue," *Journal of Surgical Research*, vol. 139, no. 2, pp. 236–242, May 2007.

[124] C. Martin, W. Sun, and J. Elefteriades, "Patient-specific finite element analysis of ascending aorta aneurysms," *American Journal of Physiology. Heart and Circulatory Physiology*, vol. 308, no. 10, H1306–1316, May 15, 2015.

[125] W. Ehlers and J. Bluhm, *Porous media: Theory, experiments and numerical applications*. Springer Science & Business Media, Mar. 9, 2013, 459 pp.

[126] R. M. Bowen, "Incompressible porous media models by use of the theory of mixtures," *International Journal of Engineering Science*, vol. 18, no. 9, pp. 1129–1148, Jan. 1, 1980.

[127] B. D. Coleman and W. Noll, "The thermodynamics of elastic materials with heat conduction and viscosity," *Archive for Rational Mechanics and Analysis*, vol. 13, no. 1, pp. 167–178, 1963.

[128] J. Pearce, "Numerical model study of radio frequency vessel sealing thermodynamics," in *Energy-based Treatment of Tissue and Assessment VIII, 7-8 Feb. 2015*, vol. 9326, 2015, 93260A–93260A–12.

[129] A. K. Datta, "Porous media approaches to studying simultaneous heat and mass transfer in food processes. II: Property data and representative results," *Journal of Food Engineering*, vol. 80, no. 1, pp. 96–110, May 2007.

[130] J. D. Cezo, V. L. Ferguson, K. D. Taylor, and M. E. Rentschler, "Measurement of bond strength of direct heat tissue fusion in arteries," in *ASME 2012 Summer Bioengineering Conference, SBC 2012, June 20, 2012 - June 23, 2012*, ser. ASME 2012 Summer Bioengineering Conference, SBC 2012, American Society of Mechanical Engineers, 2012, pp. 665–666.

[131] A. Marbn, A. Casals, J. Fernndez, and J. Amat, "Haptic feedback in surgical robotics: Still a challenge," in *ROBOT2013: First Iberian Robotics Conference*, M. A. Armada, A. Sanfeliu, and M. Ferre, Eds., vol. 252, Cham: Springer International Publishing, 2014, pp. 245–253.

[132] A. W. Bishop and G. E. Blight, "Some aspects of effective stress in saturated and partly saturated soils," *Gotechnique*, vol. 13, no. 3, pp. 177–197, Sep. 1, 1963.

[133] L. Davison, Y. Horie, and M. Shahinpoor, Eds., *High-pressure shock compression of solids IV*, DOI: 10.1007/978-1-4612-2292-7, New York, NY: Springer New York, 1997.

Chapter 9: Appendix A

Derivation of $\frac{\partial \chi}{\partial p_\ell}$

It is assumed that the effective stress parameter, χ, is equal to the liquid saturation, S_ℓ. Thus,

$$\frac{\partial \chi}{\partial p_\ell} = \frac{\partial S_\ell}{\partial p_\ell} \tag{9.1}$$

where $\frac{\partial S_\ell}{\partial p_\ell}$ is defined in equation 9.4.

Derivation of $\frac{\partial S_\ell}{\partial p_\ell}$

The derivative of liquid saturation with respect to liquid pressure can be defined as

$$\frac{\partial S_\ell}{\partial p_\ell} = \frac{\partial}{\partial p_\ell}\left(\left(\frac{1}{1 + (\frac{s}{a})^{n_{vg}}}\right)^m (S_s - S_r) + S_r\right) \tag{9.2}$$

which through applying the fact that

$$\frac{\partial s}{\partial p_\ell} = \frac{\partial(p_g - p_\ell)}{\partial p_\ell} = -1 \tag{9.3}$$

yields

$$\frac{\partial S_\ell}{\partial p_\ell} = -(1 - S_r)\left(\frac{m n_{vg}}{a}\right)\left[1 + \frac{s}{a}\right]^{-(m+1)}. \tag{9.4}$$

Derivation of $\frac{\partial p_\ell}{\partial \theta}$

$$\frac{\partial p_\ell}{\partial \theta} = 0. \tag{9.5}$$

Derivation of $\frac{\partial p_g}{\partial \theta}$

Using the definition of the Clausius-Clapeyron equation (Eqn. 5.205) it can be said that

$$\frac{\partial p_g}{\partial \theta} = p_g \frac{H_{vap} M_m}{R \theta^2} \tag{9.6}$$

Derivation of $\frac{\partial \chi}{\partial \theta}$

It is assumed that the effective stress parameter, χ, is equal to the liquid saturation, S_ℓ. Thus,

$$\frac{\partial \chi}{\partial \theta} = \frac{\partial S_\ell}{\partial \theta} \tag{9.7}$$

where $\frac{\partial \chi}{\partial \theta} = \frac{\partial S_\ell}{\partial \theta}$ is defined in equation 9.10.

Derivation of $\frac{\partial S_\ell}{\partial \theta} = \frac{\partial S_\ell}{\partial \theta}$

The derivative of liquid saturation with respect to temperature can be written as

$$\frac{\partial S_\ell}{\partial \theta} = \frac{\partial}{\partial \theta} \left(\left(\frac{1}{1 + (\frac{s}{a})^{n_{vg}}} \right)^m (S_s - S_r) + S_r \right) \tag{9.8}$$

which expanding can be written as

$$(S_r - 1) \left(\frac{m n_{vg}}{a} \right) \left[1 + \frac{s}{a} \right]^{-(m+1)} \left(\frac{\partial s}{\partial \theta} \right) \tag{9.9}$$

which can be simplified to

$$(S_r - 1) \left(\frac{m n_{vg}}{a} \right) \left[1 + \frac{s}{a} \right]^{-(m+1)} \left(\frac{\partial p_g}{\partial \theta} \right) \tag{9.10}$$

where $\frac{\partial p_g}{\partial \theta}$ is defined in 9.6.

Derivation of $\frac{\partial \rho^{\ell R}}{\partial \theta}$

The change in liquid density with respect to temperature is

$$\frac{\partial \rho^{\ell R}}{\partial \theta} = \frac{\partial \left(\rho_o^{\ell R} \left[1 - \beta_\ell^\theta (\theta - \theta_0) \right] \right)}{\partial \theta} \tag{9.11}$$

which can be simplified to

$$\frac{\partial \rho^{\ell R}}{\partial \theta} = -\rho_0^{\ell R} \beta_\ell^\theta. \tag{9.12}$$

Derivation of $\frac{\partial \rho^{gR}}{\partial \theta}$

The change in real gas density with respect to temperature is

$$\frac{\partial \rho^{gR}}{\partial \theta} = \frac{\partial}{\partial \theta} \left[\frac{p_g M_m}{\theta R} \right] \tag{9.13}$$

which expanded with the chain rule is

$$\frac{\partial \rho^{gR}}{\partial \theta} = \frac{M_m}{\theta R} \frac{\partial p_g}{\partial \theta} - \frac{p_g M_m}{R \theta^2} \tag{9.14}$$

where $\frac{\partial p_g}{\partial \theta}$ is defined in 9.6.

Derivation of $\frac{\partial S_g}{\partial \theta}$

The change in gas saturation, S_g with respect to temperature can be related the liquid saturation as

$$\frac{\partial S_g}{\partial \theta} = -\frac{\partial S_\ell}{\partial \theta} \tag{9.15}$$

where $\frac{\partial S_\ell}{\partial \theta}$ is defined in 9.10.

Derivation of $\frac{\partial v_{f_i}^D}{\partial F_{aA}}$

The derivative of the Darcy's velocity of a fluid in with respect to the deformation gradient can be written as

$$\frac{\partial v_{f_i}^D}{\partial F_{aA}} = \frac{\partial}{\partial F_{aA}}\left(\frac{k_{int}^f k_{rel}^f}{\mu_f}\frac{\partial p_f}{\partial X_I}F_{Ii}^{-1}\right) \tag{9.16}$$

which expanding is

$$\frac{\partial v_{f_i}^D}{\partial F_{aA}} = \frac{k_{int}^f}{\mu_f}\left(\frac{\partial k_{rel}^f}{\partial F_{aA}}\frac{\partial p_f}{\partial X_I}F_{Ii}^{-1} + k_{rel}^f\frac{\partial p_f}{\partial X_I}\frac{\partial F_{Ii}^{-1}}{F_{aA}}\right) \tag{9.17}$$

which applying 6.31 and 6.20 gives

$$\frac{\partial v_{f_i}^D}{\partial F_{aA}} = \frac{k_{int}^f}{\mu_f}\left(\frac{\partial k_{rel}^f}{\partial F_{aA}}\frac{\partial p_f}{\partial X_I}F_{Ii}^{-1} - k_{rel}^f\frac{\partial p_f}{\partial X_I}\left(F_{Ia}^{-1}F_{Ai}^{-1}\right)\right) \tag{9.18}$$

where $\frac{\partial k_{rel}^f}{\partial F_{aA}}$ is defined in 9.20

Derivation of $\frac{\partial k_{rel}^f}{\partial F_{aA}}$

According to the Kozemy-Carmen relationship one can write

$$\frac{\partial k_{rel}^f}{\partial F_{aA}} = \frac{\partial}{\partial F_{aA}}\left(\frac{(n)^3}{1-(n)^2}\frac{1-(n_0)^2}{(n_0)^3}\right) \tag{9.19}$$

which can be simplified using 5.11 to

$$\frac{\partial k_{rel}^f}{\partial F_{aA}} = \frac{1-(n_0)^2}{(n_0)^3}\left[\frac{3(n)^2}{1-(n)^2} + \frac{2(n)^4}{\left(1-(n)^2\right)^2}\right]\frac{\partial n}{\partial F_{aA}} \tag{9.20}$$

where $\frac{\partial n}{\partial F_{aA}}$ is defined in equation 9.23

Derivation of $\frac{\partial n}{\partial F_{aA}}$

Using the definition of porosity 5.4 it can be seen that

$$\frac{\partial n}{\partial F_{aA}} = \frac{\partial(1 - n^s)}{\partial F_{aA}} \tag{9.21}$$

which expands to

$$\frac{\partial n}{\partial F_{aA}} = \frac{\partial\left(-\frac{n_0^s}{J}\right)}{\partial F_{aA}} \tag{9.22}$$

which expands to

$$\frac{\partial n}{\partial F_{aA}} = \frac{(n-1)}{J} F_{Aa}^{-1}. \tag{9.23}$$

Derivation of $\frac{\partial v_{\ell_i}^D}{\partial p_\ell}$

Using the definition of Darcy's velocity 5.76 it can be written that

$$\frac{\partial v_{\ell_i}^D}{\partial p_\ell} = \frac{\partial}{\partial p_\ell}\left(\frac{k_{int}^\ell k_{rel}^\ell}{\mu_\ell} \frac{\partial p_\ell}{\partial X_I} F_{Ii}^{-1}\right) \tag{9.24}$$

which can be expanded to

$$\frac{\partial v_{\ell_i}^D}{\partial p_\ell} = \frac{k_{rel}^\ell}{\mu_\ell} F_{Ii}^{-1}\left(\frac{\partial k_{int}^\ell}{\partial p_\ell} \frac{\partial p_\ell}{\partial X_I} + k_{int}^\ell \frac{\partial p_\ell}{\partial X_I}\right) \tag{9.25}$$

where $\frac{\partial k_{int}^\ell}{\partial p_\ell}$ is defined in 9.27.

Derivation of $\frac{\partial k_{rel}^{\ell}}{\partial p_{\ell}}$

The partial derivative of the relative permeability with respect to liquid pressure can be written as

$$\frac{\partial k_{int}^{\ell}}{\partial p_{\ell}} = \frac{\partial}{\partial p_{\ell}}\left(\left(\frac{S_{\ell} - S_r}{1 - S_r}\right)^3\right) \tag{9.26}$$

which can be expanded to

$$\frac{\partial k_{int}^{\ell}}{\partial p_{\ell}} = 3\left(\frac{S_{\ell} - S_r}{1 - S_r}\right)^2 \frac{1}{1 - S_r}\frac{\partial S_{\ell}}{\partial p_{\ell}} \tag{9.27}$$

where $\frac{\partial S_{\ell}}{\partial p_{\ell}}$ is defined in 9.4.

Derivation of $\frac{\partial v_{g_i}^D}{\partial p_{\ell}}$

Using the definition of Darcy's velocity 5.76 it can be written that

$$\frac{\partial v_{g_i}^D}{\partial p_{\ell}} = \frac{\partial}{\partial p_{\ell}}\left(\frac{k_{int}^g k_{rel}^g}{\mu_{\ell}}\frac{\partial p_g}{\partial X_I}F_{Ii}^{-1}\right) \tag{9.28}$$

which can be expanded to

$$\frac{\partial v_{g_i}^D}{\partial p_{\ell}} = \frac{k_{rel}^g}{\mu_{\ell}}F_{Ii}^{-1}\left(\frac{\partial k_{int}^g}{\partial p_{\ell}}\frac{\partial p_g}{\partial X_I}\right) \tag{9.29}$$

where $\frac{\partial k_{int}^g}{\partial p_{\ell}}$ is defined in 9.31.

Derivation of $\frac{\partial k_{rel}^g}{\partial p_{\ell}}$

The partial derivative of the relative permeability with respect to liquid pressure can be written as

$$\frac{\partial k_{int}^{\ell}}{\partial p_g} = \frac{\partial}{\partial p_\ell}\left(1 - 1.1S_g\right) \tag{9.30}$$

which can be expanded to

$$\frac{\partial k_{int}^{\ell}}{\partial p_\ell} = 1.1\frac{\partial S_\ell}{\partial p_\ell} \tag{9.31}$$

where $\frac{\partial S_\ell}{\partial p_\ell}$ is defined in 9.4.

Derivation of $\frac{\partial v_{\ell_i}^{D}}{\partial \theta}$

The derivative of the liquid Darcy's velocity with respect to temperature can be written as

$$\frac{\partial v_{\ell_i}^{D}}{\partial \theta} = \frac{\partial}{\partial \theta}\left(\frac{k_{int}^{\ell}k_{rel}^{\ell}}{\mu_\ell}\frac{\partial p_\ell}{\partial X_I}F_{Ii}^{-1}\right) \tag{9.32}$$

which given the assumption liquid pressure is not a function of temperature can be written as

$$\frac{\partial v_{\ell_i}^{D}}{\partial \theta} = \frac{k_{irel}^{\ell}}{\mu_\ell}F_{Ii}^{-1}\frac{\partial p_\ell}{\partial X_I}\frac{\partial k_{int}^{\ell}}{\partial \theta} \tag{9.33}$$

where $\frac{\partial k_{int}^{\ell}}{\partial \theta}$ is defined in 9.35.

Derivation of $\frac{\partial k_{int}^{\ell}}{\partial \theta}$

the derivative of the relative permeability, k_{int}^{ℓ} of a liquid with respect to temperature can be written as

$$\frac{\partial k_{int}^{\ell}}{\partial \theta} = \frac{\partial}{\partial \theta}\left(\left(\frac{S_\ell - S_r}{1 - S_r}\right)^3\right) \tag{9.34}$$

which can be simplified

$$\frac{\partial k_{int}^{\ell}}{\partial \theta} = 3\left(\frac{S_\ell - S_r}{1 - S_r}\right)^2 \frac{1}{1 - S_r}\frac{\partial S_\ell}{\partial \theta} \tag{9.35}$$

where $\frac{\partial S_\ell}{\partial \theta}$ is defined in 9.10.

Derivation of $\frac{\partial v_{g_i}^D}{\partial \theta}$

The derivative of the gas Darcy's velocity with respect to temperature can be written as

$$\frac{\partial v_{g_i}^D}{\partial \theta} = \frac{\partial}{\partial \theta}\left(\frac{k_{int}^g k_{rel}^g}{\mu_g}\frac{\partial p_\ell}{\partial X_I}F_{Ii}^{-1}\right) \tag{9.36}$$

which given the assumption liquid pressure is not a function of temperature can be written as

$$\frac{\partial v_{g_i}^D}{\partial \theta} = \frac{k_{rel}^g}{\mu_g}F_{Ii}^{-1}\left[\frac{\partial p_g}{\partial X_I}\frac{\partial k_{int}^g}{\partial \theta} + \frac{\partial p_g}{\partial \theta}\frac{\partial \theta}{\partial X_I}k_{int}^g\right] \tag{9.37}$$

where $\frac{\partial k_{int}^g}{\partial \theta}$ and $\frac{\partial p_g}{\partial \theta}$ are defined in **??** and 9.6.

Derivation of $\frac{\partial k_{int}^g}{\partial \theta}$

the derivative of the relative permeability, k_{int}^g of a gas with respect to temperature can be written as

$$\frac{\partial k_{rint}^g}{\partial \theta} = \frac{\partial}{\partial \theta}\left(1 - 1.1 S_g\right) \tag{9.38}$$

which can be simplified

$$\frac{\partial k_{int}^g}{\partial \theta} = -1.1\frac{\partial S_g}{\partial \theta} \tag{9.39}$$

where

$$\frac{\partial S_g}{\partial \theta} = -\frac{\partial S_\ell}{\partial \theta} \tag{9.40}$$

where $\frac{\partial S_\ell}{\partial \theta}$ is defined in 9.10.

Derivation of $\frac{\partial \dot{S}_\ell}{\partial \dot{p}_\ell}$

The derivative of the time derivative of the liquid saturation can be described as

$$\frac{\partial \dot{S}_\ell}{\partial \dot{p}_\ell} = -(1 - S_r)\left(\frac{mn}{a}\right)\left[1 + \frac{s}{a}\right]^{-(m+1)}. \tag{9.41}$$

Derivation of $\frac{\partial H_1^{ext}}{\partial \dot{u}_j}$

The tangent stiffness of the external balance of mass forcing function is

$$\frac{\partial H_1^{ext}}{\partial \dot{u}_j} = \frac{\partial}{\partial \dot{u}_j}\left(\rho^{\ell R} S_\ell \frac{k_{int}^\ell k_{rel}^\ell}{\mu_\ell}[p_{amb} - p_\ell] + \rho^{gR} S_g \frac{k_{int}^g k_{rel}^g}{\mu_g}[p_{amb} - p_g]\right) \tag{9.42}$$

which can be expanded to

$$\frac{\partial H_1^{ext}}{\partial \dot{u}_j} = \frac{\partial}{\partial u_j}\left(\rho^{\ell R} S_\ell \frac{k_{int}^\ell k_{rel}^\ell}{\mu_\ell}[p_{amb} - p_\ell] + \rho^{gR} S_g \frac{k_{int}^g k_{rel}^g}{\mu_g}[p_{amb} - p_g]\right)\alpha\Delta t. \tag{9.43}$$

To ease the implementation into FE code it is beneficial to write 9.43

as

$$\frac{\partial H_1^{ext}}{\partial \dot{u}_j} = \frac{\partial}{\partial F_{aA}}\left(\rho^{\ell R} S_\ell \frac{k_{int}^\ell k_{rel}^\ell}{\mu_\ell}[p_{amb} - p_\ell] + \rho^{gR} S_g \frac{k_{int}^g k_{rel}^g}{\mu_g}[p_{amb} - p_g]\right)\frac{\partial F_{aA}}{\partial u_j}\alpha\Delta t \tag{9.44}$$

which can then be expanded to

$$\frac{\partial H_1^{ext}}{\partial \dot{u}_j} = \left(\rho^{\ell R} S_\ell \frac{k_{int}^\ell}{\mu_\ell} \frac{\partial k_{rel}^\ell}{\partial F_{aA}} [p_{amb} - p_l] + \rho^{gR} S_g \frac{k_{int}^g}{\mu_g} \frac{k_{rel}^\ell}{\partial F_{aA}} [p_{amb} - p_g] \right) \frac{\partial u_a}{\partial X_A} \alpha \Delta t \qquad (9.45)$$

where $\frac{\partial k_{rel}^f}{\partial F_{aA}}$ is defined in 9.20.

Derivation of $\frac{\partial H_1^{ext}}{\partial \dot{p}_\ell}$

The tangent stiffness of the external balance of mass forcing function with respect to liquid pressure is

$$\frac{\partial H_1^{ext}}{\partial \dot{p}_\ell} = \frac{\partial}{\partial \dot{p}_\ell} \left(\rho^{\ell R} S_\ell \frac{k_{int}^\ell k_{rel}^\ell}{\mu_\ell} [p_{amb} - p_\ell] + \rho^{gR} S_g \frac{k_{int}^g k_{rel}^g}{\mu_g} [p_{amb} - p_g] \right) \qquad (9.46)$$

which can be expanded to

$$\frac{\partial H_1^{ext}}{\partial p_\ell} = \frac{\partial}{\partial p_\ell} \left(\rho^{\ell R} S_\ell \frac{k_{int}^\ell k_{rel}^\ell}{\mu_\ell} [p_{amb} - p_\ell] + \rho^{gR} S_g \frac{k_{int}^g k_{rel}^g}{\mu_g} [p_{amb} - p_g] \right) \alpha \Delta t. \qquad (9.47)$$

Again expanding via the chain rule yields and applying $S_g = 1 - S_\ell$ gives

$$\frac{\partial H_1^{ext}}{\partial p_\ell} = \left(\left(\rho^{\ell R} \frac{k_{int}^\ell k_{rel}^\ell}{\mu_\ell} [p_{amb} - p_\ell] - \rho^{gR} \frac{k_{int}^g k_{rel}^g}{\mu_g} [p_{amb} - p_g] \right) \frac{\partial S_\ell}{\partial p_\ell} \right.$$
$$\left. + \rho^{\ell R} S_\ell \frac{k_{int}^\ell}{\mu_\ell} \frac{\partial k_{rel}^\ell}{\partial p_\ell} [p_{amb} - p_\ell] - \rho^{\ell R} S_\ell \frac{k_{int}^\ell k_{rel}^\ell}{\mu_\ell} \right) \alpha \Delta t \qquad (9.48)$$

where $\frac{\partial S_\ell}{\partial p_\ell}$ and $\frac{\partial k_{rel}^\ell}{\partial p_\ell}$ are defined in 9.4 and 9.27.

Derivation of $\frac{\partial H_1^{ext}}{\partial \dot{\theta}}$

The tangent stiffness of the external balance of mass forcing function with respect to temperature is

$$\frac{\partial H_1^{ext}}{\partial \dot{\theta}} = \frac{\partial}{\partial \dot{\theta}} \left(\rho^{\ell R} S_\ell \frac{k_{int}^\ell k_{rel}^\ell}{\mu_\ell} [p_{amb} - p_\ell] + \rho^{gR} S_g \frac{k_{int}^g k_{rel}^g}{\mu_g} [p_{amb} - p_g] \right) \qquad (9.49)$$

which can be written as

$$\frac{\partial H_1^{ext}}{\partial \dot{\theta}} = \frac{\partial}{\partial \dot{\theta}} \left(\rho^{\ell R} S_\ell \frac{k_{int}^\ell k_{rel}^\ell}{\mu_\ell} [p_{amb} - p_\ell] + \rho^{gR} S_g \frac{k_{int}^g k_{rel}^g}{\mu_g} [p_{amb} - p_g] \right) \alpha \Delta t. \qquad (9.50)$$

Expanding via the chain rule gives

$$\frac{\partial H_1^{ext}}{\partial \dot{\theta}} = \left(\frac{\partial \rho^{\ell R}}{\partial \theta} S_\ell \frac{k_{int}^\ell k_{rel}^\ell}{\mu_\ell} [p_{amb} - p_\ell] + \rho^{\ell R} \frac{\partial S_\ell}{\partial \theta} \frac{k_{int}^\ell k_{rel}^\ell}{\mu_\ell} [p_{amb} - p_\ell] \right.$$

$$+ \rho^{\ell R} S_\ell \frac{k_{int}^\ell}{\mu_f} \frac{\partial k_{rel}^\ell}{\partial \theta} [p_{amb} - p_\ell] + \frac{\partial \rho^{gR}}{\partial \theta} S_g \frac{k_{int}^g k_{rel}^g}{\mu_g} [p_{amb} - p_g] \qquad (9.51)$$

$$+ \rho^{gR} \frac{\partial S_g}{\partial \theta} \frac{k_{int}^g k_{rel}^g}{\mu_g} [p_{amb} - p_g] + \rho^{gR} S_g \frac{k_{int}^g}{\mu_g} \frac{\partial k_{rel}^g}{\partial \theta} [p_{amb} - p_g] - \rho^{gR} S_g \frac{k_{int}^g k_{rel}^g}{\mu_g} \frac{\partial p_g}{\partial \theta} \right) \alpha \Delta t$$

where $\frac{\partial \rho^{gR}}{\partial \theta}$, $\frac{\partial S_\ell}{\partial \theta}$, $\frac{\partial k_{rel}^\ell}{\partial \theta}$, $\frac{\partial \rho^{gR}}{\partial \theta}$, $\frac{\partial S_g}{\partial \theta}$, $\frac{\partial k_{rel}^g}{\partial \theta}$ and $\frac{\partial p_g}{\partial \theta}$ are defined in 9.12, 9.10, **??**, 9.14, 9.15, 9.38 and 9.6.

Derivation of $\frac{\partial L_1^{ext}}{\partial u_j}$

For this paper the linearization of the the balance of energy external forcing function with respect to displacement can be written as

$$\frac{\partial L_1^{ext}}{\partial \dot{u}_j} = \frac{\partial}{\partial \dot{u}_j} \left(h_t (\theta - \theta_{amb}) \right) \qquad (9.52)$$

where h_t is the heat transfer coefficient and θ_{amb} the ambient temperature. Neither of these terms is a function of displacement, therefore,

$$\frac{\partial L_1^{ext}}{\partial \dot{u}_j} = 0. \qquad (9.53)$$

Derivation of $\frac{\partial L_1^{ext}}{\partial p_\ell}$

Along the same lines as the previous section, for this paper the linearization of the the balance of energy external forcing function with respect to liquid pressure can be written as

$$\frac{\partial L_1^{ext}}{\partial \dot{p}_\ell} = \frac{\partial}{\partial \dot{p}_\ell}\Big(h_t(\theta - \theta_{amb})\Big) \tag{9.54}$$

Neither of these terms is a function of liquid pressure, therefore,

$$\frac{\partial L_1^{ext}}{\partial \dot{p}_\ell} = 0. \tag{9.55}$$

Derivation of $\frac{\partial L_1^{ext}}{\partial \theta}$

Along the same lines as the previous section, for this paper the linearization of the the balance of energy external forcing function with respect to temperature can be written as

$$\frac{\partial L_1^{ext}}{\partial \dot{\theta}} = \frac{\partial}{\partial \dot{\theta}}\Big(h_t(\theta - \theta_{amb})\Big) \tag{9.56}$$

which can be simplified to

$$\frac{\partial L_1^{ext}}{\partial \dot{\theta}} = h_t \alpha \Delta t. \tag{9.57}$$